



UNIVERSITY OF
LIVERPOOL

**Accurate Estimation of Intraocular Pressure
and Corneal Material Behaviour
Using a Non-Contact Method**

Thesis submitted in accordance with the requirements of
the University of Liverpool for the degree of Doctor in Philosophy

By

KAI-JUNG CHEN

November 2018

CONTENTS

CONTENTS	I
List of Figures	VII
List of Tables	XI
List of Abbreviations	XIV
Publications	XIX
Abstract	XXI
Acknowledgements	XXV
Chapter One	1
Introduction	1
1.1 PREFACE	1
1.2 SCOPE OF THE STUDY	8
1.3 AIM AND OBJECTIVES	9
1.4 THESIS STRUCTURE	10
Chapter Two	12
Literature Review	12
2.1 INTRODUCTION	12
2.2 STRUCTURE OF THE EYE	13
2.2.1 Eye Geometry.....	13
2.3 EYE TISSUE BIOMECHANICS	16
2.3.1 Corneal Material Behaviour	16
2.3.2 Sclera Material Behaviour.....	18
2.3.3 Ogden’s Form of Nonlinear Hyper-Elastic Material Behaviour.....	20
2.4 INTRAOCULAR PRESSURE	23
2.5 KERATOCONUS	25

2.5.1 Image Technology for Keratoconus Detection	29
2.5.2 Histopathology and Biomechanical Factors	33
2.6 GLAUCOMA	35
2.7 CATEGORIES OF TONOMETRY	38
2.7.1 The Principle of Applanation Tonometry	39
2.7.2 Goldmann Applanation Tonometry	39
2.7.3 Non-Contact Tonometry	41
2.8 ERROR SOURCES IN TONOMETRY MEASUREMENT.....	53
2.8.1 Corneal Factors that Effect Contact Tonometry (GAT)	54
2.8.2 Corneal Factors that Effect Non-Contact Tonometry	56
2.9 CONCLUDING REMARKS.....	57
<i>Chapter Three</i>	<i>59</i>
<i>Methodology</i>	<i>59</i>
3.1 INTRODUCTION	59
3.2 DISTINGUISHING BETWEEN KC AND HEALTHY DATA.....	62
3.3 NUMERICAL MODELLING	69
3.3.1 Normal/Abnormal Geometry of FEM Configuration	70
3.3.2 Regional Variation in Material Behaviour	73
3.3.2.1 Boundary Conditions.....	76
3.3.3 Loading Configuration.....	77
3.3.4 Stress-Free Configuration	79
3.3.5 Mesh Density Study	80
3.3.6 Summary of Simulation Steps.....	82
3.4 PARAMETRIC STUDY	83

3.4.1 Calculation of Dynamic Corneal Response Parameters.....	83
3.4.2 Comparisons between Clinical Data and Numerical Results	86
Comparisons of Corneal Deformation.....	86
Comparisons of CorVis-ST Dynamic Response Parameters.....	86
Comparisons of Age-matched Dynamic Response Parameters Obtained Numerically and Clinically....	87
3.5 DEVELOPMENT OF ALGORITHMS TO ESTIMATE bIOP AND CORNEAL MATERIAL BEHAVIOUR.....	89
3.5.1 Development of Algorithms to Estimate IOP and Corneal Material Behaviour in Healthy Eyes.....	90
Correlation Analysis of Dynamic Response Parameters in Healthy Eyes.....	92
Estimation Algorithm for Intraocular Pressure for Healthy Eyes.....	93
Development of an Estimation Algorithm for Corneal Material Behaviour for Healthy Eyes	94
3.5.2 Development of Algorithms to Estimate IOP and Corneal Material Behaviour in Keratoconic Eyes	98
Correlation Analysis of Dynamic Response Parameters in Keratoconic Eyes	98
Development of an Estimation Algorithm for Corneal Material Behaviour for Keratoconic Eyes.....	99
Estimation Algorithm for Intraocular Pressure for Keratoconic Eyes	100
3.6 VALIDATION OF INTRAOCULAR PRESSURE	101
3.6.1 Validation of bIOP Using Healthy Ex Vivo Human Eye Experiments.....	101
Donor Eye Details	102
Ex vivo Human Eye Testing Process	102
Statistical Analysis	104
3.6.2 Validation of bIOP using In-Vivo Clinical Data.....	105
3.6.3 Thickness Effects on the Estimation of IOP Using Clinical Data.....	106
Clinical Datasets	106
Surgical Techniques	107
Statistical Analysis	108

3.7 VALIDATION OF INTRAOCULAR PRESSURE ESTIMATION FOR PATIENTS WITH KERATOCONUS	108
3.7.1 Clinical Datasets	109
3.7.2 Statistical Analysis	111
3.8 IN-VIVO VALIDATION OF CORNEAL MATERIAL ALGORITHM(B)	111
3.8.1 Clinical Datasets	112
3.8.2 Inverse Analysis Using Patient-specific Models	112
3.8.3 Statistical Analysis	113
3.9 CONCLUDING REMARKS.....	114
<i>Chapter Four.....</i>	115
<i>Results.....</i>	115
4.1 INTRODUCTION	115
4.2 DESCRIPTIVE STATISTICS OF NUMERICAL DATASETS.....	116
4.3 VALIDATION OF NUMERICAL RESULTS	117
4.3.1 Comparisons of Corneal Deformation	118
4.3.2 Comparisons of CorVis-ST Dynamic Response Parameters	120
4.3.3 Comparisons of Age-matched Dynamic Response Parameters Obtained Numerically and Clinically	124
4.4 DEVELOPMENT OF ESTIMATION ALGORITHM FOR IOP AND CORNEAL MATERIAL BEHAVIOUR	126
4.4.1 Correlation Analysis of the Dynamic Corneal Response Parameters	126
Pearson’s Correlation Analysis of P_{DCR} for Healthy Eyes	126
Pearson’s Correlation Analysis of P_{DCR} for Keratoconic Eyes.....	129
4.4.2 IOP Estimate Algorithms for Healthy Eyes	131
4.4.3 Corneal Material Estimation Algorithms for Healthy and Keratoconic Eyes	132
4.4.4 IOP Estimation Algorithms for Keratoconic Eyes	137

4.5 VALIDATION OF bIOP-ESTIMATION ALGORITHM FOR HEALTHY EYES	138
4.5.1 Validation of bIOP Algorithm Using Ex Vivo Human Eyes.....	138
4.5.2 Validation of bIOP Algorithm Using Clinical Datasets.....	140
4.5.3 Validation of bIOP Algorithm Using Refractive Surgery Datasets.....	143
Participants of clinical datasets	143
Preoperative Results	144
Postoperative Results.....	145
Comparison between IOP measurements obtained Pre- and Post-Surgery.....	146
4.6 VALIDATION OF bIOP_{KC}-ESTIMATION ALGORITHM FOR KERATOCONIC EYES USING CLINICAL DATASETS	
.....	150
4.6.1 Analysis of Dataset 1 from Milan and Dataset 2 from Rio.....	151
Analysis of Dataset 1 (Milan).....	151
Analysis of Dataset 2 (RIO)	152
4.6.2 Correlation of IOP _{KC} Estimates with Age and Corneal Thickness.....	153
4.6.3 Comparative Analysis Based on Keratoconus Classification.....	154
4.6.4 Comparison of bIOP and bIOP _{KC} in Keratoconic Patients.....	155
Milan Dataset (1).....	155
Rio Dataset (2).....	156
4.7 IN-VIVO VALIDATION OF CORNEAL MATERIAL ALGORITHM (B).....	156
4.7.1 Comparison of β Obtained from the Estimate Algorithm and Inverse Analysis for Healthy Eyes.....	159
4.7.2 Correlation Analysis of the Material Parameter (β) with Corneal Thickness and IOP for Healthy Eyes	160
4.7.3 Validation Against Ex-Vivo Inflation Test Results in Healthy Patients.....	162
4.7.4 Comparison of β Obtained from the Algorithm and Inverse Analysis for	

Keratoconic Eyes	163
Chapter Five.....	165
Discussion and Conclusions.....	165
5.1 INTRODUCTION	165
5.2 OVERALL DISCUSSION	165
5.2.1 Correlation of bIOP with CCT and Age in Healthy Eyes.....	168
5.2.2 Validation of bIOP Algorithm through EX-Vivo Testing	170
5.2.3 Validation of bIOP on Refractive Surgery Clinical Data	174
5.2.4 IOP Estimation in Keratoconic patients.....	178
5.2.5 In Vivo Corneal Material Behaviour Estimation.....	181
Validation of Algorithm through Inverse analysis.....	183
Validation against Ex-Vivo Inflation Test Results in Healthy Eyes	185
5.3 CONCLUSIONS.....	187
5.4 LIMITATIONS.....	189
Appendix A - Diagnosis of Keratoconus	193
Appendix B - Ex-Vivo Experimental Procedure.....	208
Appendix C - Flowchart of Numerical Modelling	214
References	215

List of Figures

Figure 1-1 Applanation tonometry by Alexei Maklakoff, circa 1885 [10]	2
Figure 1-2 Contact tonometry. (A) Goldmann Applanation Tonometry; (B) Perkins Tonometry (a portable version of GAT); (C) Tono-Pen Tonometry, Avia	3
Figure 1-3 CorVis-ST developed by OCULUS Optikgeräte, Inc. (Wetzlar, Germany)	7
Figure 2-1 Horizontal section of the eye with optic nerve [3]	13
Figure 2-2 Schematic representation of eye showing rectus muscle locations [3]	14
Figure 2-3 Stress–strain relationships of corneal material with different Ages [1]	18
Figure 2-4 Tangential modulus-strain relationships of corneal material with different Ages [1]	18
Figure 2-5 Strain rate effects on average stress-strain behaviour of scleral tissue in (a) anterior, (b) equatorial and (c) posterior region [70]	20
Figure 2-6 Tangent modulus of material with non-linear behaviour: (A) Tangent modulus varies with stress; (B) Tangent modulus in constant one zone of linear behaviour at different non-linear material behaviour.	21
Figure 2-7 Schematic diagram of an aqueous humour flow pathway [105]	24
Figure 2-8 Comparison of corneal shape between (A) healthy and (B) Keratoconic eyes	26
Figure 2-9 Pentacam has a rotating Scheimpflug camera system for anterior segment analysis	30
Figure 2-10 Pentacam’s Built-in Software Overview Report. Scheimpflug image pane displays cross-sectional image, including the cornea, anterior chamber, iris and lens. Densitometry pane shows the clarity estimation of measurement. 3D corneal shape report pane provides a 3D representation of corneal shape, with the anterior corneal surface in red, posterior corneal surface in green, and iris in blue. Pachymetry map pane shows the pachymetry map in colour, which represents corneal thickness by colour and a numerical scale on the right.....	31
Figure 2-11 Pentacam Map Report. The colour map uses cooler colours for higher value and warmer colours for lower value	32
Figure 2-12 Patterns of anterior curvature map. The steep part of curvature map may form a bowtie shape, a hat shape, or an irregular shape [163].....	33
Figure 2-13 Aqueous humour drainage pathways in Glaucomatous eyes. (A) Primary open-angle Glaucoma: increased resistance makes it difficult for aqueous humour to pass through the trabecular meshwork. (B) Primary closed-angle Glaucoma: access to the drainage pathway is typically obstructed. [177].....	38
Figure 2-14 Comparison between principles of (A) Imbert–Fick law and (B) Goldmann Applanation Tonometer [10].....	40
Figure 2-15 Principles of non-contact tonometry (NCT) [192]	42

Figure 2-16 XPERT™ NCT™ PLUS Advanced Logic Tonometer by Reichert Ophthalmic Instruments.....	43
Figure 2-17 Ocular Response Analyzer® G3.....	44
Figure 2-18 Typical light signal (red) and pressure signal (green) versus time [195, 197].....	45
Figure 2-19 Sample images with markers illustrating parameters of the CorVis-ST device. (A) At ingoing first applanation phase, the anterior corneal surface is flattened. At the point of highest concavity, the radius of curvature (B), bending distance (C), and maximum deformation at the corneal apex (D) are determined. (E) As air-puff pressure decreases, the corneal surface returns to its initial state and the second applanation occurs [201].	49
Figure 2-20 Stress-strain curves for a purely elastic material with no hysteresis (A) and a viscoelastic material with hysteresis (B). The red area shows the amount of energy lost in a loading and unloading cycle, which is an indication of the magnitude of hysteresis.....	50
Figure 2-21 Dynamic Scheimpflug images at the pre-deformation phase and the oscillation phase, showing (A) cornea in pre-deformation phase (blue), at maximal corneal deflection (red), and at maximal whole eye movement (white); (B) initial corneal shape aligns with shape at maximal corneal deformation; and (C) correction for whole eye movement by aligning the cornea with maximum deflection to the initial shape [201]	51
Figure 3-1 Comparison of stiffness and topography of healthy, FFKC, and KC eyes.....	60
Figure 3-2 Flow chart of the procedure for IOP and corneal material behaviour Estimation .	61
Figure 3-3 Typical corneal geometry data plotted in 3D (A) and (B). Colour of individual points reflects their Z coordinates, and the scale of the Z coordinates is shown in a colour scale....	63
Figure 3-4 Analysis of corneal geometry elevation along meridian and circumferential lines	64
Figure 3-5 Analysis of corneal elevation data along eight main meridians of the eye	65
Figure 3-6 Analysis of corneal elevation in clinical datasets along circumferential lines with radii of 1, 2, 3, and 4 mm	67
Figure 3-7 Comparison of mean and SD of differences of variations in elevation data between (A) normal eyes and (B) KC eyes	67
Figure 3-8 Trends of variations in elevation data in normal and five KC groups	69
Figure 3-9 Geometry parameters of the eye model	71
Figure 3-10 General Equation for a general conic section (a) is given by $Y^2 = 2r_0Z - pZ^2$ and the family of conic sections with different asphericities is shown in (b) [235]	71
Figure 3-11 Model segments with different material properties in FEM (A). Stress-strain material behaviour of the cornea (B), limbus (C), anterior sclera (D), and posterior sclera (E) with age-related variation is shown [1, 70].	74
Figure 3-12 View of a FEM showing (A) full eye model and (B) cross-sectional view. Boundary conditions are highlighted in Orange.....	77
Figure 3-13 Spatial distribution (A) and time variation (B) of air-puff pressure on the cornea [46, 242, 243]. In (B), thick black line represents pressure measured in device piston and the red line represents pressure acting on the cornea.....	78

Figure 3-14 Schematic description of the approach used to obtain the stress-free configuration of the eye [233].....	79
Figure 3-15 Progress of normalised air pressure (A) and nodal deformations at the corneal apex (B) with time. When air-puff pressure increases to a maximum, corneal apex deformation reaches its max value.....	84
Figure 3-16 Corneal anterior profiles during air-puff loading.....	84
Figure 3-17 Second partial derivatives of corneal anterior edge with respect to time calculated at corneal apex.....	85
Figure 3-18 Flowchart of procedure for developing algorithms to estimate IOP and corneal material behaviour in healthy and KC eyes.....	90
Figure 3-19 Comparison of the effect of M_R value on the loading-deformation and stress-strain behaviour	94
Figure 3-20 (A) 3D point cloud plot and (B) surface plot of corneal stiffness parameter against IOP and CCT for different M_R values	96
Figure 3-21 The process of corneal material estimation. (A) When specific values of CCT ($CCT_{specific}$) and IOP ($IOP_{specific}$) are applied in the SP-HC surface plot, there are several estimates for SP-HC for different M_R . (B) When these estimates are plotted, β can be estimated using the corresponding SP-HC ($Ln(SP-HC)_{specific}$).	97
Figure 3-22 3D surface plots of stiffness parameter against IOP/20 and CCT/545 for different TopoR. Every surface corresponds to a specific value of M_R	100
Figure 3-23 Expected results of correlation analysis of IOP with CCT and Age in clinical datasets	101
Figure 3-24 Test rig showing eye sitting on a rigid support and supported from the back while being connected to a syringe pump that controls its IOP. CorVis ST is placed at a distance to enable its automatic trigger.	103
Figure 3-25 Schematic views of inflation test rig showing an ex-vivo eye [1] sitting on rigid support [2], which provided restraint against the vertical motion, and soft back support [3] that provided flexible restraint against the horizontal motion. The eye has a G14 needle [4] inserted through the posterior pole and connected to a syringe pump [5] to control the intraocular pressure using a stepper motor [6]. The needle is also connected to a pressure transducer [7] to measure the pressure inside the eye. The CorVis ST [8] is used to provide estimates of IOP through the application of an air puff.	103
Figure 4-1 Comparison of numerical predictions with clinical measurements of corneal deformation at the start of the analysis, first applanation and highest concavity.....	119
Figure 4-2 Ranges of dynamic response parameters - deformation and deflection at the first applanation and highest concavity in numerical predictions compared to the boxplot indicating the mean, range and confidence interval ranges at $p=95\%$ for the CorVis-ST output in two clinical datasets (Brazil and Milan) for healthy eyes.....	123
Figure 4-3 Ranges of dynamic response parameters - deformation and deflection at the first applanations and highest concavity in numerical predictions compared to the boxplot indicating the mean, range and confidence interval ranges at $p=95\%$ for the CorVis-ST output	

in two clinical datasets (Brazil and Milan) for keratoconic eyes	123
Figure 4-4 Effectiveness of bIOP in reducing association with CCT and age in clinical databases obtained from Smile Eye Clinics	141
Figure 4-5 Effectiveness of bIOP in reducing association with CCT and age in clinical databases obtained from Humanitas Clinical and Research Center	142
Figure 4-6 Effectiveness of bIOP in reducing association with CCT and age in clinical databases obtained from Wenzhou Medical University	142
Figure 4-7 Correlation between CCT and GAT-IOP, CVS-IOP and bIOP for (A) pre- and (B) post-operative data of LASIK group.....	149
Figure 4-8 Correlation between CCT and GAT-IOP, CVS-IOP and bIOP for (A) pre- and (B) post-operative data of SMILE group.....	149
Figure 4-9 Correlation between CCT and GAT-IOP, CVS-IOP and bIOP for (A) pre- and (B) post-operative data of both LASIK and SMILE groups.....	150
Figure 4-10 CVS-IOP, bIOP, and bIOP _{KC} values obtained for healthy and KC participants from Datasets 1 and 2. Results illustrate the stability in predicting IOP values using the bIOP and bIOP _{KC} algorithms for healthy and KC eyes, compared to the large differences found in CVS-IOP. Both bIOP and bIOP _{KC} further exhibit lower standard deviation values compared to CVS-IOP.	152
Figure 4-11 Analysis of the degree of dependency of both bIOP _{KC} and CVS-IOP on CCT and age in the Milan (a, b) and Rio dataset (c, d).....	153
Figure 4-12 Mean and standard deviation of bIOP and bIOP _{KC} in both datasets in KC patients divided based on disease stage	154
Figure 4-13 Results of the β algorithm (β_{Eq}) against β inverse analysis (β_{In}) for 158 healthy eyes shown with a red trend line against a 45-degree line denoting target perfect fit	160
Figure 4-14 Assessment of the correlation in Dataset 1 between β_{Eq} and each of (a) bIOP, (b) CCT and (c) Age	161
Figure 4-15 Assessment of the correlation in Dataset 2 between β_{Eq} and each of (a) bIOP, (b) CCT and (c) Age	162
Figure 4-16 Relationship between β and age based on in-vivo clinical data (black dots and a black trend line) and ex-vivo inflation test results (red dots) for (a) Milan dataset and (b) Rio dataset	163
Figure 4-17 Results of the β algorithm (β_{Eq}) against β inverse analysis (β_{In}) for 34 keratoconic eyes shown with a red trend line against a 45-degree line denoting target perfect fit	164

List of Tables

Table 1-1 Comparison of advantages and disadvantages between contact applanation tonometry and non-contact applanation tonometry	4
Table 2-1 Details of eye parameters on the clinical measurement data	15
Table 2-2 Keratoconus classification based on disease progression [139, 140, 148]	28
Table 2-3 Correction factors of GAT-IOP based on CCT variations.....	55
Table 2-4 Comparison of correction factors for GAT-IOP and NCT based on CCT variations...	57
Table 3-1 Details of the clinical databases	64
Table 3-2 Mean and SD of differences in elevation data between the corneal apex and points at distances of 1, 2, 3, and 4 mm from apex for healthy eyes in millimetre	66
Table 3-3 Mean and SD of differences in elevation data between the corneal apex and points at distances of 1, 2, 3, and 4 mm from corneal apex for keratoconic eyes in millimetre.....	66
Table 3-4 Comparisons of mean and SD of differences (in millimetre) between max and min elevation along circumferential lines with radii of 1, 2, 3, and 4 mm for normal and abnormal corneal geometry.....	67
Table 3-5 Trends of variations in elevation data variation trends in normal and KC groups ...	69
Table 3-6 Comparison between clinical measurement data and numerical model settings for healthy eyes	73
Table 3-7 Ogden coefficients of eye FE model in cornea, limbus, anterior sclera and posterior sclera	75
Table 3-8 Details of eight model settings tested in an initial study	80
Table 3-9 Displacements and thickness changes after IOP inflation and external loading. Values in Table are all in μm	81
Table 3-10 Cases used in Kolmogorov-Smirnov statistical analysis of healthy numerical and clinical datasets.....	88
Table 3-11 Details of clinical databases	105
Table 4-1 Results of numerical analysis for normal and keratoconic groups showing mean, standard deviation and range values	117
Table 4-2 Four randomly-selected cases considered in a validation study of numerical results	118
Table 4-3 Clinical datasets for healthy and KC patients showing mean, standard deviation and range values	121
Table 4-4 Clinical datasets for healthy and KC patients showing confidence interval ranges of CorVis-ST dynamic response parameters at $p=95\%$	122
Table 4-5 Comparisons between numerical results and clinical data in age-matching groups	125

Table 4-6 Numerical results for normal corneas showing the output of Pearson’s correlation analysis.....	127
Table 4-7 Clinical data for healthy eyes from Brazil showing the output of Pearson’s correlation analysis.....	128
Table 4-8 Clinical data for healthy eyes from Milan showing the output of Pearson’s correlation analysis.....	128
Table 4-9 Numerical results for keratoconic corneas showing the output of Pearson’s correlation analysis	130
Table 4-10 Clinical data for keratoconic eyes from Brazil showing the output of Pearson’s correlation analysis	130
Table 4-11 Clinical data for keratoconic eyes from Milan showing the output of Pearson’s correlation analysis	131
Table 4-12 Stiffness parameter in numerical results for healthy and keratoconic groups showing mean, standard deviation, and range values	133
Table 4-13 Results of Pearson’s correlation analysis of SP-HC in numerical results for healthy and keratoconic eyes.....	133
Table 4-14 Coefficients of Par_{SP-HC} in Equation 4.7 and values of CCT and IOPt	135
Table 4-15 Comparison of differences between IOPt and CVS-IOP in numerical results	136
Table 4-16 IOP measurements including uncorrected CVS-IOP and biomechanically-corrected bIOP values at controlled true IOP values between 10 and 30 mmHg. Results include mean, standard deviation and range.	139
Table 4-17 Results of three clinical datasets showing mean, standard deviation and a range value of CCT, age, CVS-IOP and bIOP	141
Table 4-18 Pre-operative data for LASIK and SMILE groups showing mean, standard deviation and range values	144
Table 4-19 Pre-operative datasets for both LASIK and SMILE groups showing results of Pearson’s correlation analysis.....	145
Table 4-20 Post-operative data for both LASIK and SMILE groups showing mean, standard deviation and range values	146
Table 4-21 Post-operative datasets for both LASIK and SMILE groups showing results of Pearson’s correlation analysis.....	146
Table 4-22 Differences between post- and pre-operative data for both LASIK and SMILE groups showing the mean, standard deviation and p value of the paired t-test results.....	147
Table 4-23 Number, mean, and standard deviation of all KC data used in Milan Dataset (1) for bIOP and bIOP _{KC} . Further, a homogeneity test was carried out to show the differences in standard deviation and the ANOVA test was performed to analyse the mean values.....	155
Table 4-24 Number, mean, and standard deviation of all KC data used in Rio Dataset (2) for bIOP, CVS-IOP, and bIOP _{KC} . Further, a homogeneity test was carried out to show the differences in standard deviation and the ANOVA test was performed to analyse the mean values.....	156

Table 4-25 Selected data from healthy and KC groups showing mean, standard deviation and range values158

Table 4-26 Clinical datasets for healthy eyes showing mean, standard deviation, a range of β and p-value of paired t-test results between β algorithm and inverse analysis.....159

Table 4-27 Clinical datasets for keratoconic eyes showing mean, standard deviation, range of β , and p-value of paired t-test results between β algorithm and inverse analysis.....164

List of Abbreviations

$\bar{\lambda}_i$	Deviatoric Principal Stretches
D_i	Compressibility of Temperature Dependent Material Parameter in Ogden Strain Energy Function
λ_i	Principal Stretches
μ_i & α_i	Temperature Dependent Material Parameter in Ogden Strain Energy Function
.odb File	Output Database File
A	Area of the Applanation of the Central Cornea
A1	First Applanation
A1DeflAmp	Maximum Deflection Amplitude of the Cornea at the Highest Concavity
A1Deflection	Deflection Amplitude of the Corneal Apex
A1Deformation	Deformation Amplitude of the Corneal Apex at the First Applanation Events
A1L	Length of the Flattened Cornea
A1T	First Applanations Times
A1V	Maximum Corneal Velocity at the First Applanation Events
A2	Second Applanation
AP1	First Applanation Pressure on the Device's Piston
b	Surface Tension Force caused by
bIOP	Biomechanically-Corrected Intraocular Pressure for Healthy Eyes
bIOP_{KC}	Biomechanically-Corrected Intraocular Pressure for Keratoconic Eyes
CCT	Central Corneal Thickness
CFD	Computational Fluid Dynamics Simulation
CVS	Corvis ST Tonometry
CVS-IOP	IOP measurement using CorVis-ST
DCR	Dynamic Corneal Response Parameters obtained from CorVis-ST
DCT	Dynamic Contour Tonometry, DCT-Pascal, Swiss Microtechnology AG, Port
DCT-IOP	IOP measurement using Dynamic Contour Tonometry
FEM	Finite Element Method

FFKC	Forme Fruste Keratoconus
GAT	Goldmann Applanation Tonometry
GAT-IOP	IOP measurement using Goldmann Applanation Tonometry
HC	Highest Concave
<i>HCDeflAmp</i>	Maximum Deflection Amplitude of the Cornea at the Highest Concavity
HCDeflection	Maximum Deflection Amplitude of the Cornea at the Highest Concavity
HCDeformation	Maximum Deformation Amplitude of the Cornea at the Highest Concavity
HCRC	Humanitas Clinical and Research Center
HCT	Time from air-puff starting until the point of HC of the Cornea
IOP	Intraocular pressure
IOPcc	Ocular Response Analyzer with its Corneal Compensated IOP estimates
IOPt	True Intraocular Pressure
I-R	Impact–Rebound Tonometer
ISO	International Standard Organization
KC	Keratoconus
K–S test	Kolmogorov-Smirnov test
LASIK	Laser-Assisted in Situ Keratomileusis
mmHg	millimeters of mercury
M_R	Ratio between the Ogden coefficients μ_i and μ at age 50
M_R(Age)	Value of M _R calculated from the Age value
NCT	Non-Contact Applanation Tonometry
OIT	Prototype Murine Optical Interference Tonometer
ORA	Ocular Response Analyzer
P	Anterior Corneal Shape Factor
<i>P</i>	Pressure inside the Sphere
P_{bIOP}	P _{DCR} has stronger correlation with IOP value than the CCT and Beta value
PCT	Peripheral Corneal Thickness
PD	Distance between the Two Peaks of the Cornea at the Time of the Highest Concavity
PPMC	Person Product Moment Correlation

PRK	Refractive Surgeries, Photorefractive Keratectomy
PSO	Particle Swarm Optimization
R	Radius of Curvature of Corneal Concavity at the Time of the Highest Deformation
R_{ab}	Abnormal Shape Factor
R_c	Corneal Central Anterior Radius of Curvature
RI	Limbal Radius
R_s	Scleral Radius
SD	Standard Deviation
SE	Spherical Equivalence
SEC	Smile Eye Clinics
SMILE	Small-Incision Lenticule Extraction
SP	Stiffness Parameter
SP-HC	Stiffness Parameter at the Highest Concavity
SP-HC_{blOP}	Stiffness Parameter at the Highest Concavity by Using blOP
SP-HC_{CVS}	Stiffness Parameter at the Highest Concavity by Using CVS-IOP
TKC	Topographic Keratoconus Classification
TopoR	Abnormal Corneal Shape Factors
W	Backpressure Flattening of the Membrane
WHO	The World Health Organization
WMU	Wenzhou Medical University
β	Corneal Material Behaviour Estimation
β_{Eq}	Corneal Material Behaviour Estimation obtained from Corneal Material Algorithm
β_{In}	Corneal Material Behaviour Estimation obtained from Inverse Analysis
ε	Strain
σ	Stress
U	Ogden strain energy
.odb File	Output Database File
A1	First Applanation
A1Deflection	Deflection Amplitude of the Corneal Apex
A1Deformation	Deformation Amplitude of the Corneal Apex at the First Applanation Events

A1L	Length of the Flattened Cornea
A1T	First Applanations Times
A1V	Maximum Corneal Velocity at the First Applanation Events
A2	Second Applanation
AP1	First Applanation Pressure on the Device's Piston
bIOP	Biomechanically-Corrected Intraocular Pressure for Healthy Eyes
bIOP_{KC}	Biomechanically-Corrected Intraocular Pressure for Keratoconic Eyes
CCT	Central Corneal Thickness
CVS	Corvis ST Tonometry
CVS-IOP	IOP measurement using CorVis-ST
DCT	Dynamic Contour Tonometry, DCT-Pascal, Swiss Microtechnology AG, Port
DCT-IOP	IOP measurement using Dynamic Contour Tonometry
FEM	Finite Element Method
FFKC	Forme Fruste Keratoconus
GAT	Goldmann Applanation Tonometry
GAT-IOP	IOP measurement using Goldmann Applanation Tonometry
HC	Highest Concave
HCDeflection	Maximum Deflection Amplitude of the Cornea at the Highest Concavity
HCDeformation	Maximum Deformation Amplitude of the Cornea at the Highest Concavity
HCT	Time from air-puff starting until the point of HC of the Cornea
HCRC	Humanitas Clinical and Research Center
IOP	Intraocular pressure
IOP_{cc}	Ocular Response Analyzer with its Corneal Compensated IOP estimates
IOP_t	True Intraocular Pressure
I-R	Impact–Rebound Tonometer
KC	Keratoconus
K–S test	Kolmogorov-Smirnov test
LASIK	Laser-Assisted in Situ Keratomileusis
mmHg	millimeters of mercury
M_R	the ratio between the Ogden coefficients μ_i and μ at age 50
M_R(Age)	The value of M _R calculated from the Age value
NCT	Non-Contact Applanation Tonometry

ORA	Ocular Response Analyzer
OIT	Prototype Murine Optical Interference Tonometer
P	Anterior Corneal Shape Factor
P_{blOP}	P _{DCR} has stronger correlation with IOP value than the CCT and Beta value
PCT	Peripheral Corneal Thickness
PD	Distance between the Two Peaks of the Cornea at the Time of the Highest Concavity
PPMC	Person Product Moment Correlation
PSO	Particle Swarm Optimization
PRK	Refractive Surgeries, Photorefractive Keratectomy
R	Radius of Curvature of Corneal Concavity at the Time of the Highest Deformation
R_{ab}	Abnormal Shape Factor
R_c	Corneal Central Anterior Radius of Curvature
RI	Limbal Radius
R_s	Scleral Radius
SEC	Smile Eye Clinics
SD	Standard Deviation
SMILE	Small-Incision Lenticule Extraction
SP	Stiffness Parameter
SP-HC	Stiffness Parameter at the Highest Concavity
SP-HC_{blOP}	Stiffness Parameter at the Highest Concavity by Using blOP
SP-HC_{CVS}	Stiffness Parameter at the Highest Concavity by Using CVS-IOP
TopoR	Abnormal Corneal Shape Factors
U	Ogden strain energy
WHO	The World Health Organization
WMU	Wenzhou Medical University
ε	Strain
λ	Stretch
σ	Stress

Publications

Journal Article

1. Chen, Kai-Jung; Joda, Akram; Vinciguerra, Riccardo; Eliasy, Ashkan; Sefat, Shervin Mir Mohi; Kook, Daniel; Geraghty, Brendan; Roberts, Cynthia J and Elsheikh, Ahmed (2018) Clinical evaluation of a new correction algorithm for dynamic Scheimpflug analyzer tonometry before and after laser in situ keratomileusis and small-incision lenticule extraction. JOURNAL OF CATARACT AND REFRACTIVE SURGERY, 44 (5). 581 - 588.

2. Eliasy, Ashkan; Chen, Kai-Jung; Vinciguerra, Riccardo; Maklad, Osama; Vinciguerra, Paolo; Ambrosio Jr; Renato, Roberts; Cynthia J and Elsheikh, Ahmed (2018) Ex-vivo experimental validation of biomechanically-corrected intraocular pressure measurements on human eyes using the CorVis ST. EXPERIMENTAL EYE RESEARCH, 175. 98 - 102.

3. Chang, Shao-Hsuan; Mohammadvali, Ashkan; Chen, Kai-Jung; Ji, You-Ren; Young, Tai-Horng; Wang, Tsung-Jen; Willoughby, Colin E; Hamill, Kevin J and Elsheikh, Ahmed (2018) The Relationship Between Mechanical Properties, Ultrastructural Changes, and Intrafibrillar Bond Formation in Corneal UVA/Riboflavin Cross-linking Treatment for Keratoconus. JOURNAL OF REFRACTIVE SURGERY, 34 (4). 264 - 272.

Under Review

1. Chen, Kai-Jung; Eliasy, Ashkan; Vinciguerra, Riccardo; Ahmed, Abass; Vinciguerra, Paolo; Ambrósio Jr, Renato; Roberts, Cynthia J. and Elsheikh, Ahmed (2018) Development and Validation of a new Intraocular Pressure Estimate for Patients with Keratoconus.

2. Eliasy, Ashkan; Chen, Kai-Jung; Vinciguerra, Riccardo; Ahmed, Abass; Vinciguerra, Paolo; Ambrósio Jr, Renato; Roberts, Cynthia J. and Elsheikh, Ahmed (2018) Determination of Corneal Biomechanical Behaviour In-vivo for Healthy Eyes Using CorVis ST Tonometry: Stress-strain Index.

Conference Paper

1. Eliasy, Ashkan; Elsheikh, Ahmed and Chen, Kai-Jung (2018) Intraocular Pressure Measurement Pre- and Post-Refractive Surgery Using GAT and CorVis ST bIOP Algorithm. In: 6th European Conference on Computational Mechanics (ECCM 6) 7th European Conference on Computational Fluid Dynamics (ECFD 7), Glasgow, UK.

2. Elsheikh, Ahmed; Eliasy, Ashkan; Chen, Kai-Jung and Vinciguerra, Riccardo (2018) Obtaining biomechanical properties of corneal tissue in-vivo using a non-contact method. In: 8th World Congress of Biomechanics, Dublin, Ireland.

3. Eliasy, Ashkan; Chen, Kai-Jung; Vinciguerra, Riccardo and Elsheikh, Ahmed (2018) Novel Intraocular Pressure Measurement Algorithm for Patients with Keratoconus. In: 8th World Congress of Biomechanics, Dublin, Ireland.

Poster

Elsheikh, Ahmed; Joda, Akram; Chen, Kai-Jung; Vinciguerra, Riccardo; Vinciguerra, Paolo; Kook, Daniel; Sefat, Shervin and Bao, FangJun (2015) Clinical Evaluation of Correction Algorithm for Corvis ST Tonometry. In: Investigative Ophthalmology & Visual Science.

Abstract

The present study is quantifying the effect of corneal parameters (including corneal geometry and material stiffness) with potential considerable influence on intraocular pressure (IOP) and corneal material estimation using finite element method to develop biomechanically-corrected IOP algorithm and biomechanically estimated material algorithm on the non-contact tonometry to estimate higher accurate IOP (with a reduced effect of CCT and age) compared to device's IOP measurement and the in-vivo corneal material behaviour (with a reduced effect of IOP).

The CorVis-ST (Oculus, Wetzlar, Germany) measures IOP using high-speed Scheimpflug technology, which can record the deformation of the cornea during the air pressure application and use this information to define the relationship between the true IOP and dynamic response parameters obtained from CorVis-ST. Hence, in this study the OCULUS CorVis-ST was used for the development of a precise method for estimation of intraocular pressure and corneal material behaviour.

Numerical analysis using the finite element method (FEM) had been adapted to represent the operation of the IOP measurement by using the CorVis-ST. The analysis considered the important biomechanical parameters of the eye including IOP, central corneal thickness (CCT), corneal geometry (central radius of curvature, R_c ; and anterior corneal asphericity, P), and corneal material behaviour. The numerical simulation results demonstrated higher association of IOP predictions with the first applanation pressure (AP1) rather than CCT and corneal material stiffness (related to age), and higher association of corneal material properties with the ratio between corneal displacement and AP1. The numerical simulation results for healthy

and Keratoconic eyes were used as a base to develop algorithms for estimating the true IOP with a reduced effect of CCT and corneal material stiffness, and corneal material behaviour (stress-strain relationship) with a reduced effect of the true IOP.

Biomechanically-corrected IOP (bIOP) algorithms for both healthy and keratoconic eyes were validated in clinical data (including healthy, KC, and refractive surgery data) with the aim of significantly reducing IOP dependence on CCT and corneal biomechanics and in experimental ex-vivo human eye tests to assess the accuracy of the bIOP algorithms.

The results of experimental ex-vivo human eye tests showed that bIOP had a higher accuracy than the IOP measurement using the CorVis-ST and exhibited no significant correlation with CCT ($p=0.756$), whereas CVS-IOP was significantly correlated with CCT ($p < 0.001$).

The correlation results in healthy datasets with no pathological conditions were tested against a large clinical data set involving 634 patients from the Smile Eyes Clinics, Germany, 1047 patients from the Humanitas Clinical and Research Center, Italy, and 912 patients from the Wenzhou Medical University, China. It was found to reduce the dependency of IOP on both CCT and age, significantly.

To compare the bIOP algorithm provided by Corvis-ST with the Goldmann Applanation Tonometry IOP (GAT-IOP) and CVS-IOP measurements before and after laser treatment in 14 situ keratomileusis (LASIK) patients and 22 refractive lenticule extraction small-incision lenticule extraction (SMILE) patients, the comparison result showed that GAT-IOP and CVS-IOP showed significant correlation with CCT in both pre-and post-operative ($p<0.05$). In contrast to GAT-IOP and CVS-IOP, no significant correlation was found between bIOP and CCT in both group($p>0.05$), In addition, no significant difference in bIOP was found between pre- and post-

operative data (0.1 ± 2.1 mmHg, $p=0.80$ for LASIK and 0.8 ± 1.8 mm Hg, $P=0.273$ for SMILE), whereas there were significant decreases after surgeries in GAT-IOP (-3.2 ± 3.4 mmHg and -3.2 ± 2.1 mmHg, respectively; both $p < 0.001$) and CVS-IOP (-3.7 ± 2.1 mmHg and -3.3 ± 2.0 mmHg, respectively, both $p < 0.001$) compared with preoperative readings.

In terms of the validations of bIOP algorithm for KC eyes (bIOP_{KC}), the bIOP_{KC} algorithm was validated using clinical data with 722 eyes of 722 participants (Dataset 1 included 164 healthy and 151 KC eyes from the Vincieye Clinic in Milan, Italy, while Dataset 2 originated from the Rio de Janeiro Corneal Tomography and Biomechanics Study Group – Rio de Janeiro, Brazil I, with 205 healthy and 202 KC eyes). Predictions of bIOP_{KC} were assessed in the KC clinical data and compared with the previously developed bIOP algorithm predictions obtained for healthy eyes. The main outcome of the study was the absence of a significant difference ($p > 0.05$) in the values of IOP between healthy and KC patients, using the bIOP and bIOP_{KC} algorithms, while there was a significant difference with CVS-IOP ($p < 0.001$) for both. Further, bIOP_{KC} predictions were significantly less influenced by both corneal thickness and age than CVS -IOP.

The corneal material estimation algorithm produced a material stiffness parameter, β , which was validated using the inverse analysis based on the clinical data. In both healthy and KC eyes the β predictions provided high accuracy compared with the inverse analysis. Moreover, in healthy eyes, the result showed no significant correlation with both CCT ($p > 0.05$) and IOP ($p > 0.05$) but was significantly correlated with age ($p < 0.01$). The stiffness estimates and their variation with age were also significantly correlated ($p < 0.01$) with stiffness estimates obtained in earlier studies on ex-vivo human tissue [1]. In addition, in KC eyes the β predications remain at approximately 80% of the normal cornea's level.

All developed algorithms for IOP and corneal material behaviour estimation demonstrated great success in significantly on providing close estimates of true IOP and corneal material behaviour and reducing the effect of corneal thickness and material stiffness on IOP measurement and the effect of IOP on the corneal material estimation.

Related to this thesis, the author has either primarily or secondarily authored the following related journal articles which are included in this thesis in modified forms:

Chen, Kai-Jung, Joda, Akram, Vinciguerra, Riccardo, Eliasy, Ashkan, Sefat, Shervin Mir Mohi, Kook, Daniel, Geraghty, Brendan, Roberts, Cynthia J and Elsheikh, Ahmed (2018) Clinical evaluation of a new correction algorithm for dynamic Scheimpflug Analyzer tonometry before and after laser in situ keratomileusis and small-incision lenticule extraction. JOURNAL OF CATARACT AND REFRACTIVE SURGERY, 44 (5). 581 - 588.

Eliasy, Ashkan, Chen, Kai-Jung, Vinciguerra, Riccardo, Maklad, Osama, Vinciguerra, Paolo, Ambrosio Jr, Renato, Roberts, Cynthia J and Elsheikh, Ahmed (2018) Ex-vivo experimental validation of biomechanically-corrected intraocular pressure measurements on human eyes using the CorVis ST. EXPERIMENTAL EYE RESEARCH, 175. 98 - 102.

Chang, Shao-Hsuan, Mohammadvali, Ashkan, Chen, Kai-Jung, Ji, You-Ren, Young, Tai-Horng, Wang, Tsung-Jen, Willoughby, Colin E, Hamill, Kevin J and Elsheikh, Ahmed (2018) The Relationship Between Mechanical Properties, Ultrastructural Changes, and Intrafibrillar Bond Formation in Corneal UVA/Riboflavin Cross-linking Treatment for Keratoconus. JOURNAL OF REFRACTIVE SURGERY, 34 (4). 264 - 272.

Acknowledgements

I would like to dedicate my paper to all those who have offered me tremendous assistance during the four years at the University of Liverpool.

First and foremost, I have huge appreciation and gratitude for my supervisor Professor Elsheikh for his extraordinary support, expert advice and encouragement throughout this thesis process.

Also, I would like to thank my examiners for their valuable time, constructive questioning and comments.

This project would have been impossible without the support of the OCULUS Optikgeräte GmbH, the Smile Eye Clinic, the Humanitas Clinical and Research Center, the Wenzhou Medical University, the Vincieye Clinic, and the Rio de Janeiro Corneal Tomography and Biomechanics Study Group.

My thanks also go to the scholars whose monographs and academic papers have enlightened me in the writing of this paper.

I also owe my sincere gratitude to my friends and colleagues, Ashkan Eliasy, JungJie Wang and Dong Zhou, who gave me their time in helping me work out my problems during my difficult times. You supported me greatly and were always willing to help.

Last but not least, my thanks would belong to my beloved family for their loving considerations and great confidence in me all through these years. Their love is always the source of my strength during the period of thesis writing.

Chapter One

Introduction

1.1 Preface

THE EYE IS THE WINDOW OF THE SOUL, THE MOUTH, THE DOOR. The intellect, the will, is seen in the eye; the emotions, sensibilities, and affections, in the mouth. The animals look for the man's intentions right into his eyes. Even a rat, when you hunt him and bring him to bay, looks you in the eye.

-Hiram Powers, American sculptor (1805–1873)

The human senses are our means of contact with the environment. The human brain combines neurons to enable our senses – seeing, hearing, smelling, tasting and touching. Moreover, 60% functioning of the brain is involved in vision. This means that the eyes are our most important sense organs. However, there is no indication of vision damage before vision loss. Consequently, maintaining healthy eyesight is a primary necessity.

Intraocular pressure (IOP) represents a fundamental factor of ocular health and disease [2]. This pressure is created by the continual renewal of fluids within the eye [3]. The normal IOP varies from person to person. The normal range of IOP for a person is 10 to 20 mmHg (millimetres of mercury), and this pressure maintains the normal conditions of the eye to present a refractive optical effect [4-6]. When the IOP level is beyond the normal range for a specific individual, the risk of vision loss increases [7, 8]. In short, IOP measurement is

important in order to evaluate ocular health.

The history of the tonometry can be traced back to 1622 when intraocular pressure was estimated using finger pressure [9]. For centuries, this method had remained the only way to evaluate IOP until 1826. The technology of intraocular pressure measurement was first witnessed when ocular tension was digitally estimated during the 1826 meeting of the British Medical Association. Since then, the technology applied to estimate IOP has developed tremendously [10]. Although the first mechanical IOP measurement concept was formed in the early 1860s, this concept was not transformed into a tool. In 1867, the first applanation tonometry (similar to Figure 1-1) was developed by Adolf Weber. The applanation tonometry had faced much scepticism for twenty years, its value was rediscovered by Alexei Maklakoff (Figure 1-1) [10, 11]. In spite of this, in the early twentieth century, digital palpation tonometry had become the “gold standard” for ophthalmologists [12].

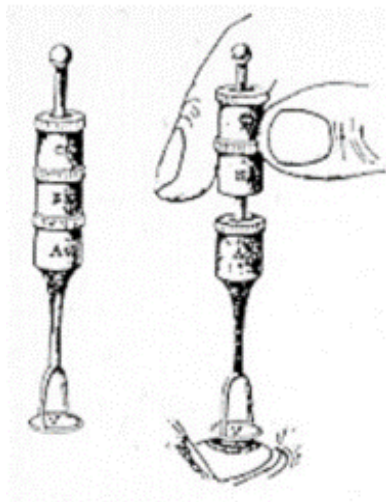


Figure 1-1 Applanation tonometry by Alexei Maklakoff, circa 1885 [10]

After nearly a decade, the first commonly used mechanical tonometry was developed by Hjalmar Schiötz, and this device became the new gold standard [12]. After its introduction in

the 1950s, the Goldmann Applanation Tonometry (GAT) (Figure 1-2, A) was widely accepted and remains the new reference standard in tonometry [13]. This technique follows the Imbert-Fick law, which is based on the relationship between intraocular pressure, the outlet force, and the applanation area. This tonometry makes a static measurement of the pressure on the cornea and attempts to avoid the effect of the bending resistance of the cornea. As it is a contact procedure, it requires a clinical license and training and application of a topical anaesthetic on the surface of the cornea [11]. For the past fifty years, the GAT has been the clinical gold standard in IOP measurement. Since then, tools for this kind of contact tonometry are being developed constantly, such as Perkins and TonoPen [10, 11] (Figure 1-2, B and C). Moreover, a better understanding of intraocular pressure has been enabled in the clinical field.



Figure 1-2 Contact tonometry. (A) Goldmann Applanation Tonometry; (B) Perkins Tonometry (a portable version of GAT); (C) Tono-Pen Tonometry, Avia

With the accelerated development in science and technology, there was a prerequisite that performing tonometry with any device was not permitted without a medical degree, as there was a need to apply topical anaesthesia. Under these restrictive conditions, the non-contact

applanation tonometry (NCT) was a timely invention by Dr Bernard Grolman, and this tonometry allowed optometrists to measure IOP without anaesthesia [10, 11]. The main characteristic of the NCT entails measuring IOP without direct contact. It applies an air puff that replaces the contact found in the applanation tonometry. Drawing a comparison with contact tonometry, the advantages and disadvantages of both methods are presented in Table 1-1. The non-contact applanation tonometry (NCT) is easier to use and does not require a higher skill level. Due to these strengths, non-medical staff can use it easily. When everything considered, it seems that NCT has a high potential in the future.

Table 1-1 Comparison of advantages and disadvantages between contact applanation tonometry and non-contact applanation tonometry

CLASSIFICATION	CONTACT APPLANATION TONOMETRY	NON-CONTACT APPLANATION TONOMETRY
ADVANTAGES	(I) Easy to use (II) Cheap (III) Comfortable (apart from anaesthetic) (IV) Quick process	(I) Quick process (II) No anaesthetic required (III) No clinical license required (IV) No contact with the cornea and low infection rate
DISADVANTAGES	(I) Need for anaesthetic (II) Need for a clinical license (III) Contact with cornea (slight chance of abrasion and high infection rate)	(I) Uncomfortable for some patients (II) Expensive to perform (III) Difficult to obtain a reading on scarred corneas

According to the World Health Organization’s (WHO) global data pertaining to blindness, over the last decade, Glaucoma has remained among the top 10 leading causes of visual impairment globally [14-16]. Worldwide, there are 67 million people affected with Glaucoma, and 10% of them are bilaterally blind [17, 18]. Owing to the rapidly ageing population, the population with Glaucoma will increase by more than 50% by 2020 [18, 19], and this will also cost over \$1.5 billion in medical expenses in the United States [17]. In addition, there are a

few reviews in previous publications pertaining to the risk to develop Glaucoma, including high and age advanced [7, 8, 16, 17, 19]. Comparing both IOP-related and age-related causes, IOP is reversible but age is not. In other words, it is possible for IOP management to be executed. Therefore, the current management strategies of Glaucoma are based on maintaining a normal IOP range, as it is the only proven method to slow the progression of Glaucomatous damage [20, 21]. Above all, measuring IOP through tonometry accurately is imperative.

The accuracy of IOP measurement using a contact applanation tonometer, such as the GAT, is potentially affected by several error sources, including variations in biomechanical parameters such as corneal stiffness, which is dominated by the central corneal thickness (CCT), corneal central anterior radius of curvature (R_c), hydration, ectasia, and age [5, 12]. Since 1957, the main error sources of GAT has been clearly indicated with regard to the variation of CCT [22]; the numerous studies related to it have been the most persuasive argument for the CCT effect [23-27]. In terms of the effect of corneal curvature, there is no significant evidence to demonstrate the correspondence of the changes in IOP and the variation in R_c ; It has been found that the IOP remains below 1.14 mmHg per 1 mm change in R_c [27, 28]. Further, the error sources of the contact applanation tonometry have been found to be correlated with the material properties of corneal tissue. The effect of material properties of corneal tissue on the GAT was found to be significant [25, 29, 30], but the current inability to perform corneal material properties measurement in vivo has limited the practical value of this finding [10]. However, besides age, it has also been found that corneal material properties are affected by disease (such as keratoconus), swelling [31, 32], ectasia [33], wound healing [34], and cross-linking processes [35-37].

Moreover, the technology of the NCT has evolved from the contact applanation tonometer. The NCT has substituted the air-puff pressure in place of the mechanical force to indent their cornea. Similar to the contact tonometer, the accuracy of IOP measurement by the NCT was affected by corneal stiffness parameters, and in particular corneal thickness, and mechanical properties [38-45]. Moreover, it indicated that no significant effect of R on IOP as it was in the contact applanation tonometer [46]. Conversely, the new NCT with image analysis, such as that of the Ocular Response Analyzer (ORA) or Ocular CorVis ST, provides more deformation parameters related to the biomechanical properties of the cornea [32]. Therefore, it means that the NCT has a higher potential to develop a method to consider the effect of the cornea's material properties in vivo.

Recently, OCULUS Optikgeräte, Inc. (Wetzlar, Germany) developed the CorVis-ST tonometry (CVS) as illustrated in Figure 1-3. It is easy to use and does not require a high skill level. Considering these strengths, non-medical staff can operate it easily. This device is characterised with high-speed Scheimpflug technology, which facilitates the measurement of IOP. The image captured by the CorVis-ST can record the deformation of the cornea during the air pressure application and use this information to define the relationship between the IOP and the air-puff pressure. The wealth of information on corneal deformation under IOP makes, the OCULUS CorVis-ST possibly the best option for the development of an accurate method for estimation of intraocular pressure and corneal material behaviour. However, this tonometer would be expected to suffer from the same error sources as other tonometry and research are needed to develop accurate estimations of IOP and corneal material behaviour. If successful, better IOP measurements can lead to better glaucoma management and in-vivo estimation of corneal material behaviour will benefit clinical applications, such as contact lens

design, refractive surgery planning, and selection of corneal implants.



Figure 1-3 CorVis-ST developed by OCULUS Optikgeräte, Inc. (Wetzlar, Germany)

Historically, corneal stiffness measurements were based on ex-vivo tensile testing. The tensile testing of corneal tissue has been accomplished by cutting strips of corneal tissue from a donor's eye and applying a tensile load while measuring the corresponding stretch of the tissue [37, 47-51]. Based on this relationship between the load and stretch, the stress-strain curve can be defined. The slope of the stress-strain curve is defined as the tangent modulus. When the material is stiffer, the slope is greater. This also can be interpreted as a stiffer material providing greater resistance to deformation than a soft material. However, the evaluation is more complex in a cornea due to its viscoelastic behaviour, in which the slope of the stress-strain relationship is a function of the strain rate or stress rate, such that higher levels of strain rate are associated with larger tangent modulus [52, 53]. Based on the principle of tensile testing, the challenge in transferring biomechanical property estimation to the in-vivo condition entails understanding of the relationship between IOP and corneal material stiffness in tonometry. While the corneal tangent modulus is the same, there are three

possible situations, that produce the same IOP measurements; low IOP with stiffer corneal tissue, high IOP with soft corneal tissue, and intermediate IOP with intermediate corneal tissue. In addition, IOP is a factor in the complex assessment of corneal biomechanics, since the corneal tangent modulus increases as IOP increases. As a result, these two factors of IOP and corneal stiffness are difficult to separate [54]. As mentioned above, the challenge faced during the estimation of IOP and corneal material behaviour lies in separating the effects between IOP and corneal material stiffness.

1.2 Scope of the Study

Advances in tonometer technology, clinical optics biomechanical, biochemical and computer engineering have enabled a better understanding of the eye and the process of vision. Building on this understanding, the main aim of this thesis is to develop a procedure that is suitable for the non-contact tonometer to achieve accurate estimations of IOP and corneal material behaviour.

The accuracy of IOP measurement is of great importance in glaucoma management. In the past, most research focused on the analysis of clinical data in the development of IOP correction algorithms. Unfortunately, this method has failed to consider all the error sources combined. To address this problem, numerical analysis using the finite element method (FEM) is used as it assesses the effect of different parameters, such as eye geometry and biomechanical properties in the development of IOP correction algorithms and estimating corneal material behaviour. These algorithms would then require validation using significant clinical data.

The Ocular CorVis-ST has been selected in this project due to the availability of corneal deformation information under the effect of air pressure. The purpose of more accurate estimation of the IOP and corneal material behaviour is to improve glaucoma management, which can decrease the probability of vision loss and improve clinical applications, such as contact lens design, refractive surgery planning and selection of corneal implants.

1.3 Aim and Objectives

The aim of this research is to develop algorithms for accurate estimations of IOP and corneal material behaviour (stress-strain relationship) using a non-contact method. This study will perform numerical analysis employing FEM and validation against clinical data to correct IOP measurements for reducing the effects of age (related to corneal stiffness) and CCT, and to estimate the corneal material behaviour in vivo.

This aim will be achieved through the following objectives:

- Develop an IOP procedure of the non-contact method for the estimation of intraocular pressure and corneal material behaviour;
- Develop a representative model of the eye's structure and the air puff produced by a non-contact instrument;
- Conduct a parametric study to relate actual IOP and the material stiffness to corneal deformation parameters and corneal IOP measurements;
- Develop an algorithm for IOP predications, with a reduced effect of corneal parameters and material stiffness;
- Develop an algorithm for in-vivo material behaviour estimation, with a reduced effect of IOP;

- Validation of both algorithms utilising clinical data obtained for healthy and keratoconus eyes, and those performed laser surgery;
- Validation of IOP algorithm through experimental testing of ex-vivo human eye globes;
- Validation of the material behaviour algorithm through applying an inverse analysis of corneal deformation data obtained in-vivo by the CorVis-ST device.

1.4 Thesis Structure

This thesis aims to provide a clear overview of the research programme, including its aim and objectives, methods, major results, and main conclusions. The thesis has been organised as follows:

- Chapter 1 introduces the background of this research, the scope of the study, and a brief outline of the aim and objectives of this study.
- Chapter 2 summarises previously conducted research pertaining to the human eye and its diseases such as glaucoma and keratoconus; the material behaviour of the eye; error sources in IOP measurement by CVS and the differences between CVS and GAT; and the material behaviour changes caused by clinical treatment.
- Chapter 3 outlines the research methodologies adopted in this study, including numerical simulation of the CVS procedure, a parametric study of CCT, material effect, and the validation using inflation tests and inverse analysis of in-vivo results.
- Chapter 4 presents the results of IOP and material behaviour algorithms for healthy and keratoconic eyes. The results are presented in the same logical order as in the methodology. The results of corrected IOP and material algorithms tested in clinical data and compared with uncorrected IOP readings of the CorVis-ST (CVS-IOP) and Goldmann

Applanation Tonometry (GAT). The validation using inflation tests and inverse analysis of in-vivo result is then presented.

- Chapter 5 provides an overall discussion of the study and its main conclusions, in addition to the limitations and several recommendations for future work.

Chapter Two

Literature Review

2.1 Introduction

The human eye is the window to the soul and is also one of the foremost means to retrieve the information from the world. It has been identified as one of the most complex organs in our body [55]. Therefore, with respect to medicine, the testing and treatment tools used for the eye must be accurate and of high quality.

There is a large volume of literature pertaining to eye structures and biomechanics (especially IOP and eye material properties), representation analysis of corneal topography under healthy and diseased conditions (especially KC), and study contact and non-contact tonometry. This body of previous research aimed to better understand the functionality of human eye components in addition to their structure and biomechanical properties, to improve disease management and treatments.

This chapter focuses on the eye's structures (including eye geometry and material properties) and intraocular pressure. Subsequently, studies related to the causes of Glaucoma and Keratoconus are reviewed and discussed. After establishing the background to tonometry, there is a brief review of the existing pool of knowledge on tonometry and its existing error sources effects. In the last part of this chapter, previous studies concerning eye material behaviour measurement are reviewed, with its achievements and limitations outlined.

2.2 Structure of the Eye

According to the brief induction of the importance of IOP in Chapter 1, understanding the various structures of an eye is helpful to improve our understanding of diseases such as glaucoma. This section summarises the main anatomical components of the human eye, its geometry, and material properties. Due to the methodology based on numerical methods, the geometry and material behaviour of the eye are important factors to be included in the base of the model.

2.2.1 Eye Geometry

The human eye has a highly complex system, however, in this research, the attention will be given to components relevant to the study. The eye comprises the cornea, limbus, and sclera (Figure 2-1).

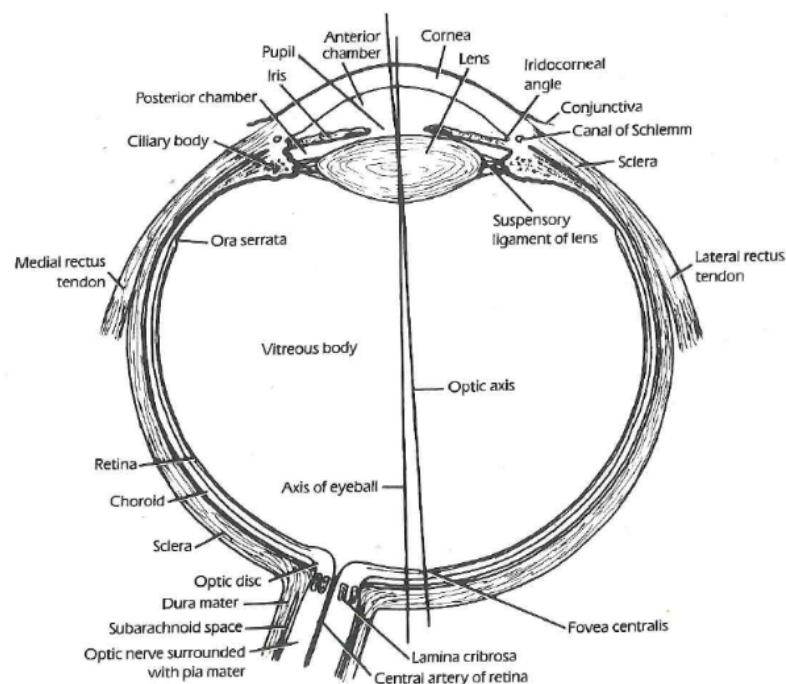


Figure 2-1 Horizontal section of the eye with optic nerve [3]

The sclera forms five-sixths of the eye at the posterior and is not a perfect sphere (Figure 2-1) [56-58]. The average thickness of the sclera in adults is approximately 1 mm thick at the posterior, thinning to 0.6 mm at the equator [56, 58], and the thickness of the thinnest part located immediately posterior to the tendinous insertions of the recti muscles is 0.3 mm [3]. At the corneoscleral junction, the sclera is 0.8 mm thick [56-58]. In other words, the thickness of the sclera in adults has been described to decrease from approximately 500–600 μm at the limbus to 400–500 μm at the equator and then increasing to 1000 μm near the optic nerve in the posterior region [56-58]. There are six muscles around the limbus linking the sclera, namely, the superior rectus muscle, medial rectus muscle, inferior rectus muscle, lateral rectus muscle, inferior oblique muscle and superior oblique muscle. The distance from the medial rectus muscle to the limbus is 5.5 mm; from the inferior rectus muscle, 6.5 mm; from the lateral rectus muscle, 6.9 mm; and from the superior rectus muscle, 7.7 mm (Figure 2-2) [3]

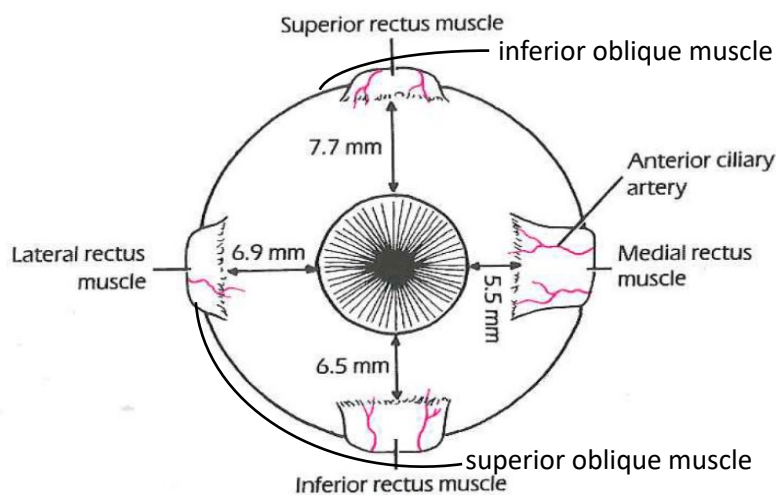


Figure 2-2 Schematic representation of eye showing rectus muscle locations [3]

The cornea forms the anterior one-sixth of the eye (Figure 2-2). The shape of the cornea from a front view is almost elliptical. The approximate measurements are 10.6 mm vertically and

11.7 mm horizontally, but the cornea is circular at the posterior, which measures approximately 11.7 mm in diameter. Moreover, the cornea is the thinnest at the centre measuring about 0.5–0.6 mm and thicker at the periphery, measuring nearly 0.7 mm [59]. The radii of curvature at the anterior and posterior surfaces of the cornea are approximately 7.7 mm and 6.9 mm respectively [3]. In conclusion, the radius of curvature of the cornea surface is changeable, but it should be highlighted that the curvature in the vertical plane is more than that in the horizontal plane in a healthy eye.

In general, the geometry of the eye is a combination of the corneal, limbal, and scleral geometry. The eye geometry includes anterior corneal central radius (R_c), anterior corneal shape factor (p , a measure of corneal asphericity), central corneal thickness (CCT), peripheral corneal thickness (PCT), limbal radius (RI), scleral radius (R_s), equatorial scleral thickness, the ratio of the equatorial scleral thickness, posterior scleral thickness, and the ratio of the posterior scleral thickness. According to the research presented above, the geometry of a healthy eye has been organised in Table 2-1.

Table 2-1 Details of eye parameters on the clinical measurement data

	<i>Clinical Data (Mean \pm SD)</i>
<i>Anterior Corneal Central Radius (R_c)</i>	7.79 \pm 0.27 mm [59-62]
<i>Anterior Corneal Shape Factor (p)</i>	0.82 \pm 0.18 [59, 61, 62]
<i>Central Corneal Thickness (CCT)</i>	0.55 \pm 0.036 mm [63-65]
<i>Limbal Radius (RI)</i>	5-6.5 mm [66-68]
<i>Scleral Radius (R_s)</i>	around 11-18 mm [66]
<i>Peripheral Corneal Thickness (PCT)</i>	CCT + 0.15 mm [63-65, 69]
<i>Equatorial Scleral Thickness</i>	0.53 \pm 0.14 mm [57, 58]
<i>Ratio of Equatorial Scleral Thickness</i>	0.8 [70]
<i>Posterior Scleral Thickness</i>	0.99 \pm 0.18 mm [57, 58]
<i>Ratio of Posterior Scleral Thickness</i>	1.2 [70]

2.3 Eye Tissue Biomechanics

Knowledge regarding the eye material behaviour is vital for predicting responses of eye globes to the effect of intraocular pressure, measurement of intraocular pressure, refractive surgery, and the action of extra-ocular muscles. According to the eye structure, the eye can be divided into three parts, namely the cornea, limbus, and sclera.

2.3.1 Corneal Material Behaviour

There are a number of research studies pertaining to the mechanical properties of the eye. Many scholars have begun studying the cornea, attempting to discover and characterise the mechanical properties of the cornea. Therefore, the biomechanics of the cornea are tested applying three methods, which are tension [37, 47-51], inflation [53, 71-73], and compression test [74, 75], to measure the relationship between displacement and loading. In the compression test, it has been found that cornea material behaviour can be considered as incompressible in ex-vivo and in-vivo test [76-78]. These three test methods are carried out in ex-vivo conditions. As a result, most clinical tests are based on these three measurement methods, and there will be certain limitations on their application. In addition, there is substantial clinical evidence, such as results from surgery to describe the cornea biomechanics [79-81]. A number of studies apply finite element models (FEM) for various corneal geometry and material properties to simulate clinical treatment conditions, such as IOP measurement and surgery. Based on the studies presented above, three different hypotheses have been posited regarding cornea material behaviour, which related to homogeneous linear elastic [82, 83], nonlinear hyper-elastic [71, 79, 84, 85], and nonhomogeneous membrane [86]. Through the tension and inflation test, it has been noted that the approximate realism of cornea

material behaviour is nonlinear hyper-elastic. In addition, the nonhomogeneous membrane material behaviour and viscoelasticity material behaviour both are difficult to measurement in the experimental test. So, these studies on corneal material behaviour are based on nonlinear hyper-elasticity in the tension and inflation test to apply in the FEM. This corneal material behaviour is more forced on the force loading than the force unloading process. Thus, this research assumed the corneal material behaviour to be a nonlinear hyper-elastic and the loading process during the measurement process is more serious in this research.

In this thesis, the characterisation of corneal material is based on Elsheikh's research, which considers the characterisation of age-related variation in corneal biomechanical properties using both uniaxial tensile test and inflation test [1]. Corneal material property has a significant correlation with age [1]. Regarding the cornea, a stress-strain relationship of the form for individuals above 30 years can take the form:

$$\sigma = (35 \times 10^{-9} \text{ age}^2 + 1.4 \times 10^{-6} \text{ age} + 1.03 \times 10^{-3}) \times [e^{(0.0013 \text{ age}^2 + 0.013 \text{ age} + 99) \varepsilon} - 1] \quad (2.1)[1]$$

where σ is the stress in MPa, ε is the strain, and the age here is presented in years.

According to Equation 2.1, the stress-strain relationship of the corneal material properties presents a nonlinear hyper-elastic behaviour in the uniaxial form (Figure 2-3). With an increase in age, corneal stiffness increases. This result clearly shows that the stiffening effect is associated with an increase in age (Figure 2-4).

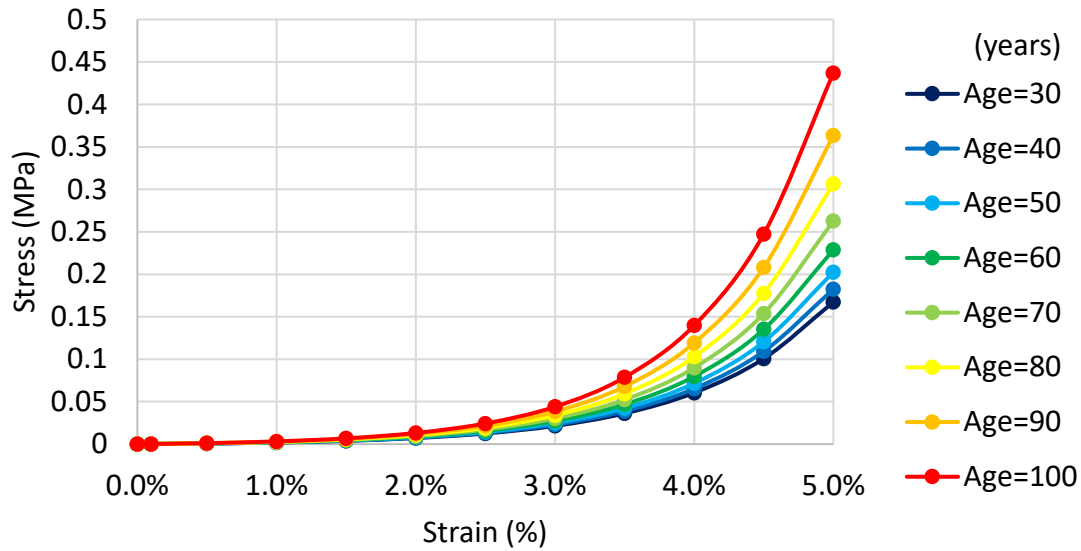


Figure 2-3 Stress–strain relationships of corneal material with different Ages [1]

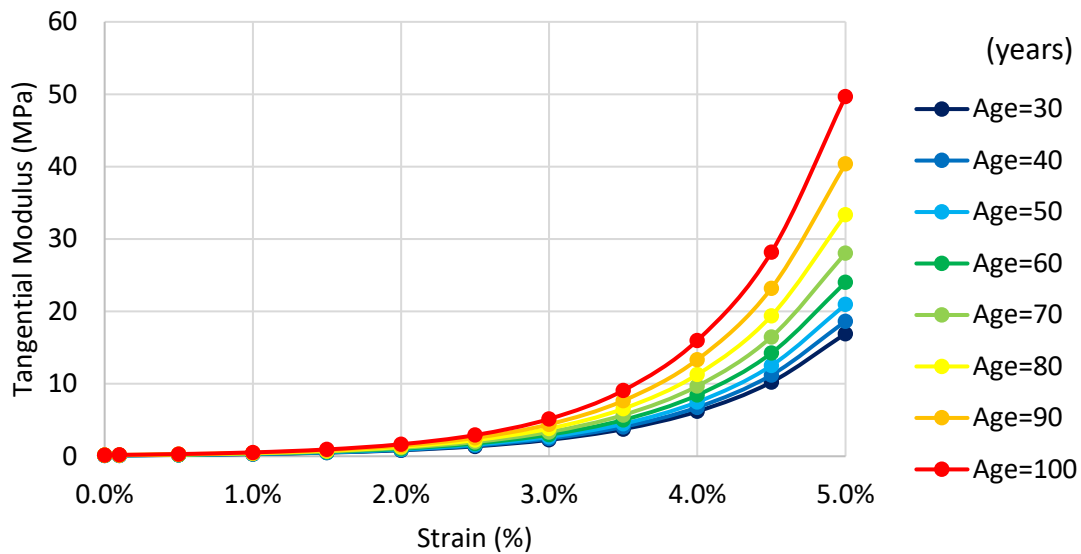


Figure 2-4Tangential modulus-strain relationships of corneal material with different Ages [1]

2.3.2 Sclera Material Behaviour

In the eye’s structure, the sclera is disproportionately larger than the cornea. The sclera is the tough, fibrous tissue that extends from the cornea to the optic nerve. It provides protection to the ocular components, resistance against the effects of intraocular pressure and external

trauma, and a connection with extraocular muscle insertions [87]. However, unlike the corneal structure, the sclera is opaque due to the irregularity of its collagen fibres [88].

For the prediction of ocular responses, the existing knowledge pertaining to the scleral material is indispensable and it is also important to numerical simulations. Numerical simulation of the globe is utilised to determine the distribution of stresses that are a result of loads and deformations. However, in the existing research on the eye's material properties, the major portion of the numerical simulation research has focused on the cornea [89-92] and the lamina cribrosa [93-96]. On the other hand, other studies have the scleral element incorporated into quantitative models developed for the eyes, but this was done assuming a uniform scleral thickness and homogenous material behaviour [84, 97]. In addition, the scleral material behaviour is characterised by changes and nonlinear hyper-elasticity in different locations, including the anterior, equatorial, and posterior region (Figure 2-5) [70]. The stiffness of the stress-strain material behaviour of the sclera decreases from the anterior to posterior. Moreover, the scleral material behaviour is also related to age level, similar to the corneal material behaviour [70].

According to these results, scleral material behaviour at the anterior region is considerably stiffer than the other regions; and scleral stiffness decreases from the anterior region to the posterior region. The number of scleral material properties considered in the numerical simulation concerns three regions: one is the region of contact with the cornea and sclera, namely, the limbus; the other two parts comprise the equatorial and posterior regions. Nevertheless, it is difficult to define the exact position of the limbus is more problematic from both a clinical and histological perspective. Hence, in the FEM, the limbal material property,

the anterior scleral material property, and posterior scleral material property were based on the experiment test in the anterior region, equatorial region and posterior region [70].

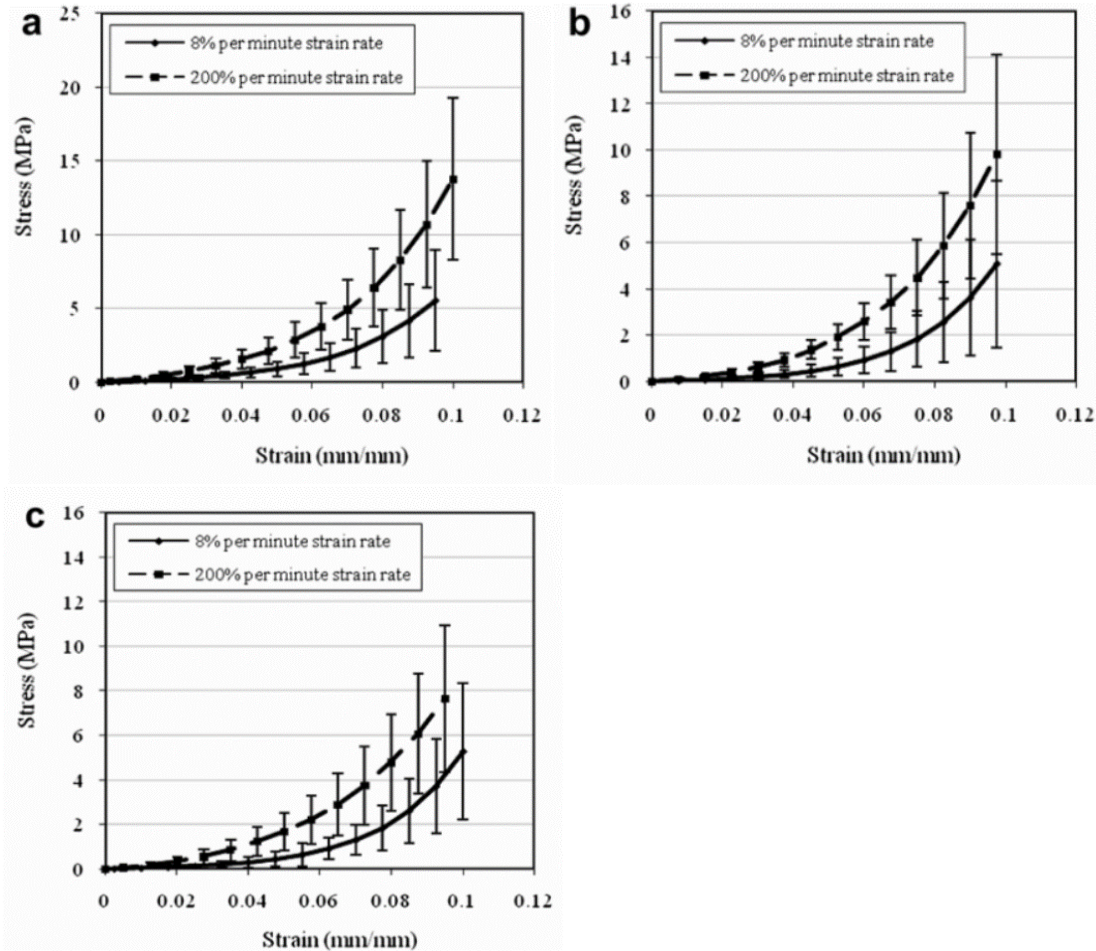


Figure 2-5 Strain rate effects on average stress-strain behaviour of scleral tissue in (a) anterior, (b) equatorial and (c) posterior region [70]

2.3.3 Ogden’s Form of Nonlinear Hyper-Elastic Material Behaviour

The Ogden material model is suitable for the hyper-elastic material and is used to describe the non-linear stress–strain behaviour of complex material behaviour as rubbers, and biological tissue. The non-linear material behaviour has several tangent moduli at the various strains (Figure 2-6 (A)). Thus, the tangent modulus can only present a characteristic stiffness

of stress–strain behaviour in one situation. There is also a limitation to tangent modulus, different non-linear material behaviours can have the same tangent modulus at the same strain or stress point (Figure 2-6 (B)). The pieces of evidence for these conditions show that the hyper-elastic material behaviour is not suitable to compare the stiffness using the tangent modulus. However, in terms of the comprehensive considerations of the characteristics of the hyperelastic material, the Ogden material model can better describe the complete material behaviour.

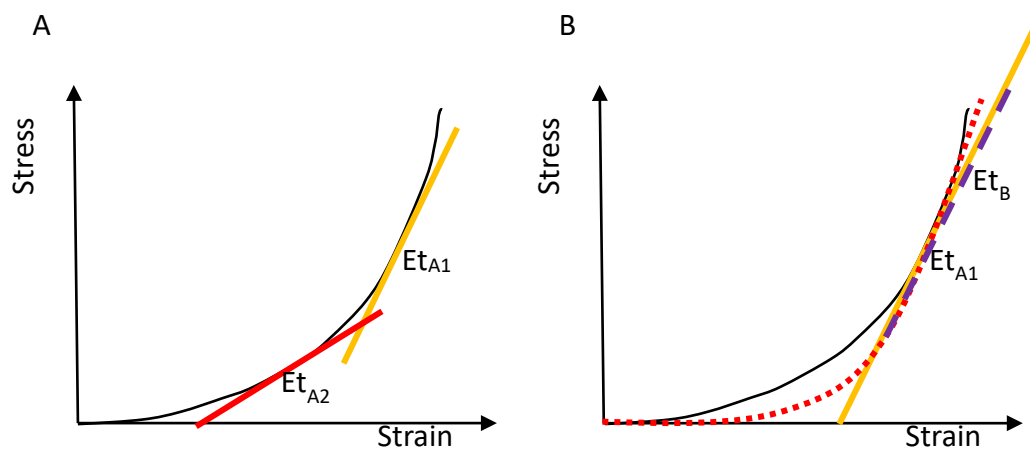


Figure 2-6 Tangent modulus of material with non-linear behaviour: (A) Tangent modulus varies with stress; (B) Tangent modulus is constant in one zone of linear behaviour at different non-linear material behaviours.

In sections 2.3.1 and 2.3.2, it has been outlined that the eye material behaviour is nonlinear hyper-elastic based on several ex-vivo tests, such as the tension test and the inflation test. Several studies pertaining to the eye's material is based on the Ogden material model to describe the eye's non-linear material behaviour [46, 91, 98, 99]. The Ogden material model assumes that material behaviour can be described by means of the strain energy density function, which has transpired from the stress-strain relationships [100].

The Ogden strain energy potential (U) is expressed in terms of the principal stretches (λ), which is similar to the strain (ϵ) but shows elongation (as provided in Equation 2.2). $\bar{\lambda}_1$ is the stretches along the X-direction, $\bar{\lambda}_2$ is the stretches along the Y-direction, and $\bar{\lambda}_3$ is the stretches along the Z-direction. The D_i values determine the compressibility of the material; if all D_i are set to zero, the material is considered fully incompressible.

$$U \stackrel{\text{def}}{=} \sum_{i=1}^N \frac{2\mu_i}{\alpha_i^2} (\bar{\lambda}_1^{\alpha_i} + \bar{\lambda}_2^{\alpha_i} + \bar{\lambda}_3^{\alpha_i} - 3) + \sum_{i=1}^N \frac{1}{D_i} (J_{el} - 1)^{2i} \quad (2.2)$$

Where U is the strain energy; $\bar{\lambda}_i$ are the deviatoric principal stretches $\bar{\lambda}_i = J^{-\frac{1}{3}}\lambda_i$
 $\rightarrow \bar{\lambda}_1\bar{\lambda}_2\bar{\lambda}_3 = 1$; λ_i are the principal stretches; $N (<6)$ is a material parameter; and μ_i , α_i , and D_i are temperature dependent material parameters.

Based on the hypothesis related to eye material behaviour and the uniaxial tension test, the Ogden strain energy's potential for the uniaxial tension can be derived from Equation 2.2 (Equation 2.3).

$$U \stackrel{\text{def}}{=} \sum_{i=1}^N \frac{2\mu_i}{\alpha_i^2} (\bar{\lambda}_1^{\alpha_i} + \bar{\lambda}_2^{\alpha_i} + \bar{\lambda}_3^{\alpha_i} - 3) \quad (2.3)$$

Where U is the strain energy; μ_i and α_i , are temperature dependent material parameters; $N (<6)$ is a material parameter, and $\bar{\lambda}_i$ are the deviatoric principal stretches.

Following the same approach as in the case of the polynomial Equation 2.3, the nominal stress-strain equation can be derived from the Ogden form. The stress-strain relationship can be described according to the nominal stress-strain algorithm (Equation 2.4).

$$\sigma = \sum_{i=1}^N \frac{2\mu_i}{\alpha_i} \left((1 + \varepsilon)^{\alpha_i - 1} - (1 + \varepsilon)^{-\frac{1}{2\alpha_i} - 1} \right) \quad (2.4)$$

Where σ is stress; ε is strain; μ_i and α_i , are temperature dependent material parameters; and N (<6) is a material parameter.

In this thesis, the eye's material behaviour in the FEM has been considered on the basis of previous findings, which is measured by means of an ex-vivo uniaxial tension test. Based on the result of the uniaxial tension, the stress-strain relationship can be described by the Ogden material model. In terms of eye's material behaviour, the eye's material in the FEM has been divided into four parts, which are the corneal, limbal, anterior scleral, and the posterior scleral regions. In order to conduct a parameter study of the Ogden material model, the considerations in this thesis are based on the Ogden form ($N = 3$), which has the regular ratio between the age and the Ogden material parameters μ_i and α_i .

2.4 Intraocular Pressure

Intraocular Pressure (IOP) is the fluid pressure within the eye. The pressure is provided by the continual renewal of fluids inside the eye. The normal IOP varies from person to person. The normal range of IOP for a person with healthy eyes is 10 to 25 mmHg [46, 101, 102], and this pressure can maintain the normal condition of the eye to present a healthy refractive optical effect.

IOP is maintained by the aqueous humour secreted by the ciliary body. This secretion will circulate in the eye and provide nutrients from the lens to the iris and the cornea. Thus, an understanding of the humour drainage systems is useful for a greater understanding of IOP.

Aqueous humour is produced by the ciliary body in the posterior chamber, following which the liquid flows into the anterior chamber. The drainage system is divided into two parts, one is for the majority of the aqueous humour, and the other is for the rest of the aqueous humour. Most aqueous humour is drained from the trabecular pathway through the trabecular meshwork and the Schlemm's canal. The remaining aqueous humour is drained through the uveoscleral pathway (Figure 2-7). Moreover, there is brief evidence in the soluble effect of aqueous humour, such as glutathione and ascorbic acid, which presents that the aqueous humour affects the ability of cells to respond and adapt to stress [103, 104].

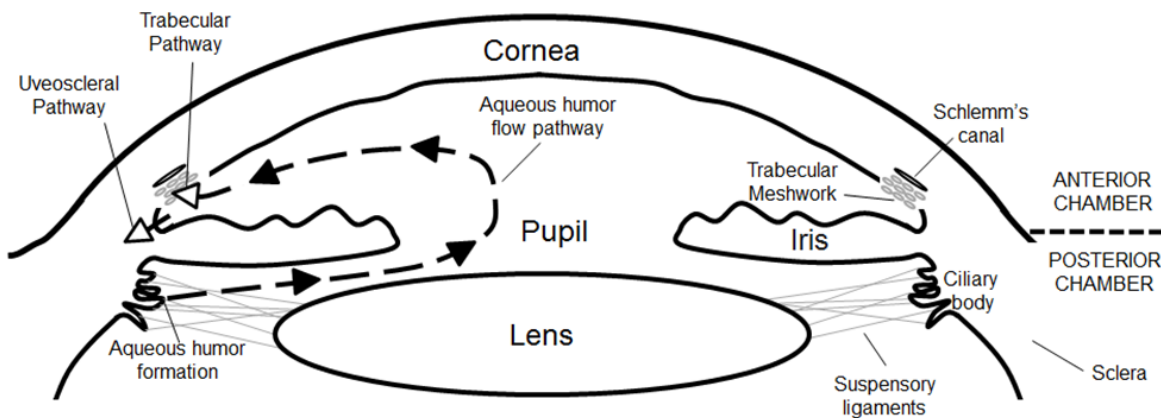


Figure 2-7 Schematic diagram of an aqueous humour flow pathway [105]

Furthermore, the volume of the aqueous humour in the chamber is constant due to the constant volume of the chamber. Under normal conditions, the production and metabolism of the aqueous humour will require a dynamic balance. When the flow in the canal is obstructed, the IOP will be anomalous. According to these conditions, there is a correlation between IOP, aqueous fluid formation rate, outflow rate, and episcleral venous pressure. An important quantitative relationship is provided by Equation 2.5 [106]. If the trabecular pathway and the uveoscleral pathway is compressed and blocked, it will lead to an increase in the IOP and may lead to retinal oppression, even Glaucoma.

$$\text{IOP} = \frac{\text{aqueous fluid formation rate}}{\text{outflow rate}} + \text{episcleral venous pressure} \quad (2.5)[107]$$

In aqueous humour, the diurnal variations will present the changing daily rates of occurrence, ranging from 3.0 $\mu\text{L}/\text{min}$ in the morning to 1.5 $\mu\text{L}/\text{min}$ at night [105]. In addition, the difference in the systolic and diastolic blood pressures create a circadian fluctuation in the IOP corresponding with the heart rate [108, 109]. On the other hand, it should be noted that the nocturnal IOP is higher than the diurnal IOP in individuals with healthy eyes [110, 111] and the variations of 24-hour IOP in the right and left eyes are similar [104, 110, 111]. According to the similarity in the eye structures of a person, differences between the right and the left eyes are less than 4 mmHg [112]. Therefore, the value of IOP undergoes a minuscule variation in a day, but it always remains in the normal range [110, 111].

In conclusion, IOP measurement is important for ensuring the eye's health. The IOP cannot be directly determined through normal check-ups, and tonometry is required for its measurement. Thus, the factors for normal IOP measurement are related to age, sex, disease such as diabetes, and geographical locations, but the correlation between the various factors for IOP measurement have not gained consensus in the literature [16, 113-118]. However, it has been agreed that the accurate estimation of IOP is important for IOP management in clinical settings.

2.5 Keratoconus

Keratoconus is the most common primary ectatic disorder of the cornea [119], which was first described in detail in 1854 [120]. The prevalence of this corneal disorder in the general population is approximately 54 per hundred thousand [121]. The early stages of this disorder

are normally ignored as well, but its impact is massive. In general, while the disease continues to progress, the risk of visual impairment increases. The reason behind this visual impairment is the thinning of the cornea. Keratoconus is a bilateral [122, 123] and asymmetric [124, 125] corneal degeneration characterised by the local thinned area, which leads to protrusion of the thinned part. Usually the thinning occurs in the central and inferotemporal cornea [126], but it has also been discovered in the superior localisations [127, 128]. Moreover, this protrusion of thin cornea leads to irregularities in the surface, which causes high myopia and irregular astigmatism and affects the quality of the vision. Due to the irregular corneal surface, Keratoconus can be detected utilising the corneal topography detection technology. Therefore, as the widespread application of corneal topography leads to improved diagnoses, the diagnostic accuracy rates of Keratoconus increase further [119].

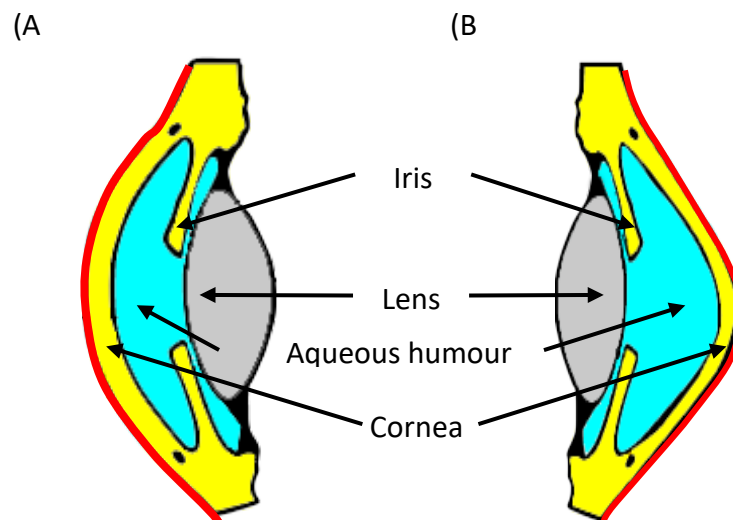


Figure 2-8 Comparison of corneal shape between (A) healthy and (B) Keratoconic eyes

Although the knowledge related to Keratoconus is limited, there is certain evidence regarding the prevalence as per genders and ethnicities and the incidence based on age. In terms of the prevalence in genders, it is unclear whether significant differences exist between males and

females. There are some evidential studies that found no differences in the prevalence among the genders [122, 129, 130]; others revealed a greater presence in females [121]; additionally, there were others that found a greater prevalence in males [131-133]. As per ethnicities, there is a prevalence of this disease by 4:1 and 4.4:1 in the Midlands area of the United Kingdom and in Asia respectively [134]. In another study conducted in Yorkshire, United Kingdom, there is evidence supporting the incidence, which was 7.5 times higher in Asians. Thus, the prevalence of Keratoconus in Asians is higher, and the reason has been attributed to consanguineous relations, especially first-cousin marriages [135]. In addition to the age incidence, this disease has been normally found to develop both at an early [136] and a late [137] stage in life. While it usually stabilises, this disease progresses until the fourth decade from the time of contraction [137]. According to a recent study, it has been observed that 50% of the non-affected eyes of patients with unilateral Keratoconus will gradually develop Keratoconus in 16 years from the time the symptoms of the disease in the affected eye have been found [129, 138]. Moreover, the incidence rates of this disease will increase in the future [119].

The symptoms and signs of Keratoconus vary depending on the severity of the disease. According to morphology, disease evolution, ocular signs, and index-based systems, Keratoconus has been classified into four stages (Table 2-2) [119, 139, 140]. During the incipient stages, such as frustre or subclinical forms (FFKC), no symptoms are observed in the cornea, and the said cornea is thereafter diagnosed [119]. Statistically, there are significant differences in the comparison of corneal topography with regard to anterior and posterior elevation, minimal corneal thickness, and anterior chamber depth parameters between normal, clinical, and subclinical Keratoconus [141]. The corneal curvature reading is commonly

within the normal range at this stage, but the surface may appear to be irregular. As disease conditions begin to deteriorate, the cornea becomes thinner [119, 139, 140], which is a sign of ectasia. The thinnest part of the cornea normally lies outside the visual axis [142-144]. Moreover, according to morphology research, Keratoconus occurs in two locations, which are the central/paracentral cornea and the inferotemporal corneal quadrant wherein the diameter from the central cornea is more than 5 mm and is located through 75% of the cornea [137, 145, 146]. Due to the advances in the corneal mapping technology, there is a new Keratoconus pattern found in the affected area at the superior, nasal, and central cornea [147]. In other words, Keratoconus is a disease that affects a number of locations in the cornea.

Table 2-2 Keratoconus classification based on disease progression [139, 140, 148]

STAGE	DESCRIPTION
1	<ul style="list-style-type: none"> • Frustre or subclinical form • No ocular signs • ~ 6/6 visual acuity (0.00 dioptries)
2	<ul style="list-style-type: none"> • Early form • Mild corneal thinning • Corneal scarring absent
3	<ul style="list-style-type: none"> • Moderate form • corneal scarring and opacities absent • Vogt’s striae; Fleischer’s ring • < 6/6 visual acuity with spectacle correction (irregular astigmatism between 2.00–8.00 dioptries) • Significant corneal thinning
4	<ul style="list-style-type: none"> • Severe form • Corneal steepening > 55 dioptries • Corneal scarring • < 6/7.5 visual acuity with contact lens correction • Severe corneal thinning and Munson’s sign

2.5.1 Image Technology for Keratoconus Detection

The detection of Keratoconus is also difficult at early stages, the disease detection has increasingly become important, particularly, for preventing iatrogenic ectasia formation [149-151]. Therefore, the detection of corneal shape loss is key to diagnosing Keratoconus. According to the research pertaining to the loss of corneal shape, there are several classification methods based on corneal topography systems to grade the severity of Keratoconus [152-159]. Rabinowitz and Mc Donnell developed the K value, as the central keratometry, and the I-S value, as the inferior-superior asymmetry, in order to measure the severity of Keratoconus [158]. As per other research, there are two index-based systems for Keratoconus detection, which are KPI and KCI percentage [157]. The KCI system is derived from eight quantitative videokeratography indices, and the other is based on KPI and an additional four indices. With the development of Artificial Intelligence, a system based on it was developed for the detection of Keratoconus and its level of severity [155, 156].

As the image technology advances increase, the diagnosis of Keratoconus is based on videokeratographic height data [154]. In addition, as a result of the above-mentioned studies, a diagnostic method has been developed by comparing the parameters comprising the K value, I-S value, Keratometric astigmatism, and relative skewing of the steepest radial axes [153]. According to the corneal topography, by utilising the slit-lamp, the index-based system is developed through corneal topography, corneal power, and higher-order first corneal surface wavefront root mean square error [152]. Besides, there is a diagnosis based on the detection of the presence or absence of Keratoconus patterns and determination of the location and magnitude of the curvature of the cornea [159]. However, the above-mentioned index-based systems for Keratoconus are based on corneal topography.

Furthermore, the assessment of corneal thickness [159] and the difference in corneal aberration [160] between normal and diseased subjects in Keratoconus detection can be performed through optical coherence tomography and corneal aberrometer instruments. Recently, there have been two types of optical instruments for the analysis of different characteristics of the anterior part of the eye, including the detection and monitoring of the corneal geometry using the Pentacam (Oculus, Wetzlar, Germany, Figure 2-10) [161].



Figure 2-9 Pentacam has a rotating Scheimpflug camera system for anterior segment analysis

The Pentacam is an instrument that is based on a rotating Scheimpflug camera system for an anterior segment analysis by capturing 12–50 images of cornea from different camera angles (Figure 2-11). Several parameters of corneal geometry, such as topography and elevation of the anterior and posterior corneal surface and the corneal thickness, are measured performing the image analysis. The basic built-in software includes Overview display, Fast

Screening Report, 1 Large Map, 4 Maps Refractive, Scheimpflug Image Overview, Virtual Eye, Tomography, Iris Image, Topometric, and Comparison displays (as illustrated in Figure 2-11).

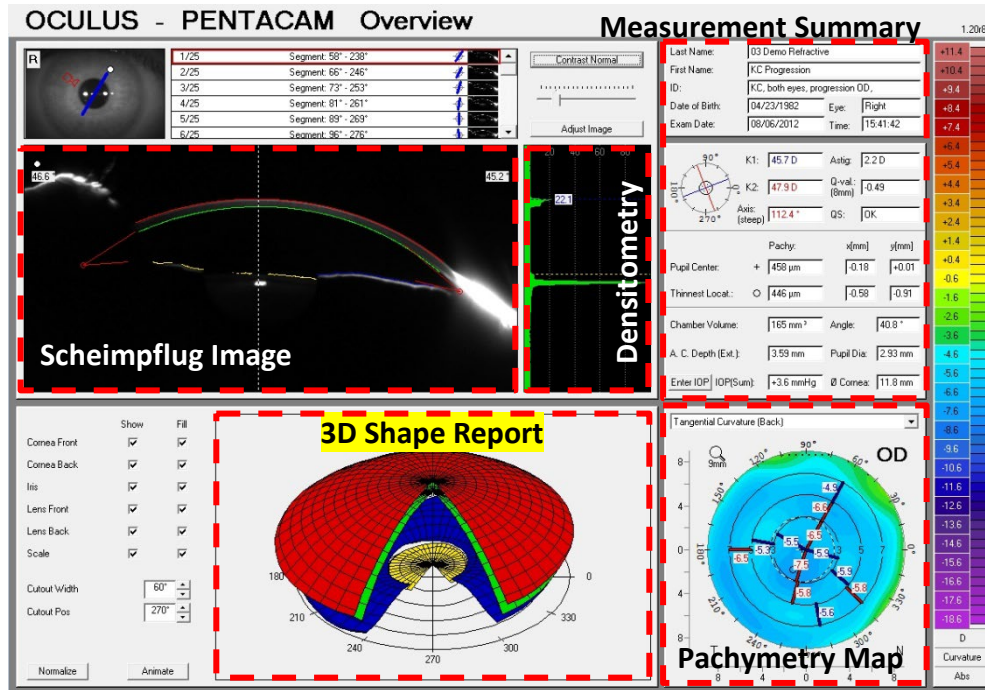


Figure 2-10 Pentacam’s Built-in Software Overview Report. Scheimpflug image pane displays cross-sectional image, including the cornea, anterior chamber, iris and lens. Densitometry pane shows the clarity estimation of measurement. 3D corneal shape report pane provides a 3D representation of corneal shape, with the anterior corneal surface in red, posterior corneal surface in green, and iris in blue. Pachymetry map pane shows the pachymetry map in colour, which represents corneal thickness by colour and a numerical scale on the right.

According to these corneal data, the method of evaluating disease severity is based on the changes in the corneal volume and anterior chamber angle, depth, and volume. This device has been found to be useful in identifying normal and Keratoconic cornea; however, in terms of the subclinical forms of Keratoconus, the sensitivity in detection has been found to be relatively lower [162]. Moreover, the difference between normal and Keratoconus eyes can be observed in the anterior axial map created using the Pentacam device [163]. The 4 Maps

Refractive, Scheimpflug Image Overview is employed to compare the anterior curvature map, presented in Figure 2-12. By performing the anterior curvature map analysis, several types of the steep part of the curvature, such as the bowtie shape, hat shape, or irregular shape, can be seen as illustrated in Figure 2-13. Normally, Keratoconus corneal topography progresses from symmetric astigmatism to asymmetric astigmatism, followed by the asymmetric astigmatism pattern presenting a skewed radial axis. With progressive Keratoconus, inferior steepening can develop in the end [163].

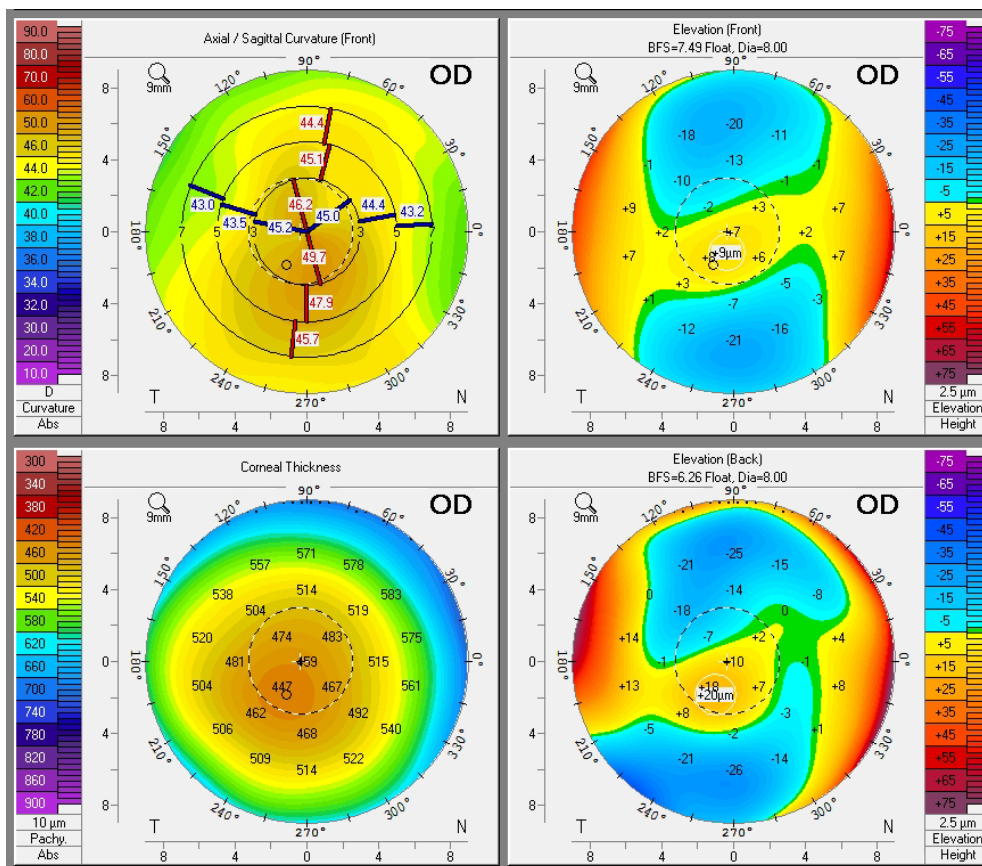


Figure 2-11 Pentacam Map Report. The colour map uses cooler colours for higher value and warmer colours for lower value

Additionally, there is a research on the aberrations of the posterior corneal surface, which is also related to Keratoconus [164]. In this research, the posterior corneal surface has more

aberrations than the anterior surface in subjects with Keratoconus. However, according to the image analysis done using the Pentacam device, it is crucial to determine the structure and function of the cornea and anterior segment for Keratoconus diagnosing.

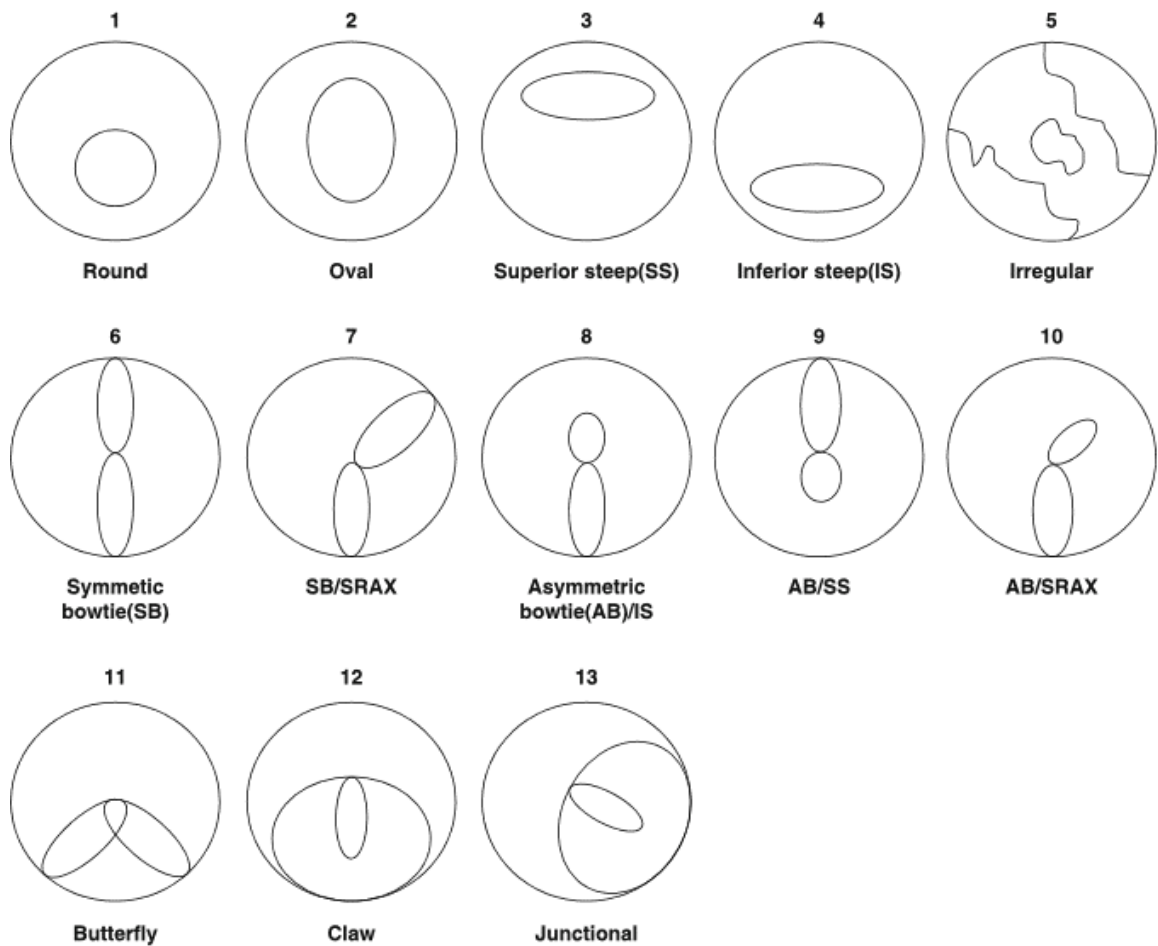


Figure 2-12 Patterns of anterior curvature map. The steep part of curvature map may form a bowtie shape, a hat shape, or an irregular shape [163]

2.5.2 Histopathology and Biomechanical Factors

According to the aberrations of cornea geometry in Keratoconus patients, the causes of abnormal corneal geometry can be explained through histopathology. There are three signs that typically characterise Keratoconus; they are stromal corneal thinning, Bowman’s layer

breakage, and iron deposits on the corneal epithelium's basal layer [121, 137]. In the Keratoconus disease, the corneal epithelium's basal cells degenerate, and subsequently, it advances towards Bowman's layer, which can be observed from the ferritin particles entering into and remaining between the epithelial cells [165]. Due to the difference between the Keratoconic and the normal cornea, the density of the basal cells also decreases in the Keratoconic cornea [166]. Bowman's layer presents breakages, and these breakages are filled with collagen from the stroma and positive nodules of Schiff's periodic acid. Consequently, there is a separation of collagen bundles in the form of Z-shaped interruptions [167]. The observation included a decrease in the number of lamellae and keratocytes, a degradation in fibroblasts, a change in the gross organisations of the lamellae, and an inhomogeneous distribution of collagen fibrillar mass and inter- and intra-lamellae in the stroma, especially around the apex of the cornea [36, 167]. Under confocal microscopy, the research has been conducted comparing the number of keratocytes between normal subjects and Keratoconic ones, which demonstrated that with a greater reduction in the number of keratocytes, the disease advances further [168]. Normally, Descemet's membrane is unaffected, excepting the breakages of this tissue; and the endothelium is also unaffected by this disease [169]. In addition, a study has demonstrated that there are thicker fibre bundles, a reduced density, and greater subepithelial plexus of corneal nerves in Keratoconus [170]. The causes of the reduction in corneal rigidity and thinning relate to the varied distribution and lower number of stromal lamellae in Keratoconus [36, 167]. However, it also has been noticed that these causes lead to the development of Keratoconus [171].

Furthermore, this histopathology is related to the connective tissue abnormality, which results in the weakening of the collagen structure. These characteristic clinical signs of Keratoconus,

including corneal topographic distortion, are an affirmation of the change in corneal biomechanical properties [121, 172]. A study by Andreassen, Simonsen, and Oxland demonstrated a statistically significantly lower Young's modulus in Keratoconus than a normal cornea [37]. In addition, there also is a difference between normal and Keratoconic cornea at high levels of stress; however, under normal physiological stresses, there is no considerable difference [33]. Due to the corneal material behaviour being non-linear, the values of Young's modulus cannot consistently be compared among studies [173]. However, Young's modulus has been demonstrated to be reduced in Keratoconus [33, 37]. In terms of the determination of corneal material behaviour through in-vivo testing, there is research pertaining to the biomechanical estimation of the cornea in Keratoconus through the development of empirically-derived ocular rigidity coefficients in 1937 [174]. According to these coefficients, the research presented no considerable variation of ocular rigidity in Keratoconic and healthy eyes [175]. On the contrary, other research has demonstrated that there is a significant difference in the ocular rigidity and the steady state elasticity among these two groups [176]. In conclusion, there is a limitation of corneal material estimation in Keratoconus through both ex-vivo and in-vivo tests, and it also poses a clinical challenge for assessing corneal biomechanical properties in vivo.

2.6 Glaucoma

Glaucoma has been identified as a leading cause of irreversible vision loss worldwide because it is asymptomatic until a significantly late stage; hence, the diagnosis is frequently delayed [177]. Glaucoma affects more than 70 million people with nearly 10% of them being bilaterally blind [178]. In the early stages, Glaucoma can remain asymptomatic, only presenting

symptoms when it becomes severe [177]. Consequently, the number of individuals affected is actually higher than the determined number [179, 180]. Over 8.4 million people were bilaterally blind as a result of primary Glaucoma as of 2010, and this has been estimated to rise by at least 3 million people by 2020 [178]. Further, Glaucoma is expected to remain one of the major eyesight-related diseases in the future.

To understand the causes of Glaucoma, first, the path through which the intraocular fluid flows must be understood. Based on the structure of an eye, the flow of intraocular fluid has been defined in chapter 2.4. The clear fluid, namely aqueous humour, is produced by the ciliary body inside the eye. The aqueous humour exits the eye through the drainage angle, which is the angle located in the anterior chamber between the iris and the peripheral cornea. Based on this path rule, any disruption in this outflow of aqueous humour results in an increased IOP. Moreover, there are longitudinal studies that had been conducted by Armaly [181] and Perkins [182] on the long-term IOP effect, showing that a small percentage of individuals with high pressure developed Glaucoma over at least a 7- to 10-year period. Strictly speaking, Glaucoma is primarily an optic neuropathy, not an intraocular pressure abnormality. Therefore, the common traits of Glaucoma include high eye pressure, damage to the optic nerve, and vision loss. Most Glaucoma cases involve elevated eye pressure, which is known as high-tension Glaucoma. However, there is an exception to Glaucoma, in which the IOP remains within the normal range, and it is known as low-tension or normal tension Glaucoma. There are no physically distinguishable characteristics of normal/low-tension and high-tension Glaucoma [183], but the former has a higher incidence of splinter haemorrhages on the optic disc than high-tension Glaucoma [184, 185]. Although it presents a higher incidence of splinter haemorrhages, the visual field loss has been discovered to be the same in normal/low-tension

and high-tension Glaucoma [183].

In general, Glaucoma has traditionally been a type of optic nerve disease, which usually follows an abnormal IOP [183]. The pathophysiology of Glaucoma has not been clearly understood until now. However, the cause of Glaucoma has been established to be a disruption in the output channel in the maintenance of an appropriate balance between the amounts of internal fluid. The balance between the input and output aqueous humour is crucial for maintaining the normal functioning of the eye. In terms of the eye's structure, there are only two independent pathways – the trabecular meshwork and the uveoscleral outflow – through which the metabolism of aqueous humour takes place, thus determining the IOP [177]. There are two types of Glaucoma patients. One kind is characterised by resistance to the aqueous outflow through the trabecular meshwork is increased (Figure 2-8(A)). This kind of Glaucoma patients is known to have open-angle Glaucoma. On the other hand, the second one is that wherein access to the drainage pathways is obstructed, namely, angle-closure Glaucoma (Figure 2-8 (B)). Due to the increased resistance of the trabecular meshwork and disruption in the drainage pathways, IOP will increase beyond the normal range. With an elevation in IOP, the lamina cribrosa was extruded to protrude out posteriorly displaced and thinner [186]. Moreover, these pathways are highly associated with the retinal ganglion cell, and the level of IOP is correlated to the death of these cells [187]. When Glaucoma progresses, the high level of IOP will injure neurons, ultimately leading to ocular damage in the form of peripheral vision loss. Therefore, maintaining IOP within the normal range will slow down and even avoid the functional impairment caused by Glaucoma [177]. However, the management of IOP is crucial for achieving this.

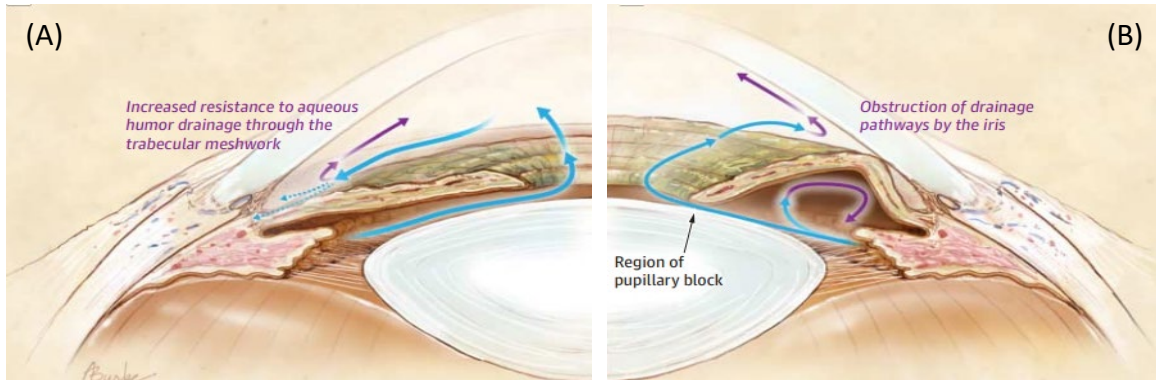


Figure 2-13 Aqueous humour drainage pathways in Glaucomatous eyes. (A) Primary open-angle Glaucoma: increased resistance makes it difficult for aqueous humour to pass through the trabecular meshwork. (B) Primary closed-angle Glaucoma: access to the drainage pathway is typically obstructed. [177]

2.7 Categories of Tonometry

The value of IOP is required, as it is the main quantifiable risk factor and a secondary diagnosis tool for Glaucoma. Theoretically, the actual IOP can be measured directly by a manometer. A catheter is fixed in the manometer for the corneal incision to measure the pressure inside. However, it is not allowed to be used in the clinical models, even if the pressure is measured with higher precision. Therefore, the clinical requirements affected the invention of the tonometry.

At present, most tonometers apply a force contact on the eye and record the resistance of the eye to deformation in order to estimate the IOP. Tonometry is performed using either the applanation or indentation tonometer. The applanation tonometer adopts different methods to flatten the cornea and subsequently relates this force to the IOP. The principle of indentation tonometry follows that a force or a weight will indent or sink into the soft eye further than into the hard eye. In this study, type of tonometer only focused on the applanation tonometer.

2.7.1 The Principle of Applanation Tonometry

The principle of applanation tonometer is based on the Imbert–Fick law [188]. The law states that the pressure inside a sphere that is filled with liquid and surrounded by a thin membrane is measured by an additional pressure flattening the membrane. This law is similar to Newton’s third law of motion: ‘If you press a stone eye with your finger, the finger is also pressed by the stone eye [189]. The relationship between the pressure inside the sphere and the counter-pressure has been presented through Equation 2.6.

$$P = \frac{W}{A} \quad (2.6)$$

where P = the pressure inside the sphere in MPa, W = backpressure flattening of the membrane in MPa, A = area of contact in cm^2 .

According to the Imbert–Fick law, it is only suitable for a dried sphere surface, a thinner wall of the body that are highly flexible, but these conditions are not present in the eye [190]. However, most principles of the applanation tonometer originate from the Imbert–Fick law. With regard to the contact, applanation tonometry is classified as either contact tonometry or non-contact tonometry. In terms of contact tonometry, Goldmann Applanation Tonometry (GAT) is the gold standard IOP test and is the most widely accepted contact method. In this research, the CorVis-ST was chosen to represent NCT.

2.7.2 Goldmann Applanation Tonometry

GAT is considered the gold standard for the measurement of IOP. The principle of the GAT also emerges from the Imbert–Fick law (Figure 2-14). However, there are some modifications

required in the pressure transducer to overcome the limitation of the Imbert-Fick law and adapt to the conditions existing in the eye [191]. In order to consider the true conditions of the cornea, the Imbert–Fick principle is modified in the form presented in Equation 2.7. Several studies [10, 24] have revealed that the effects of surface tension counterbalance bending resistance when the applanation diameter is 3.06mm; hence, the applanation area is 7.35mm². Under these conditions, the form of Equation 2.7 can be reduced to the simple form of Equation 2.6.

$$W + S = P \times A + b \quad (2.7)$$

where P = the pressure inside the sphere, W = backpressure flattening of the membrane, A = the area of the applanation of the central cornea, S = the surface tension forces caused by the tear film, and b = the surface tension forces caused by tear film and bending.

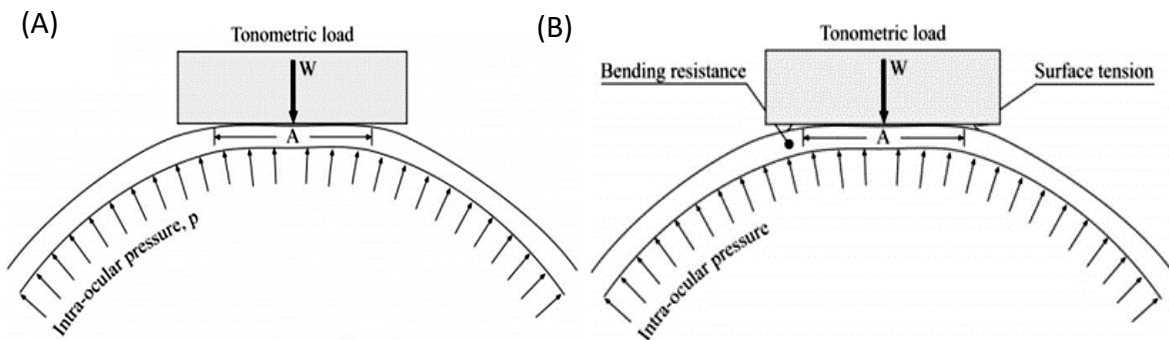


Figure 2-14 Comparison between principles of (A) Imbert–Fick law and (B) Goldmann Applanation Tonometer [10]

The GAT uses a head that is positioned against the cornea. A special disinfected truncated cone is mounted on the head of the tonometer. The force of this head against the central cornea is increased gradually until applanation is achieved. At this moment, the applanation pressure can be noted from the pressure application mechanism. Subsequently, this value is recorded and considered equal to the IOP. However, despite the GAT being the gold standard

of tonometry, the curvature and the thickness on the cornea still affect the value determined by the GAT [192].

2.7.3 Non-Contact Tonometry

In the 1970s, there was a prerequisite that performing tonometry with any device without a medical degree was not permitted, as it involved the application of topical anaesthesia [193]. Under these restrictive conditions, the NCT was a timely invention by Dr Bernard Grolman, and this tonometer allowed optometrists to measure IOP without anaesthesia [194]. The main characteristic of NCT entails measuring IOP without direct contact. It mostly uses an air puff to replace the contact head on the applanation tonometer. The advantages of NCT include easy operation, fast measurements, and the avoidance of contagious diseases and allergies.

The theory behind NCT involves using the air puff to have an impact on the cornea [192]. Subsequently, the pressure of the air puff increases with time, and the corneal behaviour is recorded during this period. When the cornea is flattened or even slightly depressed, the air puff's pressure decreases until the cornea recovers; thus, the NCT can utilise the light reflection to calculate the applanation time and pressure at the given moment. The proportional relationship between the applanation times, pressure, and IOP can be considered to measure IOP. However, this form of NCT is vulnerable and affected by uneven cornea, high astigmatism, corneal oedema, and abnormal thickness. Under these conditions, the form of Equation 2.8 can be reduced to the sample form of Equation 2.7.

$$W = P \times A + b \quad (2.8)$$

where P = the pressure inside the sphere, W = backpressure flattening of the membrane, A =

the area of the appplanation of the central cornea, and b = the surface tension force caused by tear film and bending

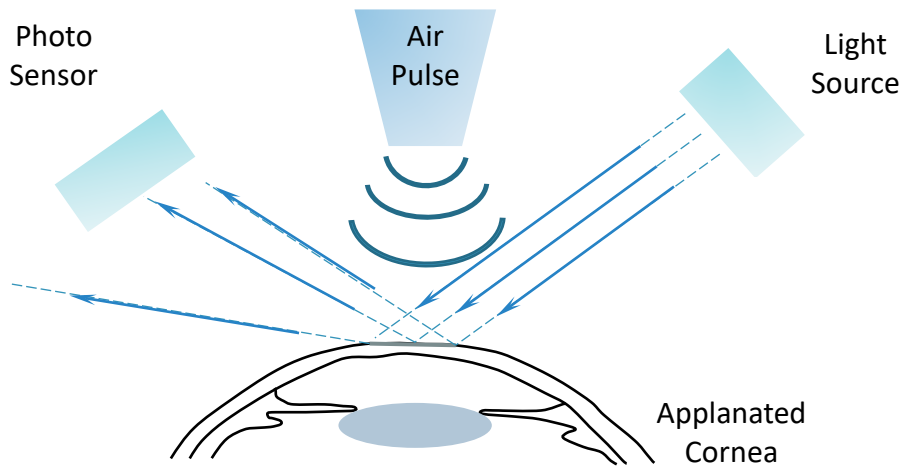


Figure 2-15 Principles of non-contact tonometry (NCT) [192]

According to the principle of the NCT (Figure 2-15), applanation was identified when the maximum reflected light reached the photo sensor as the corneal configuration was mirror-like as approximately flat. Moreover, the original design of NCT employed a constant force - linear air-pulse to applanate the cornea with an IOP.

Due to International Standard Organization's (ISO) requirements for tonometers (ISO-8612, 2001), the gold standard for IOP measurement is the Goldmann Applanation Tonometry (GAT) [13]. There is a device's internal calibration - Goldmann-like values which were used to correct the difference of IOP value between NCT and GAT [195].

In 1989, the Reichert Xpert NCT (Figure 2-16) is the first non-contact tonometer for IOP measurement by using an internal pressure transducer to measure the air-puff pressure in real time to estimate the IOP [195]. This advancement of the pressure transducer resulted in high accuracy since the minimum necessary air-puff pressure to applanate any cornea was

applied. In 2000, David Luce developed an advanced process which can extract information about corneal biomechanics from NCT measurement signal [196]. Based on this process, in 2005 the Ocular Response Analyzer(ORA) had been developed [197]. With the advances in imaging technology, the Scheimpflug technology, which has a high temporal and spatial resolution and a higher depth of focus compared to conventional slit-imaging techniques used on the NCT, had been developed. In addition, this Scheimpflug imaging can provide clinically relevant information for clinical diagnosis and is also commonly used in clinical practice.

Subsequent years of research and development resulted in the launch of what became known as the Corvis® ST, which is the first non-contact tonometer by using high-speed imaging combined with an air pulse. Regardless of how the non-contact tonometer improves, the fundamental purpose of this device remained the same ideal is to provide an IOP measurement correlated to GAT that was fast, easy, and non-contact. But, due to the indentation of the cornea by an air-puff causing a dynamic time-dependent response, ORA and CorVis device can provide extra information about corneal biomechanics.



Figure 2-16 XPERT™ NCT™ PLUS Advanced Logic Tonometer by Reichert Ophthalmic Instruments

The Ocular Response Analyzer(ORA) was the world's first device which can provide an estimation of corneal biomechanical parameters (Figure 2-17) [195, 197]. The ORA features an automated three-dimensional positioning system to detect the apex of the corneal. Once aligned, the air pulse shoots on the corneal apex for 30 ms. This 30 ms air pulse has been measured both temporally and spatially and demonstrates a Gaussian profile in the ex-vivo experiment test [195, 198]. Nevertheless, the profile of the air pressure pulse for the real eye is not symmetrical and not well fitted by a Gaussian profile, which may be explained by viscoelasticity of air [199]. However, differences in air pressure pulses for the real eye can indicate the dynamics of ocular properties during measurements [199].



Figure 2-17 Ocular Response Analyzer® G3

During the measurement process, the amplitude of the air pulse pressure at the corneal apex change over time in Figure 2-18. Moreover, the corneal movement in response to increased and decreased pressure amplitude. During the course of the measurement, the cornea deforms inward while air pulse pressure increases.

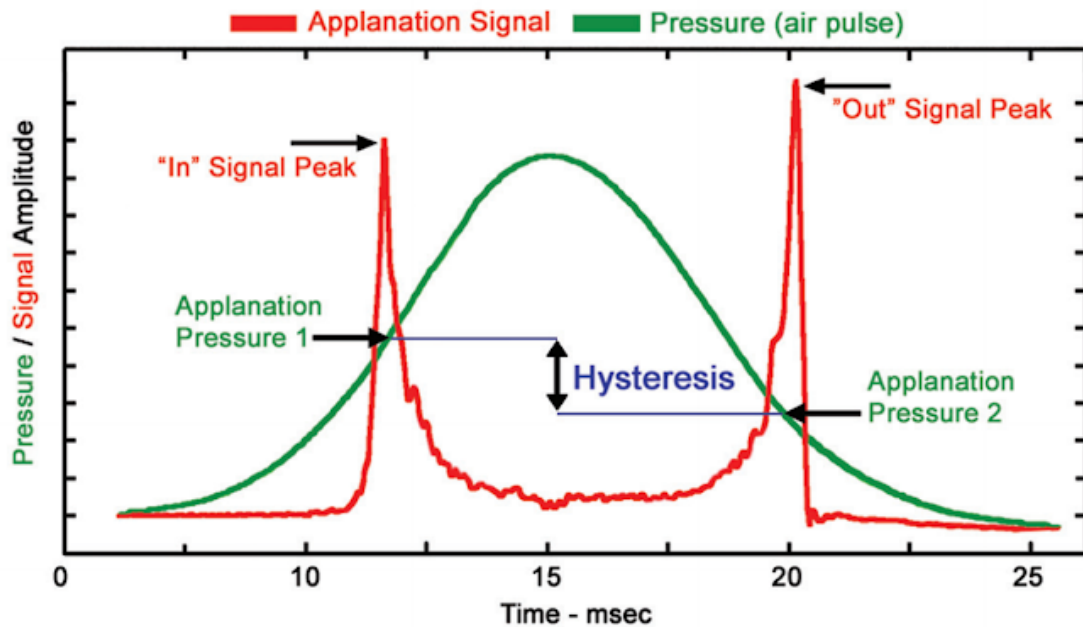


Figure 2-18 Typical light signal (red) and pressure signal (green) versus time [195, 197]

After corneal applanation, the cornea still moves into a moderate concavity and stop after maximum pressure because of viscoelasticity. As the applied pressure peaks and decreases, the cornea returns to its normal configuration, once again passing through an applanated stage. Two air pulse pressure values are recorded at the inward and outward applanation events. According to the characteristic of the corneal materials, the motion of the cornea is delayed in time by viscous damping, resulting in two different pressure values. Based on these two different pressure values, the actual IOP and the viscoelastic resistance of the cornea can be defined. Therefore, the average of both pressure provides a Goldmann-correlated IOP value and the difference between these pressure is termed Corneal Hysteresis Calibration coefficients [197]. According to these parameters, the ORA has high potential on the corneal material estimation in vivo [195, 197].

In the previous study, there is a method for measuring biomechanical properties in vivo which was introduced by Grabner *et al.* in 2005 [200]. This corneal dynamic imaging uses videotopography imaging of the cornea to analyze corneal indentation to describe the corneal biomechanical properties. Based on the corneal dynamic imaging analysis and ORA principle, the Corvis® ST has been developed. The Corvis® ST (Corneal Visualization Scheimpflug Technology) is the first non-contact tonometry by using high-speed imaging device in combination with a Gaussian shaped air-puff [195]. This ultra-high-speed Scheimpflug camera captures 140 frames during 31.93 ms measurement process, which can provide more detail of corneal indentation under air-puff. During the measurement process, the corneal deformation is related to the air-puff pressure changing which is similar to the ORA measurement process. According to the high-speed image recording, three events during the deformation process are of special interest, as the moment of first applanation, the highest concavity and second applanation.

The cornea deformation under the air-puff external load can be divided into nine different phases, and the image of the corneal deformation during this process is shown in Figure 2-19 [201].

- (I) **Pre-Deformation Phase:** The cornea geometry is maintained by the IOP and the structure of the cornea collagen fibres are extended and are under tension before the air-puff process by the CorVis-ST device.
- (II) **Ingoing Convex Phase:** When the air-puff pressure impacts the corneal surface, the cornea begins to get squished and the tension on the cornea collagen begins to reduce. Moreover, the motions of the whole eye begin to increase slowly in the posterior direction.

- (III) **Ingoing First Appplanation Phase (A1):** At the time of the first appplanation, the cornea is pressed and flattened. The force on the cornea's balance is pushed inward by the air-puff pressure and outward by the IOP. In contrast, the component of the surface tension parallel to the direction of air-puff is slight. During this process, the corneal edge profile is recorded by the CorVis-ST device (shown as Figure 2-19 A). After the duration of the first appplanation, the corneal tissue behaves under tension, changing initially to compression.
- (IV) **Ingoing Concave Phase:** As the cornea undergoes appplanation, the cornea becomes concave and the apex deformation continues to increase. The out-layer of the cornea on the concave anterior corneal surface is under compression and the in-layer of the cornea on the posterior corneal surface is under tension. While the anterior corneal surface compression gives rise to the round shape, the posterior lamellar layers are deformed toward the anterior chamber. This corneal displacement leads to the fluid in the aqueous chamber getting compressed, causing the IOP to rise with increased scleral tension. Moreover, the motions of the whole eye continue to increase slowly in the posterior direction.
- (V) **Oscillation Phase at the Highest Concave (HC):** As the air-puff pressure continues to increase, the resistance to backward corneal deflection reaches a maximum point. Furthermore, the backward motion of the cornea is limited. Until the air-puff pressure increases to maximum, the motions of the whole eye in the posterior direction continue to increase slowly. This phase is where the highest concavity (HC) shape of the cornea is observed, in addition to all maximum values for deformation, deflection, and HC deformation parameters (as shown in Figure 2-19 B, C, and D).

- (VI) **Outgoing Concave Phase:** As the air-puff pressure begins to decrease from the maximum point, the cornea begins to return to the pre-deformation phase. When the load on the corneal surface is released, the motion of the whole eye continues to increase in the backward direction, while the corneal surface is still under compression.
- (VII) **Outgoing Second Applanation Phase (A2):** At the time of the second applanation, the cornea becomes flattened again. The force on the cornea's balance is pushed inward by the air-puff pressure and outward by the IOP for a second time. In contrast, the parallel component of the surface compression to the direction of air-puff is slight. During this time, the corneal edge profile is recorded by the CorVis-ST device (as shown in Figure 2-19 E). After the duration of the second applanation, the corneal tissue behaves when compression changes to tension initially.
- (VIII) **Outgoing Convex Phase:** The air-puff pressure continues to decrease, and the corneal surface tension increases until the fully loaded state is attained. The whole eye motion decreases in magnitude in the forward direction.
- (IX) **Post Corneal Deflection Phase:** The whole eye movement continues to decrease in the forward direction until the eye fully recovers to its initial state, similar to the pre-deformation phase.

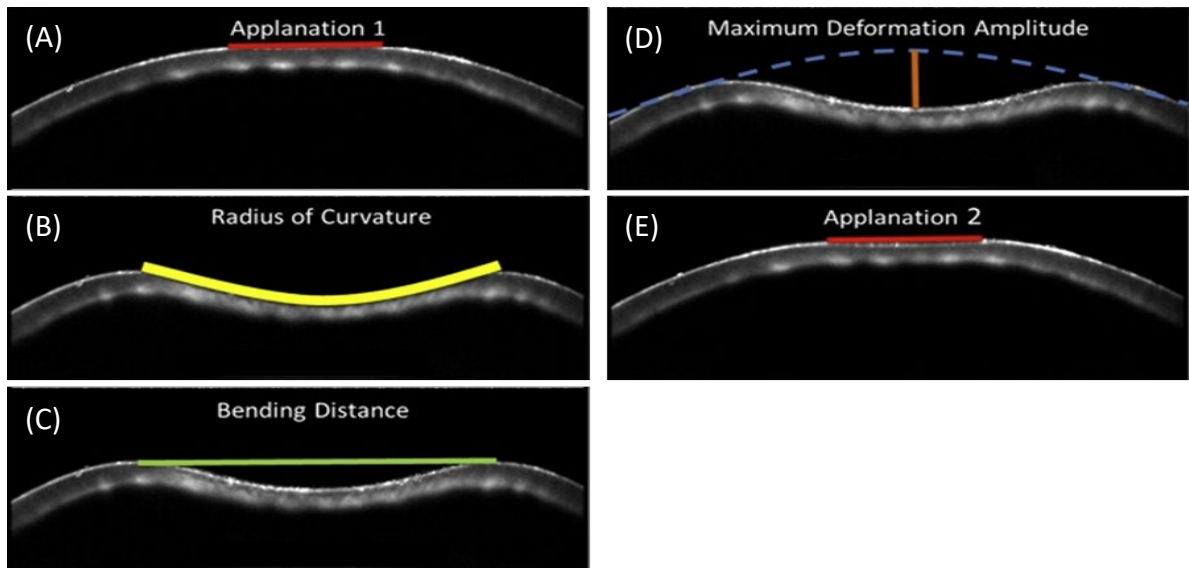


Figure 2-19 Sample images with markers illustrating parameters of the CorVis-ST device. (A) At ingoing first applanation phase, the anterior corneal surface is flattened. At the point of highest concavity, the radius of curvature (B), bending distance (C), and maximum deformation at the corneal apex (D) are determined. (E) As air-puff pressure decreases, the corneal surface returns to its initial state and the second applanation occurs [201].

According to the air-puff pressure versus duration curve, as shown in Figure 2-18, the nine phases that occur during dynamic corneal response analysis by the CorVis-ST device can be divided into two parts – loading and unloading. Moreover, eye material behaviour is similar to hyper-elastic versus viscoelastic material properties [71, 79, 82, 84-86]. In terms of hyper-elastic versus viscoelastic material properties, unlike purely elastic material properties, this material has an elastic component and a viscous component. In comparison with purely elastic and hyper-elastic versus viscoelastic materials, viscoelastic materials dissipate energy when a load is applied and then removed; on the contrary, the purely elastic materials don't behave in the same manner (Figure 2-20). The energy loss in the hyper-elastic versus viscoelastic material properties is difficult to measurement before the elastic component is defined. Hence, in this thesis, the eye materials just consider the hyper-elastic component; and it is forced on the air-puff pressure increase part in the following phases: as pre-deformation

phase, ingoing convex phase, ingoing first applanation phase, ingoing concave phase, and oscillation phase.

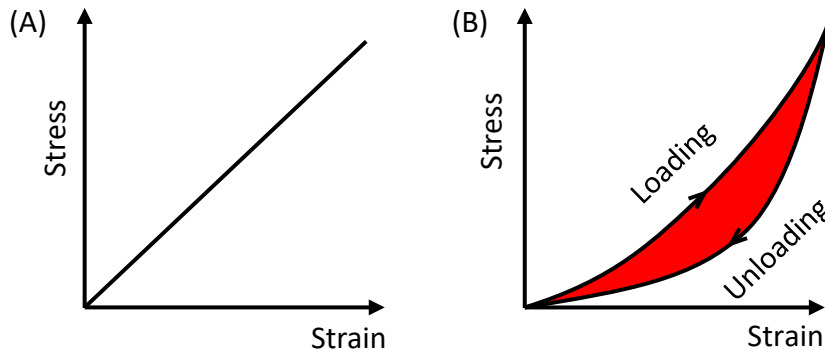


Figure 2-20 Stress-strain curves for a purely elastic material with no hysteresis (A) and a viscoelastic material with hysteresis (B). The red area shows the amount of energy lost in a loading and unloading cycle, which is an indication of the magnitude of hysteresis.

In terms of these five phases during dynamic corneal response analysis by the CorVis-ST device, there are several dynamic corneal response parameters that have been measured to describe the deformation characteristics and provide information about corneal biomechanics. According to the dynamic Scheimpflug imaging analysis of the CorVis-ST device, there are eleven parameters related to corneal deformation pertaining to the effect of air-puff pressure. At the pre-deformation phase, the initial corneal edge profile from the lateral rectus to the medial rectus is recorded, and the corneal thickness including CCT is measured. In order to describe the deformation characteristics when the cornea approaches the ingoing first applanation phase, there is the first applanation time (A1T), first applanation pressure on the device's piston (AP1), length of the flattened cornea (A1L), maximum corneal velocity at the first applanation event (A1V), deformation amplitude of the corneal apex (A1Deformation), and deflection amplitude of the corneal apex (A1Deflection) (Figure 2-19(A)). As the cornea, under the air-puff loading, approaches the oscillation phase, the following factors are

considered: The time from beginning of the air-puff until the highest concavity point of the cornea (HCT), radius of curvature of corneal concavity at the time of the highest deformation (R), bending distance between the two peaks of the cornea at the time of the highest concavity (PD), maximum deformation amplitude of the cornea at the highest concavity (HCDeformation), and maximum deflection amplitude of the cornea at the highest concavity (HCDeflection) upon maximum air-puff loading (Figure 2-19(B), (C), & (D)). Furthermore, the difference between deformation and deflection is the displacement measurement with/without the eye movement. Deformation is the distance from the original position of a point to its final location on the deformed eye, while deflection is the distance from the line that links the origin and end of the corneal apex upon air-puff loading (by using the oscillation phase as an example, as shown in Figure 2-21) [201].

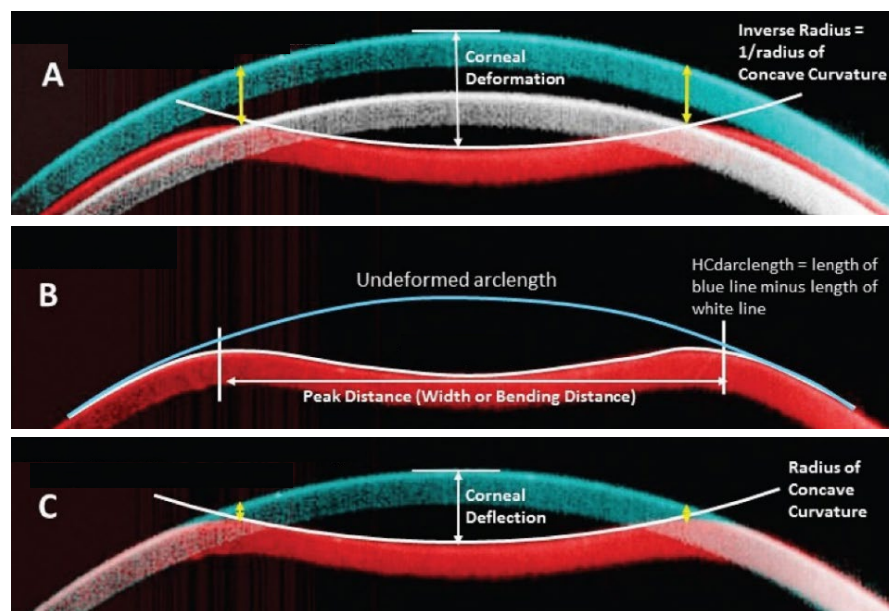


Figure 2-21 Dynamic Scheimpflug images at the pre-deformation phase and the oscillation phase, showing (A) cornea in pre-deformation phase (blue), at maximal corneal deflection (red), and at maximal whole eye movement (white); (B) initial corneal shape aligns with shape at maximal corneal deflection; and (C) correction for whole eye movement by aligning the cornea with maximum deflection to the initial shape [201]

There are several parameters obtained from the direct view of the corneal deformation to describe the specific response of the corneal deformation that is correlated with corneal biomechanical properties [202, 203]. The response parameters – the pressure at first appplanation (AP1) and the displacement between the apex in the undeformed state and the deflection at first appplanation and highest concavity showed a significant difference between different corneal material properties as normal and keratoconic eyes [201]. In addition, in 2017 Cynthia Roberts *et al.* investigate two new stiffness parameters with the dynamic corneal response parameters [201]. These stiffness parameters are defined as the relationships between inward appplanation pressure and corneal displacement. Finally, the Equations of both stiffness parameters at first appplanation time (SP-A1) and at the highest concavity time (SP-HC) are based on the biomechanically corrected IOP estimation and response deformation parameters following in Equation 2.9&2.10.

$$SP - A1 = (AP1 - bIOP)/A1DeflAmp \quad (2.9)$$

$$SP - HC = (AP1 - bIOP)/(HCDeflAmp - A1DeflAmp) \quad (2.10)$$

where $AP1$ = the pressure at first appplanation, which is used to align with the time-synchronized measured pressure signals, $bIOP$ = biomechanically corrected IOP estimation, $A1DeflAmp$ = the displacement between the apex in the undeformed state and the deflection at first appplanation, and $HCDeflAmp$ = maximum deflection near highest concavity.

Moreover, there is a significant difference in both stiffness parameters between healthy and keratoconic eyes. But both stiffness parameters still have a relationship with CCT. This means that the stiffness parameters are the overall stiffness parameters related to corneal geometry factors (as CCT, corneal curvature) and corneal material properties [201].

However, the CorVis device or ORA both have a high potential to estimate not only the IOP but also the corneal material properties. Moreover, the CorVis device can provide more information during the measurement process because of Scheimpflug technology. Due to this advantage, in this thesis, the CorVis device is selected to investigate both IOP estimated Equation and corneal estimated Equation. Some of the CorVis-ST parameters are described in the next section.

2.8 Error Sources in Tonometry Measurement

Glaucoma is a slow and irreversible progressive neuropathy that is characterised by damage to the optic nerve, which can cause visual impairment [177]. According to the causes and characteristics, this disease can be classified into the two following categories: open-angle and narrow-angle Glaucoma. It is well known that these two types of Glaucoma are closely associated with the value of IOP as discussed in Chapter one. In order to slow down the progression of Glaucomatous damage, management of IOP has been the only proven method [204]. Moreover, the principle of NCT is the same as that of GAT. There are also numerous studies pertaining to the evaluation of the factors affecting the accuracy of IOP measurements done through clinical applanation tonometry. As identified previously, the value of IOP obtained using the NCT are influenced by corneal stiffness, predominantly the CCT [192, 205, 206], central corneal radius of curvature (R_c) [5, 207], hydration [208], ectasia [33], and age [209, 210]. In this chapter, these factors of the biomechanical parameters have been discussed.

2.8.1 Corneal Factors that Effect Contact Tonometry (GAT)

The corneal factors outlined below not only affect the GAT but also affect other applanation tonometers, even the non-contact ones. As the discussion of the corneal factors specific to each applanation tonometer is beyond the scope of this paper, concentration is on the clinical gold standard, the GAT, in this section. The GAT has maintained the status of the reference standard in tonometry, even though it was developed under the inaccuracy acknowledgement in 1957 [10]. Research conducted by GAT has shown that the variation of CCT is the most remarkable. Since then, several research studies have been conducted to estimate the effect of CCT on GAT in order to develop a correction Equation to reduce this effect. In 1975, the first study showed that the value of IOP measured by GAT (denoted GAT-IOP) differed by 7.1 mmHg for every 100 μm shift in the CCT [211]. Moreover, there are also several studies exploring the association between CCT and GAT-IOP, all of which agreed with Ehlers' argument; however, the slopes of association were lower than that of Ehlers, ranging between 0.7 and 4.5 mmHg [23-25, 27, 212, 213].

Subsequently, Liu and Roberts [30] and Kirstein and Husler [214] highlighted that corneal stiffness was responsible for errors in the GAT rather than only CCT. Due to this suggestion, other corneal factors affecting corneal stiffness were noticed, such as central corneal curvature [30]. However, the studies did not agree on the magnitude of the curvature's effect on the IOP measurement using GAT (GAT-IOP) [26, 28]. Another important point to consider is that the effect of the material properties of the cornea on GAT was found to be significant [25, 30, 208], but there is a limitation in the practical value of this finding due to the current inability to measure corneal material behaviour in vivo. In addition, Elsheikh and Wang et al. have identified the relationship between age and corneal stiffness [52, 215] and were able to

determine its subsequent effects on GAT as well [216]. However, it is known that corneal material properties are affected by other factors, including age, swelling, ectasia, and healing wounds.

Table 2-3 Correction factors of GAT-IOP based on CCT variations

Authors	Year	Effect on GAT-IOP associated with the change in CCT (mmHg/ μm)	Notes
Ehlers et al. [13]	1975	0.071	Manometry study on in vivo eyes
Whitacre et al. [24]	1993	0.0228	Manometry study on 15 eyes
Wolfs et al. [23]	1997	0.019	395 participants, CCT = 537 (427–620) microns
Foster et al. [217]	2003	0.015–0.018	1232 participants
Elsheikh et al. [216]	2011	0.0165	Numerical study
Shimmyo et al. [218]	2003	0.016	1976 participants, CCT = 551 \pm 35 microns
Shah et al. [219]	1999	0.011	908 participants
Stodtmeister [220]	1998	0.007	579 participants, CCT = 585 \pm 41 (475–721) microns

Moreover, several research studies have been conducted to examine the effect of refractive surgery on the IOP measurement by GAT. The following differences between before and after surgery have been found: -3.4 ± 2.5 mmHg in Lam et al. [221]; -3.8 ± 2.2 mmHg in Zadok et al. [222]; -5.4 ± 3.0 mmHg in Siganos et al. [223]; and -1.8 ± 2.8 mmHg in Pepose et al. [224]. The cause behind this effect is the central thickness reduction and a weak link with the remaining stroma on the corneal flap [225, 226]. However, the effects of CCT and corneal material properties exist in the IOP measurement by contact tonometry.

2.8.2 Corneal Factors that Effect Non-Contact Tonometry

The value of IOP measured by NCT is known to vary with changes in biomechanical parameters, including material stiffness and geometry. For the applanation tonometer, R_c and CCT are two major influencing factors on IOP measurement. In most cases, the results indicated that the pressure reading with the applanation tonometer was affected by CCT, with the NCT being the most affected and the GAT being the least [5, 24, 206, 207]. In other words, it is true that in eyes with increased CCT, this measuring technique tends to overestimate IOP. On the contrary, NCT underestimates IOP with the presence of significantly thinner corneas. Evidenced by the same token, the effort of the radius shares a similar situation with the CCT. On the other hand, some studies found that the NCT gives better results than Goldman, especially in adult patients, and that it is also dependent on the CCT [227]. In conclusion, these influencing factors may lead to an erroneous diagnosis of Glaucoma. In terms of the effect of R on IOP, there is no significant change on IOP measurement between different R_c by noncontact tonometry [46].

All forms of tonometry are affected at present by corneal thickness. In terms of the tonometry performed using rapid corneal indentation, such as NCT and Rebound Tonometry, CCT is significantly more impactful due to the cornea's viscoelastic properties [209, 228]. In addition, there is a summary of the literature for the effect of CCT on IOP measurements considering both GAT and NCT in Table 2-4. According to the population studies, the CCT accounts for between 1% and 6% in the variation of GAT-IOP and 7% to 12% in the variation of NCT-IOP [209]. In terms of the bias of IOP measurement using different methods, the average value of the IOP measurement by NCT is normally similar to GAT. However, the trends of NCT is shown to be lower under a low IOP level and is higher with a high IOP level than GAT [229]. This

means the error effect of NCT is more than that of GAT. In order to the comparison of the effect of thickness reduction with surgery on non-contact tonometer, the reduction in IOP measurement has been found to be -4.3 ± 2.1 mmHg with non-contact tonometry (EC-5000, Nidek) [230] and -4.6 ± 2.8 mmHg with the Ocular Response Analyzer [224]

Table 2-4 Comparison of correction factors for GAT-IOP and NCT based on CCT variations

Authors	Year	Effect on IOP associated with the change in CCT (mmHg/ μm)		Notes
		GAT	NCT	
Tonnu et al [209]	2005	0.0028	0.0046	Clinic based in UK
Ko et al [206]	2004	0.0037	0.0063	Clinic based in Taiwan
Siganos et al [223]	2004	0.0026	0.0039	Clinic based in Greece
Eysteinnsson et al [231]	2002	-	0.0022 (M)/0.0028 (F)	Population based in Iceland

This research is focused on developing an accurate method of estimating IOP and corneal material behaviour implementing a non-contact method. All the influencing factors have been taken into consideration to reconfigure/redevelop the non-contact method, for CorVis-ST for example. This new method measures the IOP and reduces the effect of the geometry, including cornea size, corneal thickness, corneal curvature, and so on, and the material stiffness.

2.9 Concluding Remarks

The research studies pertaining to the behaviour of the eye have a long history, and most of them are closely related to eye diseases, especially 'Glaucoma' that indirectly resulted in the creation of the tonometer. Moreover, Glaucoma is the main cause of irreversible blindness in the world [18, 178]. Glaucoma has been described in terms of ocular disorders, with

multifactorial aetiology through the IOP association with optic neuropathy, and it can be traced back to the increased IOP in the eye [55]. IOP measurement has become an important reference for the initial diagnosis of Glaucoma. Recently, preventive medicine has started receiving greater attention, thus establishing that the management of IOP is the best way to prevent Glaucoma, and the measurement of IOP becomes of greater importance.

The first tonometer, using a force or a weight to indent the eye, was innovated back in the nineteenth century [55]. This tonometer was called the indentation tonometer, which used a plunger to delve into the cornea for measuring the IOP. Although this tonometer was not easy to use in clinical models, it was a breakthrough in the history of tonometry. At present, all tonometry techniques are based on one concept, which entails applying a mechanical force to deform the cornea for the corresponding corneal resistance to the IOP. The mechanical force can be roughly divided into two main categories, 'contact' and 'non-contact'. In terms of NCT, air tonometry is the most represented product. This air tonometry is an applanation method that does not require anaesthesia – using air puff to flatten the cornea. In addition, this type of tonometry overcomes the issue pertaining to the elastic effect of the eye, thus it has a higher impact on the IOP measurement. While comparing contact and non-contact tonometry, there are some similar error sources affecting the accuracy of IOP measurement [38-45]. On the other hand, the NCT by performing an image analysis can provide deformation parameters that are related to the biomechanical properties of the cornea [32]. Therefore, it means that the NCT has a higher potential for developing a method of the corneal material estimation in vivo.

Chapter Three

Methodology

3.1 Introduction

This section will explore the methods employed to develop and validate the biomechanically corrected IOP and the in-vivo material estimation algorithms proposed to be implemented in CorVis-ST. The pressure inside the eye has been mostly estimated in clinics by applying a force on the ocular globe (Cornea or Sclera) and relating its deformation to an assumed pressure. The dilemma in this procedure is that material properties of the tissue, its thickness and geometry, do play an important role in their deformation under pressure. Since some of these characteristics are not well understood, assumptions resulted in a less accurate estimation of IOP. In this research, experimental and laboratory data alongside accurate numerical simulations of the eye and CorVis-ST tonometry helped to better understand relationships between different parameters to satisfy the objectives including accurate IOP measurements.

This study explores healthy, Forme Fruste Keratoconus (FFKC), and Keratoconic eyes. The differences in corneal geometry and material properties between healthy and KC eyes were discussed in Chapter 2. Different corneal geometries lead to different tonometer air-puff pressure distributions on the corneal surface which is a requirement for numerical simulations. In FFKC, the corneal has a normal geometry but its material stiffness has started to become softer which affects the deformation under tonometry pressure on the corneal surface, Figure 3-1. Hence consideration of both geometry and material is necessary for this project. But it is

difficult to identify the corneal material changer in FFKC eyes, so the FFKC was ignored in this study.

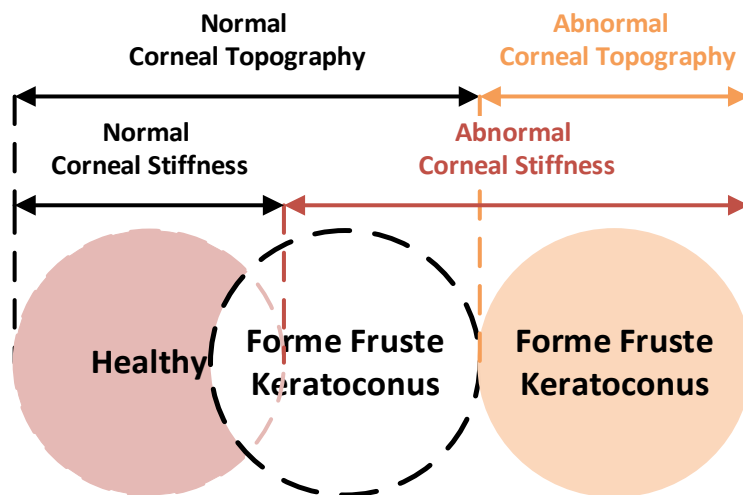


Figure 3-1 Comparison of stiffness and topography of healthy, FFKC, and KC eyes

Numerical analysis has been used to simulate variations in eye parameters, including eye geometry, IOP and material behaviour. Numerical analysis is assumed to follow three hypotheses: (I) The tissue stiffness can affect corneal deformation during the air pressure application; (II) the air pressure distribution changes with the deformation of the cornea; and (III) the IOP estimate is affected by corneal stiffness. According to these hypotheses, the FEMs adopted the following features: (I) Full representation of the eye model, considering thickness variation of the cornea and sclera; (II) regional variation of the eye material properties, including the cornea and sclera; and (III) dynamic representation of the air pressure of the CorVis-ST device.

This research was divided into two main stages of considering healthy and keratoconic eyes, respectively, Figure 3-2. At each stage, numerical modelling was used to simulate the eye geometry, IOP and CorVis-ST air-puff pressure. The results, including corneal deformation, were obtained and analysed to develop algorithms for estimation of true IOP and corneal

material properties, which were then validated using both lab experiments on ex-vivo eyes and clinical data of in-vivo eyes.

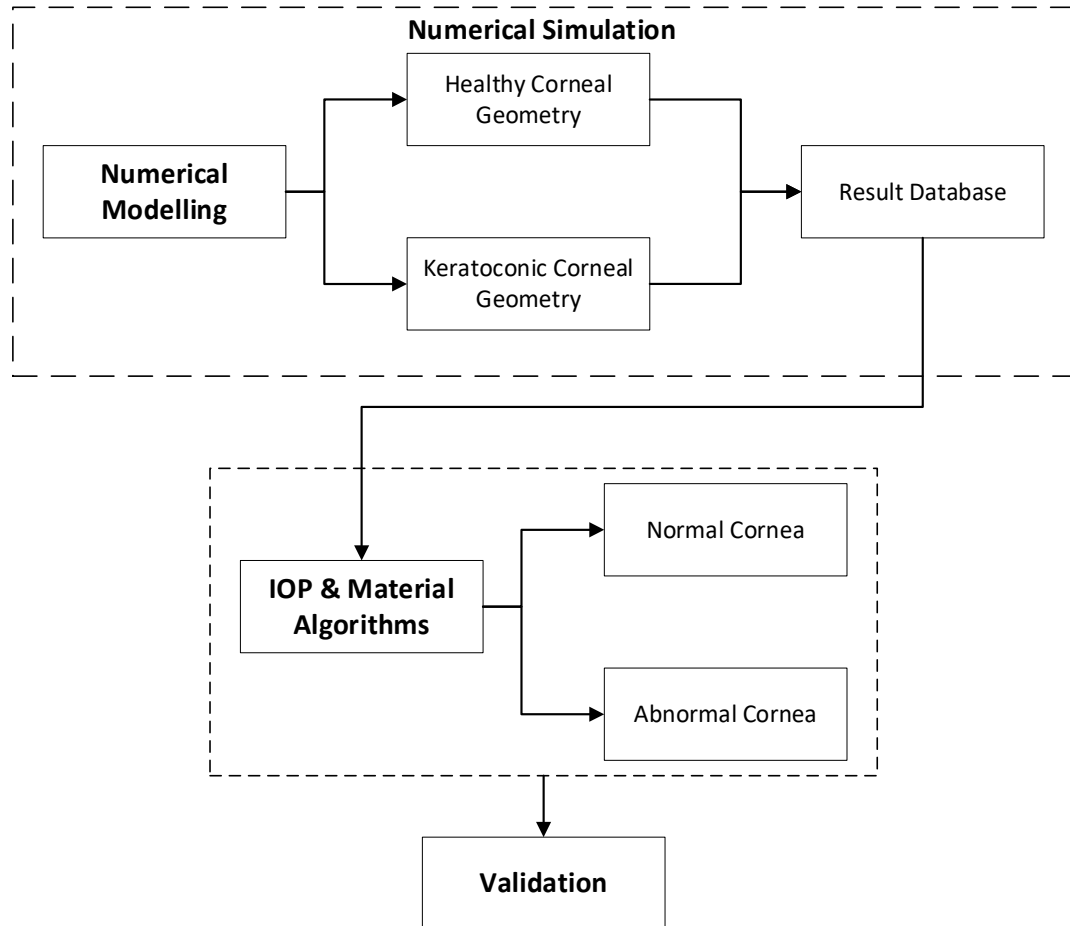


Figure 3-2 Flow chart of the procedure for IOP and corneal material behaviour Estimation

This chapter will explain the procedures undertaken to create the numerical models and develop corneal material behaviour and IOP correction algorithms. The chapter begins by developing a method that can identify the healthy eyes and KC eyes through recognition of differences in CCT, corneal geometry. The outcome was the ability to split corneal geometry into two groups: Healthy and KC (including five different corneal geometries). Thereafter, Abaqus numerical models were developed with different parameters to build a large dataset of corneal deformations under tonometer air-puff to be compared with clinical findings for

initial validation. Following this comparison, parameters that play critical roles in estimating IOP, such as corneal stiffness (which also relates to age) and central corneal thickness, were identified and used to build algorithms to estimate biomechanically corrected IOP for both healthy and KC cases. The algorithms were developed using a custom-built MATLAB code. Subsequently, following a similar method and considering previously published data, algorithms for corneal material estimation, for both healthy and KC eyes were developed. Finally, experimental and clinical studies were assessed thoroughly to validate these findings.

3.2 Distinguishing between KC and Healthy Data

Based on the Keratoconus literature review in Chapter 2, KC is associated with significant corneal distortion. Most of the clinical diagnosis of KC is based on the Scheimpflug camera system for corneal anterior segment analysis in conjunction with the mapping scanner Pentacam. However, the cause for the abnormal geometry lies in the disruption of a collagen organisation, which made the cornea lose its shape and function, resulting in a progressive visual degradation [232]. This means that the corneal material properties changed before the corneal geometry showed any changes. Therefore, both the corneal material properties and corneal geometry are important parts of abnormal corneal detection and parametric study.

As this research relied on CorVis-ST and Pentacam clinical data to develop estimation methods for IOP and corneal material behaviour, a study to distinguish between corneal geometry of healthy and KC eyes was conducted. By studying Pentacam corneal elevation maps, it was possible to categorise the topographies as normal topography (including healthy only) or abnormal topography groups (including KC only). The FFKC was ignored in this study due to it is difficult to defined the corneal material change without the corneal geometry change in the

clinical data.

The Scheimpflug technology of the Pentacam is used to measure corneal geometry. The corneal geometry measurement by the Pentacam is typically expressed in a Cartesian coordinate system as a set of regularly spaced discrete points on the corneal surface, Figure 3-3. The thickness of the cornea can be calculated based on the geometry data obtained for both anterior and posterior surfaces.

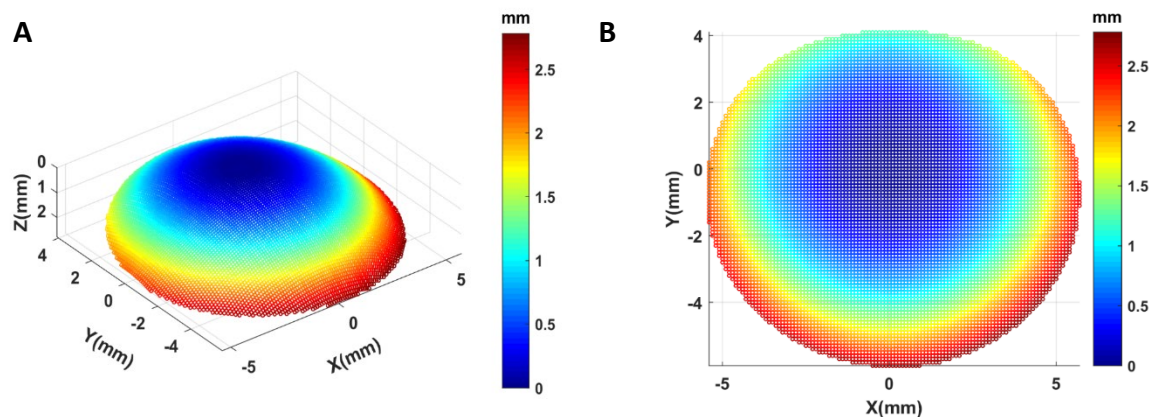


Figure 3-3 Typical corneal geometry data plotted in 3D (A) and (B). Colour of individual points reflects their Z coordinates, and the scale of the Z coordinates is shown in a colour scale.

The corneal geometry study relied on two independent clinical databases obtained from the Rio de Janeiro Corneal Tomography and Biomechanics Study Group in Brazil and the Vincieye Clinic in Milan (Table 3-1). Through a multi-centre retrospective study, a total of 722 clinical data points was available for this study. Dataset 1 (Rio) included 253 healthy and 93 Keratoconic participants, and Dataset 2 (Milan) included 227 healthy and 107 Keratoconic participants. The Institutional Review Boards of the clinical centres ruled that approval was not obligatory for this record review study.

Table 3-1 Details of the clinical databases

Database	Patients	Age (years)	CCT (μm)	CVS-IOP (mmHg)	
Dataset 1 (Rio)	Healthy	253	43 ± 16.5 (8–87)	539 ± 33.2 (454–629)	14.8 ± 3.06 (6–34)
	Keratoconus	93	38 ± 11.9 (16–72)	478 ± 37.7 (389–586)	11.8 ± 2.47 (4.5–18)
Dataset 2 (Milan)	Healthy	227	38 ± 17.2 (7–91)	543 ± 31.5 (458–635)	15.7 ± 2.35 (11–25)
	Keratoconus	107	33 ± 11.7 (13–64)	476 ± 41.2 (388–595)	13.2 ± 2.15 (6.5–19.5)

The parametric study was based on the corneal geometry with regular change on the corneal geometry, corneal material stiffness and IOP. The corneal geometry was assumed to be a symmetry shape similar to an ellipsoid in this study which is usually analysed by the variation in topography elevation along different meridia and circumferential line (Figure 3-4). Based on these geometry analyses, the difference of the corneal geometry between the patient specifically corneal geometry and symmetry idealized corneal geometry can be evaluated and used to classify the keratoconic corneal geometry into different groups for simplifying the individual difference in the parametric study.

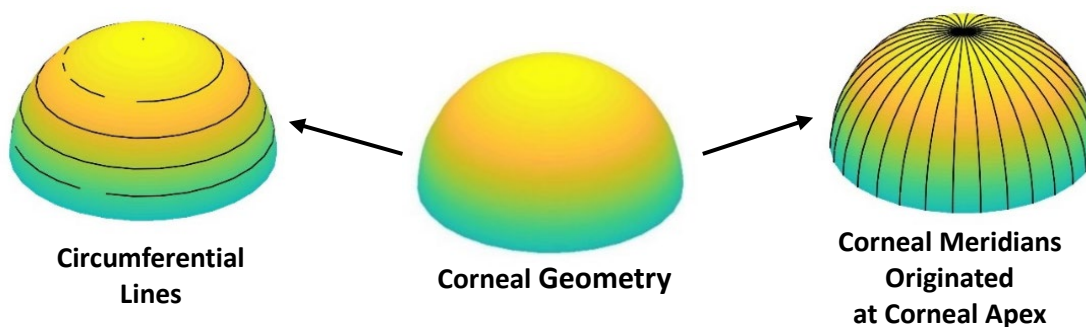


Figure 3-4 Analysis of corneal geometry elevation along meridian and circumferential lines

The original elevation data measured by the Pentacam was rotated and shifted due to the corneal geometric centre and vision centre are different. The elevation data needed to correct before geometry analysis. The corrected elevation data was rotated and shifted based on the pupil location and the corrected corneal apex also was redefined based on the pupil location. After the corrected process, the coordinate of the corrected corneal apex was located in the coordinates of the origin (0,0).

The elevation data provided for each patient was analysed by determining the changes along eight meridians with an azimuth of 45°, 90° (Superior), 135°, 180° (Temporal), 225°, 270° (Inferior), 315°, and 360° (Nasal), Figure 3-5. Along each meridian, the mean and standard deviation of the surface elevations at corneal apex and points at distances of 1, 2, 3 and 4 mm from corneal longitudinal axis were determined for normal, healthy eyes (Table 3-2) and keratoconic eyes (Table 3-3).

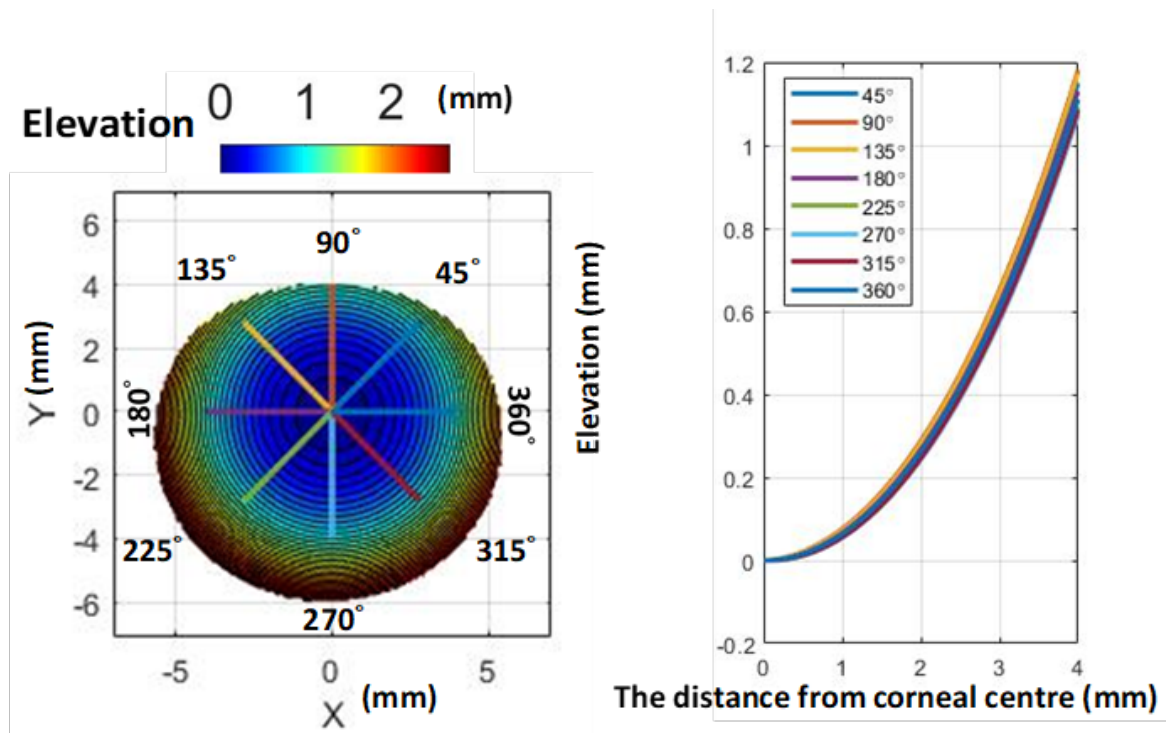


Figure 3-5 Analysis of corneal elevation data along eight main meridians of the eye

Table 3-2 Mean and SD of differences in elevation data between the corneal apex and points at distances of 1, 2, 3, and 4 mm from apex for healthy eyes in millimetre

Meridians with azimuth	Distance from corneal apex			
	1 mm	2 mm	3 mm	4 mm
45°	0.061±0.027	0.251±0.054	0.577±0.080	1.053±0.112
90°(Superior)	0.076±0.026	0.284±0.052	0.632±0.079	1.136±0.130
135°	0.085±0.023	0.304±0.048	0.664±0.074	1.180±0.105
180°(Temporal)	0.083±0.021	0.301±0.045	0.662±0.073	1.181±0.107
225°	0.070±0.024	0.279±0.047	0.637±0.073	1.158±0.106
270°(Inferior)	0.056±0.024	0.253±0.046	0.601±0.070	1.112±0.102
315°	0.048±0.021	0.233±0.043	0.563±0.069	1.047±0.101
360°(Nasal)	0.049±0.024	0.230±0.050	0.547±0.078	1.011±0.110
Overall	0.066±0.027	0.267±0.055	0.610±0.086	1.110±0.126

Table 3-3 Mean and SD of differences in elevation data between the corneal apex and points at distances of 1, 2, 3, and 4 mm from corneal apex for keratoconic eyes in millimetre

Meridians with azimuth	Distance from corneal apex			
	1 mm	2 mm	3 mm	4 mm
45°	0.075±0.038	0.276±0.079	0.611±0.122	1.088±0.169
90°(Superior)	0.095±0.038	0.317±0.075	0.674±0.115	1.179±0.162
135°	0.100±0.033	0.336±0.071	0.711±0.111	1.231±0.151
180°(Temporal)	0.086±0.032	0.317±0.069	0.698±0.111	1.234±0.159
225°	0.064±0.037	0.281±0.077	0.662±0.121	1.215±0.171
270°(Inferior)	0.049±0.036	0.258±0.076	0.635±0.119	1.190±0.163
315°	0.047±0.032	0.247±0.068	0.603±0.107	1.116±0.150
360°(Nasal)	0.057±0.035	0.250±0.074	0.582±0.118	1.055±0.164
Overall	0.072±0.040	0.285±0.080	0.647±0.123	1.163±0.174

Corneal elevations at points located at the same distance from the apex are expected to be similar in healthy eyes. Along the main meridian, the mean and standard deviation of the difference between max and min elevation in both databases (including healthy and KC eyes) were determined and shown in Figure 3-6 and Table 3-4.

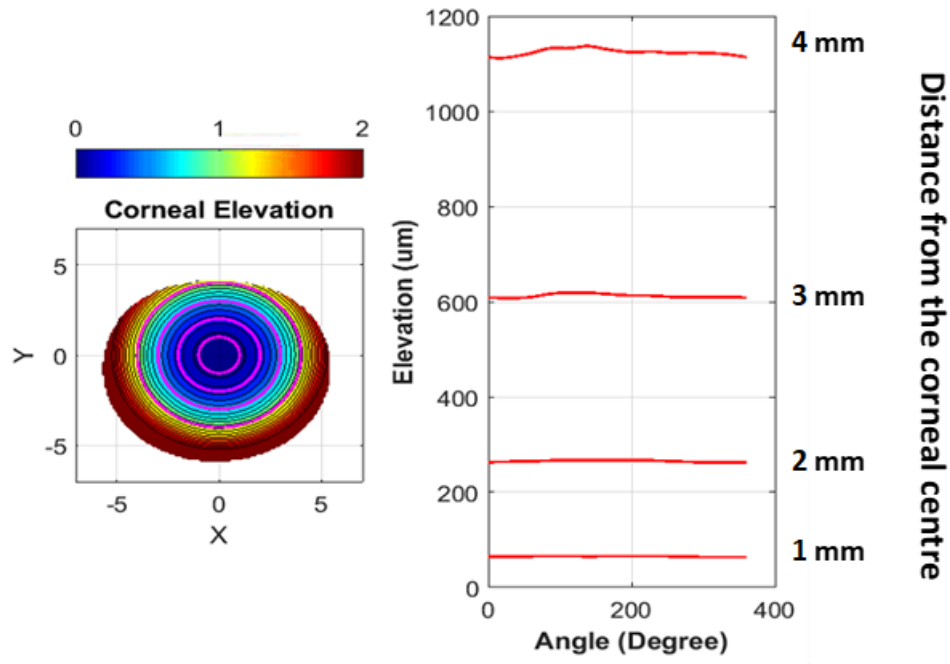


Figure 3-6 Analysis of corneal elevation in clinical datasets along circumferential lines with radii of 1, 2, 3, and 4 mm

Table 3-4 Comparisons of mean and SD of differences (in millimetre) between max and min elevation along circumferential lines with radii of 1, 2, 3, and 4 mm for normal and abnormal corneal geometry

Distance from corneal apex	1 mm	2 mm	3 mm	4 mm
Normal Corneal Geometry	0.066±0.003	0.264±0.013	0.604±0.031	1.104±0.179
Abnormal Corneal Geometry	0.072±0.035	0.285±0.073	0.647±0.115	1.163±0.161

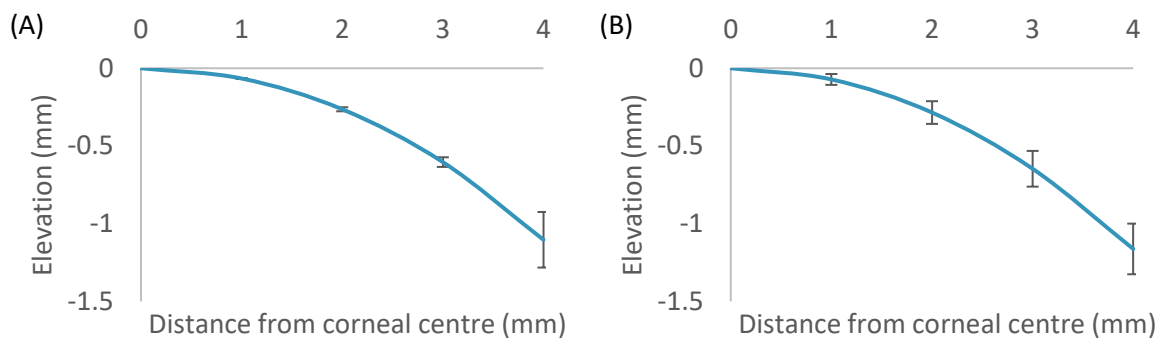


Figure 3-7 Comparison of mean and SD of differences of variations in elevation data between (A) normal eyes and (B) KC eyes

According to the results and considering variations in normal and abnormal corneal elevation across different meridian and circumferential lines, corneal topography is not rotationally symmetric and had an individual variability. These characteristics caused challenges in developing FE models. Hence, when considering corneal geometry for healthy eyes in this project, two approaches were adapted; one that assumes corneal geometry to be rotationally symmetric in FE models used to perform a parametric study; and another that relies on patient's topography data to create patient-specific models for validation.

For KC eyes, it was also assumed corneal geometry to be rotational symmetry in the parametric study even the corneal geometry was not rotationally symmetric. To reduce the effect of the corneal geometry in KC eyes, corneal geometries were divided into five different groups according to how rotationally unsymmetrical or distorted the cornea was, and this was reflected in a parameter named TopoR. These groups were decided such that the KC group 3 (TopoR=3) had a topographical shape close to healthy patients and came from the mean of all variations in KC datasets; KC group 2 (TopoR=2) was the result of mean minus SD; KC group 1 (TopoR=1) was the result of mean minus twice the SD; and similarly KC group 4 (TopoR=4) is the result of mean plus SD; and KC group 5 (TopoR=5) is the result of mean plus twice the SD (Table 3-5 & Figure 3-8). These five geometrical models for KC patients were used to develop FE models.

Table 3-5 Trends of variations in elevation data variation trends in normal and KC groups

Group name of the abnormal geometry	TopoR	Distance from corneal centre				
		0 mm	1 mm	2 mm	3 mm	4 mm
Normal group	-					
KC group 1	1	0	0	0.125	0.400	0.816
KC group 2	2	0	0.032	0.205	0.524	0.990
KC group 3	3	0	0.072	0.285	0.647	1.163
KC group 4	4	0	0.112	0.365	0.770	1.337
KC group 5	5	0	0.152	0.445	0.894	1.511

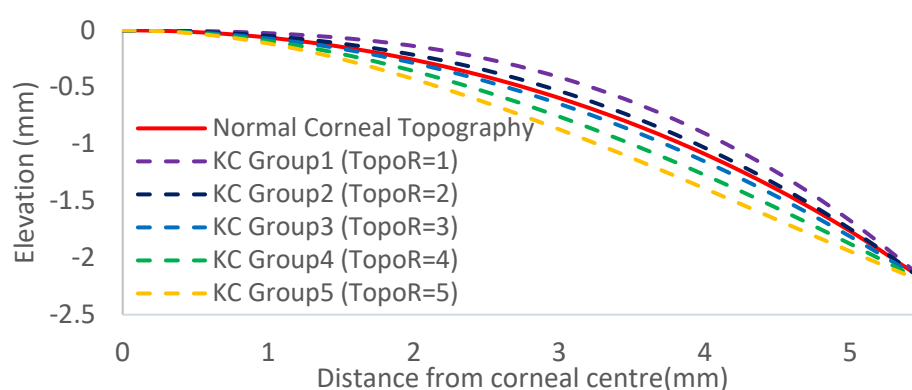


Figure 3-8 Trends of variations in elevation data in normal and five KC groups

3.3 Numerical Modelling

This study needed to conduct numerical simulations to study the relationship between intraocular pressure, air-puff pressure and corneal deformation in order to develop algorithms for estimating biomechanically corrected IOP (bIOP) and material parameters. With numerical modelling, various scenarios could be simulated which includes variations in central corneal thickness (CCT), IOP, corneal radius, topography and material parameters. Hence it brought two main advantages, first reduced the inaccuracies that could be caused by experimental methods, second it reduced cost and allowed a more thorough analysis. The finite element (FE) software ABAQUS 6.14 (Dassault Systemes Simulia Corp., Rhode Island, USA) was used to simulate eye globes and the CorVis-ST tonometry, and predict the resulting corneal

deformation data.

3.3.1 Normal/Abnormal Geometry of FEM Configuration

Eye geometry is one of the most important elements in the numerical modelling of this study. As a result of the geometry analysis mentioned in Section 3.2, normal corneas are assumed rotationally symmetry, unlike KC corneas. In order for the FE models to represent realistic conditions, they adopted the following features from previous studies [70, 100, 233]: (I) Full representation of the eye globe, considering thickness variation of cornea and sclera; (II) regional variation in the cornea & sclera material properties; and (III) dynamic representation of the CorVis-ST air pressure on the eye.

The eye model included the cornea, limbus, and sclera, and was defined using information on the anterior corneal central radius (R_c), anterior corneal shape factor (p), central corneal thickness (CCT), peripheral corneal thickness (PCT), limbal radius (RI), scleral radius (R_s), and equatorial and posterior scleral thickness (Figure 3-9).

The shape of the cornea was determined by its anterior corneal topography, CCT and PCT. Anterior corneal topography in healthy cases was assumed to be ellipsoid as also described by other researchers [60-62, 234]. The relationship between anterior corneal topography, R_c and p can take the form:

$$Z = \frac{R_c + \sqrt{R_c^2 - p(X^2 + Y^2)}}{p} \quad (3.1)$$

Where X , Y , and Z are the coordinates of a point on the corneal anterior topography; R_c is the anterior corneal central radius and p is the anterior corneal shape factor.

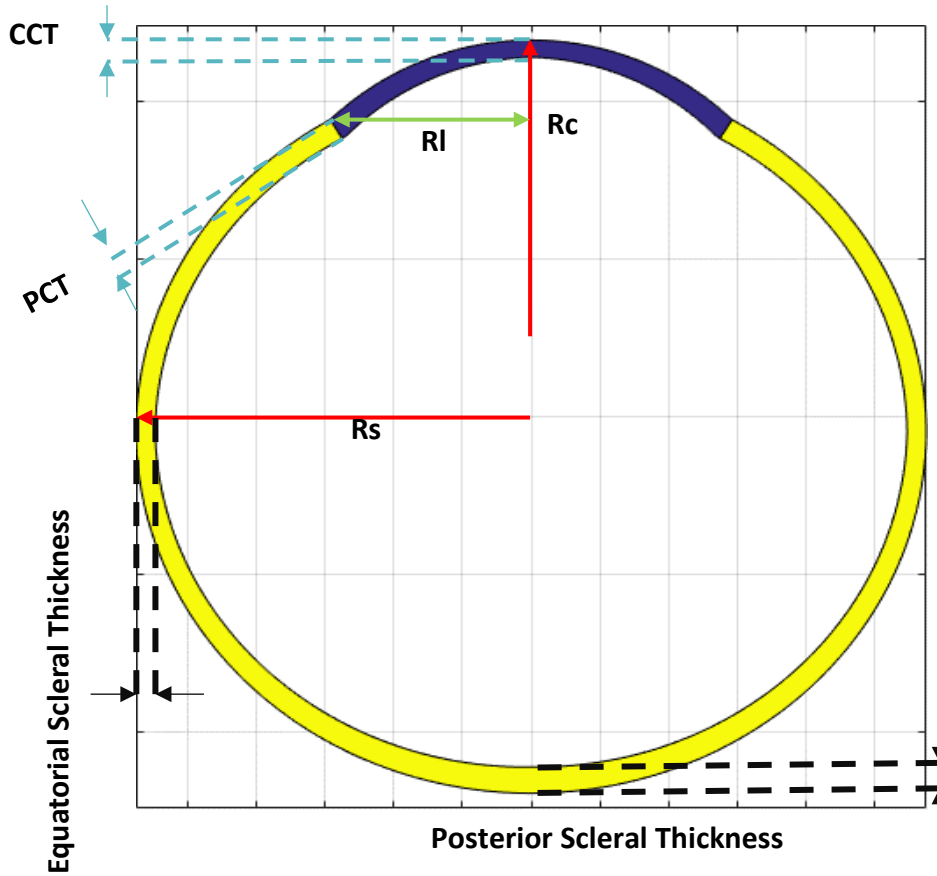


Figure 3-9 Geometry parameters of the eye model

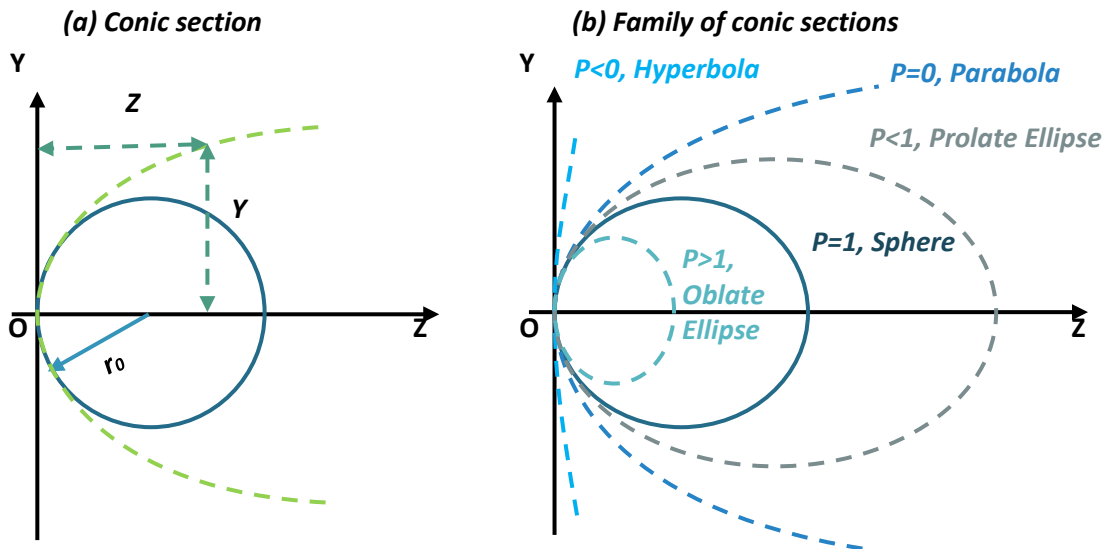


Figure 3-10 General Equation for a general conic section (a) is given by $Y^2 = 2r_0Z - pZ^2$ and the family of conic sections with different asphericities is shown in (b) [235]

The corneal thickness at any location was assumed to linearly transit from CCT to PCT. On the other hand, the sclera is assumed a roughly spherical shape [236], and its thickness is made equal to PCT at the limbus, decreasing to the equatorial sclera, then increasing to the posterior pole.

The models consider variations in the main geometry parameters as depicted in Table 3-6. These variations covered the common clinical ranges exported in the literature. In the model, the value of R_c and p was made equal to mean [59, 60], and R_l was set to the maximum value of the topography radius in the nasal-temporal cornea in the literature [237, 238]. In addition, CCT covered the range from minimum to maximum of clinical values for healthy eye, in section 3.2. The thickness variation of sclera is obtained from previous experimental and clinical evidence [56, 58, 65, 70, 239].

In order to keep the size of parametric study at a manageable level, an initial study was conducted and found that variations in some parameters, such as R_c , P and R_l had only a negligible effect on the results [46]. Consequently, constant value of the anterior corneal central radius, anterior corneal shape factor, limbal radius, and scleral radius of 7.8mm, 0.82, 5.85mm and 11.5 mm, respectively, were assumed since these parameters were not measured clinically and were found numerically to have a negligible effect on IOP estimations in the previous study [46].

Table 3-6 Comparison between clinical measurement data and numerical model settings for healthy eyes

	Clinical Data (Mean \pm SD)	Numerical model (Range)
Anterior Corneal Central Radius (Rc)	7.79 \pm 0.27 mm [59-62]	7.8 mm
Anterior Corneal Shape Factor (p)	0.82 \pm 0.18 [59, 61, 62]	0.82
Central Corneal Thickness (CCT)	0.55 \pm 0.036 mm [63-65]	0.445-0.645 mm
Limbal Radius (RI)	5-6.5 mm [66-68]	5.85 mm [46]
Scleral Radius (Rs)	around 11-18 mm [66]	11.5 mm [46]
Peripheral Corneal Thickness (PCT)	CCT + 0.15 mm [63-65, 69]	CCT+0.15 mm [70]
Equatorial Scleral Thickness	0.53 \pm 0.14 mm [57, 58]	0.8*PCT mm
Posterior Scleral Thickness	0.99 \pm 0.18 mm [57, 58]	1.2*PCT mm [70]

The abnormal corneal geometry had been classified into five different geometry groups with five values of TopoR, Section 3.2. Due to the characteristics of Keratoconus, this research assumed that the change in eye geometry affected only the cornea and the geometry on the limbus or sclera is not different between healthy and KC eye. Overall, the model was meshed by controlling the total number of element rings in corneal and sclera using 6-noded solid elements (C3D6H) arranged in one layer across the thickness.

3.3.2 Regional Variation in Material Behaviour

The eye model was divided into four main segments of the cornea, limbus, anterior sclera and posterior sclera, based on their characteristics of mechanical behaviour (Figure 3-11). In this project, third-order, hyper-elastic Ogden models were used to represent the ocular tissue's mechanical behaviour as obtained from previous experimental works and enabled sensitivity to variations in stress-strain behaviour related to age [1, 70, 99]. Moreover, scleral regional

variation in stiffness and its gradual reduction from the limbus towards the posterior pole is incorporated [240]. In all models, the optic nerve head was not considered as its effect on corneal behaviour is negligible. Based on the uniaxial tension results from a previous study [1, 70], the stress-strain relationship in the healthy eye in each segment was described in Figure 3-11.

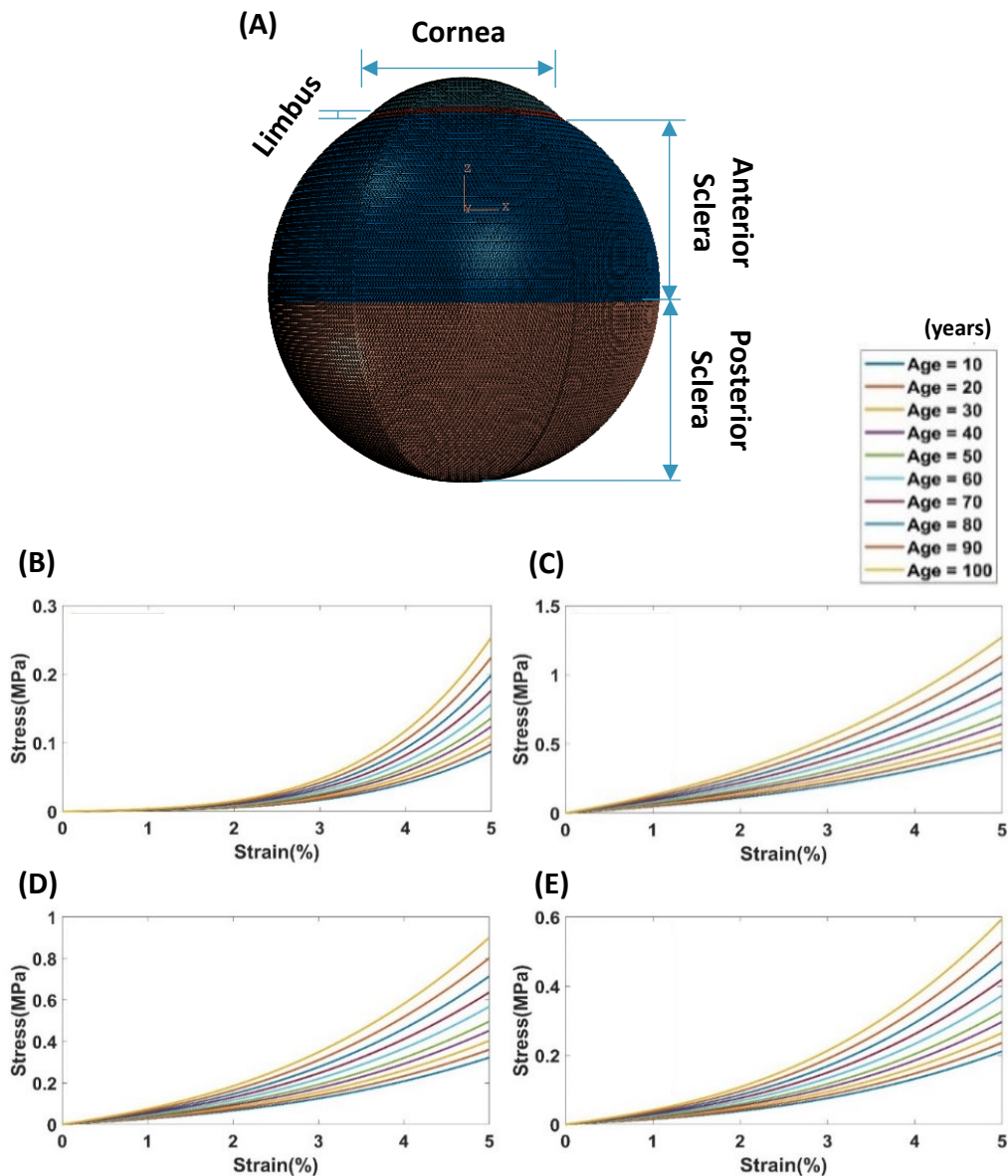


Figure 3-11 Model segments with different material properties in FEM (A). Stress-strain material behaviour of the cornea (B), limbus (C), anterior sclera (D), and posterior sclera (E) with age-related variation is shown [1, 70].

Using the stress-strain material behaviour, the Ogden coefficients, μ_i and α_i , as determined to third order in different eye regions, are shown in Table 3-7.

Table 3-7 Ogden coefficients of eye FE model in cornea, limbus, anterior sclera and posterior sclera

Region	Age (years)	μ_1 (MPa)	α_1	μ_2 (MPa)	α_2	μ_3 (MPa)	α_3
Cornea	10	-214.183	23.5457	142.131	24.9978	72.083	20.6831
	30	-267.423	23.5397	177.461	24.9995	90.000	20.6610
	50	-327.548	23.5263	217.359	24.9999	110.235	20.6187
	70	-416.894	23.5070	276.649	24.9996	140.304	20.5598
	90	-520.522	23.4835	345.416	24.9995	175.180	20.4876
Limbus	10	-391.599	2.001649	273.9372	3.999664	119.0458	- 2.00625
	30	-488.94	2.001139	342.0308	3.999936	148.6359	-2.0041
	50	-598.869	2	418.9285	4	182.0542	-2
	70	-762.223	1.998359	533.2015	3.999952	231.7134	- 1.99429
	90	-951.69	1.996362	665.7401	3.999936	289.3115	- 1.98728
Anterior Sclera	10	-407.61	2.001649	279.1595	3.999664	129.216	- 2.00625
	30	-508.931	2.001139	348.5511	3.999936	161.334	-2.0041
	50	-623.354	2	426.9148	4	197.6073	-2
	70	-885.496	2	602.1719	4	284.6928	-2
	90	-1084.96	2	735.932	4	350.5131	-2
Posterior Sclera	10	-330.079	2.001649	224.0066	3.999664	106.4883	- 2.00625
	30	-412.127	2.001139	279.6887	3.999936	132.9571	-2.0041
	50	-504.786	2	342.5702	4	162.8503	-2
	70	-642.478	1.998359	436.0146	3.999952	207.2713	- 1.99429
	90	-802.179	1.996362	544.3953	3.999936	258.7936	- 1.98728

While coefficients μ_i had a regular change with age, α_i had an almost constant value in each region. In the analysis, μ_i varied around the values obtained experimentally from ex-vivo eyes. In addition, the ratio (M_R) between the Ogden coefficient μ_i and μ at age 50 related to stiffness variations corresponding to Age. The correlation between M_R and age is presented in form:

$$M_R(\text{Age}) = 0.5852 \times e^{0.0111 * \text{Age}} \quad (3.2)$$

Where M_R is the ratio between the Ogden coefficients μ_i and μ at age 50, Age is presented in years.

Moreover, the material behaviour in KC eyes was assumed to be softer 20% than the healthy eyes. To cover the range in normal and abnormal corneal material properties observed in ophthalmic practice, relative to μ_i at age 50, M_R was allowed to vary between 10% and 300% in steps of 10%.

3.3.2.1 Boundary Conditions

The CorVis's measurement process includes few factors as air-puff shooting centre and angle etc, which affects the IOP measurement. In this study, it assumed that the air-puff shooting centre was same with the corneal centre with a vertical shooting angle. In addition, the eye material was assumed a nonlinear hyperreality homogeneous material in both healthy and KC eyes in Section 3.3.2. According to these hypotheses, all models were provided with boundary conditions that prevented their rigid body motion (Figure 3-12):

- The nodes at the corneal apex and posterior pole were restrained against displacement in the X-direction (temporal-nasal) and Y-direction (superior-inferior).

- The movement of the equatorial nodes is prevented in the Z-direction (anterior-posterior).
- To avoid the model from rigid-body rotation around the Z-axis, the equatorial nodes in the X-Z plane are fixed in the Y-direction.

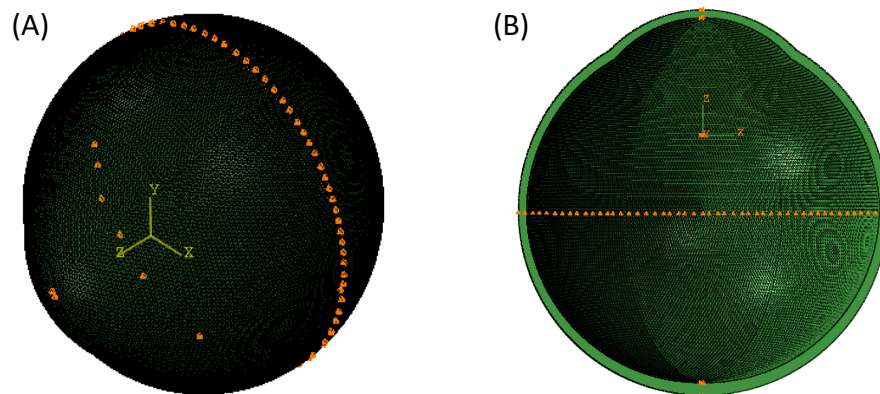


Figure 3-12 View of a FEM showing (A) full eye model and (B) cross-sectional view.

Boundary conditions are highlighted in Orange.

3.3.3 Loading Configuration

All models were subject to two loading scenarios including IOP and external tonometer air-puff pressure. The IOP varied from 10 to 30 mmHg as these values are commonly seen in ophthalmic practice. IOP was applied as a pressure change inside of the eye, modelled by defining an internal surface as a fluid cavity. Moreover, based on the assumption that aqueous and vitreous are incompressible, the ocular globe models were filled with an incompressible fluid that had a density of 1000 Kg/m^3 [241].

The external air pressure provide by the piston was applied on the central cornea. The change in piston pressure increased from 0 mmHg to 180 mmHg and reduced from 180 mmHg to 0

mmHg during the measurement was obtained from the device manufacturers (Figure 3-13 (B)), and the distribution of the air pressure was obtained based on experimental study [242] and computational fluid dynamics simulation (CFD) [243] performed on the device (Figure 3-13 (A)). When distance from the device’s shooting hole to the corneal apex is 11 mm, the maximum air pressure in the device was around 180 mmHg and was found by the manufacturer to have been reduced by approximately 50% (105mmHg) as the air puff reaches corneal apex [46, 243]. The pressure at the centre of each element was calculated using the cubic spline data interpolation in MATLAB. A new amplitude file that could be read by ABAQUS was generated to allocate the correct pressure to each element based on its location. The pressure was applied for 0.026 seconds as described in Figure 3-13 to the inflated eye, and the resulting deformations were extracted.

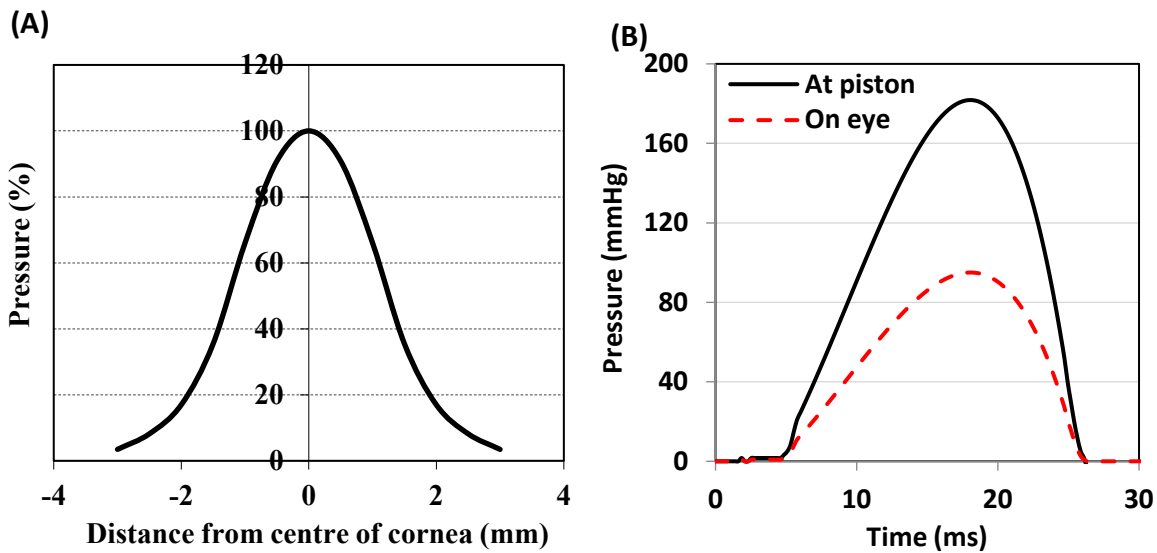


Figure 3-13 Spatial distribution (A) and time variation (B) of air-puff pressure on the cornea [46, 242, 243]. In (B), thick black line represents pressure measured in device piston and the red line represents pressure acting on the cornea.

3.3.4 Stress-Free Configuration

The eye geometry parameters adopted clinical corneal geometry measured under a stressed condition with IOP. This means that before the IOP-loading and air-puff dynamic simulation, the stress-free configuration of the FEM needs to be derived to obtain the geometry under zero IOP. An efficient iterative method was applied for deriving the stress-free condition with high accuracy [233].

The hypothesis of the stress-free process is that the nodal coordinates of the initial model with the stressed shape are equal to the sum of the nodal coordinates of the target model with the stress-free configuration and the deformations under IOP (Figure 3-14).

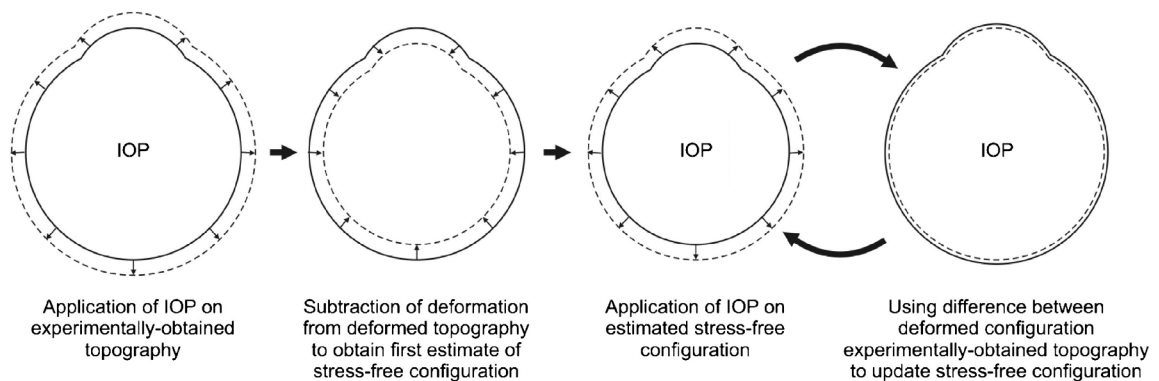


Figure 3-14 Schematic description of the approach used to obtain the stress-free configuration of the eye [233]

In the first estimation, the process began at applying the IOP to the initial model with C_0 coordinates using FE-analysis, and this led to the nodal deformation D_1 and the first estimate target model with the stress-free configuration denoted $S_1 = C_0 - D_1$. Then, the IOP was applying again to configuration S_1 to get a new IOP configuration S'_1 with a new nodal deformation D'_1 , and the difference between S'_1 and C_0 was used to compute the

error estimation using Euclidean norm in three-dimensions ($e_1 = \|S'_1 - C_0\|$). Hence, a new stress-free estimate was approximated using the new nodal deformation as $C_1 = C_0 - D'_1$. Based on this new estimate, the procedure continues by carrying out another finite element analysis and using the resulting nodal deformation D'_K to compute a new error estimate ($e_K = \|S'_K - C_0\|$) in the the K iteration. Hence, the stress-free configuration process followed this loop until the final error had magnitudes less than the pre-set tolerance of 10^5 mm.

3.3.5 Mesh Density Study

In an initial mesh density study, the numerical model assumed $R_c=7.8$ mm; $P=0.82$; $CCT=0.545$ mm; $RI=5.85$ mm; $R_s=11.5$ mm; $PCT= 0.695$ mm; equatorial scleral thickness= 0.556 mm; and posterior scleral thickness = 0.834 mm. The material properties were set to age 50 and the boundary conditions were carried out as described in Section 3.3.2. Models in these simulations differed only in the number of corneal, limbal and scleral rings and hence the number of elements/nodes used. The elements size in the corneal, limbus and sclera approximated to be the same. As detailed in Table 3-8, a total of 8 models were included.

Table 3-8 Details of eight model settings tested in an initial study

Model No.	1	2	3	4	5	6	7	8
Number of Corneal Rings	9	14	19	21	24	26	29	31
Number of Limbus Rings	3	4	6	6	7	7	8	9
Number of Scleral Rings	46	70	93	103	117	127	141	150
Number of Nodes	10096	23236	41776	50704	65716	76804	95056	108304
Number of Elements	10092	23232	41772	50700	65712	76800	95052	108300

First, inflation was performed bringing the IOP to a value of 15 mmHg. This is regarded as an initial loading and the displacement nodes at three particular locations; corneal apex, a limbal node and posterior pole were compared as shown in Table 3-9. In addition, the tissue thickness changes at these locations were recorded. Secondly, the cornea was subjected to CorVis-ST pressure up to 95 mmHg. Both deformation and tissue thickness variations at the above-mentioned locations were recorded (Table 3-9).

Table 3-9 Displacements and thickness changes after IOP inflation and external loading.

Values in Table are all in μm .

Model Number		1	2	3	4	5	6	7	8
After inflation with IOP = 15 mmHg									
Deformation	Corneal Centre	123.2	123.7	124.2	124.4	124.5	124.5	124.5	124.6
	Limbus	29	30.2	30.8	31	31.1	31.1	31.1	31.1
	Posterior Pole	24.8	24.8	24.7	24.7	24.7	24.7	24.7	24.7
Thickness Change	Corneal Centre	-15.7	-15.7	-15.7	-15.7	-15.6	-15.6	-15.6	-15.6
	Limbus	-3.1	-3.2	-3.3	-3.4	-3.4	-3.4	-3.4	-3.4
	Posterior Pole	-3.5	-3.5	-3.5	-3.5	-3.5	-3.5	-3.5	-3.5
After inflation and application of CorVis-ST Air Pressure									
Deformation	Corneal Centre	131.5	133.5	134.7	134.9	135.1	135.1	135.1	135.1
	Limbus	29.4	30.6	31.2	31.4	31.6	31.6	31.6	31.6
	Posterior Pole	24.3	24.3	24.3	24.3	24.3	24.3	24.3	24.3
Thickness Change	Corneal Centre	36.5	37.5	38	38.1	38.3	38.3	38.3	38.3
	Limbus	-2.5	-2.6	-2.7	-2.7	-2.7	-2.7	-2.7	-2.7
	Posterior Pole	-3.6	-3.6	-3.6	-3.6	-3.6	-3.6	-3.6	-3.6

It was evident from Table 3-9 that both displacements and thickness changes began to converge from the fifth model. Based on these results, the FE models used in the remainder of this project employed 65,712 six-noded elements organised in 24-element rings in the cornea, 7-element rings in the Limbus, 127-element rings in the sclera and one-element layer.

3.3.6 Summary of Simulation Steps

The development of corneal material behaviour estimation and IOP correlation algorithms were based on the simulation of the air-puff process by CorVis-ST. This simulation was divided into two steps – IOP (intrinsic loading) and air-puff (external loading). Before the simulation of the CorVis-ST process, an initial study on the model geometry was conducted to evaluate the effect of different mesh densities on the deformation under inflation in the eye and loading on the corneal centre. This initial study determined a mesh density of the model that was reliable and computationally efficient for modelling.

The input file of the simulation began with generating an idealised model and the eye setting was based on the previously mentioned factors. The idealised geometry was described in a node file using Cartesian coordinates. The models underwent a process to derive the stress-free form, under zero-IOP. These models were then used for the parametric study carried out in this project.

The main results of the simulation were recorded using nodal coordinates in the output database (.odb) file, and the deformed nodal coordinates were extracted from this file using an ABAQUS python script. Due to the time-consuming nature of the simulation, all analysis was programmed in a bespoke MATLAB environment that interacted with ABAQUS.

3.4 Parametric Study

The total number of normal and abnormal models in the parametric study was 4,500. In each model, specific values of CCT, IOP and material properties were used. The analysis of air puff application was dynamic and consisted of 300 pressure increments (time step=0.0001s) covering the 0.03 s of the CorVis-ST procedure. The coordinates of corneal anterior nodes were extracted at each time step using a Python code, and a MATLAB code was used to estimate values of CorVis-ST dynamic corneal response parameters (P_{DCR}). The results of the study were used to analyse the effect of corneal geometry and material parameters on the dynamic corneal response (DCR), and to develop algorithms providing estimates of true IOP and corneal material properties.

3.4.1 Calculation of Dynamic Corneal Response Parameters

The main dynamic corneal response parameters (P_{DCR}) were described in Chapter 2, and these parameters were estimated while following the same methods used by CorVis-ST. All simulation results were recorded in a three-dimensional space. The nodal deformations with the time variable were fitted to a 10th degree polynomial by using the least-squares method for the smooth curve on the corneal topography. with this polynomial equation, the maximum deformation at the corneal apex was determined, Figure 3-15, and the highest concavity time (HCT) and max deformation on the corneal apex at this time (HCDeformation) were determined. The corneal edge profile at the HCT phase was defined by using the cubic interpolation method (as shown by the blue line in Figure 3-16).

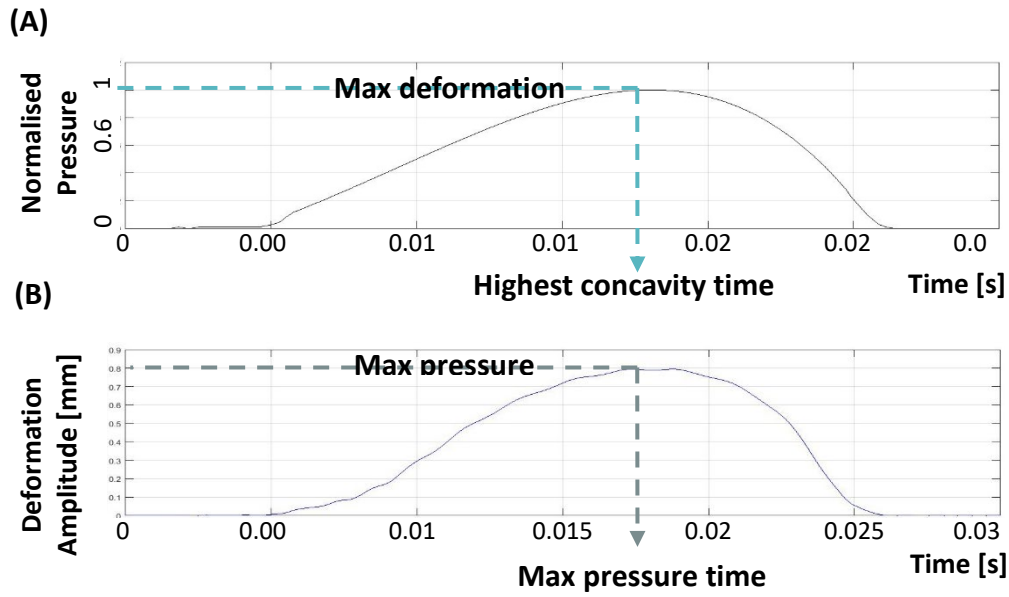


Figure 3-15 Progress of normalised air pressure (A) and nodal deformations at the corneal apex (B) with time. When air-puff pressure increases to a maximum, corneal apex deformation reaches its max value.

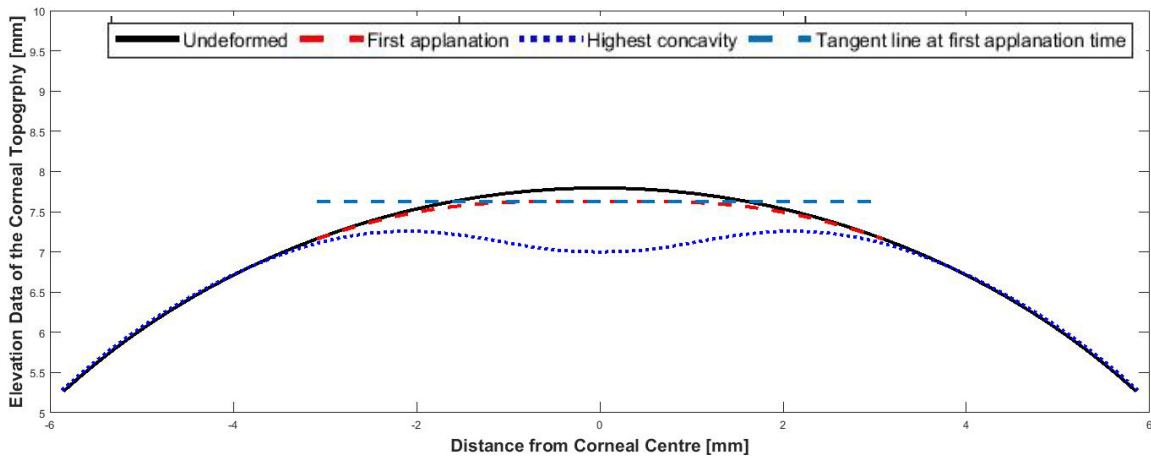


Figure 3-16 Corneal anterior profiles during air-puff loading

The two peaks of the cornea at HCT were defined using the point where the first partial derivatives were zero and the second partial derivatives were negative. Based on the two peaks of the cornea at HCT, the distance between two peaks (PD) was calculated. Subsequently, the radius of curvature of corneal concavity at HCT (R) was calculated by fitting it to a parabolic equation between two points at 1.53 mm from the corneal apex.

In terms of the time of the ongoing first applanation phase (the red line in Figure 3-16), the corneal edge profile data at different time points have fitted to a polynomial of a 10th degree by using the least-squares method and the second partial derivatives were shown in Figure 3-17). During the duration of the air-puff simulation, the location of the corneal apex changed from being at the highest point to its position at the lowest local point (under max corneal apex load) and from the lowest local point back to the highest point (under reduced apex load to zero).

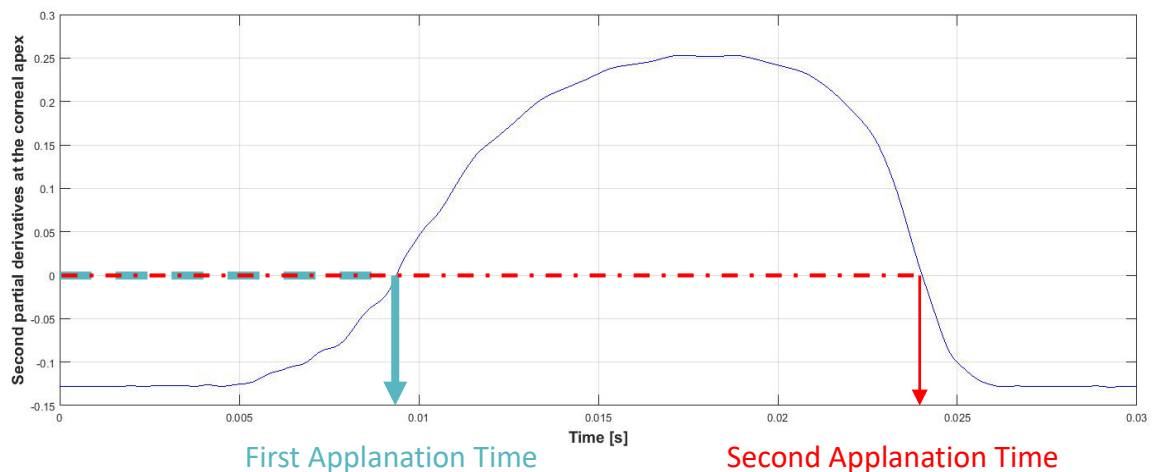


Figure 3-17 Second partial derivatives of corneal anterior edge with respect to time calculated at corneal apex

In Figure 3-17, values of the second partial derivatives of the corneal curve were zero at the first and second applanation time (APT1 and APT2). By using APT1, the corneal edge profile curve at APT1 can be defined. When the corneal surface is flattened, the slope of the tangent line through the flattened section is zero, resulting in the first partial derivatives of the corneal curve at APT1 being zero. The length of the flattened cornea is the sum of the distance which included points at the first partial derivatives of the corneal curve that were zero. Moreover, the boundary conditions of FEM are restricted to the model rotation and whole eye

movement. As a result of these conditions, the deflection is equal to deformation at each phase. The velocity at the corneal apex is equal to the value of the first derivative of corneal apex deformation with the time variable.

3.4.2 Comparisons between Clinical Data and Numerical Results

Comparisons of Corneal Deformation

To validate the performance of numerical models, their predictions were compared with clinical data. In this comparative study, IOP, CCT, and corneal material behaviour (related to age) of eye-specific models matched the parameters of four randomly selected healthy eyes, and the results were compared with a focus on corneal topography at first appplanation and the highest concavity point.

Comparisons of CorVis-ST Dynamic Response Parameters

The distribution of the main CorVis-ST dynamic corneal response parameters, as predicted numerically, were assessed to determine if their means were within the ranges expected clinically. In addition, in the numerical simulation, the input variables (as CCT, IOP and corneal material stiffness) was continuous, but the simulated input variables was only selected with groups from the grouping. As a result, the numerical results might provide biased predictions, which is difficult to compare their mean and STD between predicted numerically and expected clinically. Hence, a nonparametric statistical analysis was used to compare probability distributions of the dynamic corneal response parameters between numerical simulations and clinical measurements.

A nonparametric statistical analysis was performed to compare the predictions of these parameters with the clinical data. In the nonparametric statistical testing, a confidence interval (CI) provided an interval estimation to present the unknown population of these parameters. In this study, the numerical predictions of CorVis-ST dynamic response parameters were assumed to cover 95% of the population of these parameters clinically, when the ranges of IOP, CCT and corneal material properties in the numerical models covered their clinically expected ranges.

Comparisons of Age-matched Dynamic Response Parameters Obtained

Numerically and Clinically

Kolmogorov-Smirnov test (K-S test) was used to analyse CorVis-ST dynamic response parameters obtained from age-matched numerical and clinical data. The K-S test was used to decide whether age in healthy eyes was the only parameter that controls the material behaviour. Statistical analyses were performed using SPSS 24 (IBM, Armonk, NY).

In the healthy eyes' numerical datasets, some response parameters as deflection and applanation pressure were missing when the material configurations in ABAQUS became unstable and failed to converge because the characteristic of the incompressible material behaviour is more stringent on the control of volume changes. Hence, there were only 8 different material configurations with full IOP and CCT configurations in healthy numerical datasets

Eight different material configurations (based on Equation 3.2) in the healthy numerical datasets were shown in Table 3-10.

Table 3-10 Cases used in Kolmogorov-Smirnov statistical analysis of healthy numerical and clinical datasets

M_R	Age(M_R) [Years]	Total number of cases		Command*
		Numerical	Healthy clinical	
0.7	16	15	2	Ignored
0.8	28	15	13	Selected
0.9	38	15	9	Selected
1	48	15	12	Selected
1.1	56	15	3	Ignored
1.2	64	15	4	Ignored
1.3	71	15	6	Ignored
1.5	84	15	0	Ignored

*If the number of clinical data points was smaller than half the number of numerical data points, K-S analysis could not be performed.

In the statistical analysis, the healthy eyes' numerical dataset parameters were described by their mean, standard deviation, and range value. The results of the K-S test of these three groups (including M_R (Age)=0.8 (28), 0.9 (38), and 1 (48)) in normal numerical and healthy clinical datasets can help assess the population's homogeneity. When the p-value of any dynamic response parameter was smaller than 0.05, it indicated the age-related corneal material behaviour presented a significantly different distribution of CorVis-ST dynamic response parameters between numerical predictions and clinical outcomes. In other words, the differences in results among this study may have been due to individual difference changes in corneal biomechanical properties, despite their age-related effect.

3.5 Development of Algorithms to Estimate bIOP and Corneal Material Behaviour

Three numerical parameters, namely CCT, the ratio (M_R) of the Ogden coefficient μ with age variable based on the μ at age 50 and the true IOP (IOPt), were changed in the parametric study on healthy eyes and the models were analysed to estimate the CorVis-ST dynamic response parameters (P_{DCR}). The dilemma here is that to obtain material properties, the true IOP must be known and to obtain the true IOP, the correct material properties are required. To break this cycle, the true IOP ($IOPt$) was assumed to be a function of CCT, M_R , and P_{DCR} where M_R was expected to be strongly associated with the material behaviours and P_{DCR} was expected to be strongly associated with IOPt:

$$IOPt = f(CCT, M_R, P_{DCR}) \quad (3.3)$$

Following this strategy, material properties of the cornea were then assumed to be a function of CCT, $IOPt$, and P_{DCR} where P_{DCR} was expected to be strongly associated with the material behaviours:

$$M_R = f(CCT, IOP_t, P_{DCR}) \quad (3.4)$$

This process was followed for both healthy and KC eyes, but with slight variations. In healthy eyes the material properties were assumed to mainly dependent on age, as was established experimentally [1, 70]. This could allow the development of an Equation for estimating the true IOP based on age. However, the KC eyes, as it is known that the material properties have changed with disease progression, age could not be used as an indication of correct material behaviour. For this reason, in KC eyes, the material properties were estimated first, followed

by the estimation of true IOP, Figure 3-18.

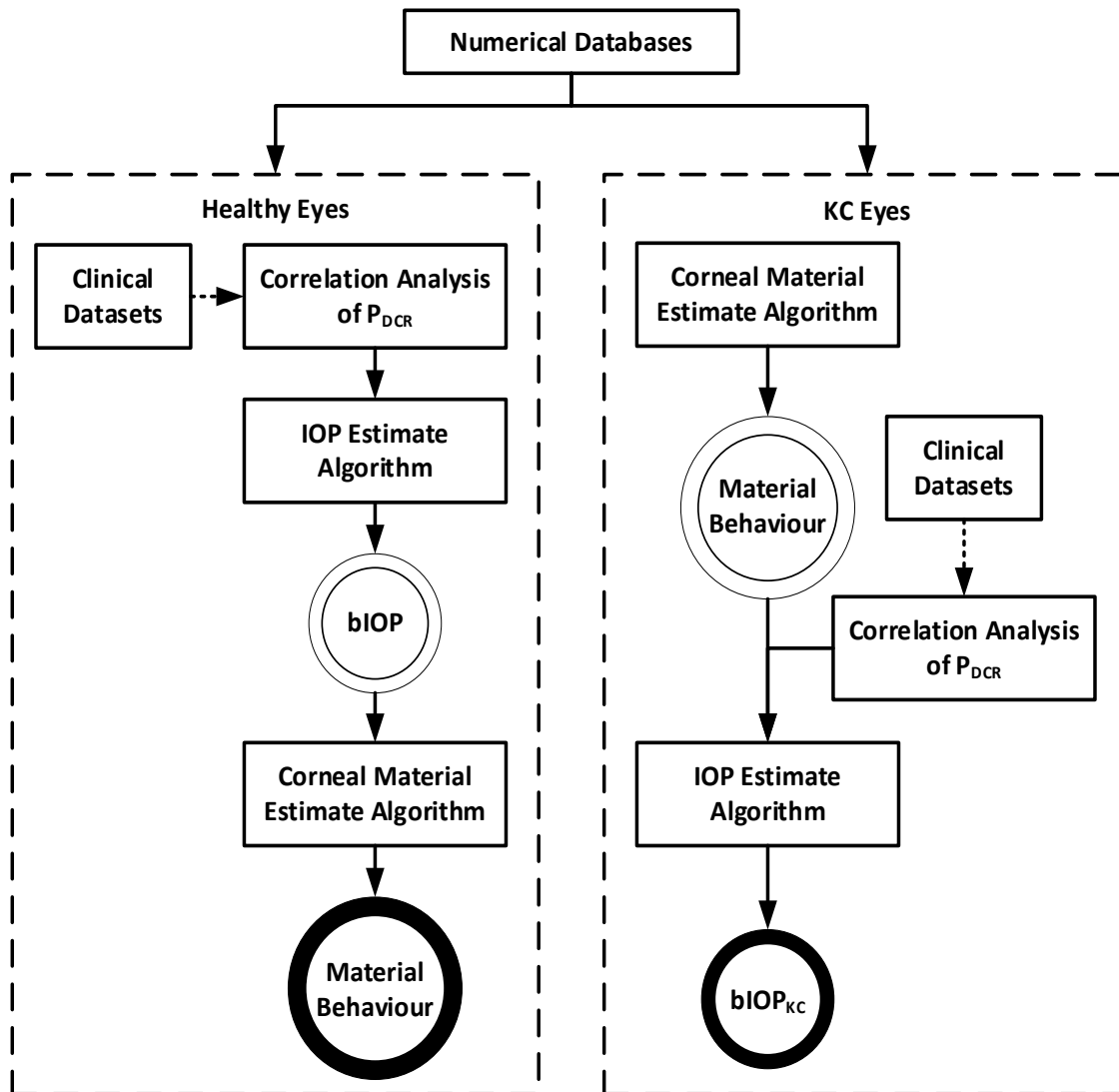


Figure 3-18 Flowchart of procedure for developing algorithms to estimate IOP and corneal material behaviour in healthy and KC eyes

3.5.1 Development of Algorithms to Estimate IOP and Corneal Material Behaviour in Healthy Eyes

In the clinical datasets, the dynamic response parameters (P_{DCR}) obtained from the CorVis-ST related to the IOP reading measured by the CorVis-ST (CVS-IOP), CCT, and Age [46], [254],

[345], [346]. In addition, the ocular tissue's mechanical behaviour is related to age [79], [91], [93]. This means that the dynamic response parameters will be a function of CVS-IOP, CCT, and corneal material stiffness. Hence, in the parametric study on healthy eyes, the numerical database took IOPt, CCT, M_R as an independent input variable and P_{DCR} provided from the numerical simulation as output variable, thus the P_{DCR} was assumed to be a function of IOPt, CCT, and M_R . By analysing the correlation between input variables (as IOPt, CCT, and M_R) and output variables (as P_{DCR}), relations between input variables and output variables were defined. Once the relations between P_{DCR} and IOPt, P_{DCR} and CCT, P_{DCR} and M_R were defined, the P_{DCR} with highly correlating with the IOPt and lowly correlating with CCT and M_R was used to develop a biomechanically-corrected IOP algorithm to reduce the effect of CCT and corneal material stiffness on the IOP estimation. On the other hand, the corneal material estimated algorithm was developed by using P_{DCR} with higher correlation with M_R and lower with CCT and IOPt to reduce the effect of IOP and CCT on the corneal material behaviour estimation.

The procedures to develop IOP and corneal material estimate in healthy eyes was divided into three stages:

- Correlation analysis of the dynamic response parameters (P_{DCR}) against IOPt, CCT and M_R in the numerical database to evaluate the effect of IOPt, CCT and M_R on the dynamic response parameters for determining which dynamic response parameter will be used to develop biomechanically-corrected IOP and corneal material estimated algorithm;
- Correlation analysis of the dynamic response parameters against IOP measurement obtained from the CorVis-ST (CVS-IOP), CCT, and Age in the clinical datasets to evaluate the effect of CVS-IOP, CCT, and Age (related to the corneal material stiffness) in the clinical datasets for comparison of the results of correlation analysis from numerical

database to validate the selected dynamic response parameters using in the biomechanically-corrected IOP and the corneal material estimated algorithm.;

- Development of a biomechanically-corrected IOP algorithm relating true IOP to CCT, M_R and highly correlating CorVis-ST parameters to reduce the effect of CCT and corneal material stiffness on the IOP estimation;
- Development of an algorithm relating corneal material properties to IOPT, CCT, and highly correlated CorVis-ST parameters to reduce the effect of IOPT and CCT on the corneal material behaviour estimation.

Correlation Analysis of Dynamic Response Parameters in Healthy Eyes

According to the hypothesis of the IOP estimation algorithm, it is important to decide which P_{DCR} can be used in the algorithm through the correlation analysis. Regarding the normal cornea, owing to the consideration of the difference in the data distribution between the clinical and numerical datasets, a correlation analysis of the dynamic response parameters with the CCT, IOP and age/ M_R (due to its association with corneal material stiffness) was conducted.

As the relationships between P_{DCR} , CCT, IOP and corneal material stiffness are unknown, the correlation analysis was done using the most common correlation method in statistics which is Person Product Moment Correlation (PPMC). In the PPMC results, the Person's correlation coefficient (r) value shows the degree of the correlation between two variables, and the p -value is used to measure the 'significance' of the relationship when it is lower than 0.05. Hence, the relation between P_{DCR} , IOP, CCT and corneal material stiffness were defined.

The P_{DCR} with highly correlated IOP and lowly correlated CCT and corneal material stiffness

(age/M_R) were denoted as P_{bIOP}. The P_{bIOP} was then used to develop the IOP algorithm for the normal cornea. Then If the algorithm still correlated highly with CCT or corneal material stiffness in the clinical datasets or sufficiently accurate in numerical database (root-mean-square error > 2 mmHg), another parameter with a stronger association to CCT or age/M_R would be added into the algorithm to correct for the effect of CCT or corneal material properties on the IOP estimation.

Estimation Algorithm for Intraocular Pressure for Healthy Eyes

According to the results of the correlation analysis based on the numerical and clinical datasets, P_{bIOP} was included in the development of the IOP algorithm (bIOP) for healthy eyes:

$$bIOP = f(CCT, Age, P_{bIOP}) \quad [For\ normal\ cornea](3.5)$$

As IOP_t, CCT, and Age are independent variables, the algorithm can take the form:

$$bIOP = f_1(CCT)f_2(Age)f_3(P_{bIOP}) \quad [For\ normal\ cornea](3.6)$$

The work started with determining the lowest possible degree of each factor before optimising to find the value of the coefficients give the minimum error between the target value (IOP_t) and estimation value (Predicted IOP) using the least-squares method:

$$\min_x \|F(x, xdata)\|_2^2 = \min_x \sum_i (F(x, xdata_i) - ydata_i)^2 \quad (3.7)$$

Where $xdata$ is input data, and $ydata$ is the observed output, and $F(x, xdata)$ is a matrix-valued or vector-valued function of the same size as $ydata$.

Development of an Estimation Algorithm for Corneal Material Behaviour for Healthy Eyes

The age-related stiffening obtained from earlier ex-vivo experiments [70, 71, 79, 84, 85] was denoted a material ratio “ M_R ” in this study. This parameter presented a comparison of stiffness in relation to the behaviour at age 50. In addition, this parameter could be developed because earlier results showed that the stress-strain curve for different ages did not cross each other, Figure 3-11. The results showed that the gradient of the curves at any stress level varied depending on age while the non-linearity of the curves remained almost unchanged, Figure 3-19.

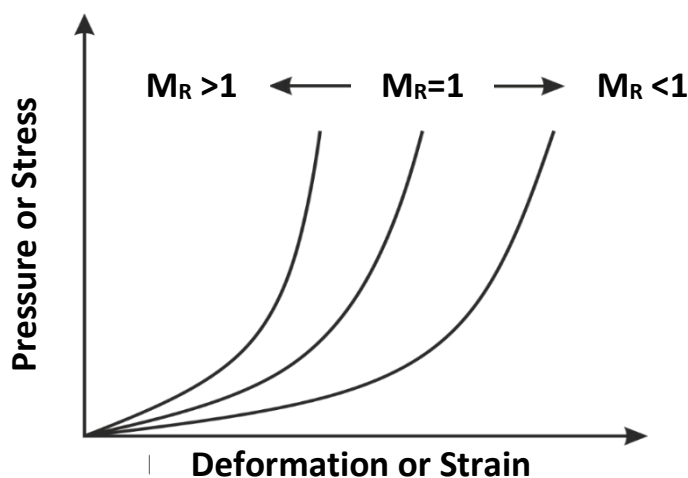


Figure 3-19 Comparison of the effect of M_R value on the loading-deformation and stress-strain behaviour

This observation is important as it allowed determination of the full stress-strain relationship instead of a tangent module (E_t) at certain stress and strain. Similar to Equation 3.3 for $IOPT_t$, an algorithm to estimate corneal material behaviour (β) can take the form:

$$\beta = f(CCT, IOPT_t, P_{DCR}) \quad [For normal cornea](3.8)$$

The only CorVis parameter that is strongly correlated with the material behaviour (i.e. P_{DCR}) was the stiffness parameter (SP), which is defined as the resultant pressure at first appplanation divided by corneal deflection at highest concavity, developed in an earlier study [201]. The stiffness parameter at the highest concavity (SP-HC) is defined as the resultant pressure at first appplanation ($A1$), divided by the difference in corneal deflection between first appplanation ($A1Deflection$) and highest concavity ($HCDeflection$), Equation 3.9 [201].

In Equation 3.9,

$$SP-HC = \frac{AP1 - IOP_t}{Deflection_{max} - Deflection_{A1}} \quad (3.9)$$

Where $AP1$ is the first appplanation pressure measured at the device's piston; $Deflection_{max}$ is the deflection amplitude at the corneal apex; $Deflection_{A1}$ is the deflection amplitude of cornea at first appplanation; and IOP_t is the true IOP value, which can be replaced by bIOP [201].

Healthy eyes are expected to have greater resistance to deflection than KC eyes, and there is evidence that SP-HC was higher for healthy eyes than KC ones [33, 37, 121, 137, 172, 173, 175, 176]. Therefore, the relationship of M_R takes the form:

$$M_R = f(CCT, IOP_t, SP-HC) \quad (3.10)$$

Values of M_R in a 3D space covering wide ranges of CCT, IOP_t and SP-HC were shown in Figure 3-20. The figure showed an association between CCT and SP-HC, and between IOP_t and SP-HC, as expected for an overall stiffness parameter. But a large variation of these parameters led to a large error on the fitting. Hence, the IOP and CCT values were divided by the mean of these parameters in the numerical datasets (as 545 μm and 20 mmHg), and the SP-HC value was applied using the natural logarithm to reduce essentially the error for predicting the

material parameter (β). Following the process, these surfaces were presented by polynomial equations related to IOP/20, CCT/545 and Ln(SP-HC), and each surface represented one material behaviour(M_R), Figure 3-20(B). Therefore, the algorithm to estimate β takes the form:

$$\beta = f(CCT, IOP_t, Ln(SP-HC)) \quad (3.11)$$

As IOPt, CCT, M_R are independent variables, the relationship between IOPt, CCT, and Ln(SP-HC) for each M_R can take the form:

$$M_R = \{Ln(SP-HC)|f(CCT, IOP_t)\} \quad (3.12)$$

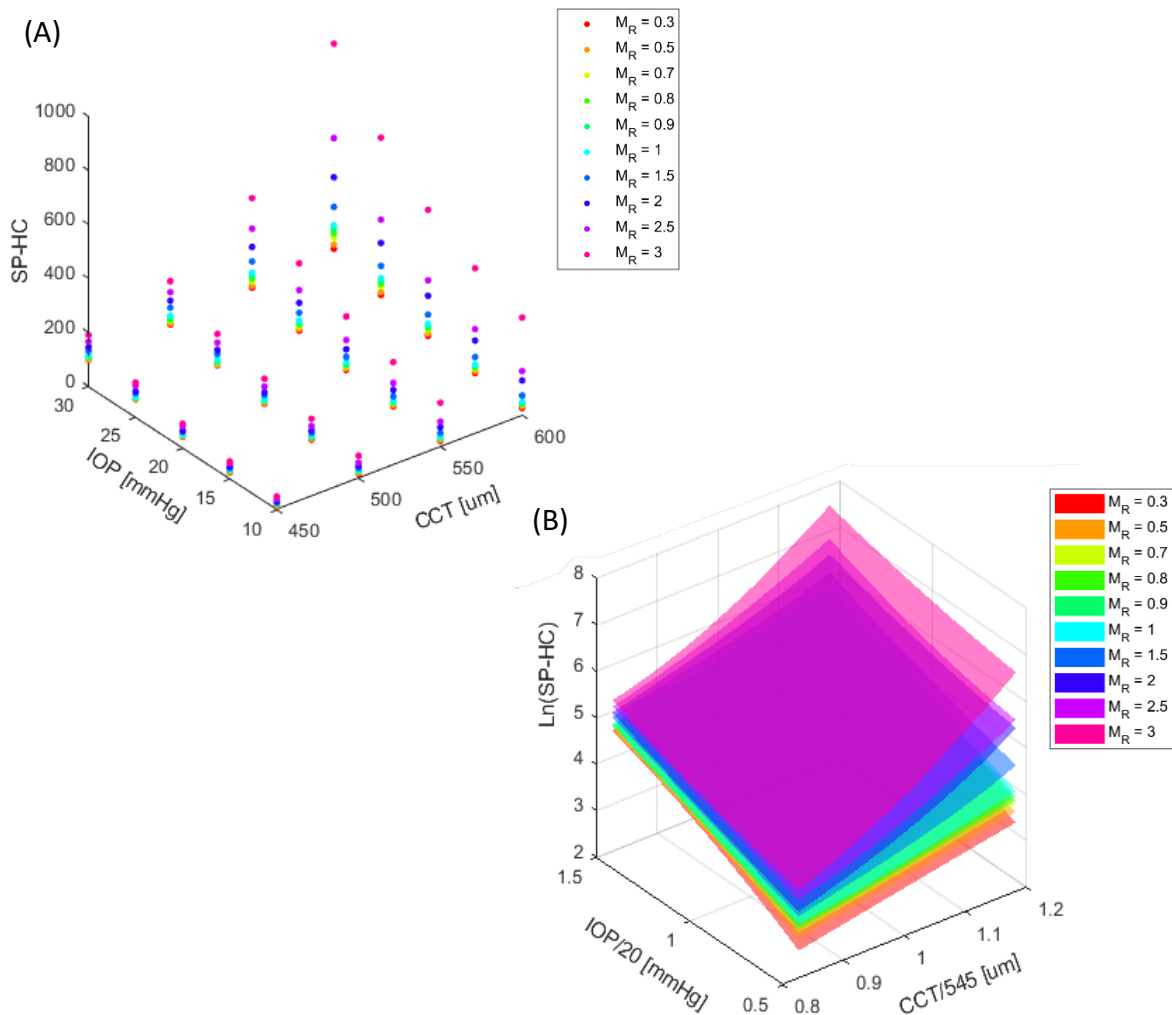


Figure 3-20 (A) 3D point cloud plot and (B) surface plot of corneal stiffness parameter against IOP and CCT for different M_R values

According to Equation 3.12, specific values of $\text{Ln}(\text{SP-HC})$ from each M_R were estimated based on the specific IOPt and CCT, Figure 3-21. Based on the relationship between M_R and $\text{Ln}(\text{SP-HC})$, the β was estimated by using cubic interpolation based on the specific $\text{Ln}(\text{SP-HC})$.

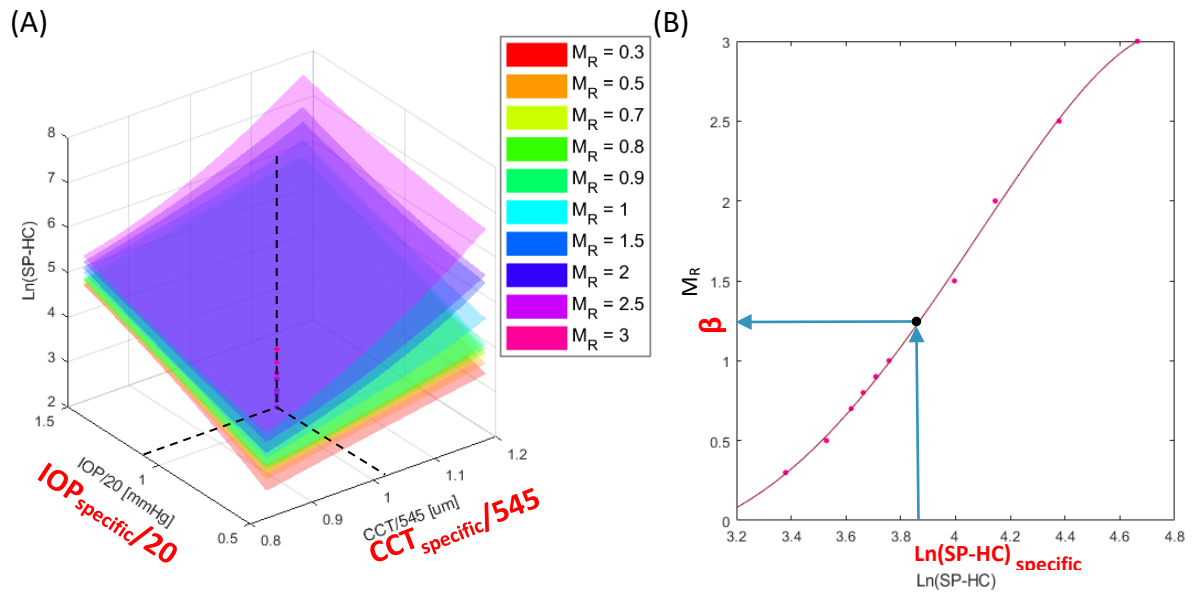


Figure 3-21 The process of corneal material estimation. (A) When specific values of CCT ($\text{CCT}_{\text{specific}}$) and IOP ($\text{IOP}_{\text{specific}}$) are applied in the SP-HC surface plot, there are several estimates for SP-HC for different M_R . (B) When these estimates are plotted, β can be estimated using the corresponding SP-HC ($\text{Ln}(\text{SP-HC})_{\text{specific}}$).

In the clinical dataset, all required parameters (as CCT, AP1, A1Deflection and HCDeflection) obtained from the CorVis-ST device. Upon development of bIOP Equation, it was found to be more reliable and closer to the true IOP values [244]. Hence bIOP was used in Equation 3.11. Following the above-mentioned process, the β healthy could be calculated using CCT, bIOP, and SP-HC value.

3.5.2 Development of Algorithms to Estimate IOP and Corneal Material Behaviour in Keratoconic Eyes

The procedure of development of the IOP & corneal material estimate algorithms for KC eyes with a slight variation was done in three stages:

- Correlation analysis of the dynamic response parameters against IOP, CCT, Age/ M_R and corneal topography parameter (TopoR)
- Development of an algorithm relating KC corneal material properties to IOP, CCT, and highly correlated CorVis-ST parameters
- Development of an algorithm relating true IOP to CCT, M_R , TopoR and highly correlated CorVis-ST parameters

Since on healthy patients, age could be used as a reliable indication of material behaviour to calculate true IOP, but, in KC eyes, the material properties have altered and age couldn't be reliably used to estimate IOP nor corneal material behaviour. Hence, the process was changed to begin estimating the corneal material behaviour, and then proceed to estimate the IOP.

Correlation Analysis of Dynamic Response Parameters in Keratoconic Eyes

Similar procedure as healthy was followed to obtain highly correlated parameters (P_{DCR}) with both IOP and material properties. In this case, CVS-IOP is the only indication of the IOP for KC eyes. Therefore, clinical datasets were used to conduct the correlation analysis of CVS-IOP with the CCT and P_{DCR} . The correlation analysis showed a significant correlation between thickness and CVS-IOP and the relationship between the P_{DCR} and CVS-IOP. These are used to correct the differences between the CVS-IOP and true IOP for material estimation. Then,

clinical datasets (used in Section 3.2) and numerical datasets were used to conduct the correlation analysis of the dynamic response parameters with the CCT, IOP, age/ M_R (due to its association with corneal material stiffness), and corneal topography (TopoR). These parameters were denoted as $P_{bIOP_{KC}}$. The $P_{bIOP_{KC}}$ was then used to develop the IOP algorithm for the keratoconic cornea.

Development of an Estimation Algorithm for Corneal Material Behaviour for Keratoconic Eyes

As mentioned, the stiffness parameter at the highest concavity (SP-HC) is lower in KC eyes than in healthy eyes [201]. Similar to Equation 3.10 for the corneal material behaviour in healthy eyes, the corneal material behaviours in KC eyes was assumed to be a function of numerically found CCT, IOP_t, SP-HC and corneal geometry factor (TopoR):

$$M_R = f(CCT, IOP_t, TopoR, SP-HC) \quad [For\ abnormal\ cornea](3.13)$$

Following the same process in Section 3.5.1, values of M_R in a 3D space covering a wide range of CCT/545, IOP_t/20, Ln(SP-HC) and five different abnormal corneal topography were shown in Figure 3-22.

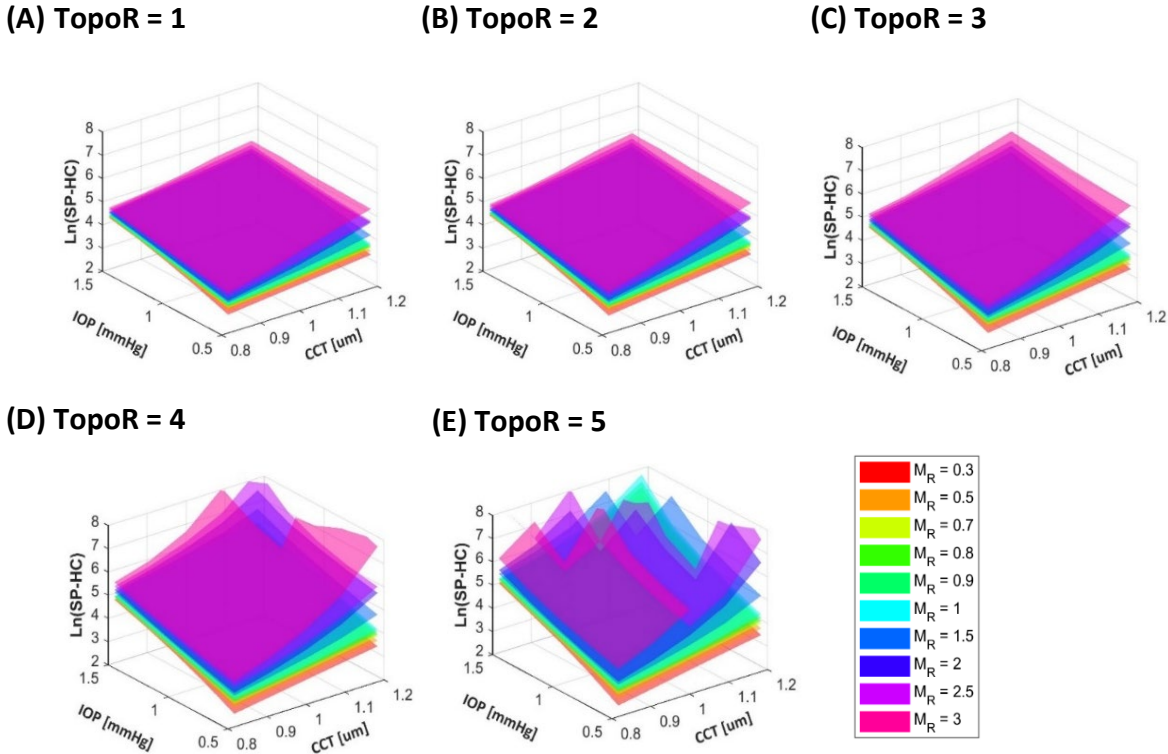


Figure 3-22 3D surface plots of stiffness parameter against IOP/20 and CCT/545 for different TopoR. Every surface corresponds to a specific value of M_R .

Based on the assumption that the only available parameter that indicates IOP in clinical data is CVS-IOP in KC eyes, an algorithm to estimate corneal material behaviours (β) for KC eyes can take the form:

$$\beta = f(CCT, CVS-IOP, Ln(SP-HC)) \quad [For\ abnormal\ cornea](3.14)$$

Estimation Algorithm for Intraocular Pressure for Keratoconic Eyes

After estimating the corneal material behaviours for KC eyes and by considering the corneal geometry effect and the results of the correlation analysis of the numerical and clinical data, an algorithm to estimate IOP ($bIOP_{KC}$) for KC eyes can take the form:

$$bIOP_{KC} = f_1(CCT)f_2(\beta)f_3(TopoR)f_3(P_{bIOP_{KC}}) \quad [For\ abnormal\ cornea](3.19)$$

3.6 Validation of Intraocular Pressure

Intraocular pressure (IOP) measurement is an essential part of the eye examination and is required to risk profile and manage Glaucoma. The reference standard tonometer used in clinics to measure IOP is the Goldmann Applanation Tonometry (GAT)³⁸. Therefore, the validation of the bIOP against GAT is important to demonstrate the feasibility and accuracy of this algorithm in clinical datasets. The evidence required in clinical datasets is a reduced correlation of bIOP values against CCT and age (Figure 3-23). On the other hand, as the true IOP is not known in clinical data, an ex vivo human eye experiment was conducted to assess the reliability of the bIOP in laboratory conditions.

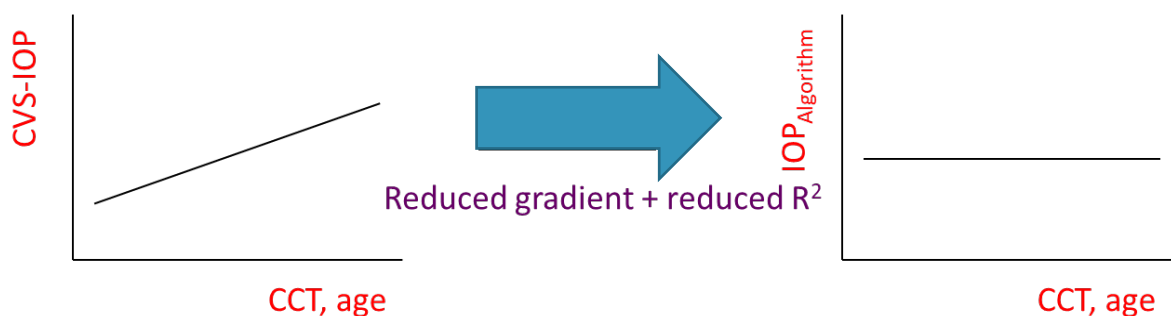


Figure 3-23 Expected results of correlation analysis of IOP with CCT and Age in clinical datasets

3.6.1 Validation of bIOP Using Healthy Ex Vivo Human Eye Experiments

This study was designed to determine the effectiveness of the CorVis ST bIOP algorithm in eliminating, or significantly reducing, the effect of biomechanics parameter variation on IOP estimates using ex-vivo human eye globes, in which the IOP was controlled and then measured with the CorVis ST (more detail of ex-vivo experiment procedure shown in Appendix B).

Donor Eye Details

Five ex-vivo human ocular globes (age 69 ± 3 years) were obtained from the Fondazione Banca degli Occhi del Veneto Onlus, Venice, Italy, and tested within 3-5 days post mortem. Ethical approval to use the specimens in research was obtained by the eye bank in accordance with the Declaration of Helsinki. The central corneal thickness (CCT) was measured using a DGH 55 Pachmate pachymeter (DGH Technology, Exton, USA). After removing the extraocular tissues, a G14 needle was inserted through the posterior pole, glued around the insertion point to prevent leakage, and used to remove the vitreous. The inside of the globe was washed with Phosphate Buffered Saline (PBS, P4417, Sigma-Aldrich, Darmstadt, Germany) a few times until a smooth movement of fluid was achieved through the needle and a syringe connected to it. The eye was then injected with a 10% Dextran solution (Sigma-Aldrich, Darmstadt, Germany) to prevent swelling during the experiment, before fitting it inside the test rig. Throughout these steps, the eye was kept moist using Everclear; a viscous tear film supplement (Melleson Pharma, Breda, Netherlands) to prevent drying.

Ex vivo Human Eye Testing Process

A custom-built inflation rig was used in the study to control the IOP in ex-vivo eye globes and measure it with the CorVis ST, Figure 3-25 and Figure 3-24. The rig included a support mechanism for the eye to allow it to sit in its natural position with the cornea horizontally facing the CorVis ST while preventing both vertical and horizontal rigid-body motion. Inside the horizontal support, a skin-safe, soft silicone rubber padding (Ecoflex® Series, Smooth-On, Pennsylvania, USA.) was placed to simulate the effect of fatty tissue around the eye.

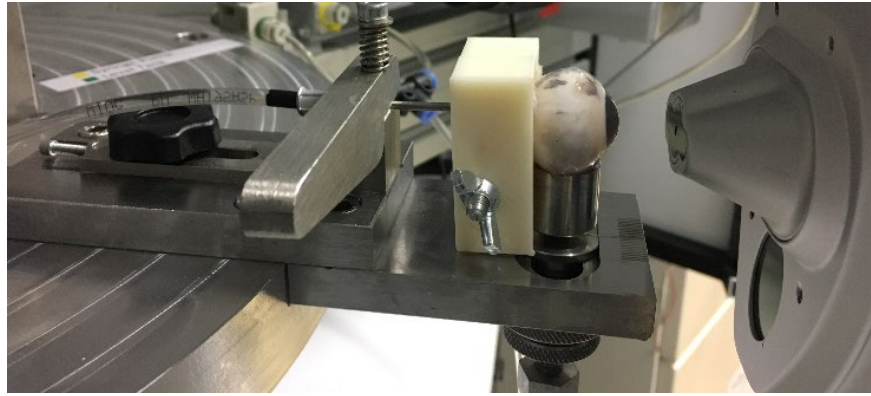


Figure 3-24 Test rig showing eye sitting on a rigid support and supported from the back while being connected to a syringe pump that controls its IOP. CorVis ST is placed at a distance to enable its automatic trigger.

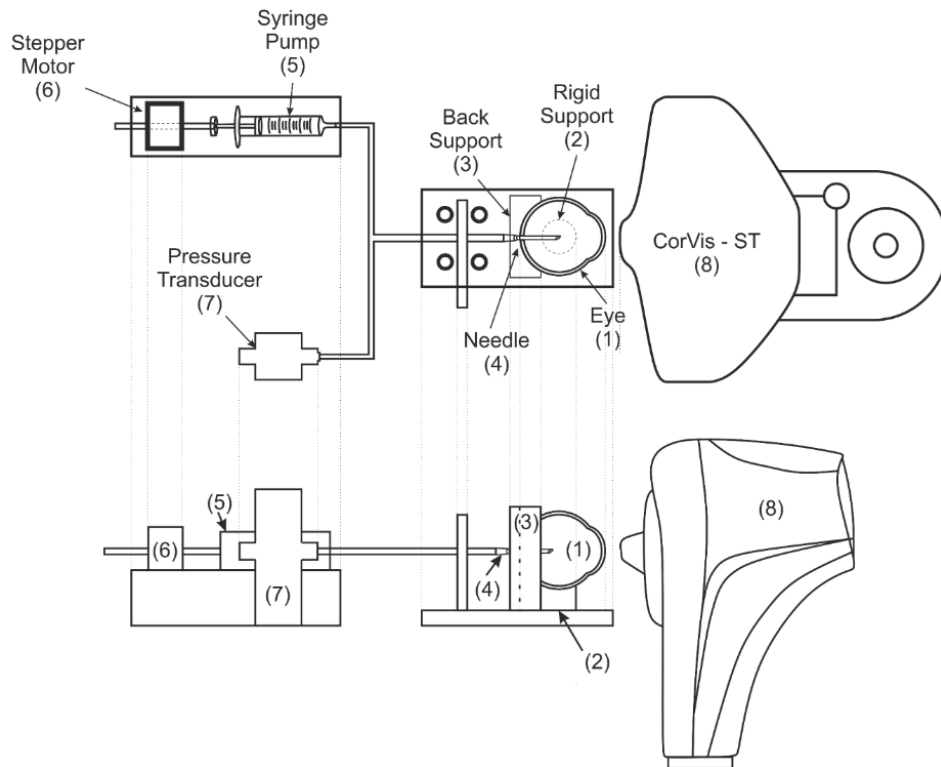


Figure 3-25 Schematic views of inflation test rig showing an ex-vivo eye [1] sitting on rigid support [2], which provided restraint against the vertical motion, and soft back support [3] that provided flexible restraint against the horizontal motion. The eye has a G14 needle [4] inserted through the posterior pole and connected to a syringe pump [5] to control the intraocular pressure using a stepper motor [6]. The needle is also connected to a pressure transducer [7] to measure the pressure inside the eye. The CorVis ST [8] is used to provide estimates of IOP through the application of an air puff.

The needle that had been inserted through the posterior pole was connected to a 4mm diameter tube attached to a syringe pump, which was controlled using bespoke LabVIEW software. The pressure applied through the syringe pump on the inside of the globe was monitored using an FDW pressure transducer (RDP Electronics, Wolverhampton, UK) fixed at the same horizontal level as the centre of the eye to avoid pressure head differences. The readings of the pressure transducer were assumed to represent the true IOP (IOPt) acting on the eye globe. IOPt was controlled to vary between values that covered the natural variation in IOP seen in ophthalmic practice; 10, 15, 20, 25 and 30 mmHg. These variations were introduced through the movement of a stepper motor connected to the syringe pump. After reaching each IOPt level, the eye was allowed to stabilise for 60 seconds (Appendix B.5) before measuring IOP using the CorVis ST, which provided an uncorrected measurement (CVS-IOP) and a biomechanically-corrected measurement (bIOP). CorVis ST measurements, which included CCT, were taken at each IOPt level until at least three readings of acceptable quality were achieved. Acceptable quality was in reference to the CorVis ST built-in standards in assessing a reading, and as part of this assessment, the device could trace and record fully the deformation profiles of the cornea during the application cycle of air puff. At least 120 seconds were allowed between successive CorVis measurements at the same IOPt that should enable the cornea to recover fully from the distortion caused by previous air puffs.

Statistical Analysis

Statistical analyses were performed on IBM SPSS version 24. The five acceptable in total 20 times CorVis-ST readings of bIOP and CVS-IOP were averaged and compared with the true IOP (IOPt) measured with the pressure transducer. After a normality analysis, the one-way ANOVA and Bonferroni Post-Hoc analysis was performed to compare the mean differences followed

by Pearson correlations used to assess the association of both bIOP and CVS-IOP with CCT and IOPt. p-values of less than 0.05 were considered indicative of statistical significance.

3.6.2 Validation of bIOP using In-Vivo Clinical Data

To evaluate the effectiveness of this algorithm for healthy and pathological eyes, three independent clinical databases were obtained from Smile Eyes Clinics (SEC), Germany; Humanitas Clinical and Research Center (HCRC), Italy; and Wenzhou Medical University (WMU), China (Table 3-11). These were used to provide estimates of the IOP. In the SEC dataset, 632 eyes were sampled from healthy participants who displayed no pathological conditions. In the HCRC dataset, 1047 eyes with pathological conditions (astigmatism, cataract, myopia, hyperopia, Emmet ropy, and retinopathy) were sampled. In the WMU dataset, however, all patients signed written informed consent. The studies were approved by their local institutional review boards and adhered to the tenets of the Declaration of Helsinki.

Table 3-11 Details of clinical databases

Database	Patients	CCT (μm)	Age (years)	CVS-IOP (mmHg)
<i>Smile Eyes Clinics</i>	632	537 \pm 42	40 \pm 12	14.5 \pm 2.8
<i>Humanitas Clinical and Research Center</i>	1047	525 \pm 38	46 \pm 18	14.1 \pm 3.5
<i>Wenzhou Medical University</i>	912	583 \pm 30	45 \pm 17	14.56 \pm 3.1

All datasets were plotted to study the correlation of IOP value (as IOP measurement and IOP_{Algorithms}) with CCT and age. The trend lines have been plotted and the Equations have been defined in Figures. The IOP algorithms, if successful, can reduce association (as slope and R²) between IOP and CCT or age.

3.6.3 Thickness Effects on the Estimation of IOP Using Clinical Data

IOP measurements by Goldmann Applanation Tonometry (GAT-IOP) are known to be significantly affected by CCT. This is because the GAT-IOP underestimates the IOP in eyes with thin corneas and overestimates IOP in eyes with thick corneas [210, 245]. In order to assess this, the corneas that were reduced in thickness after refractive surgeries, such as laser-assisted in situ keratomileusis (LASIK) and small-incision lenticule extraction (SMILE), were used to evaluate the effectiveness of bIOP algorithm by comparing pre and post-operative IOP estimates.

Clinical Datasets

A total of 48 patients (69 eyes) were treated for correcting myopia or myopic astigmatism at the Smile Eye Clinic, Munich, Germany. The inclusion criteria were myopia of fewer than 10 diopters (D), and/or astigmatism of less than 5D and a spherical equivalent (SE) greater than 1D but less than 10D. Patients with CCT less than 480 μ m or abnormal corneal topography, patients with Glaucoma, Glaucoma suspects, and patients receiving IOP-lowering medications were excluded from the study. Some of the CorVist St parameters were missing CorVis-ST in the case of some participants. A total of thirty-six patients treated with LASIK (14 patients, 20 eyes) or SMILE (22 patients, 30 eyes) were included in this retrospective case series. The study was thoroughly discussed with each patient, and informed consent was obtained from all participants. The study was approved by the local institutional review board and adhered to the tenets of the "Declaration of Helsinki". After detailed explanations to individual patients, they could freely choose whether they wanted to be treated with LASIK or SMILE.

Preoperative and postoperative (1–3 months) evaluation included slit lamp biomicroscopy of

the anterior and posterior segments, objective and manifest visual acuity, Goldmann Applanation Tonometry (GAT-IOP), Pentacam (Oculus Optikgeräte GmbH, Wetzlar, Germany) tomography, and CorVis-ST IOP measurements (CVS-IOP). All measurements with the CorVis-ST were taken by the same experienced technicians and captured using an automatic release to ensure the absence of user dependency. Only CorVis-ST exams with a quality score of “OK” were included in the analysis.

Surgical Techniques

All surgical procedures were performed by an experienced surgeon (RW). After assessing the target refraction, patients received 2 drops of topical anesthesia (Conjuncain-EDO®, Dr. Gehard Mann GmbH) and underwent periocular disinfection with povidon-iodine 10%. After standard sterile draping and insertion of the speculum, patients in the femtosecond LASIK group were treated with VisuMax® (Carl Zeiss Meditec, Jena, Germany) for flap creation and afterwards, treated with the Mel 80™ excimer laser (Carl Zeiss Meditec, Jena, Germany). After opening the corneal flap, an ultrasound pachymeter (Pachymeter SP-100, Tomey, Japan) was used to measure the remaining corneal thickness of the exposed stroma before and after ablation. On the other hand, patients receiving ReLEx SMILE were treated with VisuMax® only. The ReLEx SMILE technique was performed as described by Sekundo et al. [245] and Shah et al. [246]

The following settings were used for the femtosecond laser flap creation: Flap diameter 8.4–8.5 mm; optical zone 6.5–6.75 mm; and flap thickness 110 µm. For ReLEx SMILE, the following settings were used: Cap diameter 7.9 mm; optical zone 6.25–6.5 mm; and cap thickness 100 µm. The flap and cap thicknesses between the two groups were consciously not set equally in

order to follow the standard surgical parameters usually used in the clinical setting. Lenticule thickness was obtained from the VisuMax® SMILE planning software readout. Postoperatively, patients received polymyxin/neomycin/dexamethasone eye-drops four times a day (Isopto-Max, Alcon) for 5 days. Artificial tear supplements were prescribed for 4 weeks, starting hourly the first week, thereafter being reduced as required.

Statistical Analysis

Statistical analyses were performed using SPSS 24 (IBM, Armonk, NY). All IOP reading in these datasets has been confirmed to be the normal distribution in an earlier study [247]. The independent samples t-test was used to compare the LASIK and SMILE groups in order to determine whether there was any significant difference in the preoperative conditions. The relationship of GAT-IOP, CVS-IOP, and bIOP with CCT were assessed using Pearson's correlation analysis, and an analysis of the pre- and post-operative IOP values were conducted using the Paired t-test.

3.7 Validation of Intraocular Pressure Estimation for Patients with Keratoconus

Several studies in the literature demonstrated that the corneal thickness changes with Keratoconus [119, 139, 140], along with a reduction in corneal material stiffness [33, 37]. Normally, Keratoconic patients have thinner, steeper, and softer corneas, which poses a challenge to getting an accurate IOP measurement owing to these situations nonconformity with most of the GAT assumptions [32, 248]. As a consequence, several studies have attempted to find the best instrument to estimate IOP in Keratoconic patients [248-251].

The bIOP algorithms in this study were developed using the finite element simulations, which considered the anterior and posterior topographies of the eye using clinical data. The IOP estimated algorithms were able to consider all the changes in corneal biomechanics in Keratoconic patients. However, validating bIOP for KC patients can demonstrate its effectiveness in correcting corneal factors pertaining to IOP measurement errors.

3.7.1 Clinical Datasets

This multicentre retrospective study included 722 patients, who were enrolled in two hospitals situated in two different countries in order to include variability from more than one continent. Dataset 1 included 315 subjects (164 healthy and 151 Keratoconic) from the Vincieye Clinic in Milan, Italy, while Dataset 2 originated from the Rio de Janeiro Corneal Tomography and Biomechanics Study Group – Rio de Janeiro, Brazil – with a total of 407 participants (205 healthy and 202 Keratoconic). The Institutional Review Board (IRB) stated that approval was not obligatory for this record review study. However, the ethical standards set by the Declaration of Helsinki in 1964 and revised in 2000 were observed. All patients provided informed consent before their data was used in the study. Complete ophthalmic examination was performed on all patients, including the CorVis-ST and Pentacam (OCULUS Optikgeräte GmbH; Wetzlar, Germany) exams.

The inclusion criterion for the Keratoconic groups was the presence of bilateral Keratoconus, without a history of having had any former ocular surgeries, such as corneal collagen cross-linking or intracorneal rings. For healthy subjects, the inclusion criteria included a Belin/Ambrósio Enhanced Ectasia total deviation index (BAD-D) of less than 1.6 standard deviation (SD) from normative values in both eyes [252], no previous ocular surgery or disease,

a myopia of less than 10 D, and no concurrent or previous Glaucoma or hypotonic therapies. Moreover, to confirm the diagnosis, all examinations from each clinic were blindly re-evaluated by a corneal expert at the other clinic. Age matching between healthy and KC subjects within each database was not carried out during this study, as there was no evidence in the literature to suggest the dependence of IOP on age [253, 254].

Only CorVis-ST exams with good quality scores (QS) that enabled calculation of all DCRs were included in the analysis. All measurements with the CorVis-ST were acquired by the same experienced technicians using the automatic release to guarantee the absence of user dependency. Furthermore, an additional manual frame-by-frame evaluation of the exams, made by an independent masked examiner, was implemented to ensure the quality of each acquired measurement. Only one eye per patient was randomly included in the analysis to avoid the bias of relationships between bilateral eyes that could influence the analysis results.

Further evaluation of the IOP estimation algorithms for abnormal corneal material behaviour was carried out by considering their effectiveness in Keratoconic eyes with different stages of the disease. For this purpose, the KC datasets were divided into three groups each – mild, moderate, and advanced – based on the Topographic Keratoconus Classification (TKC) provided by the Pentacam [255]. According to this classification, mild Keratoconus was defined with a TKC classification of “Abnormal”, “Possible”, and “1”; moderate Keratoconus included TKC grades “1–2”, “2”, and “2–3”; and advanced Keratoconus included TKC grades “3”, “3–PMD”, “3–4”, and “4”.

3.7.2 Statistical Analysis

The statistical analysis was conducted using IBM SPSS Statistics 24. Before starting the analysis, the data were divided into two groups (Dataset 1-Milan and Dataset 2-Rio) and each group was further divided into two sub-groups (healthy and KC). Since the data was not expected to be normally distributed and healthy and KC groups were completely independent of each other, nonparametric Mann-Whitney U and Kruskal-Wallis tests were performed to compare the differences between various groups with regard to CCT, age, CorVis IOP, and bIOP (bIOP for healthy and bIOP_{kc} for keratoconus). The ANOVA's test was also used to assess the differences in variance in patients with KC using the two IOP estimates (bIOP, bIOP_{kc} and CorVis IOP).

3.8 In-Vivo Validation of Corneal Material Algorithm(β)

Many studies attempted to discover and characterise the mechanical properties of the cornea. There are several studies in the existing pool of literature concerning the biomechanics of the cornea defined by using three ex vivo methods – tension [33, 47, 50, 51], inflation [53, 71-73], and the compression test [75] – which are based on the relationship between loading and displacement. In addition to ex vivo methods, several parameters obtained from the CorVist –ST dynamic corneal response parameters have been developed for in vivo corneal biomechanical estimation [174-176]. These dynamic corneal response parameters have been found to be related to overall corneal stiffness including factors such as corneal geometry and material stiffness.

This validation relied on a procedure that includes a numerical inverse analysis method that

uses the pressure-deformation induced by CorVist-ST to determine the corneal hyperelastic stress–strain properties. The FE models had patient specific corneal geometry obtained from the Pentacam used to estimate material parameters. This estimates parameter was then compared by the newly developed material parameter estimation algorithm (β).

3.8.1 Clinical Datasets

As mentioned in Section 3.7, 722 patients in both clinical datasets were included in this multicentre retrospective study. In order to consider the corneal deformation during the measurement process, any CorVis readings with visible rotation in the corneal profile were excluded from the analysis. Consequently, there were only 158 healthy eyes and 34 keratoconus eyes selected for validating the corneal material estimation.

3.8.2 Inverse Analysis Using Patient-specific Models

The validation of corneal material behaviour is based on the FE method using a patient-specific model that involves real corneal geometry measured with the Pentacam device. The nodes on the anterior and posterior corneal surface in the numerical method were determined by the Zernike expression, in a manner similar to how the anterior corneal surface and their associated thickness values are determined.

In this study, The FEM is meshed using six-node solid elements (C3D6H) arranged in rings across the ocular surface and in layers across its thickness. The eye models consisted of 65710 six-node elements and were organised in 24-element rings in the cornea and 117-element rings in the sclera and consisted of a one-element layer. Steps include fitting of clinical data,

building clinical models, navigating the ABAQUS FE analysis, and conducting post-processing tasks, such as the inverse analysis. The boundary conditions and loading configurations in the FEM followed the same process as the idealised model in Section 3.3.

Based on the mesh structure of the idealised model with the same coordinate system and boundary conditions, the patient-specific model adopts the clinical measurements by only changing the coordinates of the idealised model nodes. The anterior corneal topography and corneal thickness map for each eye were fitted to Zernike polynomials up to the order 10.

For healthy or KC patients, the IOP value that was used in the calculation was the biomechanically corrected IOP parameter (bIOP). This value has been proven to be closer to the true IOP that corresponds to the true IOP value that was set in the numerical simulations.

To validate the effectiveness of the newly developed β algorithm, an inverse analysis was performed. Apex deformation under CorVis-ST air puff pressure was used as the target curve. The optimisation was performed using the Particle Swarm Optimization (PSO) algorithm that was implemented in a MATLAB code [256].

The material properties of the model were optimised until the RMS value is less than the pre-set tolerance, which means the deformation of the models matched the corneal profile deformation measured by the CorVis-ST device. Once the true material parameters were obtained in the Ogden format, they were converted to β and compared with the results obtained from the β algorithm.

3.8.3 Statistical Analysis

Statistical analyses were performed using the SPSS 24 (IBM, Armonk, NY). The analysis of the

β was conducted using the estimated algorithm (β) and the inverse analysis (β_{inv}) was performed using the paired t-test in order to compare the difference between both values.

3.9 Concluding Remarks

In this chapter, the following methodologies employed in the thesis have been highlighted: (1) Corneal geometry study to classify different types of corneal topography in normal and abnormal conditions; (2) Strategies and steps used in the numerical simulation of non-contact tonometry (such as with the CorVis-ST device); (3) Study of the dynamic corneal response analyser, including parameters and statistical analysis to compare between numerical and clinical datasets; (4) Strategies and steps taken in the development of bIOP and corneal material behaviour for normal and abnormal corneas; (5) Validation of healthy IOP-estimated algorithms using ex vivo human eye experiments; (6) Validation of bIOP using clinical datasets from patients with normal, Keratoconus, and a history of surgery; and (7) validation of corneal material behaviour estimation (β) using inverse analysis with patient-specific models

Chapter Four

Results

4.1 Introduction

Chapter 4 begins by comparing the corneal deformations under the CorVis-ST procedure obtained from FE models as discussed in the previous chapter and clinical databases to validate the feasibility of methods and algorithms developed for the IOP and corneal material behaviour. This project is divided into two parts – normal group (including normal corneal geometry & material stiffness, such as healthy, myopia, hyperopia Glaucoma patients, and refractive surgery patients) and abnormal group (including therewith abnormal corneal geometry & material stiffness, such as Keratoconus patients).

The normal group included eight parts of validation of the FE Model (including dynamic corneal response and comparison between the parameters of the CorVis-ST measurement and simulation results), parametric study, development of IOP-estimation algorithm, experimental validation of IOP algorithm, validation using clinical datasets, validation using refractive surgery datasets, development of algorithm for corneal material behaviour and its validation using inverse analysis. In terms of the abnormal group, similar steps were taken but the difficulty of validating IOP algorithm due to lack of availability of keratoconic ex-vivo human eyes forced the validation to be done by relying on clinical data.

4.2 Descriptive Statistics of Numerical Datasets

The numerical study included 4500 models with the CCT, ranging from 0.445 to 0.645 mm, with steps of 0.05 mm; the IOpt ranging from 10 to 30 mmHg, at steps of 5 mmHg; and the material stiffness (M_R) varied from 0.1 to 3.0 at steps of 0.1. There was one generic normal and five keratoconic corneal geometries. The numerical analysis usually did not converge after the air pressure relaxed and these unstable numerical models were excluded. Hence, 1950 numerical models completed the simulation successfully and included in the datasets.

From successful runs, there were eleven dynamic corneal response parameters (P_{DCR}), including the first applanation time (A1T), length of the flattened cornea (A1L), velocity of corneal apex (A1V), deformation and deflection at corneal apex (A1Deformation & A1Deflection), piston pressure (AP1) at A1T, highest concave time (HCT), and distance between the two Peaks of the cornea at point of max concavity (PD), Radius of corneal curvature(R), deformation and deflection at the corneal apex at max concavity (HCDeformation & HCDeflection), and stiffness parameter (SP-HC) at HCT, Table 4-1.

Table 4-1 Results of numerical analysis for normal and keratoconic groups showing mean, standard deviation and range values

	<i>Healthy Corneal Geometry</i>			<i>Keratoconic Corneal Geometry</i>		
<i>TopoR</i>	-	1	2	3	4	5
<i>Number</i>	325	325	325	325	325	325
<i>IOPt [mmHg]</i>	20 ± 7.1 (10–30)	20 ± 7.1 (10–30)	20 ± 7.1 (10–30)	20 ± 7.1 (10–30)	20 ± 7.1 (10–30)	20 ± 7.1 (10–30)
<i>CCT [μm]</i>	545 ± 70.8 (445–645)	545 ± 70.8 (445–645)	545 ± 70.8 (445–645)	545 ± 70.8 (445–645)	545 ± 70.8 (445–645)	545 ± 70.8 (445–645)
<i>M_R</i>	1.3 ± 0.8 (0.3–3)	1.3 ± 0.8 (0.3–3)	1.3 ± 0.8 (0.3–3)	1.3 ± 0.8 (0.3–3)	1.3 ± 0.8 (0.3–3)	1.3 ± 0.8 (0.3–3)
<i>A1T [ms]</i>	8.35 ± 1.31 (5.78–12.73)	9.00 ± 2.38 (6.42–13.38)	8.81 ± 2.01 (6.27–13.26)	8.54 ± 1.99 (5.96–12.96)	8.26 ± 1.5 (5.68–12.64)	8.07 ± 1.27 (5.60–12.50)
<i>A1L [mm]</i>	2.04 ± 0.07 (1.97–2.31)	2.64 ± 0.05 (2.57–2.91)	2.24 ± 0.06 (2.16–2.49)	1.84 ± 0.07 (1.77–2.11)	1.44 ± 0.22 (1.37–1.71)	1.04 ± 0.29 (0.97–1.31)
<i>A1V [mm/s]</i>	0.13 ± 0.03 (0.07–0.20)	0.18 ± 0.05 (0.12–0.25)	0.16 ± 0.05 (0.9–0.22)	0.14 ± 0.04 (0.08–0.21)	0.12 ± 0.03 (0.06–0.19)	0.10 ± 0.01 (0.04–0.17)
<i>HCT [ms]</i>	16.63 ± 0 (16.63–16.63)	16.63 ± 0 (16.63–16.63)	16.63 ± 0 (16.63–16.63)	16.63 ± 0 (16.63–16.63)	16.63 ± 0 (16.63–16.63)	16.63 ± 0 (16.63–16.63)
<i>PD [mm]</i>	4.43 ± 0.71 (1.58–6.08)	4.50 ± 1.13 (1.66–6.15)	4.47 ± 1.11 (1.61–6.10)	4.45 ± 0.92 (1.60–6.10)	4.41 ± 0.86 (1.56–6.16)	4.39 ± 0.73 (1.55–6.04)
<i>R [mm]</i>	13.21 ± 26.51 (5.42–307.9)	13.61 ± 26.51 (5.82–308.30)	13.31 ± 27.05 (5.50–307.97)	13.11 ± 29.24 (5.31–307.80)	12.91 ± 29.68 (5.12–308.15)	12.61 ± 29.71 (4.82–307.15)
<i>A1Deformation (A1Deflection) [mm]</i>	0.11 ± 0.02 (0.08–0.19)	0.15 ± 0.06 (0.12–0.23)	0.14 ± 0.04 (0.10–0.22)	0.12 ± 0.04 (0.07–0.21)	0.10 ± 0.03 (0.14–0.25)	0.08 ± 0.02 (0.05–0.16)
<i>HCDeformation (HCDDeflection) [mm]</i>	0.70 ± 0.25 (0.27–1.46)	1.15 ± 0.31 (0.66–1.92)	1.00 ± 0.35 (0.51–1.76)	0.81 ± 0.30 (0.31–1.56)	0.60 ± 0.28 (0.14–1.36)	0.48 ± 0.23 (0.08–1.21)
<i>AP1 [mmHg]</i>	74.53 ± 23.95 (28.28–150.3)	86.29 ± 35.11 (39.40– 159.02)	82.94 ± 26.19 (36.17–156.64)	77.89 ± 26.15 (31.41–152.91)	72.85 ± 25.39 (26.69–148.98)	69.49 ± 23.5 (23.74–146.28)

4.3 Validation of Numerical Results

In order to validate results of the numerical simulations of the CorVis-ST procedure, a comparative analysis was performed of the corneal deformation and dynamic corneal response parameters (P_{DCR}) between numerical predictions and clinical datasets obtained

using the CorVis-ST. Two parameters with good repeatability and direct relevance to IOP estimation and corneal stiffness, namely the corneal deformation at the first applanation time (AT1) and highest concavity time (HCT) were a consideration for these analyses [46, 244, 257].

4.3.1 Comparisons of Corneal Deformation

Eye-specific models representing four randomly-selected (using the simple random sample) clinical data points with wide variations in age, CVS-IOP and CCT were studied in detail, Table 4-2.

Table 4-2 Four randomly-selected cases considered in a validation study of numerical results

	<i>Age [year]</i>	<i>CVS-IOP [mmHg]</i>	<i>CCT [μm]</i>
<i>Case 1</i>	90	25	570
<i>Case 2</i>	50	15	538
<i>Case 3</i>	30	11.5	539
<i>Case 4</i>	40	15	621

Each eye-specific model was generated based on the age, CCT and CVS-IOP values. Anterior corneal central radius (R_c), anterior corneal shape factor (P), limbal radius (R_l) and sclera radius (R_s), were assumed to be constant values of 7.8, 0.82, 5.85 mm and 11.5 mm, respectively, since they were not measured clinically and found to have a negligible effect on IOP estimations [46].

The comparison concentrated on corneal deformation at AT1 and HCT with direct relevance to IOP estimation (related to the corneal deformation at AT1) [46, 244] and corneal stiffness (related to the corneal deformation at HCT) [257]. Figure 4-1 shows a comparison of corneal deformed profile between numerical predictions and CorVis-ST output at AT1 and HCT.

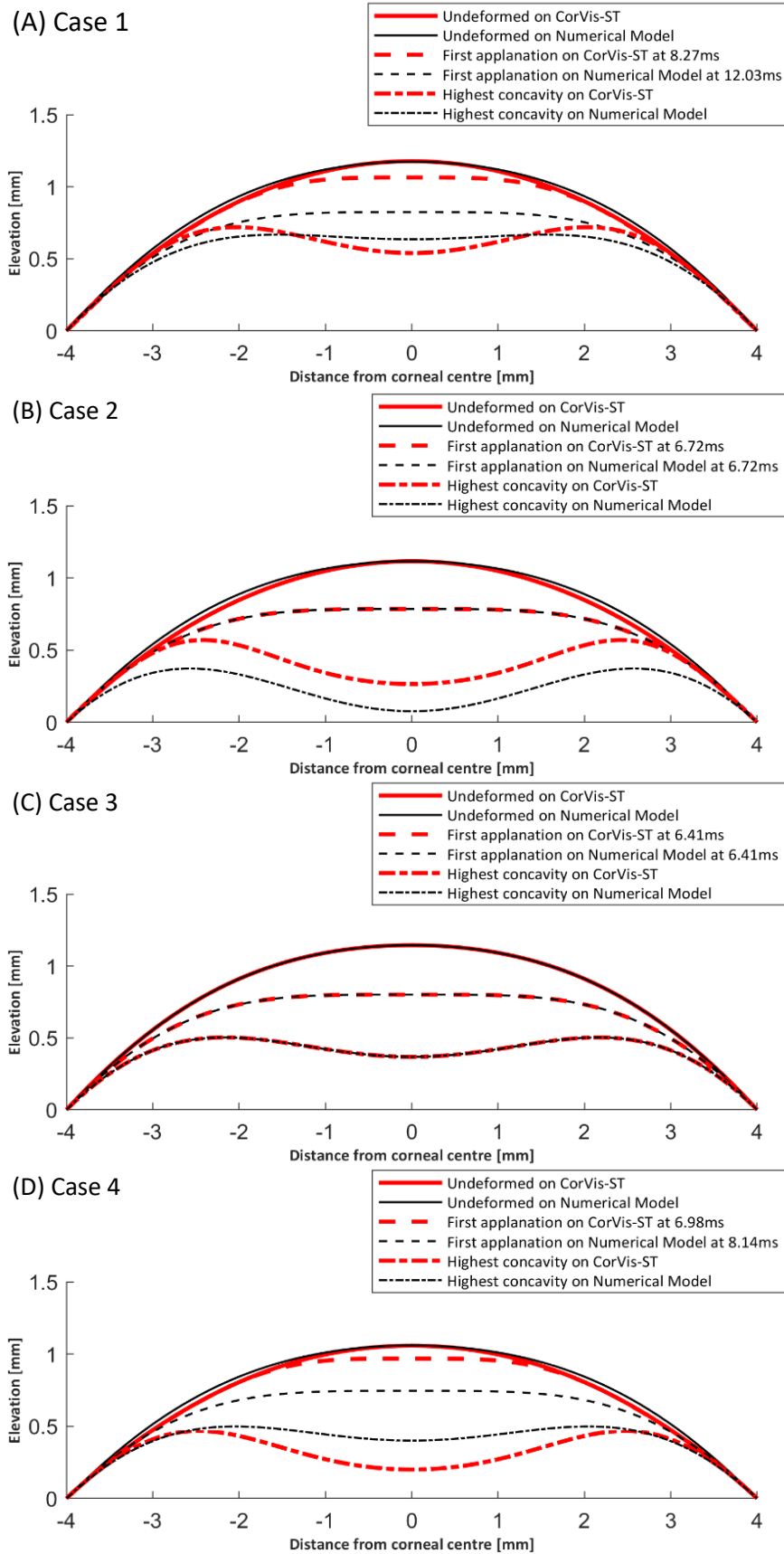


Figure 4-1 Comparison of numerical predictions with clinical measurements of corneal deformation at the start of the analysis, first applanation and highest concavity

The comparison results related to IOP estimation and corneal material behaviour presented a close match between numerical predictions and CorVis-ST measurement with the difference remaining below 5% in Case 3. By contrast, the comparisons demonstrated significant differences in corneal deformation at AT1 of around 45-50% in Cases 1&4, which means CVS-IOP cannot provide an accurate estimation of true IOP. In terms of the comparisons of the corneal material behaviours, they also demonstrated differences in corneal deformation profiles of around 30-50% in Cases 1,2&4. The results demonstrated that both CVS-IOP and corneal stiffness (based on correlation with age [1, 70, 99]) were inaccurate and led to large differences in corneal deformation between numerical predictions and CorVis-ST outcomes.

4.3.2 Comparisons of CorVis-ST Dynamic Response Parameters

In order to validate the performance of numerical models, a comparative analysis was conducted using confidence interval estimates to compare the distribution of main CorVis-ST dynamic response parameters (P_{DCR}) between numerical predictions and device's output. The numerical results of 1950 models with wide variations in true IOP (IOP_t), central corneal thickness (CCT), and the ratio of corneal stiffness (M_R), were compared with clinical data. Two clinical datasets obtained from the Rio de Janeiro Corneal Tomography and Biomechanics Study Group – Rio de Janeiro, Brazil – with a total of 253 healthy and 93 KC participants, and the Vincieye Clinic in Milan, Italy with 227 healthy and 107 KC participants presented mean, standard deviation (SD) and range value of each main P_{DCR} in Table 4-3.

Table 4-3 Clinical datasets for healthy and KC patients showing mean, standard deviation and range values

	<i>Dataset 1 from Brazil</i>		<i>Dataset 2 from Milan</i>	
	<i>Healthy</i>	<i>KC</i>	<i>Healthy</i>	<i>KC</i>
Number	227	103	253	87
CVS-IOP [mmHg]	15.71 ± 2.35 (11–25)	13.02 ± 2.32 (5–19.5)	14.8 ± 3.06 (6–34)	11.9 ± 2.33 (6–16.5)
CCT [μm]	543.9 ± 31.51 (458–635)	476 ± 49.07 (239–595)	539.3 ± 33.15 (454–629)	478.3 ± 39.58 (389–586)
Age [years]	37.64 ± 17.14 (7–90.06)	32.26 ± 11.79 (12–64)	43.11 ± 16.56 (7.51–86.33)	37.54 ± 11.84 (15–71)
TopoR	-	2.95 ± 0.21 (2.67–3.82)	-	2.82 ± 0.14 (2.59–3.37)
A1T [ms]	7.25 ± 0.36 (6.6–8.65)	6.91 ± 0.32 (6.09–7.77)	7.29 ± 0.31 (6.59–9.11)	6.96 ± 0.22 (6.58–7.61)
A1L [mm]	2.19 ± 0.36 (1.34–3.02)	1.94 ± 0.43 (1.08–2.87)	2.15 ± 0.36 (1.34–3.01)	1.87 ± 0.41 (1.15–2.81)
A1V [mm/s]	0.16 ± 0.02 (0.07–0.22)	0.18 ± 0.03 (0.13–0.34)	0.18 ± 0.02 (0.07–0.21)	0.17 ± 0.03 (0.12–0.27)
HCT [ms]	16.88 ± 0.0 (14.32–18.71)	16.78 ± 0.51 (15.48–18.02)	16.31 ± 0.0 (14.09–17.79)	16.39 ± 0.67 (14.32–17.79)
PD [mm]	5.01 ± 0.29 (3.98–5.71)	5.08 ± 0.25 (4.44–5.66)	5.07 ± 0.3 (3.85–5.81)	5.08 ± 0.23 (4.37–5.56)
R [mm]	7.27 ± 0.95 (4.51–11.28)	5.75 ± 1.18 (2.69–10.06)	7.03 ± 0.71 (5.06–9.48)	5.71 ± 0.96 (3.39–8.54)
A1Deformation [mm]	0.13 ± 0.01 (0.1–0.17)	0.14 ± 0.02 (0.09–0.21)	0.13 ± 0.01 (0.09–0.18)	0.13 ± 0.02 (0.09–0.19)
HCDeformation [mm]	1.07 ± 0.1 (0.79–1.3)	1.2 ± 0.15 (0.93–2.03)	1.09 ± 0.11 (0.8–1.47)	1.16 ± 0.12 (0.92–1.73)
AP1 [mmHg]	44.65 ± 6.11 (32.79–69.37)	37.71 ± 6.09 (17–54.32)	42.25 ± 7.93 (19.38–91.76)	34.62 ± 6.06 (19.98–46.69)
A1Deflection [mm]	0.1 ± 0.01 (0.06–0.13)	0.11 ± 0.02 (0.08–0.177)	0.09 ± 0.01 (0.06–0.13)	0.10 ± 0.02 (0.07–0.152)
HCDeflection [mm]	0.9 ± 0.11 (0.63–1.22)	1.03 ± 0.15 (0.73–1.80)	0.91 ± 0.11 (0.55–1.27)	1 ± 0.12 (0.72–1.59)

In statistics, a confidence interval (CI) is an interval estimate computed from the observed data to present the true distribution of the unknown population parameter. In this study, 95% CI range was calculated by using the mean and SD value of each P_{DCR} with a standardised normal distribution (Z-distribution) at $p=95\%$, Table 4-4.

Table 4-4 Clinical datasets for healthy and KC patients showing confidence interval ranges of CorVis-ST dynamic response parameters at p=95%

	<i>Dataset 1 from Brazil</i>		<i>Dataset 2 from Milan</i>	
	<i>Healthy</i>	<i>KC</i>	<i>Healthy</i>	<i>KC</i>
<i>CVS-IOP [mmHg]</i>	15.1 – 15.7	12.3 – 13.1	14.1 – 14.7	10.9 – 11.9
<i>CCT [μm]</i>	535.6 – 543.8	461.6 – 478.3	531.1 – 539.1	461.6 – 478.3
<i>A1T [ms]</i>	7.16 – 7.24	6.80 – 6.91	7.21 – 7.28	6.89 – 6.96
<i>A1L [mm]</i>	2.10 – 2.18	1.78 – 1.94	2.06 – 2.15	1.70 – 1.87
<i>A1V [mm/s]</i>	0.157 – 0.162	0.166 – 0.176	0.150 – 0.155	0.161 – 0.172
<i>HCT [ms]</i>	16.73 – 16.87	16.58 – 16.76	16.13 – 16.31	16.10 – 16.39
<i>PD [mm]</i>	4.94 – 5.00	4.99 – 5.08	5.00 – 5.07	4.99 – 5.08
<i>R [mm]</i>	7.02 – 7.26	5.33 – 5.77	6.85 – 7.02	5.31 – 5.71
<i>A1Deformation [mm]</i>	0.129 – 0.132	0.130 – 0.136	0.123 – 0.126	0.124 – 0.131
<i>HCDeformation [mm]</i>	1.06 – 1.07	1.14 – 1.19	1.06 – 1.09	1.12 – 1.16
<i>AP1 [mmHg]</i>	43.1 – 44.6	35.6 – 37.9	40.3 – 42.3	31.6 – 34.6
<i>A1Deflection [mm]</i>	0.098 – 0.100	0.103 – 0.108	0.091 – 0.092	0.095 – 0.101
<i>HCDeflection [mm]</i>	0.869 – 0.896	0.975 – 1.024	0.884 – 0.911	0.948 – 0.999

Figure 4-2 and Figure 4-3 presented comparisons of the four deform corneal response parameters related to IOP estimation and corneal stiffness within Max-Min range in the numerical predictions and CI range at 95% distribution in both clinical datasets for healthy and KC eyes. All numerical predictions covered 95% CI range of their CorVis-ST outcomes in both clinical datasets, in other words, the numerical modelling can be used to simulate the 95% probability of clinical situations.

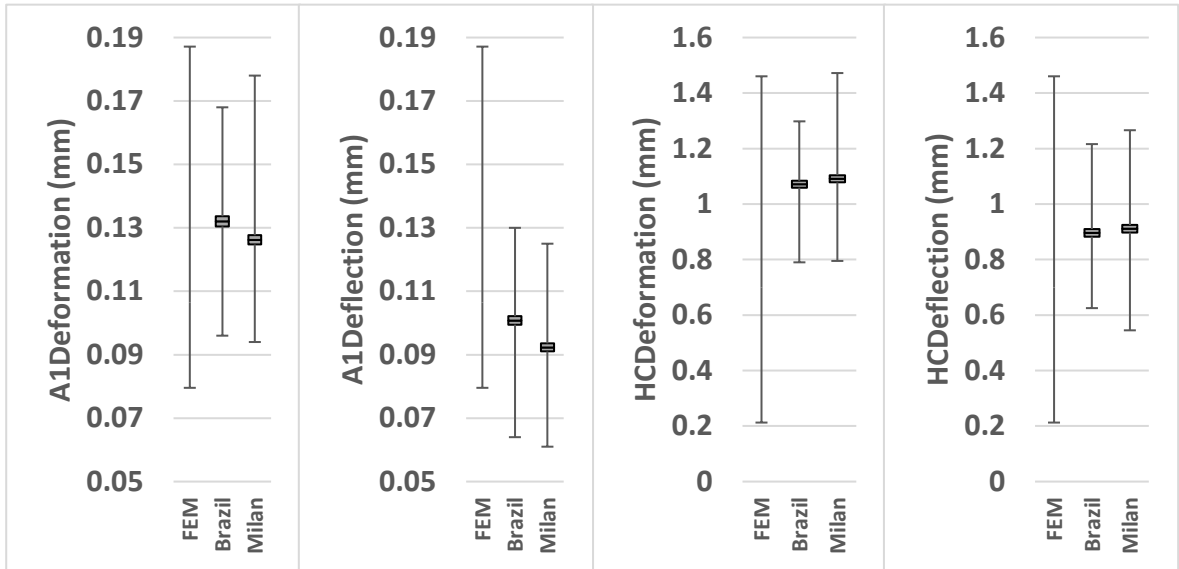


Figure 4-2 Ranges of dynamic response parameters - deformation and deflection at the first appplanation and highest concavity in numerical predictions compared to the boxplot indicating the mean, range and confidence interval ranges at p=95% for the CorVis-ST output in two clinical datasets (Brazil and Milan) for healthy eyes

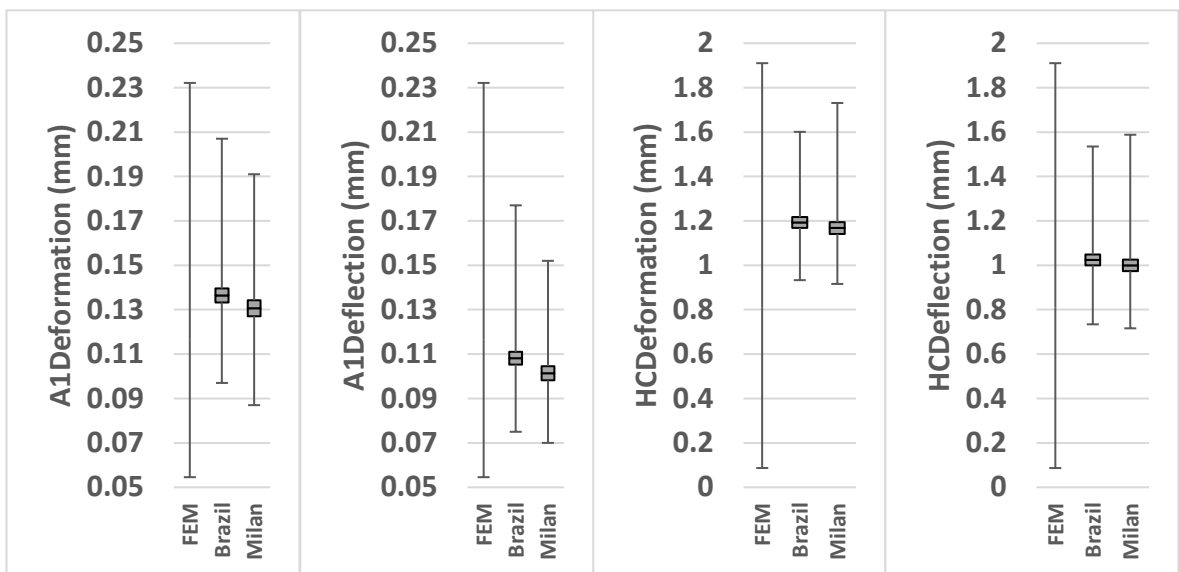


Figure 4-3 Ranges of dynamic response parameters - deformation and deflection at the first appplanations and highest concavity in numerical predictions compared to the boxplot indicating the mean, range and confidence interval ranges at p=95% for the CorVis-ST output in two clinical datasets (Brazil and Milan) for keratoconic eyes

4.3.3 Comparisons of Age-matched Dynamic Response Parameters Obtained Numerically and Clinically

The dynamic response parameters were compared between the numerical databases and combined clinical datasets (Brazil and Milan) based on age matching to reduce uncertainties associated with material stiffness, Table 4-5. The Kolmogorov–Smirnov test demonstrates the detection of the population’s homogeneity between numerical and clinical datasets.

While the distributions of IOpt, CVS-IOP and CCT between numerical models and clinical datasets were homogeneous ($P>0.05$), six P_{DCR} - A1T, A1V, PD, R, A1Deflection and HCDeflection - had homogeneous populations between numerical models and clinical datasets ($P>0.05$). By contrast, A1L in group 1 and group 3, A1Deformation and HCDeformation in all group, and AP1 in group 1 and group 3 didn’t belong to the homogeneous distributions between numerical models and clinical datasets ($P<0.05$). Moreover, the mean value of A1Deformation and HCDeformation in the numerical models were slightly smaller than the clinical datasets, and the mean value of AP1 in numerical modelling was greater than the clinical datasets. However, the reason for these differences is possibly associated with CVS-IOP or corneal material stiffness (related to the age) estimated clinically.

Table 4-5 Comparisons between numerical results and clinical data in age-matching groups

Data Source	Group 1			Group 2			Group 3		
	Numerical database	Clinical Datasets	P value	Numerical database	Clinical Datasets	P value	Numerical database	Clinical Datasets	P value
Number	15	13	-	15	9	-	15	12	-
Age(M _R) / Age [year]	28 (0.8)	28	-	38 (0.9)	38	-	48 (1)	48	-
IOPt/CVS-IOP [mmHg]	15 ± 4.23 (10–20)	14.62 ± 2.35 (10.5–19.5)	0.421	15 ± 4.23 (10–20)	16.5 ± 3.13 (14–24)	0.560	15 ± 4.23 (10–20)	15 ± 1.71 (11.5–18)	0.449
CCT [μm]	545 ± 73.19 (445–645)	521.77 ± 26.59 (477–552)	0.215	545 ± 73.19 (445–645)	558.22 ± 19.6 (527–582)	0.329	545 ± 73.19 (445–645)	554.67 ± 30.26 (528–606)	0.236
A1T [ms]	7.26 ± 0.73 (6.12–8.60)	7.22 ± 0.22 (6.86–7.65)	0.421	7.32 ± 0.73 (6.20–8.65)	7.4 ± 0.52 (6.99–8.65)	0.329	7.32 ± 0.74 (6.28–8.69)	7.29 ± 0.16 (7.04–7.6)	0.110
A1L [mm]	2.01 ± 0.03 (1.97–2.08)	1.97 ± 0.3 (1.72–2.76)	<0.01*	2.02 ± 0.03 (1.98–2.09)	2.13 ± 0.29 (1.72–2.61)	0.05	2.02 ± 0.04 (1.98–2.11)	2.22 ± 0.41 (1.64–2.72)	0.02*
A1V [mm/s]	0.15 ± 0.02 (0.12–0.19)	0.16 ± 0.02 (0.13–0.21)	0.241	0.15 ± 0.02 (0.11–0.19)	0.16 ± 0.02 (0.13–0.18)	0.476	0.15 ± 0.02 (0.11–0.19)	0.16 ± 0.01 (0.14–0.18)	0.197
PD [mm]	4.98 ± 0.41 (4.25–5.76)	5.15 ± 0.25 (4.76–5.57)	0.421	4.93 ± 0.42 (4.18–5.72)	5.03 ± 0.52 (4.06–5.71)	0.560	4.87 ± 0.42 (4.13–5.67)	5.07 ± 0.24 (4.67–5.54)	0.281
R [mm]	6.98 ± 1.05 (5.73–9.57)	6.8 ± 0.51 (6.19–7.63)	0.943	7.14 ± 1.17 (5.78–10.01)	7.26 ± 0.63 (5.99–8.17)	0.398	7.31 ± 1.3 (5.82–10.5)	7.15 ± 0.81 (5.7–8.52)	0.861
A1Deformation [mm]	0.10 ± 0.01 (0.08–0.11)	0.13 ± 0.01 (0.11–0.16)	<0.01*	0.10 ± 0.01 (0.08–0.12)	0.14 ± 0.01 (0.12–0.17)	<0.01*	0.10 ± 0.01 (0.09–0.12)	0.13 ± 0.01 (0.11–0.14)	<0.01*
HCDeformation [mm]	0.90 ± 0.19 (0.59–1.27)	1.11 ± 0.07 (1–1.21)	<0.01*	0.88 ± 0.19 (0.57–1.24)	1.11 ± 0.13 (0.9–1.27)	0.047*	0.85 ± 0.19 (0.55–1.22)	1.08 ± 0.09 (0.93–1.25)	0.02*
AP1 [mmHg]	54.6 ± 13.18 (34.2–79)	41.6 ± 6.06 (30.9–54.2)	0.02*	55.6 ± 13.35 (35.5–79.95)	46.8 ± 8.07 (40.6–66.4)	0.106	56.6 ± 13.5 (36.6–80.7)	42.8 ± 4.37 (33.7–50)	<0.01*
A1Deflection [mm]	0.10 ± 0.01 (0.08–0.11)	0.09 ± 0.01 (0.08–0.1)	0.750	0.10 ± 0.01 (0.08–0.12)	0.1 ± 0.01 (0.09–0.12)	0.819	0.10 ± 0.01 (0.09–0.12)	0.09 ± 0.01 (0.07–0.11)	0.516
HCDeflection [mm]	0.90 ± 0.19 (0.59–1.27)	0.95 ± 0.09 (0.79–1.09)	0.241	0.88 ± 0.19 (0.57–1.24)	0.89 ± 0.17 (0.63–1.13)	0.890	0.85 ± 0.19 (0.55–1.22)	0.9 ± 0.1 (0.72–1.05)	0.516

* The hypothesis of the same distribution between two datasets was rejected at P = 0.05 with two-tailed tests by K-S test.

4.4 Development of Estimation Algorithm for IOP and Corneal material behaviour

The process of the development of IOP and corneal material behaviour estimated algorithm was divided into two parts for healthy eyes and keratoconic eyes. As described in Chapter 3, in healthy eyes, the corneal material parameter (M_R) being related to age [1] led to a process that began with the IOP estimation algorithm. However, in KC, age could not be related to corneal stiffness and therefore the material algorithm was developed first and used next in IOP estimation.

4.4.1 Correlation Analysis of the Dynamic Corneal Response Parameters

The Pearson's correlation analysis of dynamic corneal response parameters (P_{DCR}) is used to find parameters, which are highly correlated with IOPT and have low correlation with CCT and M_R in healthy eyes (Table 4-6), and with CCT, M_R and TopoR in KC eyes (Table 4-9), for use in the IOP estimated algorithms for healthy and KC eyes.

Pearson's Correlation Analysis of P_{DCR} for Healthy Eyes

A Pearson's correlation analysis was run to assess the relationship between P_{DCR} and IOPT, CCT, and M_R in the numerical datasets with normal corneal geometry, Table 4-9. According to the Pearson's correlation analysis, there were six P_{DCR} – A1T, A1V, PD, HCDeformation, AP1, and HCDeflection, that had stronger correlations with IOPT than CCT and M_R , in the numerical results. Moreover, A1L and R had a stronger correlation with M_R than IOPT and CCT.

Table 4-6 Numerical results for normal corneas showing the output of Pearson's correlation analysis

	<i>IOPt [mmHg]</i>		<i>CCT [μm]</i>		<i>M_R</i>	
	<i>Pearson Correlation</i>	<i>P value</i>	<i>Pearson Correlation</i>	<i>P value</i>	<i>Pearson Correlation</i>	<i>P value</i>
<i>A1T [ms]</i>	0.807**	<0.01	0.371**	<0.01	0.398**	<0.01
<i>A1L [mm]</i>	-0.322**	<0.01	0.435**	<0.01	0.682**	<0.01
<i>A1V [mm/s]</i>	-0.716**	<0.01	-0.470**	<0.01	-0.449**	<0.01
<i>PD [mm]</i>	-0.652**	<0.01	-0.531**	<0.01	-0.491**	<0.01
<i>R [mm]</i>	0.186**	<0.01	0.262**	<0.01	0.342**	<0.01
<i>A1Deformation [mm]</i>	-0.09	0.109	0.539**	<0.01	0.656**	<0.01
<i>HCDeformation [mm]</i>	-0.685**	<0.01	-0.521**	<0.01	-0.457**	<0.01
<i>AP1 [mmHg]</i>	0.809**	<0.01	0.369**	<0.01	0.396**	<0.01
<i>A1Deflection [mm]</i>	-0.09	0.109	0.539**	<0.01	0.656**	<0.01
<i>HCDeflection [mm]</i>	-0.685**	<0.01	-0.521**	<0.01	-0.457**	<0.01

* Correlation is significant at the 0.05 level (2-tailed).

** Correlation is significant at the 0.01 level (2-tailed).

Healthy clinical datasets mentioned in Section 4.2 were utilized to perform Pearson's correlation analysis, Table 4-7 & Table 4-8. The correlation results showed that eight P_{DCR} 's had stronger correlations with IOP-CVS than with CCT and age (the parameters included A1T, A1V, PD, A1Deformation, A1Deflection, HCDeformation, HCDflection, and AP1 in Brazil's clinical dataset and A1T, A1V, PD, A1Deformation, A1Deflection, HCT, HCDflection, and AP1 in Milan's clinical dataset). In particular, there was a stronger positive linear correlation between CVS-IOP and AP1 ($r=0.998$, $p < 0.01$ in Brazilian data and $r=0.999$, $p < 0.01$ in Italian data), and CVS-IOP and A1T ($r=0.895$, $p < 0.01$ in Brazil and $r=0.984$, $p < 0.01$ in Milan), in addition, the AP1 value related to A1T.

Table 4-7 Clinical data for healthy eyes from Brazil showing the output of Pearson's correlation analysis

	<i>CVS-IOP [mmHg]</i>		<i>CCT [μm]</i>		<i>Age [years]</i>	
	<i>Pearson Correlation</i>	<i>P value</i>	<i>Pearson Correlation</i>	<i>P value</i>	<i>Pearson Correlation</i>	<i>P value</i>
<i>CVS-IOP [mmHg]</i>	1.00		0.241**	<0.01	0.04	0.51
<i>CCT [μm]</i>	0.241**	<0.01	1.00		0.08	0.25
<i>Age [year]</i>	0.04	0.51	0.08	0.25	1.00	
<i>A1T [ms]</i>	0.895**	<0.01	0.184**	0.01	0.03	0.67
<i>A1L [mm]</i>	0.263**	<0.01	0.287**	<0.01	0.07	0.30
<i>A1V [mm/s]</i>	-0.584**	<0.01	-0.247**	<0.01	-0.03	0.62
<i>HCT [ms]</i>	-0.06	0.40	0.07	0.32	0.09	0.20
<i>PD [mm]</i>	-0.730**	<0.01	-0.221**	<0.01	-0.131*	0.05
<i>R [mm]</i>	0.320**	<0.01	0.302**	<0.01	0.07	0.30
<i>A1Deformation [mm]</i>	0.588**	<0.01	0.299**	<0.01	0.244**	<0.01
<i>HCDeformation [mm]</i>	-0.752**	<0.01	-0.199**	<0.01	-0.03	0.61
<i>AP1 [mmHg]</i>	0.998**	<0.01	0.243**	<0.01	0.06	0.39
<i>A1Deflection [mm]</i>	0.466**	<0.01	0.329**	<0.01	0.277**	<0.01
<i>HCDeflection [mm]</i>	-0.711**	<0.01	-0.275**	<0.01	-0.152*	0.02

* Correlation is significant at the 0.05 level (2-tailed).

** Correlation is significant at the 0.01 level (2-tailed).

Table 4-8 Clinical data for healthy eyes from Milan showing the output of Pearson's correlation analysis

	<i>CVS-IOP [mmHg]</i>		<i>CCT [μm]</i>		<i>Age [years]</i>	
	<i>Pearson Correlation</i>	<i>P value</i>	<i>Pearson Correlation</i>	<i>P value</i>	<i>Pearson Correlation</i>	<i>P value</i>
<i>CVS-IOP [mmHg]</i>	1.00		0.313**	<0.01	0.210**	<0.01
<i>CCT [μm]</i>	0.313**	<0.01	1.00		0.06	0.35
<i>Age [year]</i>	0.210**	<0.01	0.06	0.35	1.00	
<i>A1T [ms]</i>	0.984**	<0.01	0.298**	<0.01	0.213**	<0.01
<i>A1L [mm]</i>	0.214**	<0.01	0.224**	<0.01	0.10	0.12
<i>A1V [mm/s]</i>	-0.680**	<0.01	-0.225**	<0.01	-0.141*	0.03
<i>HCT [ms]</i>	-0.330**	<0.01	-0.143*	0.02	-0.08	0.23
<i>PD [mm]</i>	-0.627**	<0.01	-0.255**	<0.01	-0.184**	<0.01
<i>R [mm]</i>	0.301**	<0.01	0.316**	<0.01	0.08	0.23
<i>A1Deformation [mm]</i>	0.327**	<0.01	0.126*	0.05	0.285**	<0.01
<i>HCDeformation [mm]</i>	-0.702**	<0.01	-0.279**	<0.01	-0.03	0.58
<i>AP1 [mmHg]</i>	0.999**	<0.01	0.313**	<0.01	0.210**	<0.01
<i>A1Deflection [mm]</i>	0.07	0.29	0.07	0.28	0.201**	<0.01
<i>HCDeflection [mm]</i>	-0.626**	<0.01	-0.304**	<0.01	-0.174**	0.01

* Correlation is significant at the 0.05 level (2-tailed).

** Correlation is significant at the 0.01 level (2-tailed).

According to the comparison of results of both correlation analyses in numerical and clinical datasets, the A1T, A1V, PD, AP1, HCDefomation and HCDeflection showed stronger correlations with IOP values (CVS-IOP and IOPT) than with CCT, and corneal material properties (age and M_R) in both numerical and clinical datasets. In these parameters, only AP1 had a stronger linear correlation with CVS-IOP in both clinical datasets. Hence, AP1 was selected for use in the IOP-estimation algorithm for healthy eyes. In addition, corneal stiffness had a weak association with age. Hence, the stiffness estimation error was adjusted using the radius of curvature at the highest concavity (R), which had the same distribution in numerical and clinical data and stronger correlation with corneal material behaviour numerically.

Pearson's Correlation Analysis of P_{DCR} for Keratoconic Eyes

A Pearson's correlation analysis was run to assess the relationship between P_{DCR} and IOPT, CCT, M_R and TopoR in the numerical datasets with five different keratoconic corneal geometries, Table 4-9. With reference to the clinical datasets of keratoconic eyes, the clinical data were similar to numerical data, Table 4-10 & Table 4-11. The results showed that three parameters – A1T, PD, and AP1 - had stronger corrections with IOPT than with CCT, M_R , and TopoR in the numerical results. In both clinical datasets, there was no correlation between P_{DCR} and age. This means that the correlation between corneal material properties and age was different in KC eyes than healthy eyes, and age was not suitable to represent corneal material properties in KC eyes. Moreover, four P_{DCR} - A1Deformation, HCDeformation, AP1 and HCDeflection in Brazil's datasets and two P_{DCR} - A1T and AP1 in Milan's datasets - had stronger associations with CVS-IOP than CCT and TopoR. Similar to correlation analysis in healthy eyes, A1T and AP1 had strong linear correlations with CVS-IOP and AP1. Hence, the AP1 was considered first for

use in the IOP-estimated algorithms for KC eyes.

Table 4-9 Numerical results for keratoconic corneas showing the output of Pearson's correlation analysis

	<i>IOPt [mmHg]</i>		<i>CCT [μm]</i>		<i>MR</i>		<i>TopoR</i>	
	<i>Pearson Correlation</i>	<i>P value</i>	<i>Pearson Correlation</i>	<i>P value</i>	<i>Pearson Correlation</i>	<i>P value</i>	<i>Pearson Correlation</i>	<i>P value</i>
<i>A1T [ms]</i>	0.781**	<0.01	0.359**	<0.01	0.385**	<0.01	-0.251**	<0.01
<i>A1L [mm]</i>	-0.041	0.098	0.055*	0.025	0.087**	<0.01	-0.992**	<0.01
<i>A1V [mm/s]</i>	-0.518**	<0.01	-0.341**	<0.01	-0.325**	<0.01	-0.690**	<0.01
<i>PD [mm]</i>	-0.651**	<0.01	-0.530**	<0.01	-0.490**	<0.01	-0.056*	0.025
<i>R [mm]</i>	0.186**	<0.01	0.262**	<0.01	0.342**	<0.01	-0.013	0.606
<i>A1Deformation [mm]</i>	-0.052*	0.03	0.316**	<0.01	0.385**	<0.01	-0.808**	<0.01
<i>HCDeformation [mm]</i>	-0.478**	<0.01	-0.346**	<0.01	-0.282**	<0.01	-0.708**	<0.01
<i>AP1 [mmHg]</i>	0.784**	<0.01	0.357**	<0.01	0.382**	<0.01	0.250**	<0.01
<i>A1Deflection [mm]</i>	-0.052*	0.035	0.316**	<0.01	0.385**	<0.01	-0.808**	<0.01
<i>HCDeflection [mm]</i>	-0.470**	<0.01	-0.346**	<0.01	-0.282**	<0.01	-0.708**	<0.01

* Correlation is significant at the 0.05 level (2-tailed).

** Correlation is significant at the 0.01 level (2-tailed).

Table 4-10 Clinical data for keratoconic eyes from Brazil showing the output of Pearson's correlation analysis

	<i>CVS-IOP [mmHg]</i>		<i>CCT [μm]</i>		<i>Age [year]</i>		<i>TopoR</i>	
	<i>Pearson Correlation</i>	<i>P value</i>	<i>Pearson Correlation</i>	<i>P value</i>	<i>Pearson Correlation</i>	<i>P value</i>	<i>Pearson Correlation</i>	<i>P value</i>
<i>CVS-IOP [mmHg]</i>	1.00		0.219*	0.03	0.10	0.33	-0.02	0.85
<i>CCT [μm]</i>	0.219*	0.03	1.00		0.08	0.42	-0.225*	0.02
<i>Age [year]</i>	0.10	0.33	0.08	0.42	1.00		0.238*	0.02
<i>TopoR</i>	-0.02	0.85	-0.225*	0.02	0.238*	0.02	1.00	
<i>A1T [ms]</i>	0.899**	<0.01	0.13	0.18	0.08	0.43	-0.01	0.95
<i>A1L [mm]</i>	0.346**	<0.01	0.369**	<0.01	0.14	0.16	0.02	0.82
<i>A1V [mm/s]</i>	-0.15	0.12	-0.462**	<0.01	-0.02	0.83	0.13	0.20
<i>HCT [ms]</i>	0.03	0.79	0.02	0.81	0.10	0.33	0.08	0.45
<i>PD[mm]</i>	-0.537**	<0.01	-0.07	0.49	-0.03	0.74	-0.12	0.23
<i>R [mm]</i>	0.316**	<0.01	0.570**	<0.01	0.03	0.77	-0.275**	0.01
<i>A1Deformation [mm]</i>	0.316**	<0.01	-0.270**	0.01	-0.02	0.84	0.271**	0.01
<i>HCDeformation [mm]</i>	-0.623**	<0.01	-0.532**	<0.01	0.05	0.61	0.263**	0.01
<i>AP1 [mmHg]</i>	0.998**	<0.01	0.219*	0.03	0.09	0.35	-0.02	0.84
<i>A1Deflection [mm]</i>	0.17	0.08	-0.342**	<0.01	-0.01	0.93	0.258**	0.01
<i>HCDeflection [mm]</i>	-0.599**	<0.01	-0.507**	<0.01	0.08	0.45	0.265**	0.01

* Correlation is significant at the 0.05 level (2-tailed);

** Correlation is significant at the 0.01 level (2-tailed).

Table 4-11 Clinical data for keratoconic eyes from Milan showing the output of Pearson's correlation analysis

	<i>CVS-IOP [mmHg]</i>		<i>CCT [μm]</i>		<i>Age [year]</i>		<i>TopoR</i>	
	<i>Pearson Correlation</i>	<i>P value</i>	<i>Pearson Correlation</i>	<i>P value</i>	<i>Pearson Correlation</i>	<i>P value</i>	<i>Pearson Correlation</i>	<i>P value</i>
<i>CVS-IOP [mmHg]</i>	1.00		0.457**	<0.01	0.09	0.38	-0.255*	0.02
<i>CCT [μm]</i>	0.457**	<0.01	1.00		0.06	0.58	-0.486**	<0.01
<i>Age [year]</i>	0.09	0.38	0.06	0.58	1.00		0.06	0.56
<i>TopoR</i>	-0.255*	0.02	-0.486**	<0.01	0.06	0.56	1.00	
<i>A1T [ms]</i>	0.861**	<0.01	0.359**	<0.01	0.08	0.44	-0.274*	0.01
<i>A1L [mm]</i>	-0.09	0.43	0.224*	0.04	-0.08	0.47	-0.223*	0.04
<i>A1V [mm/s]</i>	-0.220*	0.04	-0.272*	0.01	-0.08	0.46	0.472**	<0.01
<i>HCT [ms]</i>	-0.246*	0.02	0.05	0.67	0.04	0.70	0.01	0.93
<i>PD[mm]</i>	-0.306**	<0.01	-0.17	0.11	-0.05	0.65	-0.14	0.20
<i>R [mm]</i>	0.325**	<0.01	0.533**	<0.01	0.11	0.31	-0.517**	<0.01
<i>A1Deformation [mm]</i>	-0.03	0.79	-0.244*	0.02	0.12	0.28	0.532**	<0.01
<i>HCDeformation [mm]</i>	-0.475**	<0.01	-0.481**	<0.01	-0.01	0.96	0.475**	<0.01
<i>AP1 [mmHg]</i>	0.999**	<0.01	0.460**	<0.01	0.10	0.38	-0.262*	0.01
<i>A1Deflection [mm]</i>	-0.09	0.42	-0.258*	0.02	0.01	0.90	0.488**	<0.01
<i>HCDeflection [mm]</i>	-0.422**	<0.01	-0.498**	<0.01	-0.09	0.41	0.478**	<0.01

* Correlation is significant at the 0.05 level (2-tailed);

** Correlation is significant at the 0.01 level (2-tailed).

4.4.2 IOP Estimate Algorithms for Healthy Eyes

According to results of the correlation analysis presented in Section 4.4.1 and the comparison of P_{DCR} between numerical and clinical data described in Section 4.3, an equation that links these parameters and provides accurate estimates of true IOP is developed. The equations for a biomechanically connected IOP (bIOP) with four parameters – CCT, age, AP1 and R – is explained below.

Due to the variability of corneal stiffness, the stiffness estimation error was adjusted using the radius of curvature of corneal concavity at HCT (R), which had a stronger association with M_R than CCT and IOPt. The IOP estimate algorithm with four parameters can take the form:

$$bIOP = C_{CCT1} \times C_{AP1} \times C_{age1} + C_{CCT2} \times C_{age2} + C_R + C \quad (4.1)$$

where bIOP = biomechanically corrected IOP; C_{CCT1} and C_{CCT2} = the effect of variation in CCT; C_{AP1} = the effect of variation in the measured pressure at APT1; C_{age1} and C_{age2} = the effect of variation in age; C_R = adjustment for the stiffness effect error; and C = a constant, 3.3693 mmHg.

In Equation 4.1,

$$C_{CCT1} = 1.97 \times 10^{-2} \times CCT^3 - 31.32 \times CCT^2 + 1.5 \times 10^4 \times CCT - 6.23 \times 10^5$$

$$C_{AP1} = 3.86 \times 10^{-2} \times AP1 + 0.366$$

$$C_{age1} = 1.58 \times 10^{-7} \times [\ln(C_{M_R-Age})]^2 - 3.84 \times 10^{-7} \times \ln(C_{M_R-Age}) + 5.99 \times 10^{-6}$$

$$C_{CCT2} = -95.6 \times CCT^3 + 8.56 \times 10^3 \times CCT^2 + 5.77 \times 10^5 \times CCT - 5.87 \times 10^7$$

$$C_{age2} = -2.18 \times 10^{-10} \times [\ln(C_{M_R-Age})]^2 + 1.53 \times 10^{-10} \times \ln(C_{M_R-Age}) - 1.36 \times 10^{-10}$$

$$C_R = 0.0309 \times R - 6.15$$

$$C_{M_R-Age} = 0.5852 \times e^{0.0111 \times \text{Age}(\text{year})}$$

4.4.3 Corneal Material Estimation Algorithms for Healthy and Keratoconic Eyes

The stiffness parameter (SP) has been described in Section 3.5.2 and an earlier study demonstrated that this parameter was a useful index to reflect the corneal material behaviour [201]. Based on this evidence, the stiffness parameter at highest concavity (SP-HC) was used in the development of an algorithm to estimate corneal material behaviour. Table 4-12 presents the mean and SD value of SP-HC and Ln(SP-HC) predicted from numerical modelling with normal and keratoconic corneal geometries.

Table 4-12 Stiffness parameter in numerical results for healthy and keratoconic groups showing mean, standard deviation, and range values

TopoR	Normal Group			Keratoconic Group		
	-	1	2	3	4	5
IOPt [mmHg]	20 ± 7.1 (10–30)	20 ± 7.1 (10–30)	20 ± 7.1 (10–30)	20 ± 7.1 (10–30)	20 ± 7.1 (10–30)	20 ± 7.1 (10–30)
CCT [μm]	545 ± 70.8 (445–645)	545 ± 70.8 (445–645)	545 ± 70.8 (445–645)	545 ± 70.8 (445–645)	545 ± 70.8 (445–645)	545 ± 70.8 (445–645)
M_R	1.3 ± 0.8 (0.3–3)	1.3 ± 0.8 (0.3–3)	1.3 ± 0.8 (0.3–3)	1.3 ± 0.8 (0.3–3)	1.3 ± 0.8 (0.3–3)	1.3 ± 0.8 (0.3–3)
SP-HC [mmHg/mm]	115.8 ± 113.47 (12.63–916.68)	70.5 ± 38.60 (15.87–240.61)	79.4 ± 49.3 (15.24–315.63)	98.9 ± 78.41 (13.93–555.54)	212.39 ± 429.07 (12.97–4247.47)	308.46 ± 569.50 (11.92–4280.03)
Ln(SP-HC) [mmHg/mm]	4.57 ± 0.85 (2.59–7.58)	4.19 ± 0.54 (2.80–5.62)	4.29 ± 0.61 (2.77–5.95)	4.47 ± 0.74 (2.68–6.70)	4.74 ± 0.98 (2.56–8.35)	4.96 ± 1.14 (2.48–8.36)

Before the development of corneal material behaviour estimation, Table 4-13 presented the results of Pearson's correlation analysis between SP-HC and IOPt, CCT, M_R and TopoR in numerical models with healthy and KC corneal geometries. These results indicated that SP-HC had a significant correlation with IOPt, CCT, and M_R in healthy eyes (P<0.01). In addition to KC eyes, its correlation with IOPt, CCT, M_R and TopoR was significant (P<0.01).

Table 4-13 Results of Pearson's correlation analysis of SP-HC in numerical results for healthy and keratoconic eyes

	SP-HC [mmHg/mm]				Ln(SP-HC) [mmHg/mm]			
	Healthy Group		KC Group		Healthy Group		KC Group	
	Pearson Correlation	P value						
IOPt [mmHg]	0.351*	<0.01	0.122*	<0.01	0.638*	<0.01	0.571*	<0.01
CCT [μm]	0.402*	<0.01	0.154*	<0.01	0.515*	<0.01	0.431*	<0.01
M_R	0.494*	<0.01	0.194*	<0.01	0.519*	<0.01	0.421*	<0.01
TopoR	-	-	0.164*	<0.01	-	-	0.322*	<0.01

* Correlation is significant at the 0.01 level (2-tailed).

In this study, Ln(SP-HC) presented a low SD value and a small difference in mean values between normal and keratoconic groups. Hence, Ln(SP-HC) was related as a parameter to develop corneal material estimation algorithms.

A 3D surface plot of different corneal biomechanical parameters was drawn between the IOPt/20, CCT/545, and Ln(SP-HC); the colour of each surface presented a specific corneal material property M_R , Figures 3-20 & 3-22. Based on this, an equation for each 3D surface was developed. The form of these surfaces developed for different M_R values tools the form:

$$\beta = f(Par_{SP-HC}, \ln SP-HC) \quad [For\ normal\ cornea](4.2)$$

Where Par_{SP-HC} is a matrix of coefficients that are defined by CCT and IOPt; $\ln SP-HC$ is the natural logarithm value of the stiffness parameter at HCT; β is a material estimate obtained from a function at specific IOPt, CCT and SP-HC using Shape-preserving piecewise cubic interpolation based on values of Par_{SP-HC} .

In Equation 4.2,

$$Par_{SP-HC} = a_1 + a_2x + a_3y + a_4x^2 + a_5xy + a_6y^2 + a_7x^3 + a_8x^2y + a_9xy^2 \quad (4.3)$$

Where x is CCT in μm divided by 545; y is IOPt in mmHg divided by 20; and a_i is a coefficient that depends on CCT and IOPt (presented in Table 4-14).

Table 4-14 Coefficients of Par_{SP-HC} in Equation 4.7 and values of CCT and IOPt

M_R	a_1	a_2	a_3	a_4	a_5	a_6	a_7	a_8	a_9
0.3	-3.094	5.249	8.982	0.248	-8.423	-2.416	-0.443	1.704	2.198
0.5	-7.731	22.224	7.699	-17.455	-8.806	-1.515	5.361	2.852	1.471
0.7	0.440	0.387	4.723	2.974	-5.498	-0.403	-1.200	2.386	0.404
0.8	4.509	-10.507	3.013	12.998	-3.028	0.017	-4.315	1.583	0.002
0.9	7.603	-17.995	0.764	18.971	0.888	0.297	-5.826	-0.114	-0.259
1.0	8.047	-18.217	-0.500	18.236	3.236	0.395	-5.235	-1.242	-0.336
1.5	-8.355	30.668	1.754	-30.649	0.651	-0.519	11.572	-1.163	0.653
2.0	-3.101	16.284	-0.219	-18.494	4.480	-0.208	9.073	-3.482	0.508
2.5	4.677	-9.969	3.607	10.742	-1.410	-1.504	-1.413	-1.463	1.804
3.0	6.842	-16.245	3.244	17.519	-4.064	0.222	-3.391	1.251	0.092

Since the true IOP value is unknown in clinical practice, and the corneal material property in healthy eyes was related to age, bIOP can be calculated and used to replace the IOPt in Equation 4.2. To consider the effect of bIOP on the corneal material estimate, a close match between the predictions(β) and the true value (M_R) was expected with the differences remaining below $\pm 0.5\%$.

In keratoconic eyes, there is no way to estimate the IOP first as corneal material properties cannot be assumed to have correlation with age, but CVS-IOP is the only parameter obtained from the CorVis device, which was related to the true IOP in keratoconic eyes, even CCT has a significant effect on it in Section 4.4.1.

From the relationships between CVS-IOP and AP1 based on the two clinical datasets (Section 4.4.1), a linear relation between CVS-IOP and AP1 in healthy and KC eyes can take the form:

$$CVS-IOP = 0.384 \times AP1 - 1.44 \quad (4.4)$$

Based on this relationship, CVS-IOP value in numerical modelling was calculated and the

difference between IOPt and CVS-IOP were assessed via the root-mean-square error (RMSE) in thirty groups – IOPt varied from 10 to 30 mmHg in steps of 5 mmHg; CCT divided into two groups; thin (from 445 to 545 μm) and thick (over 545 μm); corneal material divided into several groups, soft (M_R from 0.3 to 0.7), intermediate (from 0.8 to 1.5) and stiff (M_R from 2.0 to 3.0), Table 4-15.

Table 4-15 Comparison of differences between IOPt and CVS-IOP in numerical results

Group	CCT [μm]	M_R	IOPt [mmHg]	RMSE between CVS-IOP and IOPt (%)					
				Healthy Eye	Keratoconic Eye				
					TopoR = 1	TopoR = 2	TopoR = 3	TopoR = 4	TopoR = 5
1	445-545	0.3-0.7	10	2.2	7.6	5.0	3.3	2.1	2.8
2	<545			4.8	12.0	8.0	6.1	4.5	2.8
3	445-545	0.8-1.5		4.1	10.8	7.1	5.3	3.5	2.0
4	<545			7.9	16.6	11.0	9.1	9.1	7.3
5	445-545	2-3		10.1	19.7	13.1	11.3	12.6	10.9
6	<545			23.2	39.4	26.3	24.4	32.0	30.2
7	445-545	0.3-0.7	15	2.1	10.2	5.2	3.3	2.9	1.6
8	<545			5.1	14.9	8.3	6.3	7.3	5.5
9	445-545	0.8-1.5		4.1	13.3	7.2	5.3	5.8	4.1
10	<545			8.6	20.3	11.8	9.9	12.5	10.6
11	445-545	2-3		8.7	20.2	11.9	10.0	12.8	11.0
12	<545			21.1	38.6	24.2	22.3	31.2	29.4
13	445-545	0.3-0.7	20	2.3	13.3	5.5	3.6	5.5	3.7
14	<545			5.7	18.4	8.9	7.0	10.6	8.7
15	445-545	0.8-1.5		4.5	16.4	7.6	5.7	8.7	6.9
16	<545			9.4	23.9	12.6	10.7	16.1	14.2
17	445-545	2-3		8.6	22.5	11.8	9.9	14.9	13.1
18	<545			20.2	39.5	23.2	21.4	32.4	30.5
19	445-545	0.3-0.7	25	2.6	16.2	5.8	3.9	8.3	6.4
20	<545			6.6	22.1	9.8	7.9	14.4	12.5
21	445-545	0.8-1.5		5.0	19.5	8.1	6.2	11.8	9.9
22	<545			10.2	27.5	13.4	11.4	19.8	17.8
23	445-545	2-3		8.7	25.1	11.8	10.0	17.5	15.6
24	<545			19.3	40.4	22.2	20.4	33.4	31.6
25	445-545	0.3-0.7	30	2.8	18.9	6.0	4.1	11.1	9.2
26	<545			7.4	25.7	10.5	8.7	18.1	16.2
27	445-545	0.8-1.5		5.4	22.6	8.5	6.7	14.9	13.0
28	<545			11.0	30.9	14.0	12.2	23.4	21.5
29	445-545	2-3		8.8	27.6	11.9	10.1	20.1	18.2
30	<545			19.0	42.2	21.8	20.2	35.5	33.8

Further, according to the results of the correlation analysis (Section 4.4.1), CVS-IOP was assumed to be the closest available indication of true IOP in estimating the corneal material behaviours for KC eyes. The difference in β between the predictions and the true values remained below 7% in TopoR=2-4 but was around 20% in Topo=1&5. In addition, TopoR in clinical datasets concentrated on the range between 2 and 3, which demonstrated that CVS-IOP was suitable in estimating corneal material properties in KC eyes.

4.4.4 IOP Estimation Algorithms for Keratoconic Eyes

According to the characteristic analysis of corneal geometry in Keratoconus, the effect of corneal geometry on IOP estimate was considered. The keratoconic corneal stiffness is expected to be softer than that of normal corneas. The IOP estimate in KC eyes was developed based on the correlation analysis and the influence of the geometry effect using the TopoR value:

$$bIOP_{KC} = C_{CCT1} \times C_{AP1} \times C_{Beta1} \times C_{TR1} + C_{CCT2} \times C_{Beta2} \times C_{TR2} + C_{CCT3} + C \quad (4.5)$$

where $bIOP_{KC}$ = biomechanically corrected IOP for abnormal corneas; C_{CCT1} , C_{CCT2} , and C_{CCT3} = the effect of variation in CCT; C_{AP1} = the effect of variation in the measured pressure at APT1; C_{Beta1} and C_{Beta2} = the effect of variation in corneal material estimation; C_{TR1} and C_{TR2} = adjustment of the corneal geometry effect error; and C = a constant, 3.3693 mmHg.

In Algorithm 4.5,

$$C_{CCT1} = 1.27 \times 10^{-9} \times CCT^3 - 6.06 \times 10^{-7} \times CCT^2 - 2.3 \times 10^{-3} \times CCT + 3.6$$

$$C_{AP1} = 1.5 \times 10^{-2} \times AP1 - 4.76$$

$$C_{Beta1} = 3.4 \times 10^{-2} \times [\ln(\beta)]^2 + 3.89 \times 10^{-2} \times \ln(\beta) + 5.99 \times 10^{-6}$$

$$C_{TR1} = -1.08 \times TopoR + 4.05$$

$$C_{CCT2} = 2.37 \times 10^{-9} \times CCT^3 - 1.36 \times 10^{-6} \times CCT^2 - 3.88 \times 10^{-3} \times CCT + 6.11$$

$$C_{Beta2} = 4.27 \times 10^{-2} \times [\ln(\beta)]^2 - 4.42 \times 10^{-3} \times \ln(\beta) + 7.4$$

$$C_{TR2} = -1.75 \times TopoR + 6.59$$

$$C_{CCT3} = 2.12 \times 10^{-2} \times (CCT - 475) + 5.3307$$

4.5 Validation of bIOP-Estimation Algorithm for Healthy Eyes

4.5.1 Validation of bIOP Algorithm Using Ex Vivo Human Eyes

Both uncorrected IOP values (CVS-IOP) and biomechanically-corrected values (bIOP) are presented in Table 4-16 along with the corresponding true IOP (IOPt) applied by the syringe pump system and measured by a pressure transducer. The eye donor's age and the mean and standard deviation of CCT obtained at each pressure level are also included.

The ANOVA test between the three normally distributed groups of bIOP, CVS-IOP and IOPt showed significant differences ($p < 0.001$) and allowed for Bonferroni post-hoc test to be performed in Table 4-16.

Table 4-16 IOP measurements including uncorrected CVS-IOP and biomechanically-corrected bIOP values at controlled true IOP values between 10 and 30 mmHg. Results include mean, standard deviation and range.

Specimen	Age (years)	CCT (microns)	IOP _t (mmHg)	CVS-IOP			bIOP		
				IOP (mmHg)	CVS-IOP – IOP _t (mmHg)	Error %	IOP (mmHg)	bIOP – IOP _t (mmHg)	Error %
S1	67	465±6 (458-469)	10	14.7±0.3 (14.5-15.0)	4.7	47%	12.1±0.1 (11.9-12.2)	2.1	21%
		488±13 (476-507)	15	19.3±1.0 (18.0-20.5)	4.3	29%	16.4±0.8 (15.5-17.3)	1.4	9%
		493±2 (492-496)	20	23.5±0.0 (23.5-23.5)	3.5	18%	20.5±0.1 (20.4-20.6)	0.5	3%
		498±1 (496-499)	25	28.0±0.4 (27.5-28.5)	3.0	12%	25.1±0.6 (24.3-25.6)	0.1	0%
		487±6 (477-494)	30	31.9±1.0 (31.0-33.0)	1.9	6%	29.7±0.9 (28.7-30.7)	-0.3	-1%
S2	67	618±22 (594-639)	15	25.5±0.9 (24.5-26.5)	10.5	70%	17.3±1.2 (16.0-18.2)	2.3	15%
		619±1 (618-620)	20	30.5±0.5 (30.0-31.0)	10.5	53%	22.2±0.3 (22.0-22.6)	2.2	11%
		621±9 (613-632)	25	36.2±0.3 (36.0-36.5)	11.2	45%	27.4±0.5 (26.8-27.7)	2.4	10%
		624±2 (622-627)	30	41.3±0.6 (41.0-42.0)	11.3	38%	32.2±0.6 (31.7-32.8)	2.2	7%
S3	76	607±10 (597-618)	10	17.0±0.5 (16.5-17.5)	7.0	70%	9.5±0.9 (8.7-10.5)	-0.5	-5%
		599±18 (584-619)	15	21.8±0.8 (21.0-22.5)	6.8	45%	14.4±0.4 (14.1-14.8)	-0.6	-4%
		594±4 (590-598)	20	27.2±0.3 (27.0-27.5)	7.2	36%	19.4±0.3 (19.1-19.7)	-0.6	-3%
		603±1 (602-604)	25	31.2±1.0 (30.0-32.0)	6.2	25%	23.0±1.0 (21.9-23.7)	-2.0	-8%
S4	68	829±68 (750-870)	10	16.3±0.6 (16.0-17.0)	6.3	63%	7.1±1.2 (5.8-8.3)	-2.9	-29%
		808±3 (805-810)	15	26.9±0.5 (26.5-27.5)	11.9	79%	16.0±0.5 (15.6-16.8)	1.0	7%
		834±8 (828-840)	20	32.0±1.2 (30.0-33.0)	12.0	60%	21.0±1.1 (19.0-22.0)	1.0	5%
		808±3 (805-810)	25	38.0±1.3 (36.5-39.5)	13.0	52%	26.6±1.1 (25.2-28.0)	1.6	6%
		870±14 (860-880)	30	40.6±0.8 (40.0-41.5)	10.6	35%	29.1±0.8 (28.4-29.9)	-0.9	-3%
S5	67	553±6 (548-557)	10	15.8±1.1 (15.0-16.5)	5.8	58%	10.6±1.1 (9.8-11.4)	0.6	6%
		576±5 (572-584)	15	20.9±1.4 (19.5-22.5)	5.9	39%	14.9±1.2 (13.8-16.2)	-0.1	-1%
		582±15 (565-593)	20	27.5±0.5 (27.0-28.0)	7.5	38%	21.0±0.9 (20.3-22.0)	1.0	5%
		603±4 (599-608)	25	31.5±0.5 (31.0-32.0)	6.5	26%	24.0±0.4 (23.7-24.5)	-1.0	-4%
		605±12 (596-624)	30	35.0±1.7 (33.0-37.0)	5.0	17%	27.1±1.3 (25.4-28.1)	-2.9	-10%

(1) IOP_t = manometric, true intraocular pressure; CCT = central corneal thickness; CVS-IOP = uncorrected intraocular pressure measurement by the CorVis ST; bIOP = biomechanically-corrected intraocular pressure measurement with four parameters.

(2) The pressure at 30 mmHg for S3 and the pressure at 10 mmHg for S2 is excluded from the table. These measurements could not be obtained using the device's automatic triggering mechanism despite repeated attempts.

The average difference for all specimens and at all IOPt levels between CVS-IOP and IOPt was 7.5 ± 3.2 (1.9 to 13.0) mmHg, while it was 0.3 ± 1.6 (-2.9 to 2.4) between bIOP and IOPt. While the difference between CVS-IOP and IOPt was significant ($p < 0.001$), the difference between bIOP and IOPt was not significant ($p = 0.989$). The error in CVS-IOP (CVS-IOP – IOPt) decreased significantly, in percentage values, with higher IOPt. However, while there was also a reduction in CVS-IOP error, in absolute values, with higher IOPt, the association of the reduction in error with IOPt was not significant ($p = 0.617$). On the other hand, no correlation was found for bIOP errors with IOPt in either percentage ($p = 0.756$) or values ($p = 0.617$). Further, the CVS-IOP error increased significantly with higher CCT (0.0196 mmHg/ μm , $p < 0.001$), unlike the errors in bIOP, which were smaller and not correlated with CCT (-0.002 mmHg/ μm , $p = 0.482$).

4.5.2 Validation of bIOP Algorithm Using Clinical Datasets

As mentioned above regarding the accuracy of the IOP-estimation algorithms, the bIOP value has higher accuracy than the CVS-IOP. As a result, there are two IOP values – bIOP, and CVS-IOP – in correction analysis, which use the trend to illustrate the association between IOP and CCT, and IOP and age.

In this study, three clinical datasets with no pathological conditions, obtained from Smile Eye Clinic (SEC), Germany; Humanitas Clinical and Research Center (HCRC), Italy; and Wenzhou Medical University (WMU), China, were used to provide IOP estimates. The results pertaining to the three clinical datasets is shown in Figure 4-4, Figure 4-5 & Figure 4-6.

Table 4-17 Results of three clinical datasets showing mean, standard deviation and a range value of CCT, age, CVS-IOP and bIOP

Database	Patients	CCT (μm)	Age (years)	CVS-IOP (mmHg)	bIOP (mmHg)
Smile Eye Clinics	632	547 \pm 32.35 (404–650)	38 \pm 11.1 (19–82)	14.45 \pm 2.83 (6.5–35.5)	13.26 \pm 2.19 (7.53–28.92)
Humanitas Clinica and Research Center	1047	538 \pm 37.33 (364–646)	45 \pm 17.7 (7–94)	14.13 \pm 3.57 (6–48.5)	12.85 \pm 2.61 (4.9–36.87)
Wenzhou Medical University	912	583 \pm 8.55 (474–595)	45 \pm 17.4 (8–94)	14.56 \pm 3.1 (7–34)	13.02 \pm 2.26 (7.44–25.5)

The correction algorithm of bIOP was successful in significantly reducing the strength of the association between CVS-IOP and CCT in the three datasets as follows: from 0.0306 mmHg/ μm ($R^2 = 0.204$) to 0.0014 mmHg/ μm ($R^2 = 0.0007$) in the SEC set; from 0.0288 mmHg/ μm ($R^2 = 0.095$) to -0.0053 mmHg/ μm ($R^2 = 0.0059$) in the HCRC set; and from 0.0314 mmHg/ μm ($R^2 = 0.090$) to -0.005 mmHg/ μm ($R^2 = 0.0044$) in the WMU set.

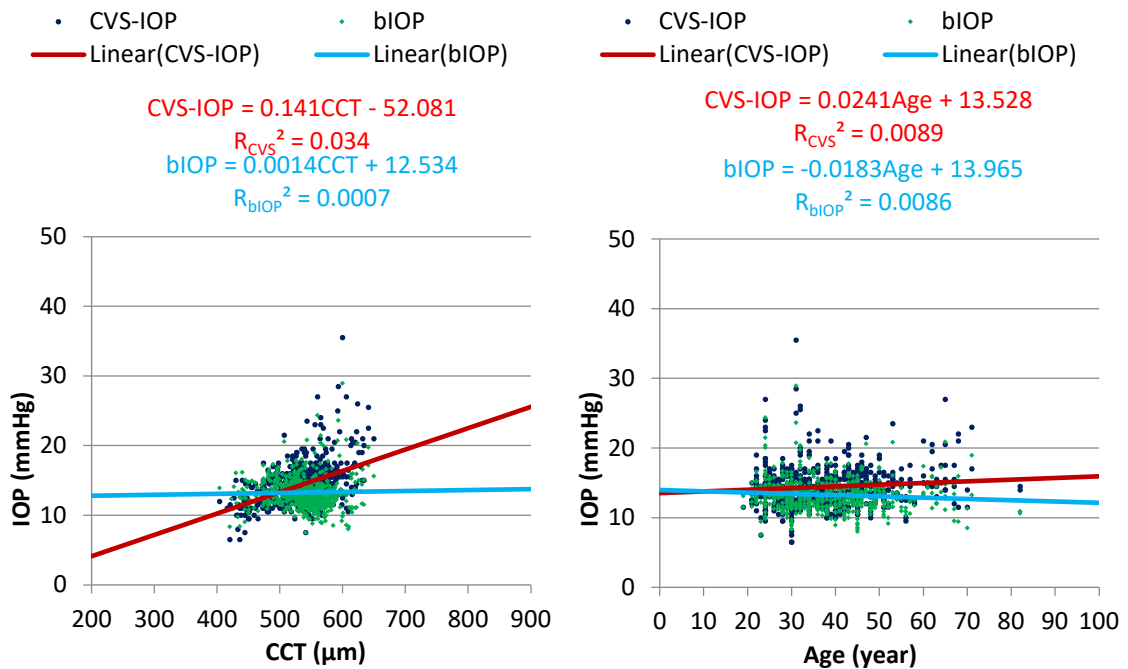


Figure 4-4 Effectiveness of bIOP in reducing association with CCT and age in clinical databases obtained from Smile Eye Clinics

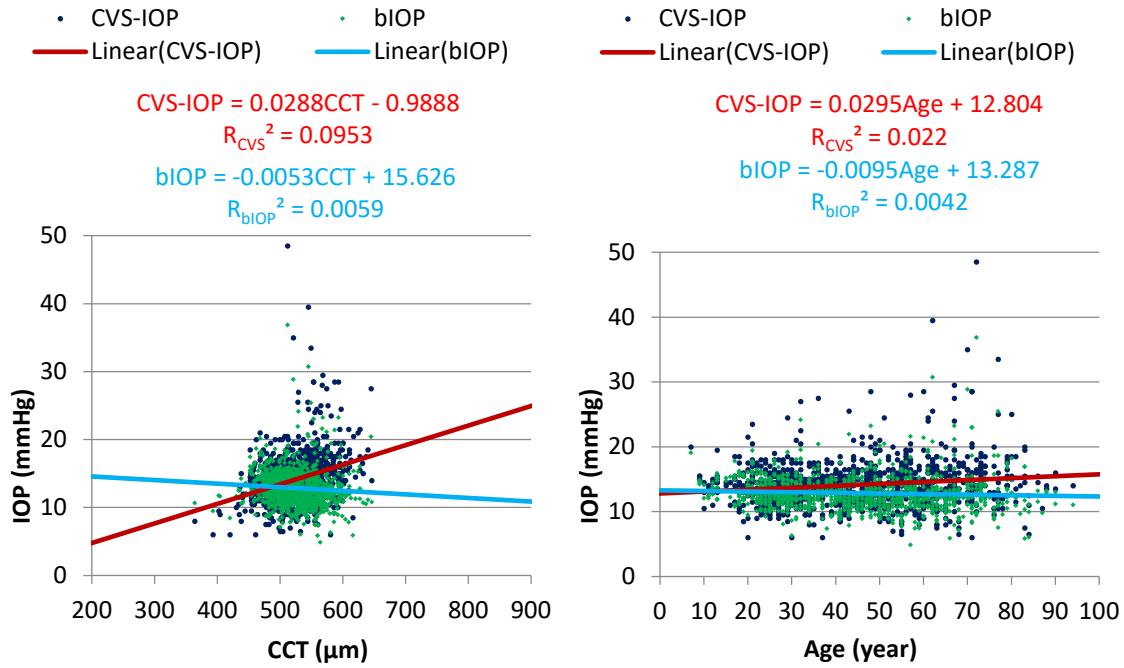


Figure 4-5 Effectiveness of bIOP in reducing association with CCT and age in clinical databases obtained from Humanitas Clinical and Research Center

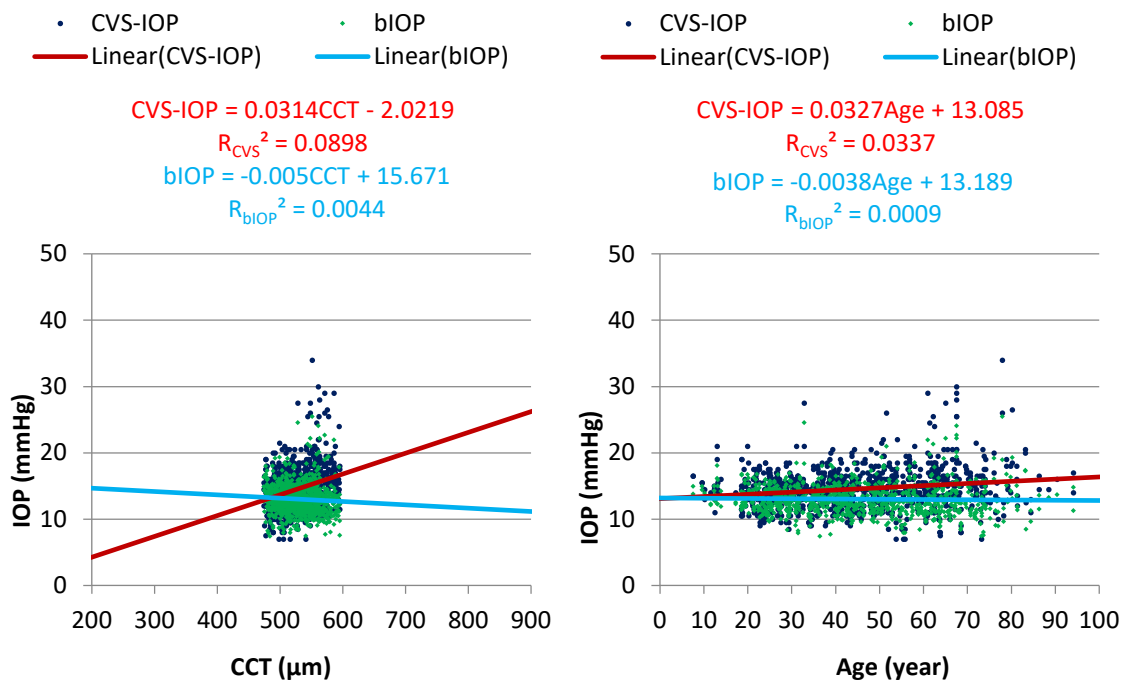


Figure 4-6 Effectiveness of bIOP in reducing association with CCT and age in clinical databases obtained from Wenzhou Medical University

In addition, the association between bIOP and age reduced in the three datasets (Figure 4-4, 4-5 & 4-6) from 0.0241 mmHg/year ($R^2 = 0.0089$) to -0.0183 mmHg/year ($R^2 = 0.0086$) in the SEC set; from 0.0295 mmHg/year ($R^2 = 0.022$) to -0.0095 mmHg/year ($R^2 = 0.0042$) in the HCRC set; and from 0.0327 mmHg/year ($R^2 = 0.0337$) to -0.0038 mmHg/year ($R^2 = 0.0009$) in the WMU set.

4.5.3 Validation of bIOP Algorithm Using Refractive Surgery Datasets

The IOP measurements by CorVis-ST are known to be significantly affected by CCT such that CVS-IOP underestimates IOP in eyes with thin corneas and overestimates IOP in eyes with thick corneas [46, 209]. In addition to considering the natural variation in CCT in the healthy population, corneal thickness is also reduced in laser refractive surgeries such as a laser in situ keratomileusis (LASIK) and small-incision lenticule extraction (SMILE, Carl Zeiss Meditec AG) [209, 258]. Hence, to evaluate the effect of corneal thickness on IOP measurement, the results concentrated on comparing the results with the correction algorithm, Goldmann Applanation Tonometry and CorVis-ST in measuring IOP before and after LASIK and SMILE.

Participants of clinical datasets

Forty-eight patients (69 eyes) were treated for correction of myopia or myopic astigmatism; however, dynamic Scheimpflug analyzer IOP parameters were missing for some participants (first applanation pressure, AP1 for 18 eyes and CCT for 1 eye). Therefore, the study comprised only 36 patients treated with LASIK (14 patients, 20 eyes [11 male, 9 female]) or SMILE (22 patients, 30 eyes [15 male, 15 female]) with an optical zone of 6.5 mm in all cases, for which there was a match in preoperative SE between LASIK group and SMILE group, Table 4-18.

Table 4-18 Pre-operative data for LASIK and SMILE groups showing mean, standard deviation and range values

	LASIK Group (n = 20)	SMILE Group (n = 30)	P value	Combined Group (n = 50)
CCT (μm)	559.7 \pm 31.0 (505–616)	542.6 \pm 30.0 (499–606)	0.06	549.6 \pm 31.2 (499–616)
Age (years)	36.7 \pm 7.4 (27–48)	35.6 \pm 7.7 (25–51)	0.62	36.0 \pm 7.5 (25–51)
Spherical Equivalence (D)	-3.65 \pm 1.12 (-5.38–-1.25)	-3.81 \pm 0.95 (-5.63–-2.00)	0.78	-3.75 \pm 1.02 (-5.63–-1.25)
Refraction manifest (Sphere)	-2.75 \pm 1.36 (-5.00–0.00)	-3.30 \pm 1.11 (-5.5–-1.5)	0.13	-3.08 \pm 1.23 (-5.50–0.00)
Refraction manifest (Cylinder)	-1.84 \pm 1.32 (-4.50–-0.25)	-0.86 \pm 0.61 (-2.25–0.00)	0.00	-1.25 \pm 1.06 (-4.5–0.00)
Refraction manifest (Axis)	68.16 \pm 65.88 (0.00–175)	90.00 \pm 71.34 (0.00–178)	0.29	81.35 \pm 69.36 (0.00–178)
GAT-IOP (mmHg)	16.1 \pm 1.7 (13.0–20.0)	15.6 \pm 2.5 (11.0–22.0)	0.39	15.8 \pm 2.2 (11.0–22.0)
CVS-IOP (mmHg)	15.2 \pm 2.3 (11.5–20.5)	14.4 \pm 2.3 (10.5–19.5)	0.22	14.7 \pm 2.3 (10.5–20.5)
bIOP (mmHg)	14.2 \pm 1.4 (11.8–18.4)	14.3 \pm 1.9 (11.5–19.0)	0.93	14.3 \pm 1.7 (11.5–19.0)

CCT = Central Corneal Thickness; GAT-IOP = IOP measured by Goldman Applanation Tonometer; CVS-IOP = IOP measured by CorVis-ST; bIOP= Biomechanically corrected IOP measured by CorVis-ST.

Preoperative Results

Table 4-18 presents the preoperative mean, SD, and range of central corneal thickness (CCT), age, spherical equivalence (SE), and IOP measurements obtained from Goldmann (GAT-IOP) and CorVis-ST (CVS-IOP and bIOP) for both the LASIK and SMILE groups, separately and combined. An independent-samples t-test found no significant difference between the preoperative values of all parameters between the two groups.

Results of Pearson’s analysis between the IOP and CCT values in both the LASIK and SMILE groups, separately and combined, are shown in Table 4-19. In all cases, the analysis showed a significant preoperative correlation between either GAT-IOP or CVS-IOP with CCT, but not between bIOP and CCT. Hence, the first main observation of the study is that the bIOP algorithm was successful in reducing correlation with CCT before refractive surgery.

Table 4-19 Pre-operative datasets for both LASIK and SMILE groups showing results of Pearson's correlation analysis

		<i>LASIK Group</i>		<i>SMILE Group</i>		<i>Combined Group</i>	
		<i>R-value</i>	<i>P-value</i>	<i>R-value</i>	<i>P-value</i>	<i>R-value</i>	<i>P-value</i>
<i>Pre-Operative CCT vs</i>	<i>GAT-IOP</i>	0.481*	0.032	0.259*	0.045	0.345*	0.015
	<i>CVS-IOP</i>	0.480*	0.032	0.329**	0.002	0.418**	0.003
	<i>bIOP</i>	0.006	0.980	0.005	0.978	0.005	0.972

CCT = Central Corneal Thickness; GAT-IOP = IOP measured by Goldman Applanation Tonometer; CVS-IOP = IOP measured by CorVis-ST; bIOP = Biomechanically corrected IOP measured by the CorVis-ST device

* Correlation is significant at the 0.05 level (2-tailed).

** Correlation is significant at the 0.01 level (2-tailed).

Postoperative Results

Table 4-20 presents the postoperative mean, SD, and range of CCT, SE, GAT-IOP, CVS-IOP, and bIOP for both the LASIK and SMILE groups, separately and combined. In Table 4-21, the Pearson's analysis showed significant correlation between postoperative GAT-IOP and CCT ($R = 0.22$, $p = 0.047$ in the LASIK group; $R = 0.17$, $p = 0.037$ in the SMILE group; $R = 0.034$, $p = 0.043$ in the combined group) and between postoperative CVS-IOP and CCT ($R = 0.362$, $p = 0.05$ in the LASIK group; $R = 0.354$, $p = 0.003$ in the SMILE group; $R = 0.374$, $p = 0.008$ in the combined group). In contrast, there was no significant correlation between postoperative bIOP and CCT in all cases ($R = 0.09$, $p = 0.705$ in the LASIK group; $R = 0.068$, $p = 0.706$ in the SMILE group; $R = 0.061$, $p = 0.678$ in the combined group). These results illustrate the second main observation of the study, which is that the bIOP correction was successful in removing the correlation of IOP measurements obtained after LASIK and SMILE with CCT.

Table 4-20 Post-operative data for both LASIK and SMILE groups showing mean, standard deviation and range values

	LASIK Group (n = 20)	SMILE Group (n = 30)	Combined Group (n = 50)
CCT (μm)	483.3 \pm 33.6 (420–548)	466.0 \pm 33.9 (413–558)	473.0 \pm 34.5 (413–558)
Spherical Equivalence (D)	-0.13 \pm 0.33 (-1.00–0.50)	-0.04 \pm 0.26 (-0.75–0.75)	-0.07 \pm 0.30 (-1.00–0.75)
GAT-IOP (mmHg)	12.9 \pm 2.5 (10–17)	12.3 \pm 2.3 (8–18)	12.6 \pm 2.4 (8–18)
CVS-IOP (mmHg)	11.6 \pm 1.6 (8.5–15)	11.1 \pm 1.9 (6–14.5)	11.3 \pm 1.8 (6–15)
biOP (mmHg)	14.1 \pm 1.5 (11.6–16.9)	13.5 \pm 1.9 (9.2–17.5)	13.7 \pm 1.8 (9.2–17.5)

CCT= Central Corneal Thickness; GAT-IOP= IOP measured by Goldman Applanation Tonometer; CVS-IOP= IOP measured by CorVis-ST; biOP= Biomechanically corrected IOP measured by CorVis-ST

Table 4-21 Post-operative datasets for both LASIK and SMILE groups showing results of Pearson's correlation analysis

		LASIK Group (n = 20)		SMILE Group (n = 30)		Combined Group (n = 50)	
		R-value	P-value	R-value	P-value	R-value	P-value
Post-Operative CCT vs	GAT-IOP	0.220*	0.047	0.170*	0.037	0.034*	0.043
	CVS-IOP	0.362**	0.005	0.354**	0.003	0.374**	0.008
	biOP	0.09	0.705	0.068	0.706	0.061	0.678

CCT = Central Corneal Thickness; GAT-IOP = IOP measured by Goldman Applanation Tonometer; CVS-IOP = IOP measured by CorVis-ST; biOP = Biomechanically corrected IOP measured by the CorVis-ST device

* Correlation is significant at the 0.05 level (2-tailed).

** Correlation is significant at the 0.01 level (2-tailed).

Comparison between IOP measurements obtained Pre- and Post-Surgery

Table 4-22 presents the results of the paired-samples t-test that aimed to compare the values of GAT-IOP, CVS-IOP, and biOP pre- and post-operation for the LASIK and SMILE groups, separately and combined. After the treatment, there was a significant decrease in GAT-IOP (-3.2 \pm 3.4 mmHg, $p < 0.001$ in the LASIK group; -3.2 \pm 2.1 mmHg, $p < 0.001$ in the SMILE group; -3.2 \pm 2.6 mmHg, $p < 0.001$ in the combined group) and in CVS-IOP (-3.7 \pm 2.1 mmHg, $p < 0.001$ in the LASIK group; -3.3 \pm 2.0 mmHg, $p < 0.001$ in the SMILE group; -3.4 \pm 2.0 mmHg, $p < 0.001$ in the combined group). On the other hand, the preoperative and postoperative biOP did not

differ significantly (0.1 ± 2.1 mmHg, $p = 0.80$ in the LASIK group; 0.8 ± 1.8 mmHg, $p = 0.273$; 0.2 ± 1.9 mmHg in the SMILE group, $p = 0.58$ in the combined group). These results have led to the third main observation of the study, which is that bIOP was successful in reducing the differences in IOP measurements obtained before and after refractive surgery.

Table 4-22 Differences between post- and pre-operative data for both LASIK and SMILE groups showing the mean, standard deviation and p value of the paired t-test results

Post-Pre	LASIK Group (n = 20, M = 11, F = 9)		SMILE Group (n = 30, M = 15, F = 15)		Combined Group (n = 50, M = 26, F = 24)	
	Mean \pm SD	P-value	Mean \pm SD	P-value	Mean \pm SD	P-value
CCT (μ m)	-76.4 \pm 19.9	< 0.001	-76.6 \pm 19.6	< 0.001	-76.4 \pm 19.5	< 0.001
GAT-IOP (mmHg)	-3.2 \pm 3.4	< 0.001	-3.2 \pm 2.1	< 0.001	-3.2 \pm 2.6	< 0.001
CVS-IOP (mmHg)	-3.7 \pm 2.1	< 0.001	-3.3 \pm 2.0	< 0.001	-3.4 \pm 2.0	< 0.001
bIOP (mmHg)	-0.1 \pm 2.1	0.795**	-0.8 \pm 1.8	0.273**	-0.2 \pm 1.9	0.58**

CCT = Central Corneal Thickness, GAT-IOP = IOP measured by Goldman Applanation Tonometer; CVS-IOP = IOP measured by CorVis-ST; bIOP = Biomechanically corrected IOP measured by CorVis-ST

** No significant difference between means of pre-and post-values.

The results of the trend line analysis of pre- and post-surgery datasets is shown in Figure 4-7, Figure 4-8 & Figure 4-9. The correlations between CVS-IOP and CCT significantly increase the strength between GAT-IOP and CCT in the pre- and post-surgery datasets as follows: From 0.0266 mmHg/ μ m ($R^2=0.2318$) to 0.0348 mmHg/ μ m ($R^2=0.2301$) in the pre-operative dataset of the LASIK group; from -0.0166 mmHg/ μ m ($R^2=0.0484$) to 0.0177 mmHg/ μ m ($R^2=0.1312$) in the post-operative dataset of the LASIK group; from 0.0212 mmHg/ μ m ($R^2=0.067$) to 0.0248 mmHg/ μ m ($R^2=0.108$) in the pre-operative dataset of the SMILE group; from 0.0114 mmHg/ μ m ($R^2=0.029$) to 0.0201 mmHg/ μ m ($R^2=0.1256$) in the post-operative dataset of the

SMILE group; from 0.0241 mmHg/ μm ($R^2=0.1194$) to 0.0304 mmHg/ μm ($R^2=0.1749$) in the pre-operative datasets of both LASIK and SMILE groups; and from 0.0023 mmHg/ μm ($R^2 = 0.0011$) to 0.0196 mmHg/ μm ($R^2=0.1402$) in the post-operative datasets of both LASIK and SMILE groups.

On the contrary, the correction algorithm of bIOP was successful in significantly reducing the strength of the association between GAT-IOP and CCT in the pre- and post-surgery data sets, using bIOP as follows: From 0.0266 mmHg/ μm ($R^2=0.2318$) to 0.0003 mmHg/ μm ($R^2=4E-5$) in the pre-operative dataset of the LASIK group; from -0.0166 mmHg/ μm ($R^2=0.0484$) to -0.0041 mmHg/ μm ($R^2=0.0081$) in the post-operative dataset of the LASIK group; from 0.0212 mmHg/ μm ($R^2=0.067$) to -0.0003 mmHg/ μm ($R^2=3E-5$) in the pre-operative dataset of the SMILE group; from 0.0114 mmHg/ μm ($R^2=0.029$) to 0.0041 mmHg/ μm ($R^2=0.0053$) in the post-operative dataset of the SMILE group; from 0.0241 mmHg/ μm ($R^2=0.1194$) to -0.0003 mmHg/ μm ($R^2=3E-5$) in the pre-operative datasets of both LASIK and SMILE groups; and from 0.0023 mmHg/ μm ($R^2=0.0011$) to 0.0021 mmHg/ μm ($R^2=0.0037$) in the post-operative datasets of both LASIK and SMILE groups.

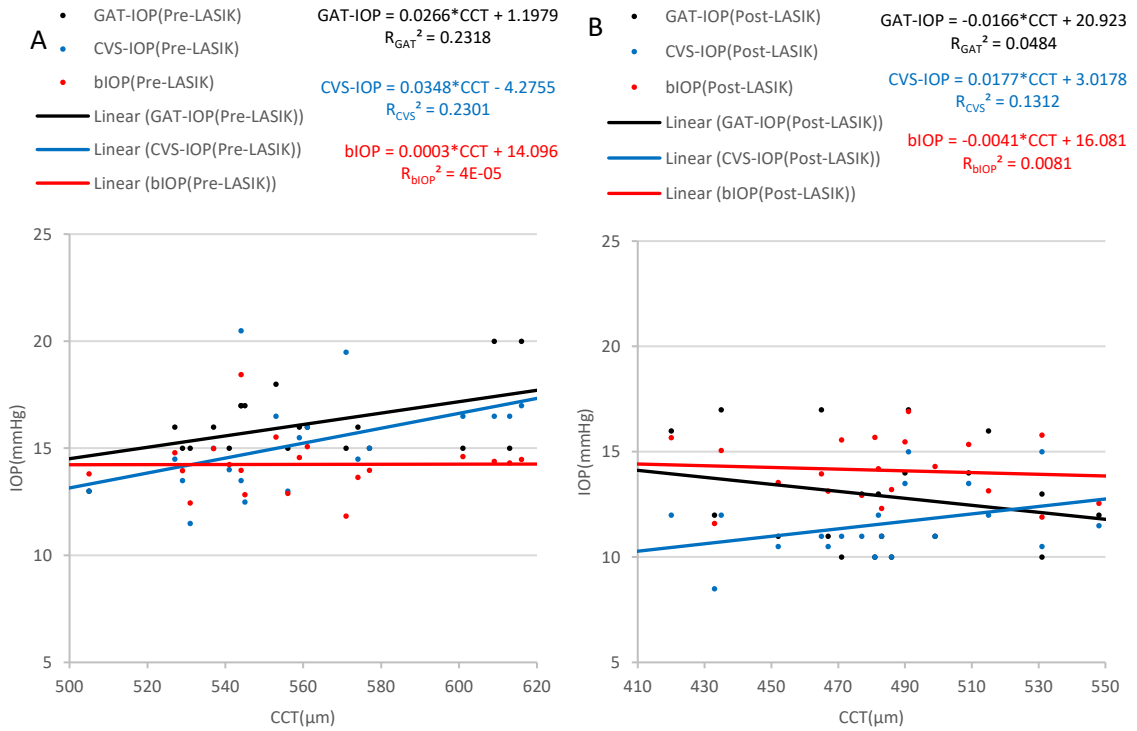


Figure 4-7 Correlation between CCT and GAT-IOP, CVS-IOP and bIOP for (A) pre- and (B) post-operative data of LASIK group.

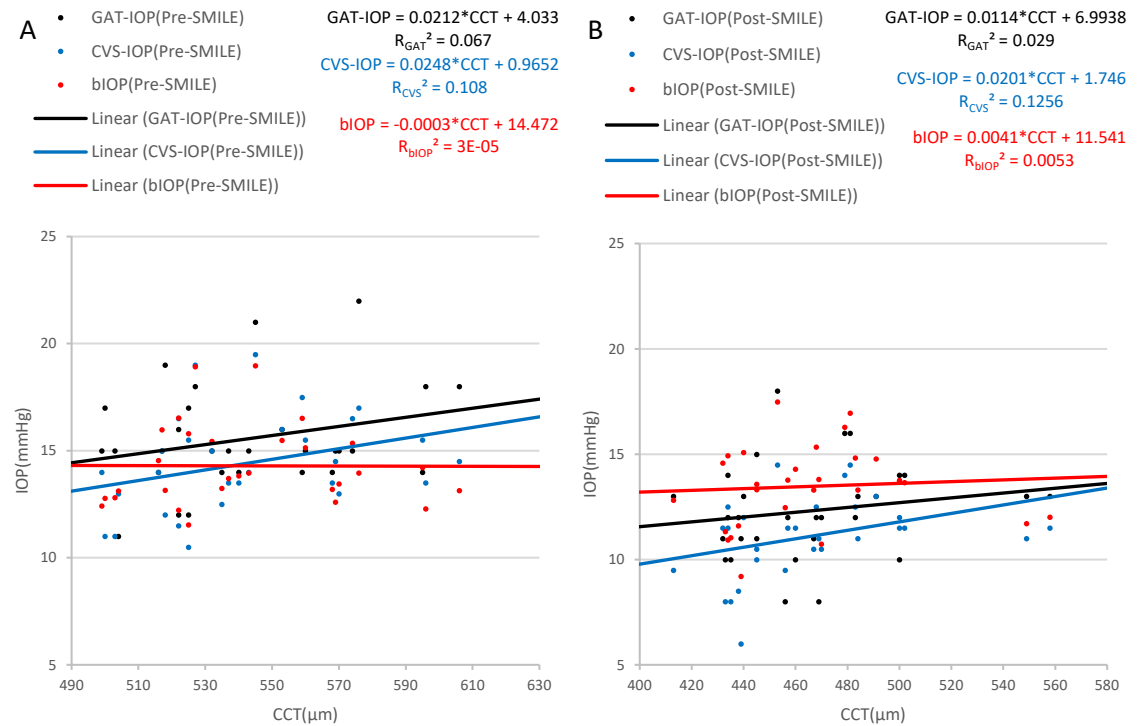


Figure 4-8 Correlation between CCT and GAT-IOP, CVS-IOP and bIOP for (A) pre- and (B) post-operative data of SMILE group.

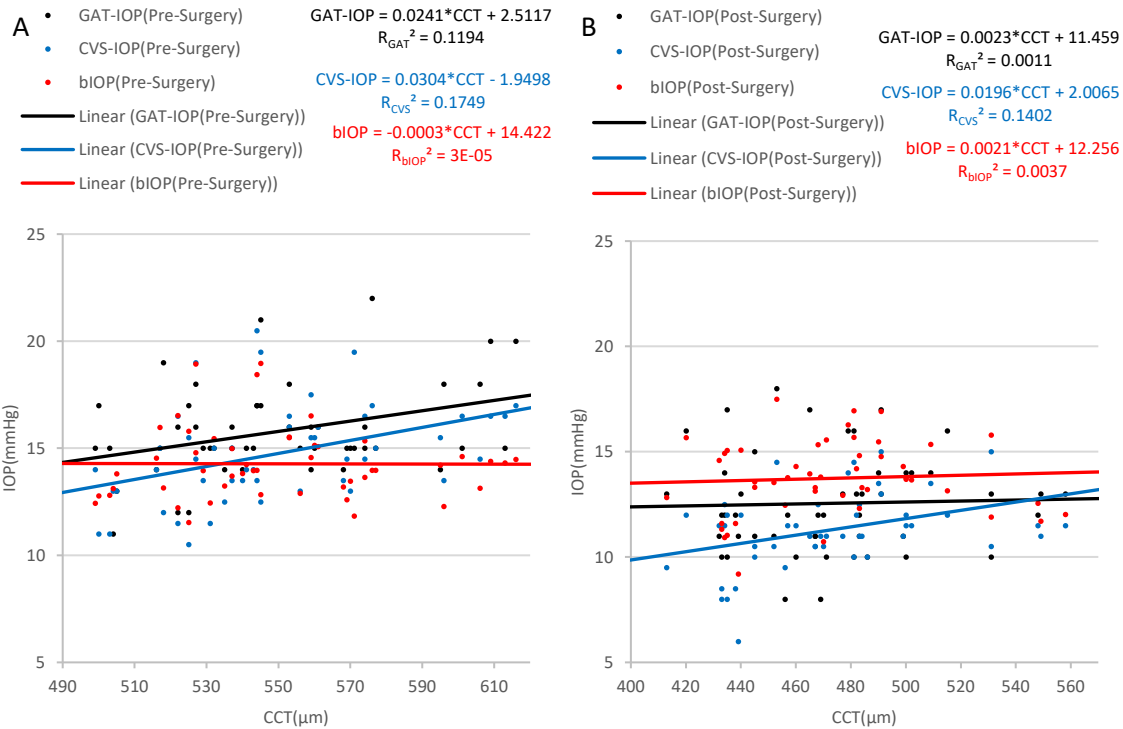


Figure 4-9 Correlation between CCT and GAT-IOP, CVS-IOP and bIOP for (A) pre- and (B) post-operative data of both LASIK and SMILE groups.

Overall, there was no significant difference in the mean values of bIOP estimation, which implies that the bIOP values of the pre- and post-operative datasets are not different when the P-value is greater than 0.05 in either the LASIK or SMILE group. The linear association test revealed that the association between bIOP and age, and between bIOP and CCT in pre-and post-operative data was lower than for GAT-IOP and CVS-IOP. This means that the effect of CCT and age was less on the bIOP value.

4.6 Validation of bIOP_{KC}-Estimation Algorithm for Keratoconic Eyes Using Clinical Datasets

The clinical validation of bIOP_{KC} algorithm for keratoconic patients was performed with the expectation of a significant reduction in dependency of corneal biomechanics. The results

compared the IOP values between healthy and keratoconic patients using the bIOP and bIOP_{KC} algorithms, respectively, followed by their correlation with corneal thickness and age in two large clinical datasets from two different continents. There are 315 participants (164 healthy and 151 Keratoconic) from the Vincieye Clinic in Milan, Italy in Dataset 1, and 407 participants (205 healthy and 202 Keratoconic) from the Rio de Janeiro Corneal Tomography and Biomechanics Study Group – Rio de Janeiro, Brazil in Dataset 2 to include variability from more than one continent.

4.6.1 Analysis of Dataset 1 from Milan and Dataset 2 from Rio

Analysis of Dataset 1 (Milan)

In Dataset 1, the mean age of healthy participants was 35 ± 13 years (range 14–73), which was similar to the mean age of KC patients, 33 ± 12 (14–73) years ($p = 0.507$). In contrast, the CCT was considerably higher, as expected, in healthy eyes [543 ± 32 (458–635) μm] than in KC eyes [482 ± 45 (239–595) μm] ($p < 0.001$). For both groups, the mean bIOP was almost the same – 14.7 ± 1.6 (10.6–20.4) mmHg for healthy eyes and 14.6 ± 1.2 (10.9–18.1) mmHg for KC eyes ($p = 0.121$) – while the CorVis IOP was lower in KC eyes [13.1 ± 2.2 (5.0–19.5) mmHg] than in healthy cases [15.1 ± 1.6 (11.0–23.0) mmHg] ($p < 0.001$) (Figure 4-10). There were also significant differences between bIOP and CorVis IOP obtained for KC patients ($p < 0.0001$), but the same was not observed for healthy participants ($p = 0.103$) (Figure 4-10). Furthermore, there was a significant difference in variances of bIOP_{KC} as compared to CVS-IOP in KC patients ($p < 0.0001$, Figure 4-10).

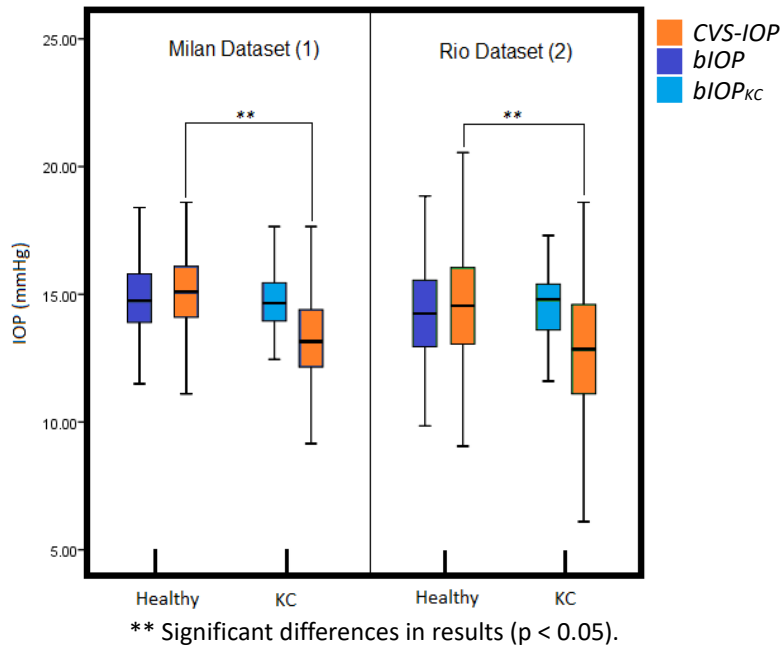


Figure 4-10 CVS-IOP, bIOP, and bIOP_{KC} values obtained for healthy and KC participants from Datasets 1 and 2. Results illustrate the stability in predicting IOP values using the bIOP and bIOP_{KC} algorithms for healthy and KC eyes, compared to the large differences found in CVS-IOP. Both bIOP and bIOP_{KC} further exhibit lower standard deviation values compared to CVS-IOP.

Analysis of Dataset 2 (RIO)

Similar to Dataset 1, healthy and KC participants in Dataset 2 had similar age ranges of $[40 \pm 13$ (18-72)] years and $[39 \pm 13$ (18-72)] years, respectively ($p = 0.228$). However, they had different CCT ranges of $[540 \pm 33$ (454-629)] μm and $[491 \pm 41$ (381-586)] μm respectively ($p < 0.001$). Similar IOP results were obtained with the mean bIOP being similar in healthy eyes [bIOP 14.4 ± 2.2 (9.9-24.3)] mmHg and KC eyes [bIOP_{KC} 14.4 ± 1.1 (11.5-17.2)] mmHg ($p = 0.319$); while the CVS-IOP in KC eyes, $[12.6 \pm 2.5$ (4.5-20.0)] mmHg, was significantly lower than in healthy eyes $[14.8 \pm 2.6$ (9.0-29.0)] mmHg ($p < 0.001$). The bIOP_{KC} values were also significantly different from the CVS-IOP in KC eyes ($p < 0.0001$, Figure 4-10), while there were no significant differences between bIOP and CVS-IOP in healthy eyes ($p = 0.091$). Analogous to the results

obtained in Dataset 1, the comparative analysis of KC patients showed significantly different variances of $bIOP_{KC}$ as compared to CVS-IOP ($p < 0.0001$, Figure 4-10).

4.6.2 Correlation of IOP_{KC} Estimates with Age and Corneal Thickness

The degree of dependency of $bIOP_{KC}$ and CVS-IOP on CCT and age in KC patients of both datasets have been assessed in Figure 4-11.

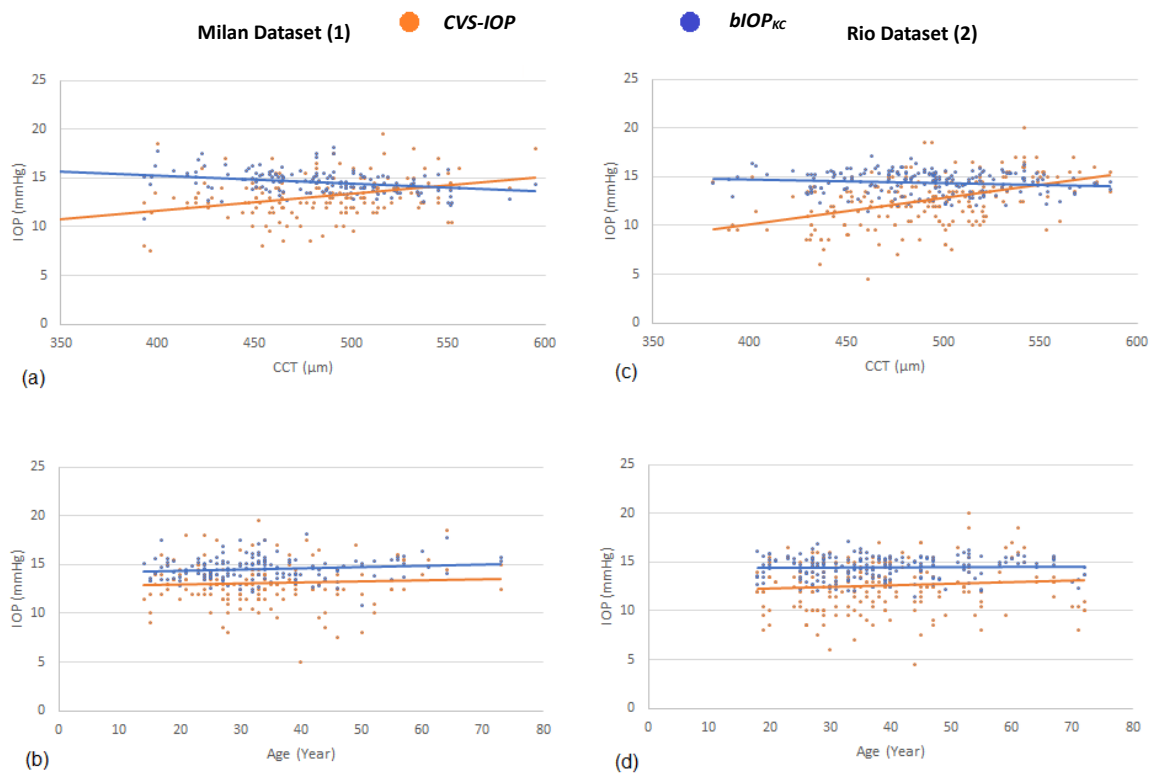


Figure 4-11 Analysis of the degree of dependency of both $bIOP_{KC}$ and CVS-IOP on CCT and age in the Milan (a, b) and Rio dataset (c, d)

The results show large $bIOP_{KC}$ reductions in IOP dependency on CCT: From 1.7 mmHg/100 μm (with CVS-IOP) to -0.8 mmHg/100 μm (with $bIOP_{KC}$) in Dataset 1 and from 2.7 mmHg/100 μm (with CVS-IOP) to -0.3 mmHg/100 μm (with $bIOP_{KC}$) in Dataset 2. On the other hand, the dependency of IOP on age, which was small in the case of CVS-IOP, experienced only small

reductions. With $bIOP_{KC}$, it changed from 0.12 mmHg/decade (with CVS-IOP) to 0.10 mmHg/decade (with $bIOP_{KC}$) in Dataset 1 and from 0.17 mmHg/decade (with CVS-IOP) to 0.02 mmHg/decade (with $bIOP_{KC}$) in Dataset 2.

4.6.3 Comparative Analysis Based on Keratoconus Classification

The Keratoconic group in Dataset 1 was decomposed in accordance with the TKC classification into 30 mild, 50 moderate, and 29 advanced cases. Similarly, in Dataset 2, the subgroups included 20 mild, 51 moderate, and 19 advanced cases. Figure 4-12 shows $bIOP_{KC}$ and CVS-IOP in KC patients, split into the TKC classification groups. The results present evidence of the non-significant difference in $bIOP_{KC}$ and CVS-IOP in the three KC stage groups ($p = 0.095$ and $p = 0.413$ for Dataset 1 and $p = 0.693$ and $p = 0.579$ for Dataset 2 with Kruskal-Wallis). However, as described previously, the CVS-IOP values were significantly lower and had significantly larger standard deviations than the $bIOP_{KC}$ in both datasets and all patient subgroups.

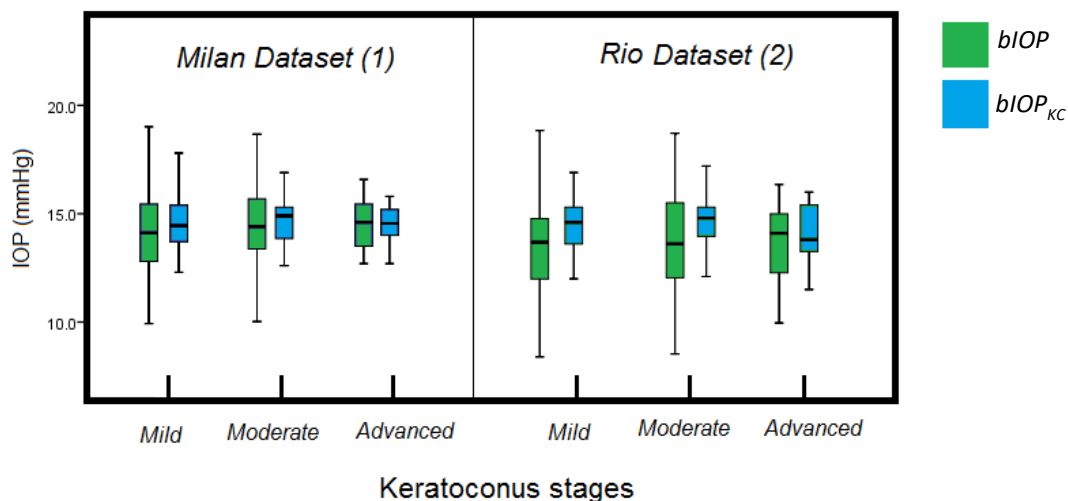


Figure 4-12 Mean and standard deviation of $bIOP$ and $bIOP_{KC}$ in both datasets in KC patients divided based on disease stage

4.6.4 Comparison of bIOP and bIOP_{KC} in Keratoconic Patients

Milan Dataset (1)

There were no significant differences in the mean values and standard deviations of bIOP and bIOP_{KC} between patients with mild, moderate, and advanced Keratoconus ($p > 0.05$; see Table 4-23). When comparing the values of bIOP and bIOP_{KC}, the main outcome of this sub-analysis was the significantly smaller standard deviations of bIOP_{KC} as compared to bIOP in all stages of Keratoconus, except the advanced cases ($p < 0.001$ for mild, $p = 0.035$ for moderate, and $p = 0.067$ for advanced cases). Conversely, the mean values of bIOP and bIOP_{KC} were not significantly different in mild, moderate, and advanced Keratoconus (respectively $p = 0.168$, $p = 0.649$, and $p = 0.329$).

Table 4-23 Number, mean, and standard deviation of all KC data used in Milan Dataset (1) for bIOP and bIOP_{KC}. Further, a homogeneity test was carried out to show the differences in standard deviation and the ANOVA test was performed to analyse the mean values.

		<i>N</i>	<i>Mean</i>	<i>Standard Deviation</i>	<i>Homogeneity of Variances</i>	<i>ANOVA</i>
	<i>Mild</i>	106	14.2	2.1		
<i>bIOP</i>	<i>Moderate</i>	27	14.5	1.9	P = 0.677	P = 0.508
	<i>Advanced</i>	18	13.8	2.5		
	<i>Mild</i>	106	14.6	1.2		
<i>bIOP_{KC}</i>	<i>Moderate</i>	27	14.7	1.1	P = 0.813	P = 0.749
	<i>Advanced</i>	18	14.4	1.3		

Rio Dataset (2)

Similarly, there were no significant differences in the mean values and standard deviations of bIOP and bIOP_{KC} in patients with mild, moderate, and advanced Keratoconus ($p > 0.05$; see Table 4-24). The comparative analysis of bIOP and bIOP_{KC} in patients with KC showed, as the main outcome, significantly smaller standard deviations of bIOP_{KC} when compared with bIOP in all stages of Keratoconus ($p < 0.001$ for mild and moderate and $p = 0.035$ for advanced). Likewise, the mean values of bIOP were significantly lower in mild and moderate Keratoconus as compared to bIOP_{KC} (respectively $p < 0.001$ and $p = 0.008$).

Table 4-24 Number, mean, and standard deviation of all KC data used in Rio Dataset (2) for bIOP, CVS-IOP, and bIOP_{KC}. Further, a homogeneity test was carried out to show the differences in standard deviation and the ANOVA test was performed to analyse the mean values.

		<i>N</i>	<i>Mean</i>	<i>Standard Deviation</i>	<i>Homogeneity of Variances</i>	<i>ANOVA</i>
	<i>Mild</i>	128	13.5	2.0		
<i>bIOP</i>	<i>Moderate</i>	51	13.7	2.2	P = 0.627	P = 0.769
	<i>Advanced</i>	23	13.3	2.4		
	<i>Mild</i>	128	14.4	1.1		
<i>bIOP_{KC}</i>	<i>Moderate</i>	51	14.6	1.1	P = 0.155	P = 0.270
	<i>Advanced</i>	23	14.1	1.3		

4.7 In-Vivo Validation of Corneal Material Algorithm (β)

The main challenge in estimating the corneal biomechanical behaviour in vivo stems from the difficulty in separating the effects of this behaviour from those of the IOP on ocular response

to mechanical stimuli. A positive development towards achieving a solution to this problem was the introduction of the biomechanically-corrected IOP (bIOP) and corneal material parameter (β) estimates based on the CorVis-ST output.

The bIOP algorithm was developed using a combination of numerical modelling, experimental and clinical validation, and used corneal deformation parameters (measured by the CorVis ST) to reduce the effect of stiffness on IOP estimates on the basis of the above-mentioned results. In the following development procedure in Chapter 3.1, this study takes the next logical step in providing an algorithm for estimation of the material mechanical behaviour in Section 4.4.3.

In this Section, the algorithm was validated by comparing the result between predictions from the algorithm and results from the inverse analysis for healthy and keratoconic datasets, assessing the correlation between its material stiffness predictions and patient's age in healthy datasets, and against earlier results of inflation experiments on ex-vivo human eyes [1].

For inverse analysis, due to the time-consuming nature of procedure, there were only 84 healthy and 17 keratoconic eyes from Milan, and 84 healthy and 17 keratoconic eyes from Brazil selected to validate corneal material parameter (β), Table 4-25.

Table 4-25 Selected data from healthy and KC groups showing mean, standard deviation and range values

	Healthy Group (N = 168)	Keratoconic Group (N = 34)
Age [years]	39.89 ± 16.66 (7–81)	35.62 ± 11.07 (16–59)
CCT [μm]	543.8 ± 29.42 (454–621)	477 ± 37.59 (389–551)
CVS-IOP [mmHg]	15 ± 2.56 (9.5–29)	13.19 ± 2.35 (9–18)
bIOP/bIOP_{KC} [mmHg]	14.47 ± 2.28 (9.79–24.27)	15.56 ± 1.21 (13.18–19.33)
A1T [ms]	7.25 ± 0.31 (6.65–8.78)	7.05 ± 0.33 (6.7–7.77)
A1L [mm]	2.12 ± 0.35 (1.34–2.76)	1.88 ± 0.42 (1.3–2.82)
A1V [mm/s]	0.16 ± 0.02 (0.07–0.22)	0.18 ± 0.03 (0.14–0.27)
PD. [mm]	5.06 ± 0.28 (3.85–5.81)	5.06 ± 0.28 (4.37–5.49)
R [mm]	7.05 ± 0.81 (5.54–10.75)	5.89 ± 0.9 (4.25–8.61)
A1Deformation [mm]	0.13 ± 0.01 (0.1–0.16)	0.13 ± 0.01 (0.11–0.16)
HCDeformation [mm]	1.09 ± 0.09 (0.8–1.34)	1.15 ± 0.13 (0.9–1.41)
A1Deflection [mm]	0.1 ± 0.01 (0.07–0.13)	0.1 ± 0.01 (0.08–0.13)
HCDeflection [mm]	0.91 ± 0.1 (0.55–1.23)	0.99 ± 0.13 (0.72–1.21)
AP1 [mmHg]	42.23 ± 6.35 (29.3–74.8)	37.44 ± 7.12 (26.9–52.3)

4.7.1 Comparison of β Obtained from the Estimate Algorithm and Inverse Analysis for Healthy Eyes

A total of 168 healthy patients were selected from the Milan and Brazil clinical datasets. To evaluate the effectiveness of the β algorithm, the results from the inverse analysis were assumed to represent the true material parameters.

Table 4-25 and Table 4-26 presents the mean, SD, and range of the central corneal thickness (CCT), age, IOP measurements by the CorVis-ST device (CVS-IOP), the biomechanically-corrected IOP (bIOP), and β values obtained from the estimated algorithm (β_{Eq}) and inverse analysis (β_{In}) for healthy eyes.

Table 4-26 Clinical datasets for healthy eyes showing mean, standard deviation, a range of β and p-value of paired t-test results between β algorithm and inverse analysis

<i>Number</i>	168
β_{Eq} <i>(from estimated algorithm)</i>	0.93 ± 0.19 (0.56–1.67)
$\beta_{I.}$ <i>(from inverse analysis)</i>	0.93 ± 0.21 (0.47–1.55)
<i>Differences of Mean ± SD</i>	0.00 ± 0.12
<i>p value</i>	0.998

** Significant differences between means of β_{Eq} and β_{In}

The β_{In} obtained from inverse analysis of numerical models simulating the 168 eyes included in the study had a mean of 0.93±0.21 (0.47-1.55) and the β algorithm provided a β_{Eq} mean of 0.93±0.19 (0.56-1.67), Table 4-26. There were no significant differences between the two sets of β values (p=0.99), Figure 4-13.

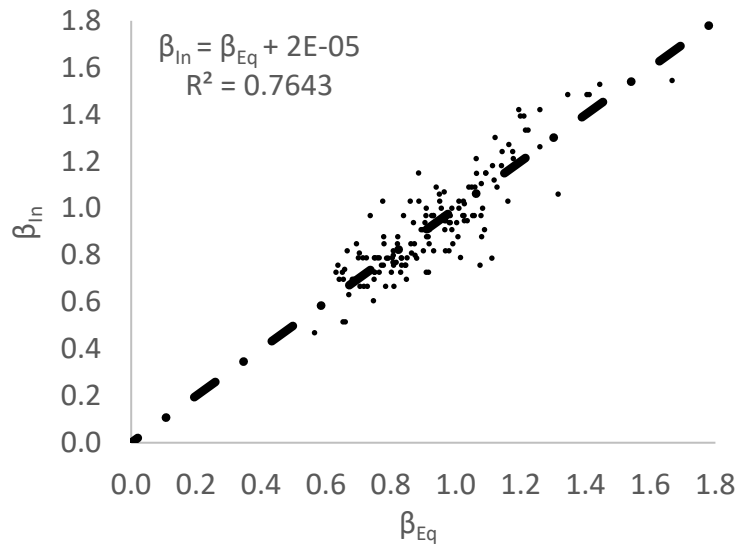


Figure 4-13 Results of the β algorithm (β_{Eq}) against β inverse analysis (β_{In}) for 158 healthy eyes shown with a red trend line against a 45-degree line denoting target perfect fit

4.7.2 Correlation Analysis of the Material Parameter (β) with Corneal Thickness and IOP for Healthy Eyes

The material estimate algorithm has been able to successfully predict the in-vivo material behaviour of corneal tissue as estimated using an inverse analysis procedure. The β algorithm was assessed against clinical data obtained from 480 healthy participants enrolled at the Vincieye Clinic in Milan, Italy (Dataset 1, 253 patients) and Corneal Tomography and Biomechanics Study Group – Rio de Janeiro, Brazil (Dataset 2, 227 patients).

Dataset 1 (Milan)

253 Participants included in Dataset 1 had a mean age of 43.1 ± 16.6 (8-87) years, CCT of 539.3 ± 33.2 (454-629) microns and bIOP of 14.3 ± 2.6 (7.7-29.3) mmHg. Analysis of CCT, bIOP, age and β_{Eq} values confirmed the hypothesis that β_{Eq} was not dependant on CCT ($p=0.792$) or IOP ($p=0.745$) but significantly correlated with age ($P<0.01$), Figure 4-14. Statistical analysis

was performed using Pearson correlation for bIOP and CCT as the data were normally distributed and with Spearman's rho correlation for an age where the data were not normally distributed.

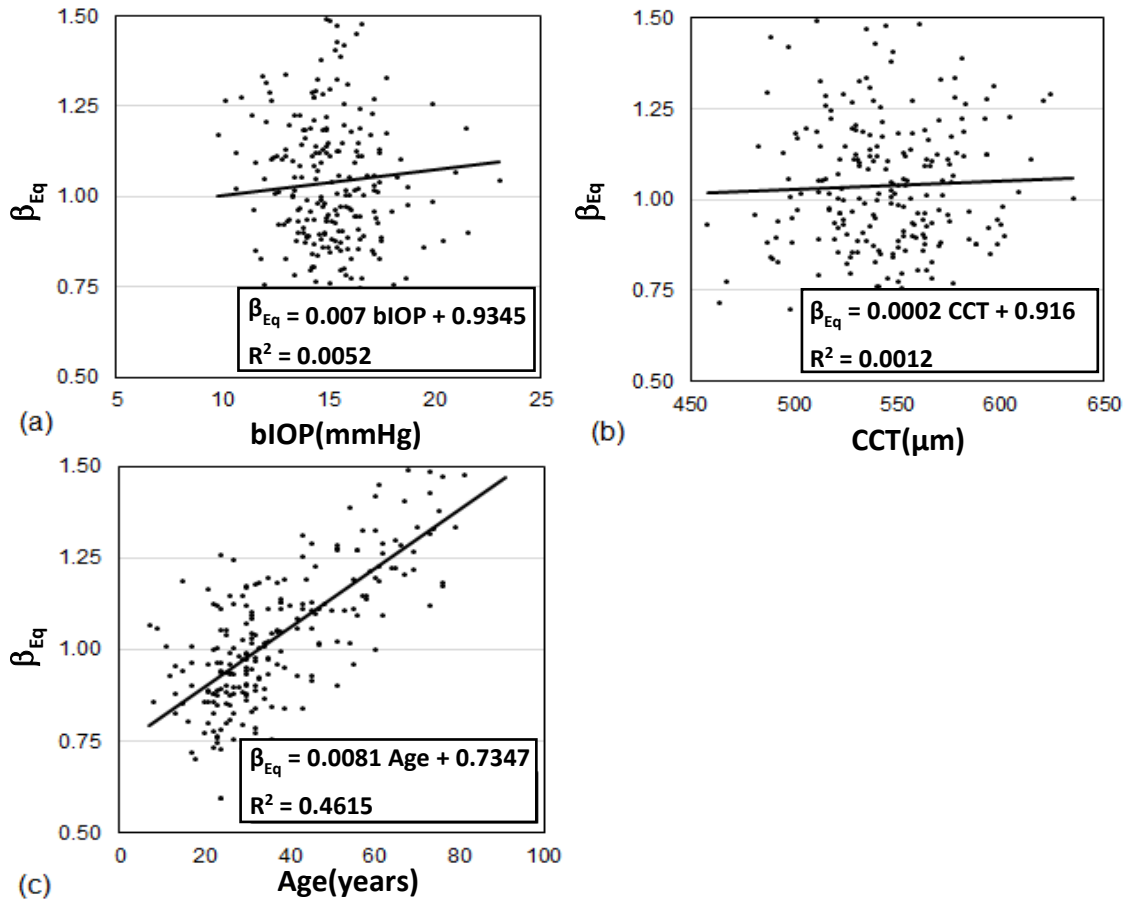


Figure 4-14 Assessment of the correlation in Dataset 1 between β_{Eq} and each of (a) bIOP, (b) CCT and (c) Age

Dataset 2 (Rio)

In Dataset 2, participants had a mean age of 37.6 ± 17.1 (7-90) years, CCT of 543.8 ± 31.5 (454-635) microns and bIOP of 14.5 ± 2.3 (9.8-24.3). Similar to Dataset 1, the analysis showed that β_{Eq} was not dependant on CCT ($p = 0.599$) or bIOP ($p = 0.281$), but was significantly correlated with age ($P < 0.01$), Figure 4-15. Statistical analysis was performed using Pearson correlation

with bIOP and CCT and Spearman's rho correlation with age for the reasons described above.

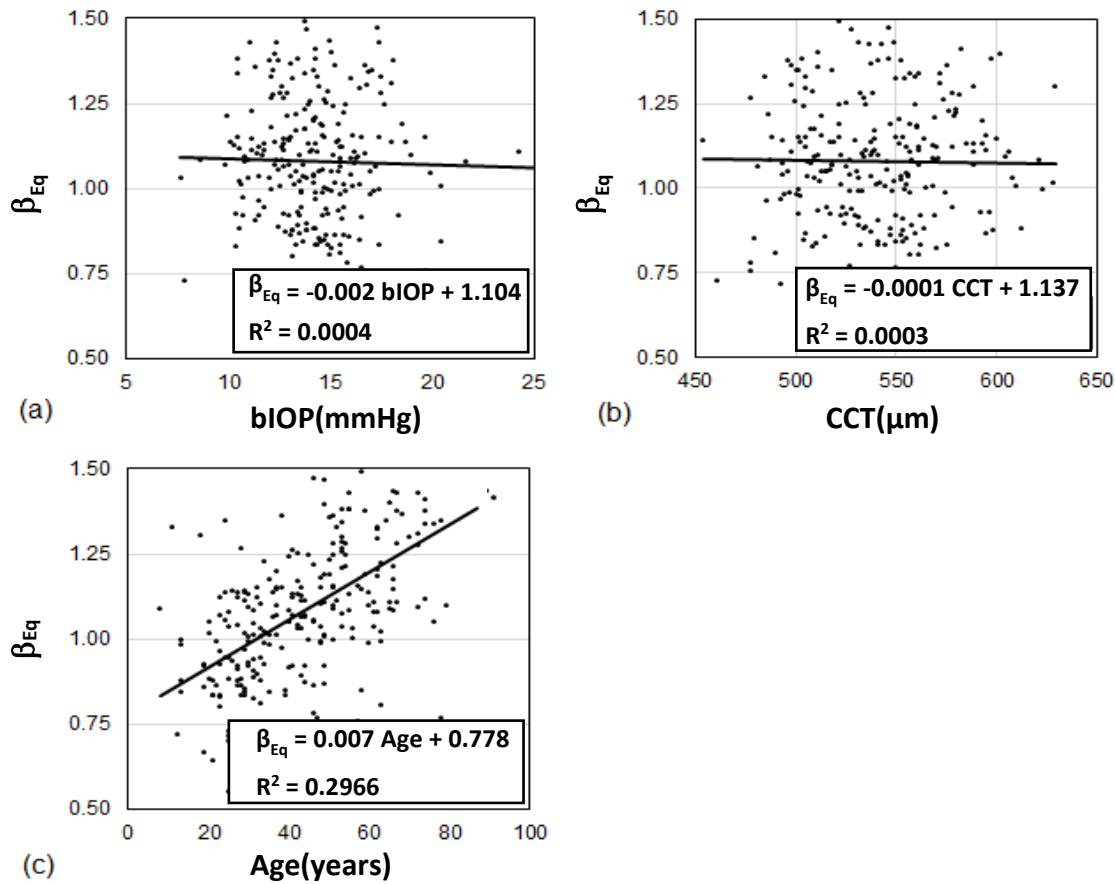


Figure 4-15 Assessment of the correlation in Dataset 2 between β_{Eq} and each of (a) bIOP, (b) CCT and (c) Age

4.7.3 Validation Against Ex-Vivo Inflation Test Results in Healthy Patients

The relationship between β_{Eq} and age plotted in Figure 4-14 and Figure 4-15 for Datasets 1 and 2, respectively, is re-plotted in Figure 4-16 and compared with the relationship based on ex-vivo inflation test results. The comparison shows a close correlation between the two relationships with the differences being 0.09 ± 0.20 ($p < 0.01$) and 0.10 ± 0.21 ($p < 0.01$) for Datasets 1 and 2, respectively. Statistical analysis was performed using Spearman's rho correlation as the data were not normally distributed.

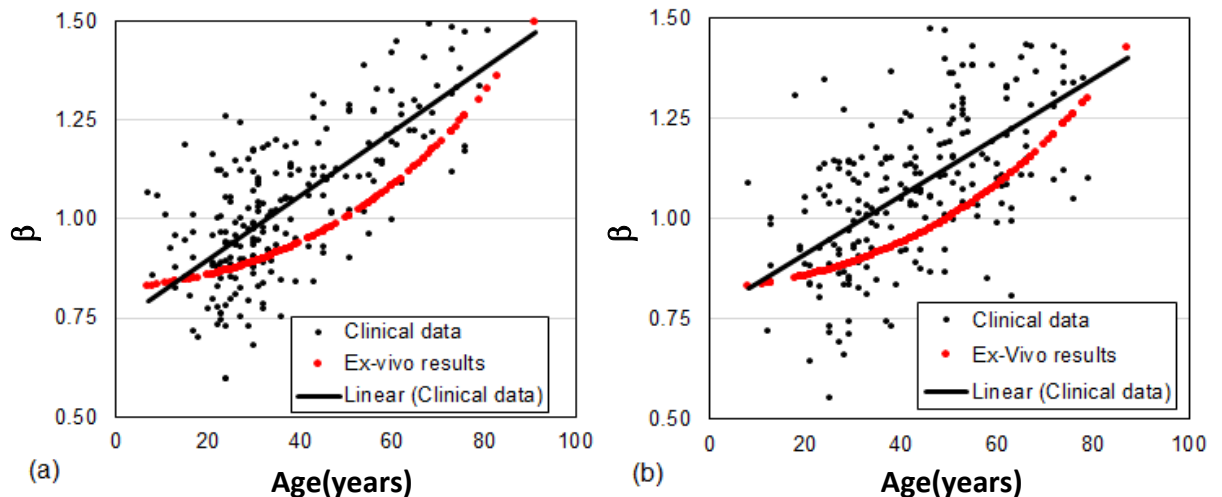


Figure 4-16 Relationship between β and age based on in-vivo clinical data (black dots and a black trend line) and ex-vivo inflation test results (red dots) for (a) Milan dataset and (b) Rio dataset

4.7.4 Comparison of β Obtained from the Algorithm and Inverse Analysis for Keratoconic Eyes

A total of 32 keratoconic patients were selected from the Milan and Brazil clinical datasets. To evaluate the effectiveness of the β algorithm, the results from the inverse analysis were assumed to represent the true material parameters. Table 4-25 and Table 4-27 presents the mean, SD, and range of the central corneal thickness (CCT), age, IOP measurements by the CorVis-ST device (CVS-IOP), the biomechanically-corrected IOP for keratoconic ($bIOP_{KC}$), and β values obtained from the estimated algorithm (β_{Eq}) and inverse analysis (β_{In}) for healthy eyes.

Table 4-27 Clinical datasets for keratoconic eyes showing mean, standard deviation, range of β , and p-value of paired t-test results between β algorithm and inverse analysis

Number	34
β_{Eq} (from estimated algorithm)	0.76 ± 0.21 (0.38–1.23)
β_{In} (from inverse analysis)	0.76 ± 0.29 (0.36–1.55)
Differences of Mean \pm SD	0.00 ± 0.20
p value	0.99

** Significant differences between means of β_{Eq} and β_{In}

The β_{In} obtained from inverse analysis of numerical models simulating the 34 eyes included in the study had a mean of 0.76 ± 0.29 (0.36-1.55) and the β algorithm provided a β_{Eq} mean of 0.76 ± 0.21 (0.38-1.23). There were no significant differences between the two sets of β values ($p=0.99$), Figure 4-17.

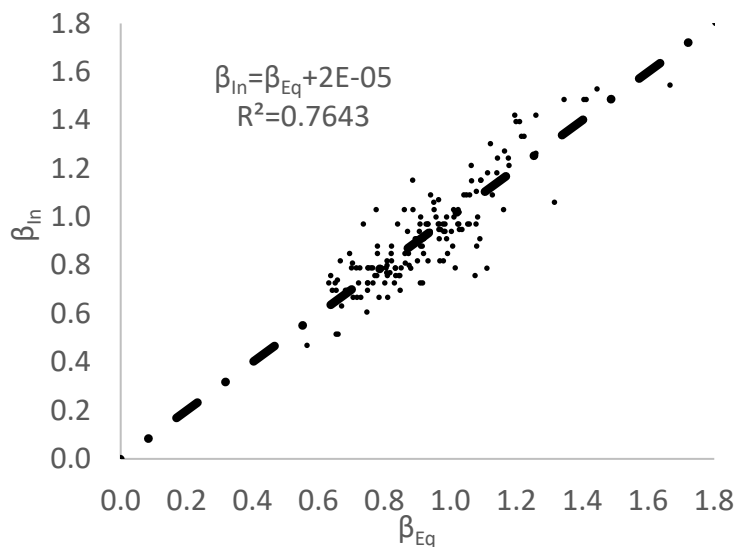


Figure 4-17 Results of the β algorithm (β_{Eq}) against β inverse analysis (β_{In}) for 34 keratoconic eyes shown with a red trend line against a 45-degree line denoting target perfect fit

Chapter Five

Discussion and Conclusions

5.1 Introduction

The information presented in previous chapters concerning the validation of biomechanically-corrected intraocular pressure (bIOP) and in-vivo corneal material behaviour estimation is discussed in this chapter. Overall conclusions are then provided, followed by recommendations for future work.

5.2 Overall Discussion

Measurement of intraocular pressure (IOP) is of great clinical importance for a number of applications including the management and risk profiling of glaucoma. Several methods have been developed to provide estimates of IOP, most of which rely on a simple concept involving the application of a mechanical force – usually on the cornea – and correlating the resistance to deformation under this force to the value of IOP. While this technique is simple to apply, it introduces inaccuracies that are difficult to eliminate. It has long been realised that corneal stiffness, which is influenced by the tissue's thickness and material biomechanics, also influences the resistance to deformation under the applied force, and hence can cause changes in the IOP measurement. The difficulty to separate the effects of IOP and tissue biomechanics on the IOP measurement has been the subject of numerous research studies and has not been entirely possible to date [259].

The CorVis-ST, a relatively new non-contact tonometer (NCT), aims to address this challenge. It acquires detailed cross-sectional profiles of the cornea's anterior and posterior surfaces recorded during the application of the external, dynamic air pressure. This information, along with measurements of thickness over the central corneal region, was used to distinguish between the effects of IOP and corneal biomechanics on corneal deformation, and hence provide an estimate of IOP that is designed to be less dependent on the corneal biomechanical parameters including central corneal thickness (CCT) and age (related to the corneal stiffness) [46, 260].

A numerical simulation was found to be a reliable tool for modelling the cornea's response to mechanical loads, such as those applied by tonometers [46]. Hence, this study through the use of numerical simulations evaluated effects of IOP and overall eye material behaviour (including corneal geometry, and eye material stiffness) on the dynamic corneal response parameters obtained from the CorVis-ST. Based on the numerical results, the influence of each parameter on the IOP measurement could be defined and eliminated. As the literature presented previously, the association of the accurate IOP with geometrical parameters (such as CCT) or age (material stiffness) has not been investigated widely in clinical models as of now. Corneal material estimation influences IOP estimation and vice versa which forced these algorithms to be interrelated [54]. This means that the estimation process entails a set of activities that interact with one another, using the IOP or corneal material properties to define each.

Several experimental studies concern the characteristics of corneal material behaviour, which are based on the uniaxial tension [33, 47, 50, 51], inflation [53, 71-73], and compression tests [75]. These studies assumed the material properties of the cornea to be: homogeneous linear

elastic [82, 83], nonlinear hyper-elastic [71, 79, 84, 85], and nonhomogeneous [86]. According to the tension and inflation tests, the obtained corneal material behaviour demonstrated nonlinear hyper-elastic material behaviour. Moreover, based on Elsheikh's research, the uniaxial test [1] and the inflation test [1, 52, 91, 261] demonstrated an association between biomechanical properties and age. According to these findings, there is a regular change in corneal material behaviour with an increase in age. Nevertheless, there are significant differences in individual corneal material behaviour among those with the same age. Hence, a new corneal material stiffness parameter (β) has developed to overcome the challenge of corneal material behaviour differences in individuals and to enable obtaining these variations using tonometry.

In this study, the aim was to develop algorithms to better estimate IOP and corneal material behaviour, based on the dynamic corneal response parameters obtained from a non-contact method. Through numerical simulations, all algorithms were developed and clinically, experimentally and numerically validated. More accurate estimation of IOP can have a huge impact on the prediction of glaucoma [213]. Moreover, a better estimation of corneal material properties can help with customising clinical procedures.

The development of an IOP estimation algorithm for application in the CorVis-ST initially relied on the numerical simulation that represents the eye model and CorVis-ST procedure. The similarity between the numerical and clinical results, including the values of central displacement at first appplanation (A1) and highest concavity (HC), demonstrated the reliability of the simulations and their ability to model the CorVis-ST procedure with a high level of accuracy. Subsequently, a parametric study considering a wide range of variation in CCT, corneal material properties, and IOP was conducted. This study confirmed that the first

applanation pressure (AP1) has a stronger association with IOP than with CCT and age. Applying the least squares method, an algorithm quantifying the corneal material behaviour was developed, and that helped to provide a biomechanically-corrected IOP estimation that is more accurate and less affected by variations in corneal mechanical stiffness and its geometry as compared to either not corrected IOP measured with a CorVis-ST or Goldmann Applanation Tonometry (GAT).

There are several studies regarding corneal material properties [33, 47, 50, 51, 53, 71-73, 75, 79, 82-86], but most measurement methods involve ex-vivo tests and cannot be used clinically. Hence, it is necessary to develop an in-vivo method for assessing corneal material behaviour, which has high potentials in clinical application. As mentioned above, the analysis of dynamic corneal response parameters is indispensable while quantifying the corneal material behaviour. A new stiffness parameter (SP) introduced in the literature has been demonstrated to reflect overall corneal stiffness [201]. Hence the corneal material behaviour estimation algorithm has been developed using the most influential parameters, which are the highest concave stiffness parameter (SP-HC), IOP, and CCT. This method was effective in determining material properties and showed high accuracy in comparison to the results of inverse analysis of clinical data. However, there are several points that require further discussion in this section.

5.2.1 Correlation of bIOP with CCT and Age in Healthy Eyes

A biomechanically-corrected IOP (bIOP) estimation algorithm for healthy eyes is developed through numerical methods, which represent realistic eye material behaviour and the air-puff procedure similar to the CorVis-ST device. Based on this numerical simulation, the effect of corneal factors, such as corneal geometric parameters (central corneal thickness, CCT; corneal

central anterior radius of curvature, R_c ; and anterior corneal shape factor, P) and corneal material stiffness (assuming correlation with age [1]), on IOP measurement has been quantified. There has been no influence of R_c or P on IOP measurement in literature [46]. For this reason, this study only considered the effect of both CCT and age (related to the corneal material stiffness [1]) on the IOP measurement. The results clearly demonstrate the effect of CCT and age on measured not corrected IOP with a CorVis-IOP (CVS-IOP), and these are similar to other findings using the GAT and NCT [10, 13, 23, 24, 206, 209, 217, 218, 223, 231]. For reducing the effects of both CCT and age on IOP measurement, a number of correction equations were formulated for GAT, ORA, and CorVis, which have been successfully validated clinically [46, 242, 262, 263]. The numerical simulations of the Corvis procedure in this study were validated against clinical results obtained in vivo for four randomly selected eyes of four age groups at same CCT and CVS-IOP, and compared the distribution of main CorVis-ST dynamic response parameters (P_{DCR}) between numerical predictions and two clinical datasets obtained from the Rio de Janeiro Corneal Tomography and Biomechanics Study Group – Rio de Janeiro, Brazil – with a total of 253 healthy participants, and the Vincieye Clinic in Milan, Italy with 227 healthy participants.

The similarity between the numerical and clinical results and the confirmation of statistical analysis demonstrated the reliability of the simulations. Subsequently, a wide range of variations in CCT, true IOP, and the different material properties of the eye were simulated in the parametric study for the dynamic corneal response analysis. The parametric study affirmed that the AP1 has a strong association with true IOP, and a weak association with CCT and corneal material behaviour. Using polynomial fitting, an IOP estimation algorithm (Equation 4.1) was developed considering the correlation of IOP estimation with CCT and age

in order to estimate the IOP with a less impact of corneal factors.

The measured IOP by the CorVis-ST (CVS-IOP) were tested against three clinical datasets of 634 healthy eyes from Smile Eye Clinics (SEC), Germany, 1047 eyes of pathological conditions (astigmatism, cataract, myopia, hyperopia, Emmet ropy, and retinopathy) from Humanitas Clinical and Research Center (HCRC), Italy, and 634 healthy eyes from and Wenzhou Medical University (WMU), China. CVS-IOP measurements were significantly correlated with CCT ($r^2 = 0.204$, slope = 0.0306 mmHg/ μm) and age ($r^2 = 0.009$, slope = 0.024 mmHg/year) in the SEC set, Figure 4-4; CCT ($r^2 = 0.095$, slope = 0.0288 mmHg/ μm) and age ($r^2 = 0.022$, slope = 0.0295 mmHg/year) in the HCRC set, Figure 4-5; and CCT ($r^2 = 0.09$, slope = 0.0314 mmHg/ μm) and age ($r^2 = 0.0337$, slope = 0.0327 mmHg/year) in the WMU set, Figure 4-6, respectively.

Introducing the bIOP algorithm reduced its dependency even further on both CCT ($r^2 = 0.0007$, slope = 0.0014 mmHg/ μm) and age ($r^2 = 0.0086$, slope = -0.0183 mmHg/year) in the SEC set, Figure 4-4; CCT ($r^2 = 0.0059$, slope = -0.0053 mmHg/ μm) and age ($r^2 = 0.0042$, slope = -0.0095 mmHg/year) in the HCRC set, Figure 4-5; and CCT ($r^2 = 0.0044$, slope = -0.005 mmHg/ μm) and age ($r^2 = 0.0009$, slope = -0.0038 mmHg/year) in the WMU set, Figure 4-6, considerably.

The biomechanically-corrected IOP estimation algorithm presented in this study offers a simple and effective method to obtain IOP estimates with less effect of the main corneal stiffness parameters and less dependency on a major error source to provide more reliable IOP estimates for glaucoma management.

5.2.2 Validation of bIOP Algorithm through EX-Vivo Testing

The evaluation of intraocular pressure (IOP) is a fundamental part of eye examination and is

essential for the screening and treatment of pathologies such as glaucoma and ocular hypertension. The association between elevated intraocular pressure (IOP) and glaucoma development and progression has since been confirmed, making IOP the main modifiable risk factor for glaucoma, and establishing IOP measurement as an essential part of glaucoma risk-profiling and management [194, 264]. For this reason, an accurate IOP estimate is highly desirable.

The reference standard in IOP measurement is the Goldmann Applanation Tonometry (GAT), which makes the device susceptible to the natural variations in corneal stiffness, caused by variations in tissue thickness and biomechanics from average levels, and introduces inaccuracies in IOP measurements [265, 266]. Based on these findings, several attempts were made to create IOP estimates that corrected for biomechanics including, most notably, the dynamic contour tonometer (DCT, DCT-Pascal, Swiss Microtechnology AG, Port, Switzerland) [267], the ocular response analyzer (ORA) [268] with its corneal compensated IOP (IOP_{cc}) estimates, and more recently the CorVis-ST [269] through its biomechanically corrected IOP measurements [46, 270].

In the ex-vivo animal-based experiments, there are existing literatures on the comparison between IOP estimation and the true IOP on porcine [271-273], rabbit [261], sheep [274], cows [274], cat [274, 275] and mice [274, 276] using the impact–rebound tonometer (I-R), a prototype murine optical interference tonometer (OIT), Goldmann Applanation Tonometry (GAT), Tono-Pen, Pneumo-tonometry, Ocular Response Analyzer (ORA), CorVis-ST and Schiøtz tonometer. Moreover, several studies assess the accuracy of tonometer using experiments on ex-vivo human eyes [12, 277-280]. These ex-vivo studies were conducted on an inflation rig which is developed in house by the research group and enabled simulation of IOP on full eye

globes. However, these tonometries are calibrated for use in humans and not applicable to the animal eyes. For these reasons, this study relied on ex-vivo experiments to validate the bIOP algorithms for healthy eyes.

In this study, the results are providing an assessment of the biomechanical correction (bIOP) algorithm in determining the intraocular pressure (IOP) using a direct experimental technique, in which the IOP is controlled in ex-vivo human eyes followed by measuring the pressure using the CorVis-ST and providing bIOP estimates. The technique showed that while uncorrected IOP estimates exhibited inaccuracies, and appeared to be influenced by corneal biomechanics, bIOP values were significantly more accurate and closer to the values of true IOP.

In this ex-vivo study, the donor's eye was connected through a pipe network to a motor-driven syringe pump, which was used to control the IOP. The true IOP was measured using a pressure transducer (FDW 060-K262-01, RDP Electronics, USA) having a 0.1 mmHg resolution. The IOP measured using tonometer was compared to the true IOP value and used to validate the findings of this study in regards to bIOP algorithm.

For the five ex-vivo eye globes employed in this study, for which age varied little between 67 and 76 years, and CCT varied between 458 and 880 μm , IOP was maintained at specific values between 10 and 30 mmHg in 5 mmHg increments. At each true IOP (IOP_t) level, at least three acceptable-quality IOP readings by the CorVis-ST were obtained, along with estimates of bIOP. While the uncorrected CVS-IOP measurements resulted in large and significant errors (7.5 ± 3.2 mmHg, $p < 0.001$), bIOP was closer to IOP_t with small and non-significant errors of (0.3 ± 1.6 mmHg, $p=0.989$). Further, the CVS-IOP errors were significantly correlated with, and possibly caused by, the increases in CCT beyond average values ($p < 0.001$).

These results, although based on a limited number of human globes, are promising when compared to previous studies, in which either Perkins or GAT was employed and exhibited significant errors ranging from a mean of 1.7 ± 1.8 to 5.2 ± 1.6 mmHg [264, 277, 278]. Conversely, when considering DCT readings, the published literature shows inconsistent results with reports showing minimal differences compared to true IOP [0.58 ± 0.70 mmHg18 or 0.50 mmHg (95% CI=0.40–0.60) [278]] and another showing higher error values (2.3 ± 2.4 mmHg) [277]. On the other hand, there is no published work on the evaluation of ORA IOPcc versus to true IOP by using healthy ex-vivo human eye experiments.

Several studies have showed a significant correlation between CCT and IOP for instance in the GAT tonometry (from 0.26 to 0.37 mmHg with a 100 μ m change in CCT) and NCT tonometry (from 0.39 to 0.63 mmHg with a 100 μ m change in CCT) [10, 13, 23, 24, 206, 209, 217, 218, 223, 231]. Since individuals have different corneal geometries the variation of IOP estimates found to be large in most tonometries. However, using bIOP on ex-vivo human eyes was found no correlation for bIOP errors with IOPt in either percentage ($p=0.756$) or values ($p=0.617$). Further, the CVS-IOP error increased significantly with higher CCT (0.0196 mmHg/ μ m, $p < 0.001$), unlike the errors in bIOP, which were smaller and not correlated with CCT (-0.002 mmHg/ μ m, $p=0.482$), Table 4-16. But, this observation was not repeated with bIOP [264].

In conclusion, this study provides further evidence of the capability of the bIOP algorithm in providing a close estimate of the true IOP in the range of 10–30 mmHg in healthy eyes and the reduction in the association with the cornea's stiffness parameters, most notably the thickness. Based on this and the previously published studies, the bIOP may provide a possible solution to the long-standing challenge of offering IOP estimates that are significantly less affected by corneal biomechanics than other, commonly used, tonometry methods.

5.2.3 Validation of bIOP on Refractive Surgery Clinical Data

The accuracy of current methods of IOP measurement is influenced by corneal stiffness, which varies with thickness and the tissue's material behaviour [281]. The resulting errors potentially lead to failure to correctly risk profile glaucoma, and this has been estimated to affect more than 20% of patients [213]. Previous studies showed that IOP measurements by Goldmann Applanation Tonometry (GAT-IOP), the reference standard in tonometry, are affected by an error margin that varied between 0.7 mmHg and 7.1 mmHg per each 100 μm change in CCT [209, 211, 282]. The significance of this error margin should be seen in the light of an earlier estimate that the risk for glaucoma progression increased by 10% for each 1 mmHg increase in IOP [204], and the potential that this error can lead to significant numbers of false-positives and false-negatives in glaucoma risk profiling. Within the context of the present study, refractive surgery raises important questions regarding the implications of tissue loss and change in biomechanical properties (because of both ablation and weak connection of flap or cap with residual stroma) on IOP measurement and the accuracy of glaucoma risk profiling. A previous study showed that the well-known reduction of IOP with applanation tonometry after refractive surgery was only partly related to corneal thickness change [283]. In that study, the change in CCT associated with the refractive change explained less than 1.0% of the change in measured GAT-IOP, and therefore parameters other than CCT might influence IOP measurement error using applanation tonometry.

Several attempts have been made to address this problem by either quantifying the effect of CCT (and other parameters that affect corneal stiffness) on IOP measurement or developing techniques that seek to reduce the dependence of IOP measurement on stiffness in general and CCT in particular [46, 209, 284]. Among attempts aiming to quantify the effect of stiffness

parameters on IOP measurements [25, 211, 245, 285, 286], algorithms were produced to enable more accurate GAT-IOP estimates based on quantifying the errors caused by variations in the stiffness parameters. On the other hand, efforts to develop new techniques to reduce dependence on stiffness parameters have been more substantial, resulting in the dynamic contour tonometer (DCT, SMT Swiss Microtechnology AG) and the Ocular Response Analyzer (ORA, Reichert Technologies).

The DCT is a digital tonometer designed to be less affected by the corneal thickness than the GAT; this claim was confirmed by studies evaluating normal and glaucoma patients [204, 287], although others did not agree, showing significant correlation with thickness [288]. Furthermore, it has been reported that the changes in IOP values obtained with the DCT after refractive surgeries, photorefractive keratectomy (PRK), and laser in situ keratomileusis (LASIK) remained nonsignificant, suggesting a low correlation with CCT [223, 224, 288].

Similarly, the ORA with its corneal-compensated intraocular pressure (IOP_{cc}), produced by the dynamic bidirectional applanation device is claimed with some success to compensate for CCT [223, 289, 290], and researchers [223, 291, 292] found that IOP_{cc} was less altered after refractive surgery than GAT-IOP. Preoperative CCT showed correlation with only the GAT equivalent but not with the IOP_{cc}. A particularly relevant study of this work has been carried out by the authors to develop an algorithm to reduce dependency on corneal properties in the dynamic Scheimpflug analyzer IOP (CVS-IOP) [46, 204, 269, 270, 293]. The resulting bIOP algorithm has been assessed clinically and showed effectiveness in producing IOP estimates that were largely independent of CCT and the cornea's biomechanical properties [270, 294].

The aim of this study was to provide a further assessment of the bIOP algorithm by comparing

it with the GAT-IOP and CVS-IOP measurements before and after the refractive surgery procedures LASIK and small-incision lenticule extraction (SMILE, Carl Zeiss Meditec AG). These procedures have a number of main effects on corneal stiffness in (1) reducing the thickness through ablation, (2) reducing interaction between the flap or cap and the residual stromal tissue, and (3) possibly affecting the mechanical properties of stromal tissue caused by the wound-healing process. The effective thickness reduction in both LASIK and SMILE, attributable to both tissue ablation and the flap or cap creation, is commonly between 10% and 20% of the stroma's original thickness, which is expected to result in a notable reduction in corneal stiffness and hence affect IOP measurements [295-298]. On the other hand, the wound healing effect on corneal biomechanics has not been quantified and therefore its effect on tonometry results cannot be considered at present [34, 299].

The clinical data was collected from the Smile Eye Clinic, Munich, Germany and included 36 patients (50 eyes) patients who had undergone refractive surgery by LASIK (14 patients, 20 eyes [11 male, 9 female]) and SMILE (22 patients, 30 eyes [15 male, 15 female]) for correction of myopia or myopic astigmatism [247]. The first result of the study is the confirmation that the bIOP correction is able to reduce the known correlation (confounding factor) between CCT and IOP readings before and after LASIK and SMILE. This was demonstrated with Pearson coefficients that showed significant correlations between both GAT-IOP and CVS-IOP with CCT ($p < 0.05$), but no correlation between bIOP and CCT in both the LASIK and SMILE groups, separately and combined ($p > 0.5$).

The study further provides an important test of the bIOP algorithm after laser refractive surgery and shows that the bIOP readings are not different before and after LASIK (-0.1 ± 2.1 mmHg, $p=0.795$) and SMILE (-0.8 ± 1.8 mmHg, $p=0.273$), Table 4-22. In particular, statistical analyses showed that after LASIK and SMILE, there was a significant decrease in GAT-IOP and CVS-IOP values (>3 mmHg, $p<0.001$), whereas there was no significant difference between preoperative and postoperative bIOP readings.

This last finding and considering that the optical zone stayed the same (6.5 mm) suggest that bIOP algorithm is not only able to correct for the changes in CCT induced by the 2 procedures but also for the dissimilar volume of tissue removed with the 2 refractive techniques. The results of our study are in agreement with a previous report that showed significant decreases in CVS-IOP after LASIK and SMILE [247]. Similarly, Osman et al. [300] showed reductions of CVS-IOP values after SMILE, although these did not reach statistical significance.

The preoperative analysis showed mean values of bIOP and CVS-IOP lower than GAT-IOP. However, the mean values of bIOP have been shown in a large normative study to be very similar to Goldmann values [270]. For this reason, this result might be an incidental Findings in this clinical data. Moreover, the difference between Goldmann and bIOP and the CVS-IOP is not constant in the 2 groups (1.9 mmHg between bIOP and Goldmann in the LASIK group and 1.3 mmHg in the SMILE group), and GAT-IOP is known to have a test–retest repeatability of ± 2.5 mmHg [301].

In conclusion, this study shows that the new biomechanically corrected bIOP was not significantly correlated with CCT before and after LASIK and SMILE laser refractive surgery, unlike GAT-IOP and CVS-IOP. Furthermore, the IOP readings using the bIOP algorithm were

different before and after LASIK and SMILE. These results suggest that the bIOP algorithm should be able to compensate for the effect of laser surgeries on ocular biomechanics including the loss of tissue caused by ablation and flap or cap cutting. not significantly.

5.2.4 IOP Estimation in Keratoconic patients

The reliable measurement of IOP in patients with Keratoconus (KC) has always been a challenge [248]. Being thinner, steeper, softer, and less regular than healthy tissue, Keratoconic corneas usually suffer from systematic underestimations of IOP [250], which can cause problems when using eye-drops (such as steroids [302]) or undergoing procedures that can induce a rise in IOP – making it difficult to evaluate whether a borderline IOP measurement represents a clear abnormality.

The challenge in accurately measuring IOP stems from the way in which tonometry techniques work, where the cornea's resistance to deformation, under an external mechanical effect, is correlated to IOP. This common methodology means that the natural variations in corneal stiffness, caused by several factors such as changes in thickness, curvature or tissue biomechanical properties, affect the accuracy of IOP measurements. This problem becomes particularly serious in keratoconus, where the cornea experiences significant reductions in thickness and tissue stiffness in addition to notable changes in geometry. This study is an attempt to separate the effects of corneal mechanical stiffness from those of IOP in the IOP measurement process, and hence provide more representative IOP values compared with CorVis IOP. The method used relied on numerical simulation of the CorVis-ST procedure in eye models with wide variations in true IOP, anterior surface profile, CCT, thickness profile and material properties. The method, which was similar to that reported earlier for healthy eyes

[46, 303]. led to the development of an algorithm providing estimates of biomechanically-corrected IOP values for kc eyes (bIOP_{kc}).

Validation of the bIOP_{kc} algorithm involved applying it to keratoconic populations and comparing the results to those of bIOP for healthy populations recruited in the same clinical centres. While the CorVis IOP measurements in healthy and kc eyes were significantly different, Figure 4-10 – being lower in kc eyes, as expected – the bIOP_{kc} and bIOP for kc and healthy participants were similar (Figure 4-12). Given that there is no reason to hypothesize that patients with kc should have a “true” IOP that is different from a healthy population with a similar composition, this result provides evidence that bIOP_{kc} was able to correct for the confounding biomechanical factors that make IOP measurements in kc patients unreliable (Table 4-23 and Table 4-24). Further evidence is in the reduced dependency of bIOP_{kc} estimates on two major stiffness parameters; corneal thickness and age, similar to what has been found in the results of the bIOP algorithm when applied to eyes with healthy tomography [46, 270].

The inclusion of two large datasets from two different continents was necessary to assess the reliability of the bIOP_{kc} algorithm in populations with different ethnic backgrounds. It is the first time, to the authors’ knowledge, that an IOP estimate for kc was able to show the same mean values and standard deviations as for healthy eyes in such a large dataset. Previous studies illustrated the variable performance of different tonometers with disagreement still persisting on which tonometer provides the most reliable measurement of IOP in kc. Earlier reports noted the relatively low reliability of the Goldmann and Tono-pen tonometers [248, 249, 304] and the ability of both the ocular response analyzer (ORA, ORA-Reichert Ophthalmic Instruments, Depew, NY, USA) or the dynamic contour tonometer (DCT, DCT-Pascal, Swiss Microtechnology AG, Port, Switzerland) to provide more reliable estimates of IOP [248-251,

305, 306]. Nevertheless, neither the ORA with its corneal compensated IOP (IOP_{cc}) nor the DCT-IOP estimates were able to provide IOP values for kc patients that were not significantly different from those of healthy subjects in the same populations [307].

Another important finding of the study was provided by the analysis of the variances in kc severity. The differences in $bIOP_{kc}$ between sub-groups with mild, moderate and advanced kc were limited to 0.2 mmHg in Milan Dataset (2) and 0.5 mmHg in Rio Dataset (1) and were not significant, and in all sub-groups, $bIOP_{kc}$ provided a smaller spread compared to CorVis IOP (Figure 4-11). While this finding is of significant importance when evaluating the IOP in patients with keratoconus, where measurements are known to vary much between devices [248], note should be made of the differences in the number of kc patients included in each sub-group, which may have affected the statistical analysis of IOP results. A similar finding was reported in an earlier study, which demonstrated no significant differences in the DCT and IOP_{cc} measurements among patients with different Amsler-Krumeich kc classifications, but in that study, the mean IOP values were still different compared to healthy subjects [248].

Finally, a comparative analysis of $bIOP$ and $bIOP_{kc}$ in patients with keratoconus showed the absence of significant differences in means between $bIOP$ and $bIOP_{kc}$ estimations, a finding that was repeated in patient sub-groups with mild, moderate and advanced kc. However, $bIOP_{kc}$ values had significantly smaller standard deviations compared to $bIOP$ in most sub-groups (Figure 4-12). These results indicate that while $bIOP$ could potentially be used to estimate IOP in kc patients, the results may not be as reliable as with the $bIOP_{kc}$.

In conclusion, based on the findings, this research proposed $bIOP_{kc}$ as a new algorithm for a more reliable estimate of intraocular pressure in patients with keratoconus. The routine use

in clinical practice of this algorithm may help take into account the well-known systematic errors that affect other tonometers, including Goldmann, caused by the particular irregularities in material properties, anterior topography and thickness profile of the corneas of keratoconic patients.

5.2.5 In Vivo Corneal Material Behaviour Estimation

The biomechanical characterisation of in-vivo tissue is a developing field in clinical management and treatment planning. Estimating the characterisation of the mechanical behaviour of the cornea may enable the clinician to simulate its response to any clinical manipulation performed during an intervention. Since the corneal material behaviour displays a great variability from individual to individual, understanding the corneal material behaviour has become an important subject for future research. Moreover, the cornea has a strong sensitivity to age and temperature, which is used to condition its biomechanical behaviour in clinical treatment [52]. Furthermore, the estimation of the corneal mechanical response can be applied to detect some pathologies whose symptoms may change corneal stiffness [308]. For these reasons, there are several studies, which demonstrate that the in-vivo estimation of the corneal material behaviour is the core of the analysis with regard to the real response during treatment interventions [34, 309-312].

The main challenge in estimating the corneal biomechanical behaviour in vivo stems from the difficulty in separating the effects of this behaviour from those of the IOP on ocular response to mechanical stimuli. This challenge has made it difficult to produce accurate IOP estimates, that are free of the effects of corneal biomechanics [30], and the same challenge exists in determining the tissue's biomechanics that is free of the effects of IOP. Nevertheless, the

compound nature of this challenge has meant that finding a solution for either IOP or corneal biomechanics would lead to a solution for the other problem.

What complicates matters further is that the stress-strain behaviour of biological tissue, including cornea and sclera, is nonlinear [52, 70], and therefore the tangent modulus (E_t) – a measure of material stiffness – does not have a constant value, but increases with stress and strain. This effectively means that as the IOP in the eye increases, the stress and strain to which the eye is subjected increases, causing a rise in the tangent modulus. Therefore, the problem is not only that the effects of IOP and corneal biomechanics on eye behaviour are difficult to separate; IOP also effects the immediate corneal stiffness.

This study attempts to address a long-standing challenge related to the in-vivo measurement of corneal biomechanics, and in doing so it attempts to overcome two major obstacles. First, the nonlinear nature of the tissue behaviour makes it necessary to determine the whole stress-strain behaviour, rather than a tangent modulus value which would be valid only at a particular level of stress or strain. This obstacle was overcome through observation that stress-strain relationships obtained earlier for ex-vivo ocular tissue had similar trends that saw almost proportional decreases in strain with increases in tissue age [1, 52, 70]. By taking the average experimental behaviour obtained for corneal tissue with age 50 years [1, 52, 70] as the benchmark, at which the new biomechanically parameter (β) was assumed equal to 1.0, other stress-strain relationships for stiffer or softer material could be derived by multiplying the strain values by the relevant value of the β parameter.

The second challenge stems from the effect of IOP and corneal thickness on corneal deformation under the action of internal or external mechanical actions. However, while the

effect of corneal thickness on overall behaviour is large, it can be estimated and removed as the thickness and its effect can be measured and excluded accurately. On the other hand, IOP presents a more difficult challenge since IOP measurement methods – through tonometry – are affected by corneal stiffness, creating a challenging dilemma with the stiffness affecting IOP measurement and IOP affecting corneal mechanical behaviour, which is used to estimate the stiffness. In this study, this challenge was addressed through consideration of a CorVis-ST parameter – the stiffness parameter at highest concavity, SP-HC – which is more strongly correlated with corneal stiffness than IOP.

In 2011, the OCULUS CorVis-ST (OCULUS Optikgerate GmbH, Mtinchholzhauser Str. 29 D-35582 Wetzlar, Germany) was presented. This tonometer includes the functions of pachymetry and video/image recording of the corneal deformation using an Ultra-High-Speed Scheimpflug camera. Additionally, these images and videos display the in-vivo biomechanical responses of the cornea to the air puff. Therefore, the corneal material behaviour can be assessed for each patient by utilising the CorVis device.

This study presented an algorithm for in-vivo estimation of the corneal material behaviour based on the dynamic corneal response analysis. The corneal material estimated (β) algorithm was generated based on predictions of corneal behaviour using finite element (FE) numerical modelling simulating the effects of IOP and CorVis-ST air puff.

Validation of Algorithm through Inverse analysis

In general, to obtain corneal material properties, two main approaches have been attempted. A classical method is based on the standard experiments (as tension [33, 47, 50, 51], inflation [53, 71-73], and compression test [75]), which involve ex-vivo measurements with

simplifications and assumptions. Other method is to combine numerical model and experiment to compute the material properties using an inverse finite element method [313-315]. In the inverse finite element method, the corneal stiffness was obtained through inverse analysis method using Particle Swarm Optimisation (PSO) algorithm to match patient specific corneal behaviour obtained from CorVis-ST. Hence, to validate the β algorithm, the predicted β value was compared with the true β obtained from the inverse analysis (β_{in}).

There were 168 healthy eyes (including 84 healthy eyes in Dataset 1 from Milan, and 84 healthy eyes in Dataset2 from Brazil) and 34 keratoconic (KC) eyes (including 17 KC eyes in Dataset 1 from Milan, and 17 KC eyes in Dataset2 from Brazil) to validate the accuracy of corneal material estimation algorithm; this refers to how close a β value, obtained by CorVis-ST (β_{Eq}), matches the true β defined by the inverse analysis (β_{in}).

The inverse results present that the mean and standard deviation of β_{in} is 0.93 ± 0.21 (range: 0.47–1.55) in the healthy eyes and 0.76 ± 0.29 (range: 0.36–1.55) in the KC eyes. Introducing the corneal material estimation algorithm into CorVis-ST, the mean and standard deviation of β value (β_{Eq}) obtained to be 0.93 ± 0.19 (range: 0.56–1.67) in the healthy eyes and 0.76 ± 0.21 (range: 0.38–1.23) in the KC eyes. But there was no significant difference between β_{Eq} and β_{in} (0.00 ± 0.12 , $p = 0.998$ in healthy and 0.00 ± 0.20 , $p = 0.99$ in KC eyes). That is to say, the estimated corneal material behaviour (β_{Eq}) value was highly accurate in explaining corneal mechanical behaviour in vivo.

Keratoconus, the most common ectatic disorder of the cornea, is a non-inflammatory progressive thinning disease [32]. Recently, it has been demonstrated that increased distensibility of the Keratoconic cornea tissue appears to be an important pathogenic factor

in the development of Keratoconus [316]. Previous studies have also shown that the corneal biomechanical behaviour is related to the uniform distribution of collagen fibrils assimilating into well-organised lamellae layers [317, 318]. Moreover, it has been noted that the number of collagen lamellae in Keratoconic tissue is less than in normal ones [167], and the native collagen fiber network is disorganised and loses the preferred directions [36, 319]. Therefore, there is a difference in the corneal biomechanical behaviour between healthy and Keratoconic eyes due to these characteristics of the keratoconic tissues.

With regard to the corneal material behaviour, several studies have demonstrated that the decreased ocular rigidity was found in Keratoconus compared to normal [33, 175]. Moreover, the Keratoconic corneas lose their rigidity and remain approximately 60–70% of the level of normal corneas [32]. Other studies have demonstrated that the ratio of Young's modulus between Keratoconic and healthy cornea, is within the range of 0.5 to 0.9 [33, 37, 176, 320]. Therefore, this evidence outlined that corneal material behaviour is softer in Keratoconus than in normal.

In this study, the results of β values obtained from the corneal material estimation algorithm (β_{Eq}) and the inverse analysis (β_{In}) are smaller in the KC patients than in healthy patients. In addition, the results also evidence that the KC material behaviour in the non-linear hyper-elastic material model remains at approximately 80% of the normal cornea's level similar to the rigidity stiffness coefficient defined by Shah [32] and Young's modulus defined by Edmund [319].

Validation against Ex-Vivo Inflation Test Results in Healthy Eyes

The β algorithm for healthy eyes was then validated through assessment of its correlation with

IOP, CCT and age in two large clinical datasets (including 84 healthy eyes in both Dataset 1 from Milan and Dataset2 from Brazil). As expected, β_{Eq} was found to be independent of both IOP ($p= 0.745$ in Dataset 1, $p= 0.281$ in Dataset 2) and CCT ($p= 0.792$ in Dataset 1, $p= 0.599$ in Dataset 2), while being correlated with age ($p< 0.01$ in Dataset 1, $p< 0.01$ in Dataset 2), which, in turn, was found earlier – in an experimental study on ex-vivo human eyes) to be strongly associated with material stiffness [1, 52].

Another validation exercise was conducted by comparing the relationship between β_{Eq} and age established in the two datasets against the results of the earlier ex-vivo study[1]. The comparisons showed there were no significant differences between the relationships ($p< 0.01$ in both Datasets 1 and 2).

The use of the β algorithms in clinical practice could enable customisation of the diagnosis and management of ocular diseases and allow optimisation of clinical procedures that either interact or interfere mechanically with the eye. With successful validation, β could help in identifying eyes with keratoconus, possibly increasing the sensitivity and specificity of indexes such as the CorVis Combined Biomechanical Index (CBI) [321] or the Tomography and Biomechanical Index (TBI) [322]. Moreover, it could help in the detection of patients with higher risk or susceptibility for ectasia development or progression after refractive surgery and could aid in surgery planning [323].

Glaucoma management could also benefit from the accurate measurement of corneal biomechanics. Quantifying the stiffness using the β algorithm could lead to improvements in IOP measurement and possibly better glaucoma management outcomes [30].

There have been previous attempts to measure corneal mechanical properties in vivo. These

included the Corneal Hysteresis (CH) and Corneal Resistance Factor (CRF) produced by the Ocular Response Analyzer (ORA) [197], and the Stiffness Parameter (SP) [201] by the CorVis-ST. These parameters were correlated with the diagnosis of keratoconus [321] and showed significant increases after collagen cross-linking (CXL) [324] but could not provide measurements of material behaviour that were separate from the effects of geometry and IOP. Another attempt is the elastic modulus provided by Brillouin microscopy [325], which, while related to the cornea's material stiffness, is not compatible with the nonlinear stress-strain behaviour. It means the tissue does not have a unique modulus, but has a tangent modulus, which increases gradually with stress or applied pressure.

In conclusion, this study introduced in this study a new method for estimating the material behavior of healthy corneal tissue that can aid in the optimisation of procedures that interact or interfere mechanically with the cornea such as refractive surgeries and intraocular pressure measurement.

5.3 Conclusions

The aim of this study was to accurately estimate intraocular pressure (IOP) and corneal material behaviour, based on dynamic corneal response parameters obtained from CorVis-ST, a non-contact tonometer. This study relied on numerical simulations to develop idealised and patient-specific eye models and perform through studies to quantify the effect of IOP and corneal stiffness on corneal deformations under air-puff. Upon this understanding, the estimated algorithms were developed to estimate IOP and material behaviour for healthy and keratoconic (KC) patients.

All findings have been validated clinically, experimentally and numerically [244, 260, 326, 327]. The biomechanically-corrected IOP algorithms for healthy eyes (bIOP) present higher accuracy and a lower correlation with central corneal thickness (CCT) and age (related to the corneal material stiffness) on the IOP in the ex-vivo experiment. Moreover, a study performed that bIOP on patients from before and after refractive surgeries can reduce the effect of CCT and corneal stiffness on IOP estimation significantly.

In terms of the effect of Keratoconus on the IOP measurement, the results of the biomechanically-corrected IOP algorithms for KC eyes (bIOP_{KC}) presents that there is no difference between the means of bIOP values in the healthy group and bIOP_{KC} in the KC group. Hence, it showed that the new bIOP_{KC} algorithm is a more reliable method of estimating IOP in patients with Keratoconus, which may help account for the well-known systematic errors that affect another tonometer.

The corneal material estimation (β) algorithm was successful in reflecting the biomechanical behaviour of the cornea in individual eyes and in-vivo. This β algorithm was validated through inverse analysis and demonstrated high accuracy and low correlations with IOP and CCT. In addition, the result of β algorithm in healthy eyes has a similar relationship between β and age in comparison to the previous ex-vivo human eye experiment [1].

All developed algorithms for IOP and corneal material behaviour estimation demonstrated great success. The bIOP algorithm has been implemented by the manufacturer of CorVis-ST into their device. Both bIOP_{KC} algorithm and β algorithm are planned to be added to the CorVis device very soon. This study will have a significant effect on the early diagnosis of patients with glaucoma by producing more accurate IOP measurements. With the use of β parameter

to quantify the corneal material behaviour, future developments on the patient specific treatments (as refractive surgery, corneal cross-linking treatment) and the contact lenses of contact lenses will be possible.

5.4 Limitations

In this study, there were several limitations with respect to eye's geometry and material properties, which hindered a simulation of the corneal response to deformation under the air-puff loading on the cornea. These limitations are also important parameters for clinical applications, such as surgery planning or customised contact lens design. In the future, there should be focused on eliminating these limitations.

The corneal material behaviour in this study was assumed to have homogeneous nonlinear hyperelastic material properties [71, 79, 84, 85]. In addition, the material behaviour of sclera and limbus was assumed to fix based on its correlation with age. However, in reality, it is a nonhomogeneous membrane [86] due to the irregular distribution of the fibre. Furthermore, the material behaviour of sclera and limbus are also similar to the hypothesis regarding corneal material behaviour, which varies between individual patients due to the high variability in composition and heterogeneity of the population. Hence, the hypothesis of these eye's material behaviour limited that the corneal material behaviour estimation only can provide the one material estimated value on the corneal, but this estimation can't detect the area of the specific local material change, which is a common symptom of keratoconus. On the other hand, based on this hypothesis of corneal material behaviour, this study ignored the characteristic of material viscoelasticity, as hysteresis, which also is observed after air-puff stop on the CorVis-ST. Hence, the numerical method in this study only can provided the

information about the hyperelastic material properties during air-puff pressure increasing.

The amplitude profile of air-puff pressure with time variable used in this study is measured by using the anemograph and the distribution of the air pressure was obtained based on experimental study [242] and computational fluid dynamics simulation (CFD) [243], which did not consider the effect of corneal deformation [243] and viscoelasticity of air [199] during the CorVis measurement process. In the future, the FE-model will be changed to the fluid–structure interaction model, which can simulate the air-puff loading on the corneal and consider the corneal response deformation during the process.

Additionally, there is an error effect about the effect of the position of the air-puff on the cornea. The FE-model only can simulate that the air-puff pressure always applied at its centre. To consider about the air- puff position effect, the parametric study is necessary to include a condition of the air-puff position on the different corneal factors to make sure the position effect is lower on the IOP measurement and corneal material estimation.

In this study, the validations of estimated algorithms were based on the ex-vivo human eye testing and in-vivo clinical validations. In the ex-vivo human eye testing, human specimens are limited quantity and nonreusable. And, the Fondazione Banca degli Occhi del Veneto Onlus, Venice, Italy only can provide the healthy human specimens with no pathological conditions due to the specification in the Institutional Review Board. These limitations make validations of the performance on bIOP and material behaviour estimation algorithm more difficult in healthy eyes, even keratoconic eyes. In addition, the in-vivo clinical validations by using clinical datasets took a large number of medical resources to diagnosis. For this reason, the number of the clinical validation in this study was limited.

However, the method can be improved by these three points, which make the error effect of the corneal factors on IOP and corneal material estimation lower. In addition, in this study, three estimated algorithms of IOP and corneal material behaviour have been developed, but the clinical validation and ex-vivo human eye test are not enough to prove the feasibility and credibility of these algorithms. As a result, the most important thing in the future is to do a large number of clinical trials.

Overall, according to these limitations, few points should be considered for future works:

- The corneal material behaviour in this study was assumed to have homogeneous nonlinear hyperelastic material properties [71, 79, 84, 85]. However, in reality, it is a nonhomogeneous membrane [86] due to the irregular distribution of the fibre.
- The material behaviour of sclera and limbus was fixed based on its correlation with age. They are similar to the hypothesis regarding corneal material behaviour, which varies between individual patients due to the high variability in composition and heterogeneity of the population.
- The amplitude profile of air-puff pressure with time variable used in this study was measured by using the anemobiograph which do not consider the corneal deformation effect during the CorVis process. In the future, FSI models may be required to simulate the air-puff loading on the corneal and consider the corneal response deformation during the process.
- The air-puff nozzle distance was fixed to 11mm in this study and it was located at a perpendicular distance from the apex. In reality there may be a variation in terms of both distance and direction of the air-puff on the cornea. These may provide more accurate simulations and help to improve the accuracy of the algorithms.

- There is a variation between equations developed for KC and Healthy eyes. If possible, these two equations should be combined to eliminate the need for diagnosis before applying an equation. It would help with a wider application of this algorithm in clinics and daily practices.
- β for Keratoconus relied on CorVis IOP as an indication of internal pressure. Upon availability of more accurate information from the instrument, adjustments can be made to eliminate the need for usage of CorVis IOP in the determination of material characteristics.
- Models for keratoconic patients assumed rotationally symmetric. If more information is available about topography of KC eyes, more accurate assumptions can be made to improve the accuracy of this work. It may help with combining both equations into one single algorithm.

Appendix A - Diagnosis of Keratoconus

A.1 Introduction

In early treatment of keratoconus, early diagnosis of ectasia is of paramount importance. Loss of corneal strength and alteration of corneal shape are a central feature of keratoconus progression [149-159, 328]. Normally, the detection of the corneal shape alteration as thinning and decreased curvature is based on the corneal topography analysis or image analysis with either videokeratography or optical coherence tomography instruments. Nevertheless, these instruments cannot measure corneal material properties, even after the significant changes in the corneal morphology [328]. For this reason, to develop an instrument to measure in-vivo corneal material stiffness is important to aid the diagnosis of keratoconus when corneal topography is normal.

The CorVis-ST (Oculus Optikgeräte GmbH, Wetzlar, Germany) is introduced as a noncontact tonometer which measures the response of the cornea under an air puff using an ultra-high speed Scheimpflug camera to provide estimates of IOP and dynamic response parameters.

A stiffness parameter (SP), found in the literature, was used by the CorVis-ST for diagnosing the corneal diseases as Keratoconus which affect corneal material stiffness [201]. After biomechanically-corrected IOP algorithms were developed, the SP-HC was calculated for two clinical datasets from the Rio de Janeiro Corneal Tomography and Biomechanics Study Group in Brazil and the Vincieye Clinic in Milan (Table 3-1). A total of 722 clinical data points was available for this study. Dataset 1 (Rio) included 253 healthy and 93 keratoconic participants, and Dataset 2 (Milan) included 227 healthy and 107 keratoconic participants. The Institutional

Review Boards of the clinical centres ruled that approval was not obligatory for this record review study. A 3D plot was developed for healthy and KC eyes, with the axis representing CCT, age, and SP-HC, as shown in Figure A-1. The SP-HC with CCT and age has a cover area between the healthy and KC clinical dataset. This implies that the classification of corneal material diagnosis using SP-HC still has a blind area. However, the SP is not enough to diagnose the keratoconus.

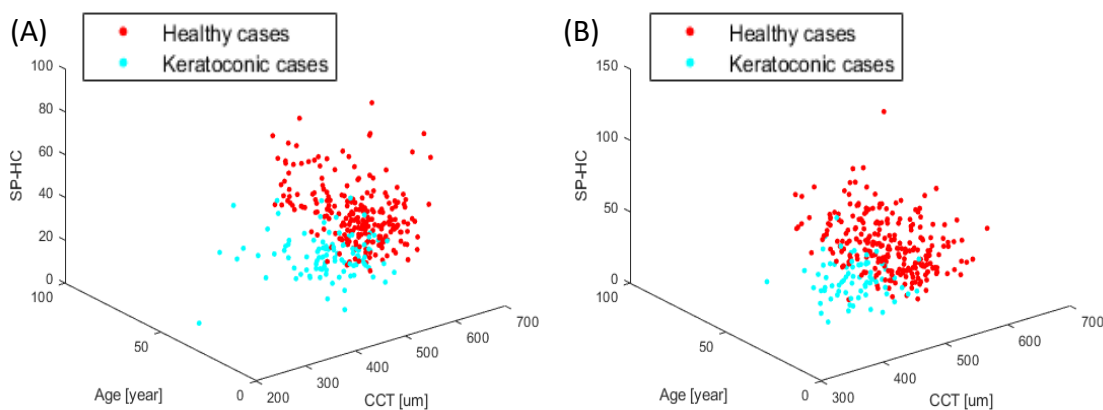


Figure A-1 A 3D plot of the SP-HC with CCT and age by using the healthy and KC clinical dataset in (A)Brazil and (B)Milan

The automatic diagnosis technique is important and suitable for users, including medical and non-medical staff, to separate between healthy and Keratoconus. As this research relied on the CorVis-ST and the Pentacam to develop better estimation methods for IOP and corneal material behaviour, it was required to develop a method that allows quick identification of patient data using the CorVis-ST. Hence, the aim of this research was to develop an automatic diagnosis process based on corneal thickness and different dynamic corneal response parameters provided by the Corvis ST to detect corneal mechanical changes noninvasively for separating keratoconic from normal eyes.

A.2 Participants and Methods

Clinical Datasets

1342 patients were included in this multicenter retrospective study. The patients from two clinics located in two different countries were selected to include variability from different continents and to develop an automatic diagnosis process to separate healthy and keratoconic eyes in more than one ethnic group. The patients were divided into two groups – training group and validation group. The training group included a total of 346 patients (253 healthy and 93 keratoconic) enrolled from the Rio de Janeiro Corneal Tomography and Biomechanics Study Group, Rio de Janeiro, Brazil and 334 patients (227 healthy and 107 keratoconic) from the Vincieye Clinic in Milan, Italy. The validation group included 407 participants (205 healthy and 202 Keratoconic) from the Rio de Janeiro Corneal Tomography and Biomechanics Study Group – Rio de Janeiro, Brazil, and 315 participants (164 healthy and 151 Keratoconic) from the Vincieye Clinic in Milan, Italy.

The Institutional Review Boards of the clinical centres ruled that approval was not obligatory for this record review study. However, participants provided informed consent before using their data in the study. Complete ophthalmic examination was performed on all patients, including the CorVis-ST and Pentacam (OCULUS Optikgeräte GmbH; Wetzlar, Germany) exams.

The inclusion criterion for the Keratoconic groups was the presence of bilateral Keratoconus, without a history of having had any former ocular surgeries, such as corneal collagen cross-linking or intracorneal rings. For healthy subjects, the inclusion criteria included a Belin/Ambrósio Enhanced Ectasia total deviation index (BAD-D) of less than 1.6 standard deviation (SD) from normative values in both eyes [252], no previous ocular surgery or disease,

a myopia of less than 10 D, and no concurrent or previous Glaucoma or hypotonic therapies. Moreover, to confirm the diagnosis, all examinations from each clinic were blindly re-evaluated by a corneal expert at the other clinic. Age matching between healthy and KC subjects within each database was not carried out during this study, as there was no evidence in the literature to suggest the dependence of IOP on age [253, 254].

Only CorVis-ST exams with good quality scores (QS) that enabled calculation of all DCRs were included in the analysis. All measurements with the CorVis-ST were acquired by the same experienced technicians using the automatic release to guarantee the absence of user dependency. Furthermore, an additional manual frame-by-frame evaluation of the exams, made by an independent masked examiner, was implemented to ensure the quality of each acquired measurement. Only one eye per patient was randomly included in the analysis to avoid the bias of relationships between bilateral eyes that could influence the analysis results.

Automatic Diagnosis Process Using Corneal Thickness and Dynamic Corneal

Response Parameters

The automatic diagnosis process was constructed by using corneal thickness classification and dynamic corneal response parameter classification.

The common symptoms of keratoconus are a bilateral [122, 123] and asymmetric [124, 125] degeneration of the cornea characterized by the local thinned area, resulting in the thinned part protrusion. In addition, the location of corneal thickness thinning is a random occurrence [126-128]. Hence, the corneal thickness classification was based on the corneal thickness variation.

The corneal thickness classification was developed by using the evaluation data of corneal topography obtained by the Pentacam device from the training group. Before developing the corneal thickness classification, the evaluation data needed to rotate with an axis of rotation along the corneal apex and a plane of rotation in the plane based on the pupil to reduce the error of the measurement. The rotated evaluation data on the anterior and posterior corneal surface were determined by the Zernike expression, and then the corneal thinness along four meridians with an azimuth of 90° (Superior), 180° (Temporal), 270° (Inferior), and 360° (Nasal) was determined, Figure A-2. In addition, the recorded image of the IOP measurement on the CorVis-ST is recording the corneal topography in the temporal-nasal cross-section following with corneal apex response deformation in the anterior-posterior direction. Hence, the corneal thickness classification was based on the average difference in corneal thickness between corneal apex and four different points from the corneal longitudinal axis.

The mean and standard deviation of the difference in corneal thickness between the corneal apex and points at distances of 1, 2, 3 and 4 mm from the corneal longitudinal axis were determined for healthy eyes, Table A-1.

Table A-1 Mean and SD value of the difference in corneal thickness between corneal apex and points at distances of 1, 2, 3, and 4 mm from the corneal apex in micrometer

The distance from the corneal centre	1 mm	2 mm	3 mm	4 mm
Mean and SD of difference in corneal thickness between corneal apex and different points at distances (um)	3.345 ± 2.3441	13.465 ± 4.6294	32.555 ± 7.1472	65.453 ± 10.2465

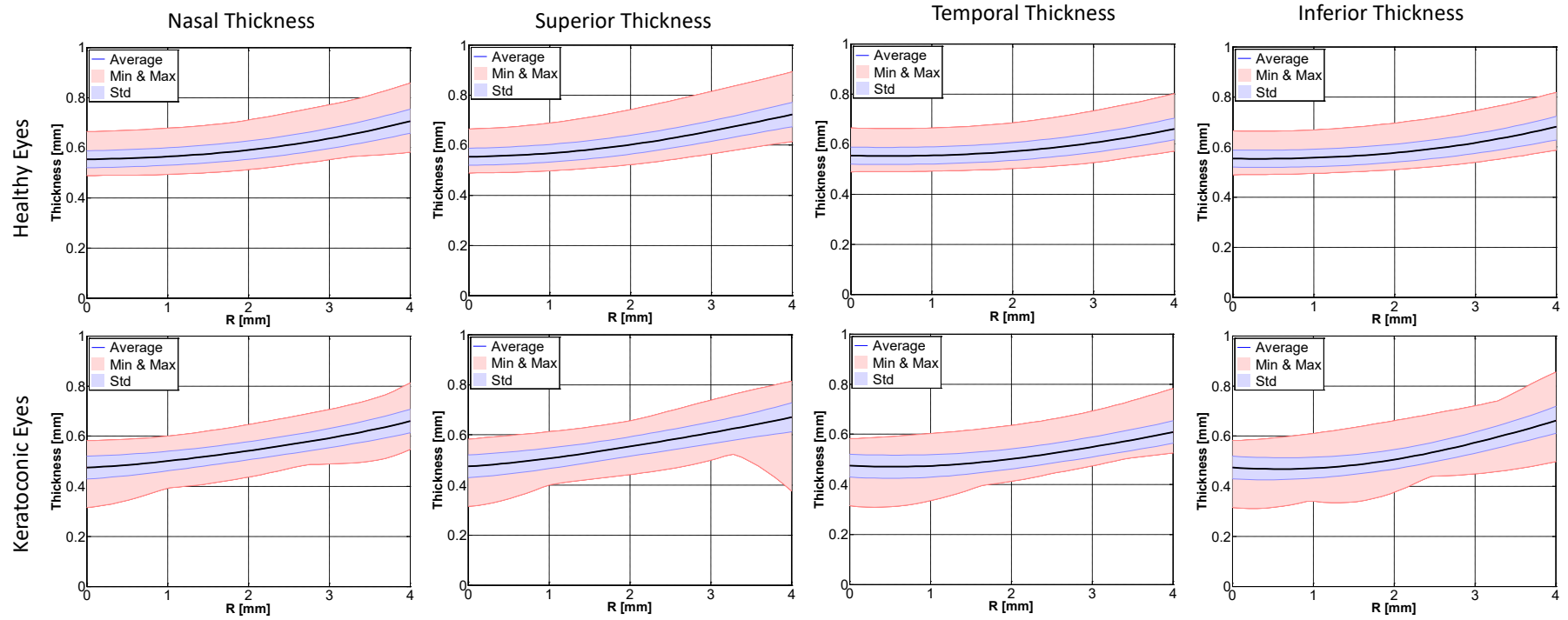


Figure A-2 Comparison of corneal thickness along four meridians with an azimuth of 90° (Superior), 180° (Temporal), 270° (Inferior), and 360° (Nasal) between healthy and keratoconic eyes in millimetre

The first condition of the healthy/keratoconic corneal classification is defined by the changes in corneal thickness with the distance variable. If the change in corneal thickness between the corneal apex and points at a distance of 1, 2, 3 and 4 mm from the corneal apex lies within the range of the mean \pm SD value, the corneal is categorised in the healthy cornea geometry. On the other hand, if it is beyond the range, it is categorised in the keratoconic corneal geometry.

Both corneal shape and corneal material stiffness are important elements for the diagnosis of the keratoconus. In the CorVis-ST process, there are 25 dynamic corneal response parameters related to IOP, CCT, corneal geometry, and corneal material behaviour. Due to the material stiffness was assumed to be a nonlinear hyper-elasticity in this research, the dynamic corneal response parameter analysis was only focused on the loading phase during the IOP measurement. Hence, only 13 dynamic corneal response parameters (as bIOP, CCT, A1T, A1L, A1V, HCT, PD, R, A1Deformation, A1Deflection, HCDeformation, HCDeflection, and AP1) was also considered for addition to the diagnosis process.

In pattern classification, to allocate the object described by varieties of measurements into one amongst a finite set of categories is the final goal. There is a particular characterization method based on the k-nearest neighbor (KNN) algorithm, which works well in practice [329]. Therefore, the dynamic corneal response parameter's analysis was based on the KNN method to detect the loss of the corneal stiffness for the early diagnosis of the keratoconus.

The KNN method is a non-parametric lazy learning algorithm, which does not make any assumptions regarding the underlying data distribution. It assumes that the data points in the feature space have a factor of distance. According to these distances in the feature space, a

class label is associated with each vector in the training data. In addition, there is a single number, K , that decides how many neighbours influence the classification. Based on the K neighbours, the weight factors of the distance metric can be defined to determine the breakaway points for classification. Basically, any point can find the K -nearest breakaway points used to determine the classification. In the KNN MATLAB toolbox, there is an automatic method to define the K value using the distance scale. Hence, the dynamic corneal response parameter's analysis was developed using a custom-built MATLAB code.

In this study, the KNN training process used the Leave-p-out cross-validation to test the ability of the training model in order to exclude the problem of overfitting or selection bias. The training data was an automatic random selection of 70% of clinical data from the training group and the results were validated by 30% of clinical data from the training group. Due to define the best value of K neighbours, the code used the automatic hyperparameters optimization to minimize cross-validation loss. For reproducibility, the code set the random selection and used the expected-improvement-plus acquisition function. Once the KNN training process was finished, the value of the K neighbours and the distance algorithm also was defined automatically in the KNN MATLAB toolbox.

Validation of Automatic Diagnosis of Keratoconus

The automatic diagnosis process allocated patients to the healthy or keratoconic eyes according to the results of the analysis of corneal thickness and dynamic corneal response parameters obtained from the CorVis-ST. The process of the automatic diagnosis was developed by using the clinical data in the training group from two medical organization and used the doctor's diagnoses as the "gold standard. The parameters included in the diagnosis

process were the result of corneal thickness classification and the dynamic corneal response parameters (including bIOP, CCT, A1T, A1L, A1V, HCT, PD, R, A1Deformation, A1Deflection, HCDeformation, HCDeflection, and AP1).

To make corneal thickness classification less effect of the measurement error, the evaluation data obtained from the CorVis-ST removed the eye rotation and redefined the corneal apex by using the location of the maximum corneal curve. The corneal thickness was calculated by using the rotated evaluation data and new corneal apex.

Subsequently, to exclude overfitting in the dynamic corneal response parameter analysis, the process was independently validated by using clinical data from the validation group. In addition, to reduce the effect of human error and machine error in the IOP measurement, a total of 722 patients in the validation group were collected from the same medical organization.

A.3 Result

The clinical datasets were divided into the training group for developing the automatic diagnosis of keratoconus and the validation group for evaluating the performance of the automatic diagnosis. All independent clinical databases were obtained from the Rio de Janeiro Corneal Tomography and Biomechanics Study Group in Brazil and the Vincieye Clinic in Milan.

A total of 1392 patients (617 left and 775 right eyes) were included in this research. The training group included 304 left and 366 right eyes and the validation group included 617 left and 775 right eyes. The mean and SD value of age in normal patients was 41 ± 17 years in the training group and 38 ± 13 years in the validation group, while the mean and SD value of age in

keratoconic patients was 35 ± 12 years in the training group and 36 ± 13 years in the validation group. In addition, the training group comprised 305 women and 365 men with a sex ratio (male to female) of 0.89 in healthy patients and 2.68 in keratoconic patients and the validation group comprised 298 women and 424 men with a sex ratio (male to female) of 0.84 in healthy patients and 2.61 in keratoconic patients.

The automatic diagnosis was constructed with corneal thickness classification and dynamic corneal response parameter classification. The results of corneal thickness classification provided by the Pentacam and the CorVis-ST for clinical datasets of the training group were summarized in Table A-2. The results showed that the corneal thickness classification by using the Pentacam had a higher correct classification with 85% specificity and 99% sensitivity than using the CorVis-ST with 58% specificity and 95% sensitivity. Hence, the results demonstrated that only using the corneal thickness measured in the temporal-nasal cross-section by using the CorVis-ST not enough to separate healthy and keratoconic patients. To consider addition more parameters in the automatic diagnosis was necessary to increase the specificity and sensitivity of the diagnosis process.

Table A-2 Results of corneal thickness classification using the Pentacam and the CorVis-ST for clinical datasets of the training group

		<i>Corneal Thickness Classification</i>			
		<i>Using Pentacam</i>		<i>Using CorVis-ST</i>	
<i>Predicted Outcome</i>		<i>Clinical Diagnosis</i>			
		<i>Health Eye</i>	<i>Keratoconic Eye</i>	<i>Health Eye</i>	<i>Keratoconic Eye</i>
<i>Health Eye</i>		475	28	456	80
<i>Keratoconic Eye</i>		5	162	24	110

The dynamic corneal response parameter classification of the training group by using the KNN method. The parameters in this classification including bIOP, CCT, A1T, A1L, A1V, HCT, PD, R, A1Deformation, A1Deflection, HCDeformation, HCDeflection, and AP1. The dynamic corneal response parameter classification of the training dataset showed that 670 patients using 4 neighbours and standardized euclidean distance in the KNN method without considering the result of corneal thickness classification were correctly classified with 80% specificity and 95% sensitivity (Table A-3).

Table A-3 Comparison of the results of the classification in the training group between dynamic corneal response parameter classification with and without the result of corneal thickness classification

<i>Train Group Total = 670 patients (480 Healthy and 190 KC eyes)</i>	<i>Dynamic Corneal Response Parameter Classification without Corneal Thickness Classification</i>	<i>Dynamic Corneal Response Parameter Classification With Corneal Thickness Classification</i>
<i>Positive Predictive Value</i>	92.3%	99.2%
<i>False Discovery Rate</i>	7.7%	0.8%
<i>False Omission Rate</i>	13.6%	2.6%
<i>Negative Predictive Value</i>	86.4%	97.4%
<i>Ture Positive Rate (Sensitivity)</i>	95.0%	99.0%
<i>False Positive Rate</i>	20.0%	2.1%
<i>False Negative Rate</i>	5.0%	1.0%
<i>False Positive Rate</i>	20.0%	2.1%
<i>True Negative Rateb (Specificity)</i>	80.0%	98.0%
<i>Positive likelihood Ratio</i>	475.0%	4702.5%
<i>Negative likelihood Ratio</i>	6.3%	1.1%
<i>F1-Score</i>	93.6%	99.1%
<i>G-Measure</i>	93.6%	99.1%
<i>Accuracy</i>	90.7%	98.7%

Additionally, when the parameters of dynamic corneal response parameter classification included the result of the corneal thickness classification, the specificity, sensitivity, and accuracy of the classification in the training group increased to 98%, 99%, and 98.7%,

respectively (Table A-3). Hence, the 4-nearest neighbour KNN classification model with standardized euclidean distance based on the input variables (including dynamic corneal response parameters and the result of the cornea thickness classification) was used in the automatic diagnosis of keratoconus.

In the validation group, the automatic diagnosis of keratoconus correctly classified 97% of the cases with specificity and 98% sensitivity (Table A-4). The result of the combined datasets including 670 patients (480 healthy and 190 keratoconic eyes) in the training group and 722 patients (369 healthy and 353 keratoconic eyes) in the validation group showed a good predictive accuracy of this diagnosis was 98.1% (with 97.2% specificity and 98.6% sensitivity), .

Table A-4 Results of automatic diagnosis of keratoconus in the training group, validation group and combined group

	<i>Training Group</i> <i>Total = 670 patients</i> <i>(480 Healthy / 190 KC eyes)</i>	<i>Validation Group</i> <i>Total = 722 patients</i> <i>(369 Healthy / 353 KC eyes)</i>	<i>Combined Group</i> <i>Total = 1392 patients</i> <i>(849 Healthy / 543 KC eyes)</i>
<i>Positive Predictive Value</i>	99.2%	97.1%	98.2%
<i>False Discovery Rate</i>	0.8%	2.9%	1.8%
<i>False Omission Rate</i>	2.6%	2.0%	2.2%
<i>Negative Predictive Value</i>	97.4%	98.0%	97.8%
<i>Ture Positive Rate</i> <i>(Sensitivity)</i>	99.0%	98.0%	98.6%
<i>False Positive Rate</i>	2.1%	3.1%	2.8%
<i>False Negative Rate</i>	1.0%	1.9%	1.4%
<i>False Positive Rate</i>	2.1%	3.1%	2.8%
<i>True Negaive Rate</i> <i>(Specificity)</i>	98.0%	97.0%	97.2%
<i>Positive likelihood</i> <i>Ratio</i>	4702.5%	3144.9%	3568.8%
<i>Negative likelihood</i> <i>Ratio</i>	1.1%	2.0%	1.5%
<i>F1-Score</i>	99.1%	160808.2%	245520.0%
<i>G-Measure</i>	99.1%	97.5%	98.4%
<i>Accuracy</i>	98.7%	97.5%	98.4%

A.4 Discussion

There are 1 in 2000 people in the general population affected by Keratoconus [121]. Normally, characteristics of the keratoconus are thinning and steepening of the cornea. A large amount of literature supports the observation that keratoconic cornea has a lower tangent modulus value than healthy cornea [36, 37, 98]. According to existing biomechanical models, clinical topographic and tomographic data, and studies at the genetic and molecular level, these observations have shed light on biomechanical pathogenesis and aetiology of keratoconus [33, 36, 37, 176, 328-332]. In particular, collagen and extracellular matrix pathways were found to be related to the mechanical stability of the keratoconic cornea [36, 37, 332]. These results were later confirmed by the studies of Scarcelli et al [328], Nash et al. [33] and Edmund [176]. The loss of biomechanical stability leads to the corneal morphologic change as the softer area on the cornea strains more than the surrounding stiffer areas [33, 176, 328, 330]. In addition, the increase in curvature is also related to the loss of biomechanical stability. All of the corneal morphologic change contributes to an overall stress redistribution [328, 330]. Therefore, observed deterioration in mechanical properties before the resulting changes in thickness and corneal topography may be an appropriate target for the early diagnosis of keratoconus [330, 333, 334].

To achieve this aim, dynamic corneal response parameters and corneal thickness obtained from the Corvis-ST were used to develop an automatic diagnosis of keratoconus aimed to separate normal from keratoconic eyes.

This study included 1392 cases from two different continents, Italy and Brazil. The inclusion of only one eye per patient eliminated the risk of bias due to the relationship between bilateral

eyes. Only clinical data with clear keratoconus and clearly normal eyes were included in this study. In this study, forme fruste keratoconus and subclinical cases were excluded from the databases, because it is difficult to detect the corneal material change by using in-vivo instrument. Moreover, the doctor's diagnoses as the "gold standard" were used to develop the automatic diagnosis of keratoconus by using corneal thickness and dynamic corneal response parameters.

All data were divided into training group (480 healthy and 200 keratoconic eyes) and validation group (414 healthy and 353 keratoconic eyes). The training group was used to develop the automatic diagnosis process to distinguish between normal and keratoconic eyes. The results indicated that once the corneal thickness added to the input variables of the KNN model, the KNN classification created showed high sensitivity and specificity with an accuracy of 98.7%. Moreover, using the automatic hyperparameters optimization to minimize cross-validation loss, the optimum number of neighbour points and the optimum distance algorithm in the KNN classification were defined. Following the determination of the optimum parameter combination of the KNN model, in the validation group, the predicted outcome also showed high sensitivity and specificity with an accuracy of 97.5%. The correctly classified more than 95% of the cases in both groups.

To compare the earlier studies about the diagnosis of keratoconus, most results provided both sensitivity and specificity lower than 90% [330, 335], but a new biomechanical index, CBI, provided higher sensitivity, specificity and accuracy of the keratoconus diagnosis than this research [321]. Furthermore, all studies are based on the dynamic Scheimpflug CorVis-ST device. Hence, the CorVis-ST has high potentiality on detecting the loss of biomechanical stability.

Additionally, many similar studies performed with the ocular response analyzer, which is also a non-contact tonometer using the air puff. These results showed sensitivity and specificity of the diagnosis lower than 90% [336-338]. However, this study provided a new method for the diagnosis of keratoconus using the dynamic corneal response parameters and corneal thickness based on the CorVis-ST.

The external validation of foremost importance to exclude overfitting and test reproducibility when considering a multi-input variable in the KNN classification. This validation included in this study, which produced a close result to the training group. In other words, this last finding excluded the risk of overfitting and confirmed the diagnostic capability of the method for keratoconus.

This study introduces a new method for keratoconus diagnosis, which showed highly sensitive, specific and accuracy to separate healthy from keratoconic eyes. The results of external validation datasets also confirm the feasibility of this method combined with topography to aid the diagnosis of keratoconus.

Appendix B - Ex-Vivo Experimental Procedure

B.1 Introduction

This Appendix B was to provide a detailed explanation on how the CorVis's ex-vivo human eye's test was performed and how CorVis's measurement data obtained from the test was analysed.

B.2 Specimen preparation

The fresh donor's eye was collected from the Fondazione Banca degli Occhi del Veneto Onlus, Venice, Italy, and tested within 3-5 days post mortem. Soft muscular tissue around the eye was removed by using surgical tongs and curved scissors. The superior direction based on the location of the superior rectus muscle and the medial direction based on the location of the anterior medial rectus muscle was marked to determine the side of the donor's eye. To define the location of the posterior pole, a 3D printed component was designed by using the previous experiment data [70]. The eye globe was placed in a 3D printed component to allow for accurate needle insertion through the posterior pole. The internal components of the eye were removed through the posterior pole with a 14G needle. Due to the glue to affect the material property, the needle needed to be lightly glued around the posterior pole with tiny amounts of glue. The intra-ocular cavity was then washed with Phosphate-buffered saline (PBS, Sigma, Dorset, United Kingdom). During this procedure, the outer surface of the eye was kept hydrated by the PBS drops every 2 minutes. Finally, the prepared specimen was injected with a 10% Dextran solution (Sigma-Aldrich, Darmstadt, Germany) to prevent swelling during

the experiment, and then transferred on the test rig.

B.3 Test Rig

A new test rig was developed to accurately and quickly test the performance of the biomechanically-Corrected intraocular pressure algorithm with the specimens under different IOP by using the CorVis-ST (Figure B-1).

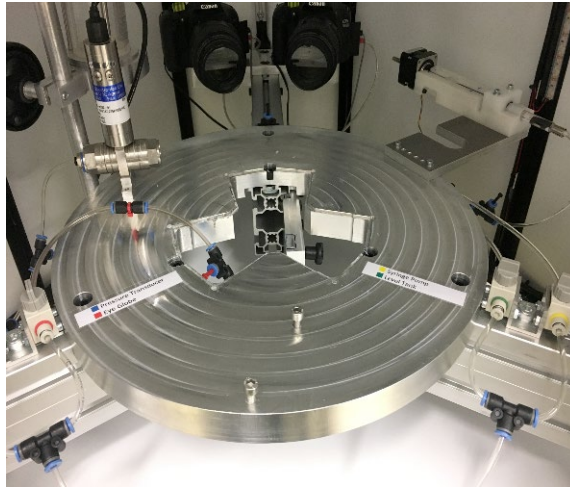


Figure B-1 Ex-Vivo Experimental equipment the custom-designed clamp

The test equipment (Figure 3-25) was built in-house, and all equipment was set inside a tailored-fit tent to assure no light disturbance, which would affect the CorVis' measurement during the testing. In addition, the IOP control system was made of an FDW pressure transducer (RDP Electronics, Wolverhampton, UK) to measure the IOP accurately, a stepper motor and a syringe to regulate the pressure in the circuit, and the control software was written in LabVIEW (version 10.0.1). The software was connected to the pressure transducer, the stepper motor and the syringe that allowed the user to regulate any pressure inside the eye in a dynamic or a constant manner. Before the specimen set on the test rig, a jar open to

atmosphere to level the pressure in the circuit to almost 0 mmHg at the beginning of the test and finally a custom-designed clamp allows the specimen to sit on a circular based with the needle attached to the posterior pole.

The custom-designed clamp was constructed with two parts, as the specimen holder and the posterior pole cast (Figure 3-24). The specimen holder was designed by the previous experiment data which provided a smooth contour to hold the inferior region of the specimen. The posterior pole cast was 3D printed by silicone which can support the eye from being pushed back by the air puff. In addition, the soft material is playing the role of fat tissues around ocular.

For pressure transducer to accurately measure the pressure, two important rules must be respected:

- The length of all pipes to any junction should be equal.
- The height of the nozzle of pressure transducer should be equal to the height of the syringe pump and they all have to be in the same height as the needle which is located at the centre of the eye pointing toward apex.

B.4 Testing Control and Protocols

The control software was used to control the stepper motor of the syringe to regulate the IOP of the specimen, and the IOP was monitored by using the pressure transducer. The experiments started with 3 pre-conditioning cycle which increased pressure to 40 mmHg and decreased to 0 mmHg in each cycle. The pre-conditioning cycle ensured that the specimen was sitting stably and comfortably on the custom-designed clamp and the tissue's material

behaviour was stable and repeatable [52]. Once the pre-conditioning cycle had finished, an initial pressure was regulated to 2.5 mmHg for increasing the accuracy and sensitivity of the pressure transducer. The testing IOP was controlled to vary between values that covered the natural variation in IOP seen in ophthalmic practice - 10, 15, 20, 25 and 30 mmHg. Between each testing IOP, the eye should be relaxed to 2.5 mmHg and waiting a period of 2 min. This time was determined by the previous experiment to allow the tissue to recover its initial state. In each setting IOP, the IOP measurement process was triggered automatically from the CorVis device. During the ex-vivo testing, each measurement (as CCT, CVS-IOP, and AP1 et. al) was shown on the CorVis monitor. The deformation at the corneal apex at the first applanation and the highest concave, CCT and AP1 should be consistent for 10 readings in the same pressure. If not, more measurements will be taken to decrease errors. Normally, each IOP was taken 20 times IOP measurement to select 10 reading, which was used in post statistics analysis. Throughout these steps, the eye was kept moist using Everclear; a viscous tear film supplement (Melleson Pharma, Breda, Netherlands) to prevent drying.

B.5 Reliability Test of Test Rig

The test rig was used to validate the biomechanically-corrected intraocular pressure algorithm for healthy eyes. For this reason, to validate the reliability of the pressure support system and the accuracy of the pressure transducer in the experimental equipment is important.

In this study, 5 fresh porcine eyes were used in the reliability test. All of the fresh porcine eyes were collected from a local abattoir and tested within 6-9 hours after death. Then, specimen preparation and testing protocols in the validation test followed the same protocols with the ex-vivo experiment. In addition, the testing IOP was controlled to vary from 10 to 30 mmHg,

and the rate of pressure increase by 0.5 mmHg per second.

The validation test was used to test the sensitivity of the pressure transducer and the stability of the pressure support system by using 5 porcine eyes. Following the process, the IOP inside the porcine eyes was recorded beginning at 2.5 mmHg and stopping when the IOP achieved the setting value and became stable. After the testing, the eye should be relaxed to 2.5 mmHg and waiting a period of 2 min. In addition, the test of each specimen repeated 3 times on each setting IOP to validate the reproducibility of the test rig.

The results of the validation test were shown in Figure B-2. The accuracy of the pressure support system was validated by using repeated measured ANOVA. The result of the repeated testing was shown that there was no significant difference in IOP between the set level and the final stable level ($p>0.05$) with the Bartlett's Sphericity Test. In addition, all results showed that the IOP was still unstable after the IOP achieved the setting IOP, Figure B-2. The mean and STD of the time period from the first time of the setting IOP achieved to the final time of the IOP stable condition was 61.0 ± 0.7 second in 10 mmHg of IOP setting, 61.0 ± 1.0 second in 15 mmHg of IOP setting, 60.7 ± 0.8 second in 20 mmHg of IOP setting, 61.0 ± 1.0 second in 25 mmHg of IOP setting, and 60.7 ± 0.6 second in 30 mmHg of IOP setting. According to these results, after reaching each setting IOP level, the eye was allowed to stabilise for 60 seconds before measuring IOP using the CorVis-ST. Hence, the reliability of the test rig has been validated that the process with the rate of pressure increase by 0.5 mmHg per second and range of IOP varied from 10 mmHg to 30 mmHg has high accuracy to be used to validate the biomechanically-corrected intraocular pressure algorithm for healthy eyes ex-vivo.

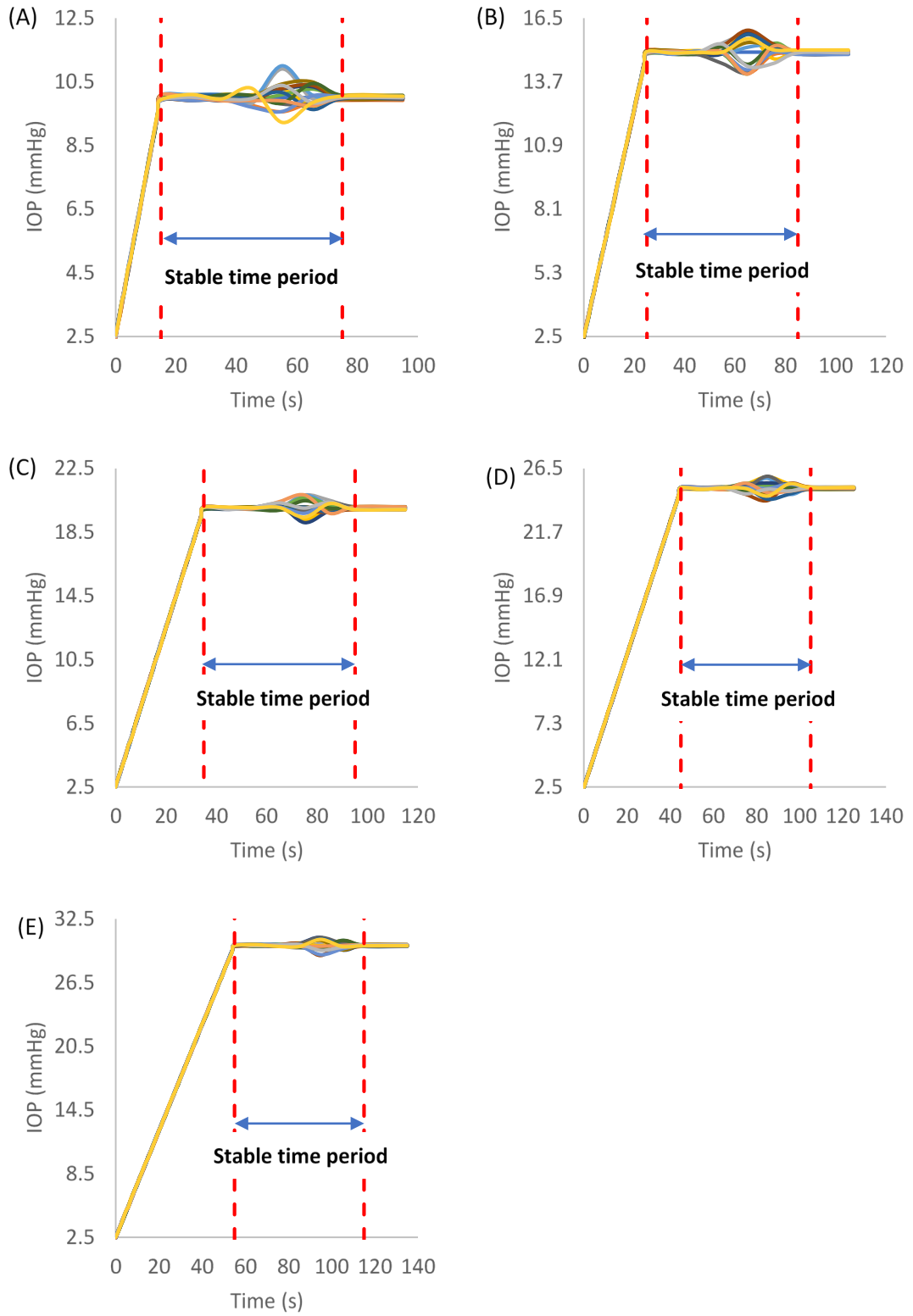


Figure B-2 Results of the reliability of test rig

Appendix C - Flowchart of Numerical Modelling

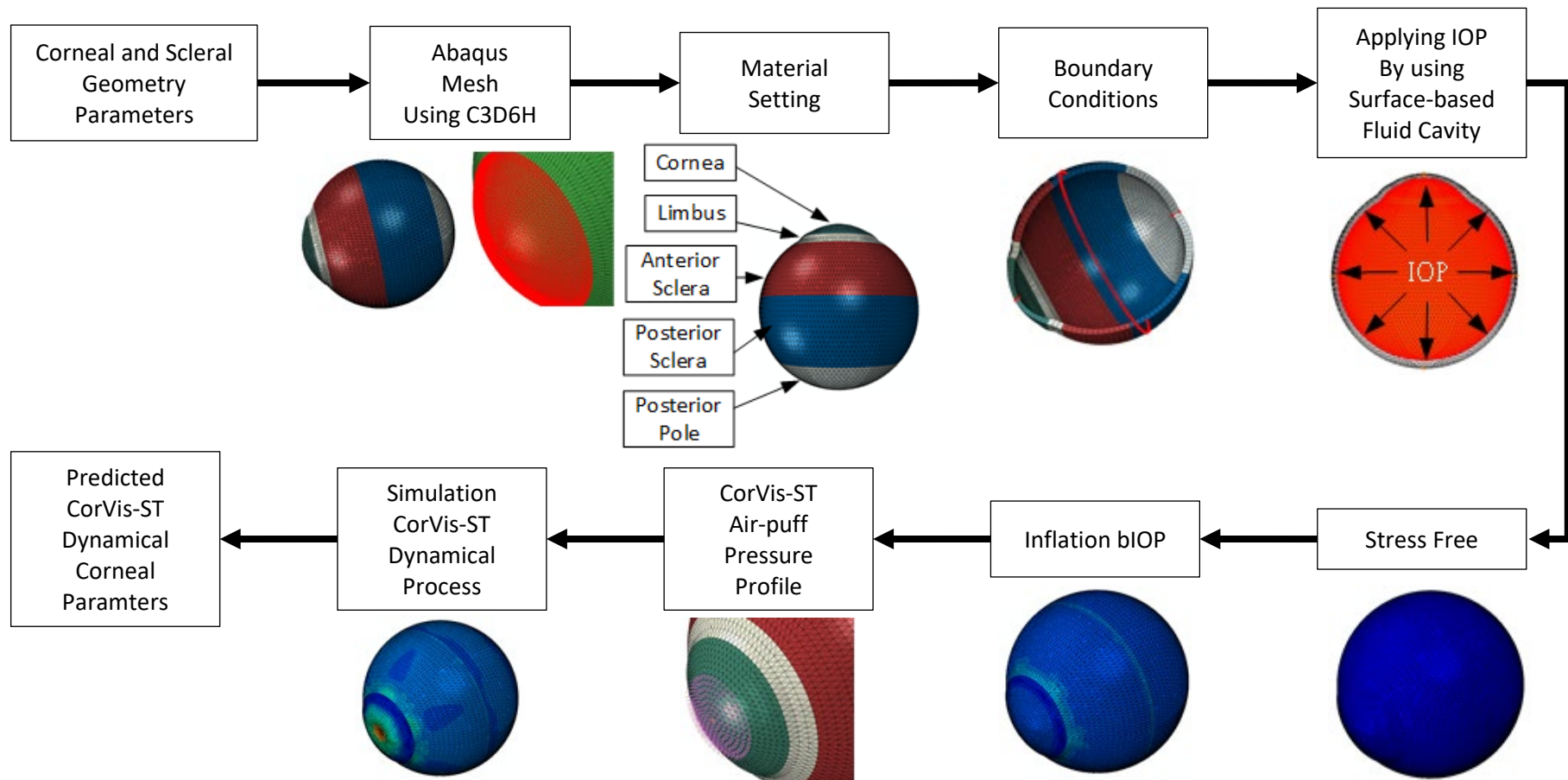


Figure C-1 Flowchart is demonstrating the process behind the analysis of numerical modelling

References

- [1] A. Elsheikh, B. Geraghty, P. Rama, M. Campanelli, and K. M. Meek, "Characterization of age-related variation in corneal biomechanical properties," vol. 7, no. 51, pp. 1475-1485, 2010.
- [2] F. Grehn and R. L. Stamper, *Glaucoma. [electronic book]* (Essentials in ophthalmology). Berlin ;New York : Springer, 2006., 2006.
- [3] R. S. Snell, M. A. Lemp, and I. Grunther, *Clinical anatomy of the eye*, 2nd ed. ed. (Online access with purchase: Wiley Online Library). Blackwell Science Ltd,. 1998.
- [4] F. A. Medeiros and R. N. Weinreb, "Evaluation of the influence of corneal biomechanical properties on intraocular pressure measurements using the ocular response analyzer," (in English), *Journal of Glaucoma*, Article vol. 15, no. 5, pp. 364-370, 10 / 01 / 2006.
- [5] C. Kaufmann, L. M. Bachmann, and M. A. Thiel, "Comparison of Dynamic Contour Tonometry with Goldmann Applanation Tonometry," *Investigative Ophthalmology & Visual Science*, vol. 45, no. 9, pp. 3118-3121, 2004.
- [6] P.-B. Ouyang, C.-Y. Li, X.-H. Zhu, and X.-C. Duan, "Assessment of intraocular pressure measured by Reichert Ocular Response Analyzer, Goldmann Applanation Tonometry, and Dynamic Contour Tonometry in healthy individuals," *International journal of ophthalmology*, vol. 5, pp. 102-107, 2012.
- [7] S. Hong, J. S. Gong, and J. H. Young, "Long-term intraocular pressure fluctuation and progressive visual field deterioration in patients with glaucoma and low intraocular pressures after a triple procedure," (in English), *Archives of Ophthalmology*, Article vol. 125, no. 8, pp. 1010-1013, 08 / 01 / 2007.
- [8] N. G. Congdon, D. S. Friedman, and T. Lietman, "Important causes of visual impairment in the world today," (in English), *Journal of the American Medical Association*, Review vol. 290, no. 15, pp. 2057-2060, 10 / 15 / 2003.

- [9] P. Davey, *Ophthalmology-current clinical and research updates*. IntechOpen, 2014.
- [10] E. M. Kirstein, A. Elsheikh, and P. Gunvant, "Tonometry—past, present and future," in *Glaucoma-Current Clinical and Research Aspects*, D. P. Gunvant, Ed.: InTech, 2011.
- [11] M. Chakrabarti, S. R. John, and A. Chakrabarti, "180 years of evolution in Tonometry," *Kerala Journal of Ophthalmology*, p. 173, 2009.
- [12] C. Kniestedt, M. Nee, and R. L. Stamper, "Dynamic contour tonometry: a comparative study on human cadaver eyes," *Archives of ophthalmology*, vol. 122, no. 9, pp. 1287-1293, 2004.
- [13] S. IOF., *Ophthalmic Instruments—Tonometers: ISO8612: 2001*, Geneva, Switzerland, 2001.
- [14] T. Vos, C. Allen, M. Arora, R. M. Barber, Z. A. Bhutta *et al.*, "Global, regional, and national incidence, prevalence, and years lived with disability for 310 diseases and injuries, 1990–2015: a systematic analysis for the Global Burden of Disease Study 2015," *The Lancet*, vol. 388, no. 10053, pp. 1545-1602, 2016/10/08/ 2016.
- [15] D. Pascolini and S. P. Mariotti, "Global estimates of visual impairment: 2010," *British Journal of Ophthalmology*, vol. 96, no. 5, pp. 614-618, 2012.
- [16] A. Sommer, J. M. Tielsch, J. Katz, H. A. Quigley, J. D. Gottsch *et al.*, "Relationship between intraocular pressure and primary open angle glaucoma among white and black Americans: the Baltimore Eye Survey," *Archives of ophthalmology*, vol. 109, no. 8, pp. 1090-1095, 1991.
- [17] A. V. Mantravadi and N. Vadhar, "Glaucoma," *Primary Care: Clinics in Office Practice*, vol. 42, no. 3, pp. 437-449, 2015/09/01/ 2015.
- [18] H. A. Quigley, "Number of people with glaucoma worldwide," *British journal of ophthalmology*, vol. 80, no. 5, pp. 389-393, 1996.
- [19] H. A. Quigley and S. Vitale, "Models of open-angle glaucoma prevalence and incidence in the United States," *Investigative Ophthalmology & Visual Science*, vol.

- 38, no. 1, pp. 83-91, 1997.
- [20] S. European Glaucoma, *Terminology and guidelines for glaucoma*. Savona: Dogma, 2008.
- [21] R. N. Weinreb and P. T. Khaw, "Primary open-angle glaucoma," *The Lancet*, vol. 363, no. 9422, pp. 1711-1720, 2004/05/22/ 2004.
- [22] H. Goldmann and T. Schmidt, "Über Applanationstonometrie," *Ophthalmologica*, vol. 134, no. 4, pp. 221-242, 1957.
- [23] R. C. W. Wolfs, C. C. W. Klaver, J. R. Vingerling, D. E. Grobbee, A. Hofman, and P. T. V. M. de Jong, "Distribution of central corneal thickness and its association with intraocular pressure: the Rotterdam study," *American Journal of Ophthalmology*, vol. 123, no. 6, pp. 767-772, 1997/06/01/ 1997.
- [24] M. M. Whitacre and R. Stein, "Sources of error with use of Goldmann-type tonometers," *Survey of Ophthalmology*, vol. 38, no. 1, pp. 1-30, 1993/07/01/ 1993.
- [25] G. J. Orssengo and D. C. Pye, "Determination of the true intraocular pressure and modulus of elasticity of the human cornea in vivo," *Bulletin of Mathematical Biology*, vol. 61, no. 3, pp. 551-572, 1999/05/01/ 1999.
- [26] R. Munger, W. G. Hodge, G. Mintsoulis, P. J. Agapitos, W. B. Jackson, and K. F. Damji, "Correction of intraocular pressure for changes in central corneal thickness following photorefractive keratectomy," *Canadian journal of ophthalmology. Journal canadien d'ophtalmologie*, vol. 33, no. 3, pp. 159-165, 1998.
- [27] J. D. Brandt, J. A. Beiser, M. A. Kass, and M. O. Gordon, "Central corneal thickness in the ocular hypertension treatment study (OHTS)," *Ophthalmology*, vol. 108, no. 10, pp. 1779-1788, 2001/10/01/ 2001.
- [28] U. Rehany, V. Bersudsky, and S. Rumelt, "Paradoxical hypotony after laser in situ keratomileusis," *Journal of Cataract & Refractive Surgery*, vol. 26, no. 12, pp. 1823-1826, 2000/12/01/ 2000.

- [29] K. E. Hamilton and D. C. Pye, "Young's modulus in normal corneas and the effect on applanation tonometry," *Optometry and Vision Science*, vol. 85, no. 6, pp. 445-450, 2008.
- [30] J. Liu and C. J. Roberts, "Influence of corneal biomechanical properties on intraocular pressure measurement: Quantitative analysis," *Journal of Cataract & Refractive Surgery*, vol. 31, no. 1, pp. 146-155, 2005/01/01/ 2005.
- [31] A. Kotecha, E. White, P. G. Schlottmann, and D. F. Garway-Heath, "Intraocular pressure measurement precision with the Goldmann Applanation, dynamic contour, and Ocular Response Analyzer tonometers," *Ophthalmology*, vol. 117, no. 4, pp. 730-737, 2010/04/01/ 2010.
- [32] S. Shah, M. Laiquzzaman, R. Bhojwani, S. Mantry, and I. Cunliffe, "Assessment of the biomechanical properties of the cornea with the Ocular Response Analyzer in normal and keratoconic eyes," *Investigative Ophthalmology & Visual Science*, vol. 48, no. 7, pp. 3026-3031, 2007.
- [33] I. S. Nash, P. R. Greene, and C. S. Foster, "Comparison of mechanical properties of keratoconus and normal corneas," *Experimental Eye Research*, vol. 35, no. 5, pp. 413-424, 1982/11/01/ 1982.
- [34] W. J. Dupps and S. E. Wilson, "Biomechanics and wound healing in the cornea," *Experimental Eye Research*, vol. 83, no. 4, pp. 709-720, 2006/10/01/ 2006.
- [35] W. Radner, M. Zehetmayer, R. Aufreiter, and R. Mallinger, "Interlacing and cross-angle distribution of collagen lamellae in the human cornea," (in eng), *Cornea*, vol. 17, no. 5, pp. 537-543, 1998/09// 1998.
- [36] K. M. Meek, S. J. Tuft, Y. Huang, P. S. Gill, S. Hayes *et al.*, "Changes in collagen orientation and distribution in keratoconus corneas," *Investigative Ophthalmology & Visual Science*, vol. 46, no. 6, pp. 1948-1956, 2005.
- [37] T. T. Andreassen, A. Hjorth Simonsen, and H. Oxlund, "Biomechanical properties of keratoconus and normal corneas," *Experimental Eye Research*, vol. 31, no. 4, pp. 435-

441, 1980/10/01/ 1980.

- [38] M. J. Moseley, N. M. Evans, and A. R. Fielder, "Comparison of a new non-contact tonometer with Goldmann applanation," *Eye*, vol. 3, no. 3, pp. 332-337, 1989/05/01 1989.
- [39] A. A. Yücel, J. Stürmer, and B. Gloor, "Comparison of tonometry with the Keeler air puff non-contact tonometer "Pulsair" and the Goldmann applanation tonometer," (in ger), *Klinische Monatsblätter für Augenheilkunde*, vol. 197, no. 4, pp. 329-334, 1990/10// 1990.
- [40] S. W. Mackie, J. L. Jay, R. Ackerley, and G. Walsh, "Clinical comparison of the Keeler Pulsair 2000, American Optical MkII and Goldmann applanation tonometers," *Ophthalmic and Physiological Optics*, vol. 16, no. 2, pp. 171-177, 1996/03/01/ 1996.
- [41] O. E. Babalola, A. V. Kehinde, A. C. Iloegbunam, T. Akinbinu, C. Moghalu, and I. Onuoha, "A comparison of the Goldmann applanation and non-contact (Keeler Pulsair EasyEye) tonometers and the effect of central corneal thickness in indigenous African eyes," vol. 29, no. 2, pp. 182-188, 2009.
- [42] S. Mohan, S. Tiwari, A. Jain, J. Gupta, and S. K. Sachan, "Clinical comparison of Pulsair non-contact tonometer and Goldmann applanation tonometer in Indian population," *Journal of Optometry*, vol. 7, no. 2, pp. 86-90, 2014/04/01/ 2014.
- [43] B. C. Chauhan and D. B. Henson, "Clinical evaluation of the Non-Contact Tonometer Mark II," (in eng), *American journal of optometry and physiological optics*, vol. 65, no. 9, pp. 751-756, 1988/09// 1988.
- [44] V. Gupta, P. Sony, H. Agarwal, R. Sihota, and A. Sharma, "Inter-instrument agreement and influence of central corneal thickness on measurements with Goldmann, pneumotonometer and noncontact tonometer in glaucomatous eyes," *Indian journal of ophthalmology*, Original Article vol. 54, no. 4, pp. 261-265, October 1, 2006 2006.
- [45] D. Wang, W. Huang, Y. Li, Y. Zheng, P. J. Foster *et al.*, "Intraocular pressure, central corneal thickness, and Glaucoma in Chinese adults: the Liwan eye study," *American*

Journal of Ophthalmology, vol. 152, no. 3, pp. 454-462.e1, 2011/09/01/ 2011.

- [46] A. A. Joda, M. M. S. Shervin, D. Kook, and A. Elsheikh, "Development and validation of a correction equation for Corvis tonometry," *Computer Methods in Biomechanics and Biomedical Engineering*, vol. 19, no. 9, pp. 943-953, 2016/07/03 2016.
- [47] D. A. Hoeltzel, P. Altman, K. Buzard, and K.-i. Choe, "Strip extensometry for comparison of the mechanical response of bovine, rabbit, and human corneas," *Journal of Biomechanical Engineering*, vol. 114, no. 2, pp. 202-215, 1992.
- [48] A. Elsheikh and K. Anderson, "Comparative study of corneal strip extensometry and inflation tests," vol. 2, no. 3, pp. 177-185, 2005.
- [49] E. Spoerl, V. Zubaty, N. Terai, L. E. Pillunat, and F. Raiskup, "Influence of high-dose cortisol on the biomechanics of incubated porcine corneal strips," (in English), *Journal of Refractive Surgery, Conference Paper* vol. 25, no. 9, pp. S794-S798, 09 / 01 / 2009.
- [50] T. Seiler, M. Matallana, S. Sandler, and T. Bende, "Does Bowman's layer determine the biomechanical properties of the cornea?," *Journal of Refractive Surgery* vol. 8, no. 2, pp. 139-142, 1992.
- [51] J. Gloster, E. S. Perkins, and M. L. Pommier, "Extensibility of strips of sclera and cornea," (in eng), *The British journal of ophthalmology*, vol. 41, no. 2, pp. 103-110, 1957.
- [52] A. Elsheikh, D. Wang, M. Brown, P. Rama, M. Campanelli, and D. Pye, "Assessment of corneal biomechanical properties and their variation with age," *Current Eye Research*, vol. 32, no. 1, pp. 11-19, 2007/01/01 2007.
- [53] S. L. Y. Woo, A. S. Kobayashi, W. A. Schlegel, and C. Lawrence, "Nonlinear material properties of intact cornea and sclera," *Experimental Eye Research*, vol. 14, no. 1, pp. 29-39, 1972/07/01/ 1972.
- [54] C. J. Roberts, "Concepts and misconceptions in corneal biomechanics," *Journal of*

Cataract & Refractive Surgery, vol. 40, no. 6, pp. 862-869, 2014/06/01/ 2014.

- [55] M. F. Land and R. D. Fernald, "The evolution of Eyes," *Annual review of neuroscience*, vol. 15, no. 1, pp. 1-29, 1992.
- [56] T. W. Olsen, S. Sanderson, X. Feng, and W. C. Hubbard, "Porcine sclera: thickness and surface area," *Investigative Ophthalmology & Visual Science*, vol. 43, no. 8, pp. 2529-2532, 2002.
- [57] S. Vurgese, S. Panda-Jonas, and J. B. Jonas, "Scleral thickness in human eyes," *PLOS ONE*, vol. 7, no. 1, p. e29692, 2012.
- [58] L. Shen, Q. S. You, X. Xu, F. Gao, Z. Zhang *et al.*, "Scleral thickness in Chinese eyes," *Investigative Ophthalmology & Visual Science*, vol. 56, no. 4, pp. 2720-2727, 2015.
- [59] M. Dubbelman, H. A. Weeber, R. G. L. Van Der Heijde, and H. J. Völker-Dieben, "Radius and asphericity of the posterior corneal surface determined by corrected Scheimpflug photography," *Acta Ophthalmologica Scandinavica*, vol. 80, no. 4, pp. 379-383, 2002.
- [60] M. Dubbelman, V. A. D. P. Sicam, and G. L. Van der Heijde, "The shape of the anterior and posterior surface of the aging human cornea," *Vision Research*, vol. 46, no. 6, pp. 993-1001, 2006.
- [61] R. Lindsay, G. Smith, and D. Atchison, "Descriptors of corneal shape," (in eng), *Optometry and vision science : official publication of the American Academy of Optometry*, vol. 75, no. 2, pp. 156-158, 1998/02// 1998.
- [62] J. Ying, M. Shi, B. Wang, and B. Wang, *Anterior corneal asphericity calculated by the tangential radius of curvature* (no. 7 %J Journal of Biomedical Optics). SPIE, 2012, pp. 1-10, 10.
- [63] S. Feizi, M. R. Jafarinasab, F. Karimian, H. Hasanpour, and A. Masudi, "Central and peripheral corneal thickness measurement in normal and keratoconic eyes using three corneal pachymeters," (in eng), *Journal of ophthalmic & vision research*, vol. 9,

no. 3, pp. 296-304, Jul-Sep 2014.

- [64] S. Al-Ageel and A. M. Al-Muammar, "Comparison of central corneal thickness measurements by Pentacam, noncontact specular microscope, and ultrasound pachymetry in normal and post-LASIK eyes," *Saudi Journal of Ophthalmology*, vol. 23, no. 3, pp. 181-187, 2009/10/01/ 2009.
- [65] I. A. Chaudhry, "Measurement of central corneal thickness in health and disease," (in eng), *Saudi journal of ophthalmology : official journal of the Saudi Ophthalmological Society*, vol. 23, no. 3-4, pp. 179-180, 2009.
- [66] J. M. Tiffany, B. S. Todd, and M. R. Baker, "Computer-assisted calculation of exposed area of the human eye," in *Lacrimal Gland, Tear Film, and Dry Eye Syndromes 2: Basic Science and Clinical Relevance*, D. A. Sullivan, D. A. Dartt, and M. A. Meneray, Eds. Boston, MA: Springer US, 1998, pp. 433-439.
- [67] J. C. Barry and A. Backes, "Limbus versus pupil center for ocular alignment measurement with corneal reflexes," *Investigative Ophthalmology & Visual Science*, vol. 38, no. 12, pp. 2597-2607, 1997.
- [68] J. C. Barry and A. Backes, "Limbus versus pupil center for ocular alignment measurement with corneal reflexes," *Journal of American Association for Pediatric Ophthalmology and Strabismus*, vol. 2, no. 3, p. 191, 1998/06/01/ 1998.
- [69] T. Avitabile, F. Marano, M. G. Uva, and A. Reibaldi, "Evaluation of central and peripheral corneal thickness with ultrasound biomicroscopy in normal and keratoconic eyes," (in eng), *Cornea*, vol. 16, no. 6, pp. 639-644, 1997/11// 1997.
- [70] A. Elsheikh, B. Geraghty, D. Alhasso, J. Knappett, M. Campanelli, and P. Rama, "Regional variation in the biomechanical properties of the human sclera," *Experimental Eye Research*, vol. 90, no. 5, pp. 624-633, 2010/05/01/ 2010.
- [71] M. R. Bryant and P. J. McDonnell, "Constitutive Laws for Biomechanical Modeling of Refractive Surgery," *Journal of Biomechanical Engineering*, vol. 118, no. 4, pp. 473-481, 1996.

- [72] B. Jue and D. M. Maurice, "The mechanical properties of the rabbit and human cornea," *Journal of Biomechanics*, vol. 19, no. 10, pp. 847-853, 1986/01/01/ 1986.
- [73] J. Ø. Hjortdal, "Extensibility of the normo-hydrated human cornea," *Acta Ophthalmologica Scandinavica*, vol. 73, no. 1, pp. 12-17, 1995.
- [74] H. Hatami-Marbini and E. Etebu, "Hydration dependent biomechanical properties of the corneal stroma," *Experimental Eye Research*, vol. 116, pp. 47-54, 2013/11/01/ 2013.
- [75] J. L. Battaglioli and R. D. Kamm, "Measurements of the compressive properties of scleral tissue," *Investigative Ophthalmology & Visual Science*, vol. 25, no. 1, pp. 59-65, 1984.
- [76] H. Hatami-Marbini and E. Etebu, "An experimental and theoretical analysis of unconfined compression of corneal stroma," *Journal of Biomechanics*, vol. 46, no. 10, pp. 1752-1758, 2013/06/21/ 2013.
- [77] M. Ahearne, Y. Yang, A. J. El Haj, K. Y. Then, and K. K. Liu, "Characterizing the viscoelastic properties of thin hydrogel-based constructs for tissue engineering applications," vol. 2, no. 5, pp. 455-463, 2005.
- [78] H. Hatami-Marbini and E. Etebu, "Rate dependent biomechanical properties of corneal stroma in unconfined compression," *Biorheology* vol. 50, no. 3-4, pp. 133-147, 2013.
- [79] W. M. Petroll, P. Roy, C. J. Chuong, B. Hall, H. D. Cavanagh, and J. V. Jester, "Measurement of surgically induced corneal deformations using three-dimensional confocal microscopy," (in eng), *Cornea*, vol. 15, no. 2, pp. 154-164, 1996/03// 1996.
- [80] K. A. Buzard, J. F. Ronk, M. H. Friedlander, D. J. Tepper, D. A. Hoeltzel, and K. I. Choe, "Quantitative measurement of wound spreading in radial keratotomy," *Journal of Refractive Surgery*, vol. 8, no. 3, pp. 217-223, 1992.
- [81] J. Ø. Hjortdal and N. Ehlers, "Acute tissue deformation of the human cornea after

- radial keratotomy," *Journal of refractive surgery*
vol. 12, no. 3, pp. 391-432, 1996.
- [82] S. A. Velinsky and M. R. Bryant, "On the computer-aided and optimal design of keratorefractive surgery," *Journal of Refractive Surgery*, vol. 8, no. 2, pp. 173-182, 1992.
- [83] R. P. Vito and P. H. Carnell, "Finite element based mechanical models of the cornea for pressure and indenter loading," *Journal of Refractive Surgery*, vol. 8, no. 2, pp. 146-151, 1992.
- [84] K. D. Hanna, F. E. Jouve, G. O. Waring, and P. G. Ciarlet, "Computer simulation of arcuate keratotomy for astigmatism," *Journal of Refractive Surgery*, vol. 8, no. 2, pp. 152-163, 1992.
- [85] W. O. Wray, E. D. Best, and L. Y. Cheng, "A mechanical model for radial keratotomy: toward a predictive capability," *Journal of Biomechanical Engineering*, vol. 116, no. 1, pp. 56-61, 1994.
- [86] P. M. Pinsky and D. V. Datye, "Numerical modeling of radial, astigmatic, and hexagonal keratotomy," *Journal of Refractive Surgery*, vol. 8, no. 2, pp. 164-172, 1992.
- [87] G. K. Lang, *Ophthalmology: a pocket textbook atlas* (Online access: Thieme Medical Publishers, Inc. MedOne Education). Thieme Medical Publishers Incorporated.
- [88] K. M. Meek and N. J. Fullwood, "Corneal and scleral collagens—a microscopist's perspective," *Micron*, vol. 32, no. 3, pp. 261-272, 2001/04/01/ 2001.
- [89] V. Alastrué, B. Calvo, E. Peña, and M. Doblaré, "Biomechanical modeling of refractive corneal surgery," *Journal of Biomechanical Engineering*, vol. 128, no. 1, pp. 150-160, 2005.
- [90] D. C. Fernández, A. M. Niaz, R. M. Kurtz, G. P. Djotyan, and T. Juhasz, "A finite element model for ultrafast laser–lamellar keratoplasty," *Annals of Biomedical*

Engineering, journal article vol. 34, no. 1, pp. 169-183, January 01 2006.

- [91] A. Elsheikh and D. Wang, "Numerical modelling of corneal biomechanical behaviour," *Computer Methods in Biomechanics and Biomedical Engineering*, vol. 10, no. 2, pp. 85-95, 2007/04/01 2007.
- [92] L.-y. Li and B. Tighe, "Nonlinear analysis of static axisymmetric deformation of the human cornea," *Computational Materials Science*, vol. 38, no. 4, pp. 618-624, 2007/02/01/ 2007.
- [93] C. F. Burgoyne, J. C. Downs, A. J. Bellezza, and R. T. Hart, "Three-dimensional reconstruction of normal and early glaucoma monkey optic nerve head connective tissues," *Investigative Ophthalmology & Visual Science*, vol. 45, no. 12, pp. 4388-4399, 2004.
- [94] I. A. Sigal, J. G. Flanagan, I. Tertinegg, and C. R. Ethier, "Predicted extension, compression and shearing of optic nerve head tissues," *Experimental Eye Research*, vol. 85, no. 3, pp. 312-322, 2007/09/01/ 2007.
- [95] I. A. Sigal, J. G. Flanagan, I. Tertinegg, and C. R. Ethier, "Finite element modeling of optic nerve head biomechanics," *Investigative Ophthalmology & Visual Science*, vol. 45, no. 12, pp. 4378-4387, 2004.
- [96] A. J. Bellezza, R. T. Hart, and C. F. Burgoyne, "The optic nerve head as a biomechanical structure: initial finite element modeling," *Investigative Ophthalmology & Visual Science*, vol. 41, no. 10, pp. 2991-3000, 2000.
- [97] P. D. Hassett and C. C. Kelleher, "The epidemiology of occupational penetrating eye injuries in Ireland," *Occupational Medicine*, vol. 44, no. 4, pp. 209-211, 1994.
- [98] K. Anderson, A. El-Sheikh, and T. Newson, "Application of structural analysis to the mechanical behaviour of the cornea," *Journal of the Royal Society Interface*, vol. 1, no. 1, pp. 3-15, 2004.
- [99] A. Elsheikh, "Finite element modeling of corneal biomechanical behavior," *Journal of*

Refractive Surgery, vol. 26, no. 4, pp. 289-300, 2010.

- [100] R. W. Ogden and R. Hill, "Large deformation isotropic elasticity - on the correlation of theory and experiment for incompressible rubberlike solids," *Proceedings of the Royal Society of London. A. Mathematical and Physical Sciences* vol. 326, no. 1567, pp. 565-584, 1972.
- [101] C. R. Ethier, M. Johnson, and J. Ruberti, "Ocular Biomechanics and Biotransport," *Annual Review of Biomedical Engineering*, vol. 6, no. 1, pp. 249-273, 2004.
- [102] T. Theelen, C. F. M. Meulendijks, D. E. M. Geurts, A. van Leeuwen, N. B. M. Voet, and A. F. Deutman, "Impact factors on intraocular pressure measurements in healthy subjects," *British journal of ophthalmology*, vol. 88, no. 12, pp. 1510-1511, 2004.
- [103] F. J. Giblin, J. P. McCready, T. Kodama, and V. N. Reddy, "A direct correlation between the levels of ascorbic acid and H₂O₂ in aqueous humor," *Experimental Eye Research*, vol. 38, no. 1, pp. 87-93, 1984/01/01/ 1984.
- [104] K. C. Bhuyan and D. K. Bhuyan, "Regulation of hydrogen peroxide in eye humors effect of 3-amino-1H-1,2,4-triazole on catalase and glutathione peroxidase of rabbit eye," *Biochimica et Biophysica Acta (BBA) - General Subjects*, vol. 497, no. 3, pp. 641-651, 1977/05/26/ 1977.
- [105] S. Rumelt, *Glaucoma-basic and clinical aspects*. IntechOpen, 2013.
- [106] M. Jeelani, R. H. Taklikar, A. Taklikar, V. Itagi, and A. Bennal, "Variation of intraocular pressure with age and gender," *National Journal of Physiology, Pharmacy and Pharmacology*, vol. 4, no. 1, p. 57, 2014.
- [107] !!! INVALID CITATION !!! .
- [108] A. I. Dastiridou, H. S. Ginis, D. De Brouwere, M. K. Tsilimbaris, and I. G. Pallikaris, "Ocular rigidity, ocular pulse amplitude, and pulsatile ocular blood flow: the effect of intraocular pressure," *Investigative Ophthalmology & Visual Science*, vol. 50, no. 12, pp. 5718-5722, 2009.

- [109] A. Vogel, S. Beck, O. Schwenn, F. Grus, F. Krummenauer, and N. Pfeiffer, "Reproducibility of measurement of ocular pulse amplitude and intraocular pressure using Smartlens," (in ger), *Der Ophthalmologe : Zeitschrift der Deutschen Ophthalmologischen Gesellschaft*, vol. 98, no. 10, pp. 944-949, 2001/10// 2001.
- [110] A. J. Sit, "Continuous monitoring of intraocular pressure: rationale and progress toward a clinical device," *Journal of glaucoma*, vol. 18, no. 4, pp. 272-279, 2009.
- [111] J. H. K. Liu, A. J. Sit, and R. N. Weinreb, "Variation of 24-hour intraocular pressure in healthy individuals: right eye versus left eye," *Ophthalmology*, vol. 112, no. 10, pp. 1670-1675, 2005/10/01/ 2005.
- [112] W. Leydhecker, "The intraocular pressure: clinical aspects," *Annals of ophthalmology*, vol. 8, no. 4, pp. 389-92, 395-9, 1976.
- [113] H. Hashemi, A. H. Kashi, A. Fotouhi, and K. Mohammad, "Distribution of intraocular pressure in healthy Iranian individuals: the Tehran Eye Study," *British journal of ophthalmology*, vol. 89, no. 6, pp. 652-657, 2005.
- [114] J. S. Lee, S. H. Lee, B. S. Oum, J. S. Chung, B. M. Cho, and J. W. Hong, "Relationship between intraocular pressure and systemic health parameters in a Korean population," vol. 30, no. 4, pp. 237-241, 2002.
- [115] L. M. Weih, B. N. Mukesh, C. A. McCarty, and H. R. Taylor, "Association of demographic, familial, medical, and ocular factors With intraocular pressure," *Archives of Ophthalmology*, vol. 119, no. 6, pp. 875-880, 2001.
- [116] S.-Y. Wu and M. C. Leske, "Associations with intraocular pressure in the Barbados eye study," *Archives of ophthalmology*, vol. 115, no. 12, pp. 1572-1576, 1997.
- [117] M. C. Leske, A. M. S. Connell, S.-Y. Wu, L. Hyman, and A. P. Schachat, "Distribution of intraocular pressure: the Barbados eye study," *Archives of ophthalmology*, vol. 115, no. 8, pp. 1051-1057, 1997.
- [118] B. E. Klein, R. Klein, and K. L. Linton, "Intraocular pressure in an American community.

the Beaver Dam eye study," *Investigative Ophthalmology & Visual Science*, vol. 33, no. 7, pp. 2224-2228, 1992.

- [119] M. Romero-Jiménez, J. Santodomingo-Rubido, and J. S. Wolffsohn, "Keratoconus: a review," *Contact Lens and Anterior Eye*, vol. 33, no. 4, pp. 157-166, 2010/08/01/ 2010.
- [120] A. Gokul, D. V. Patel, and C. N. McGhee, "Dr John Nottingham's 1854 landmark treatise on conical cornea considered in the context of the current knowledge of keratoconus," *Cornea*, vol. 35, no. 5, pp. 673-678, 2016.
- [121] J. H. Krachmer, R. S. Feder, and M. W. Belin, "Keratoconus and related noninflammatory corneal thinning disorders," *Survey of Ophthalmology*, vol. 28, no. 4, pp. 293-322, 1984/01/01/ 1984.
- [122] R. H. Kennedy, W. M. Bourne, and J. A. Dyer, "A 48-year clinical and epidemiologic study of keratoconus," *American Journal of Ophthalmology*, vol. 101, no. 3, pp. 267-273, 1986/03/01/ 1986.
- [123] K. Zadnik, J. T. Barr, M. O. Gordon, and T. B. Edrington, "Biomicroscopic signs and disease severity in keratoconus. Collaborative Longitudinal Evaluation of Keratoconus (CLEK) Study Group," (in eng), *Cornea*, vol. 15, no. 2, pp. 139-146, 1996/03// 1996.
- [124] I. Chopra and A. K. Jain, "Between eye asymmetry in keratoconus in an Indian population," *Clinical and Experimental Optometry*, vol. 88, no. 3, pp. 146-152, 2005.
- [125] K. Zadnik, K. Steger-May, B. A. Fink, C. E. Joslin, J. J. Nichols *et al.*, "Between-eye asymmetry in keratoconus," *Cornea*, vol. 21, no. 7, pp. 671-679, 2002.
- [126] G. U. Auffarth, L. Wang, and H. E. Völcker, "Keratoconus evaluation using the Orbscan topography system 1," *Journal of Cataract & Refractive Surgery*, vol. 26, no. 2, pp. 222-228, 2000/02/01/ 2000.
- [127] K. H. Weed, C. N. J. McGhee, and C. J. MacEwen, "Atypical unilateral superior keratoconus in young males," *Contact Lens and Anterior Eye*, vol. 28, no. 4, pp. 177-

- 179, 2005/12/01/ 2005.
- [128] O. Prisant, J.-M. Legeais, and G. Renard, "Superior keratoconus," *Cornea*, vol. 16, no. 6, pp. 693-694, 1997.
- [129] X. Li, Y. S. Rabinowitz, K. Rasheed, and H. Yang, "Longitudinal study of the normal eyes in unilateral keratoconus patients," *Ophthalmology*, vol. 111, no. 3, pp. 440-446, 2004/03/01/ 2004.
- [130] B. A. Fink, H. Wagner, K. Steger-May, C. Rosenstiel, T. Roediger *et al.*, "Differences in keratoconus as a function of gender," *American Journal of Ophthalmology*, vol. 140, no. 3, pp. 459.e1-459.e12, 2005/09/01/ 2005.
- [131] H. Wagner, J. T. Barr, and K. Zadnik, "Collaborative longitudinal evaluation of keratoconus (CLEK) study: methods and findings to date," *Contact Lens and Anterior Eye*, vol. 30, no. 4, pp. 223-232, 2007/09/01/ 2007.
- [132] K. H. Weed and C. N. J. McGhee, "Referral patterns, treatment management and visual outcome in keratoconus," *Eye*, vol. 12, no. 4, pp. 663-668, 1998/07/01 1998.
- [133] H. Owens and G. Gamble, "A profile of keratoconus in New Zealand," *Cornea*, vol. 22, no. 2, pp. 122-125, 2003.
- [134] A. R. Pearson, B. Soneji, N. Sarvananthan, and J. H. Sandford-Smith, "Does ethnic origin influence the incidence or severity of keratoconus?," *Eye*, vol. 14, no. 4, pp. 625-628, 2000/07/01 2000.
- [135] T. Georgiou, C. L. Funnell, A. Cassels-Brown, and R. O'Conor, "Influence of ethnic origin on the incidence of keratoconus and associated atopic disease in Asians and white patients," *Eye*, vol. 18, no. 4, pp. 379-383, 2004/04/01 2004.
- [136] W. Rahman and S. Anwar, "An unusual case of keratoconus," *Journal of pediatric ophthalmology strabismus*, vol. 43, no. 6, 2006.
- [137] Y. S. Rabinowitz, "Keratoconus," *Survey of Ophthalmology*, vol. 42, no. 4, pp. 297-319, 1998/01/01/ 1998.

- [138] A. Gordon-Shaag, M. Millodot, E. Shneor, and Y. Liu, "The genetic and environmental factors for keratoconus," *BioMed research international*, vol. 2015, 2015.
- [139] M. Amsler, "Kératocône classique et kératocône fruste; arguments unitaires," *Ophthalmologica*, vol. 111, no. 2-3, pp. 96-101, 1946.
- [140] M. Amsler, "Le kératocône fruste au Javal," *Ophthalmologica*, vol. 96, no. 2, pp. 77-83, 1938.
- [141] A. Arntz, J. A. Durán, and J. I. Pijoán, "Subclinical keratoconus diagnosis by elevation topography," (in spa), *Archivos de la Sociedad Espanola de Oftalmologia*, vol. 78, no. 12, pp. 659-664, 2003/12// 2003.
- [142] A. Ertan and O. Muftuoglu, "Keratoconus clinical findings according to different age and gender groups," *Cornea*, vol. 27, no. 10, pp. 1109-1113, 2008.
- [143] C. Edmund, "Corneal topography and elasticity in normal and keratoconic eyes. A methodological study concerning the pathogenesis of keratoconus," (in eng), *Acta ophthalmologica. Supplement*, vol. 193, pp. 1-36, 1989 1989.
- [144] H. Serdarogullari, M. Tetikoglu, H. Karahan, F. Altin, and M. Elcioglu, "Prevalence of keratoconus and subclinical keratoconus in subjects with astigmatism using pentacam derived parameters," (in eng), *Journal of ophthalmic & vision research*, vol. 8, no. 3, pp. 213-219, 2013.
- [145] H. D. Perry, J. N. Buxton, and B. S. Fine, "Round and oval cones in keratoconus," *Ophthalmology*, vol. 87, no. 9, pp. 905-909, 1980/09/01/ 1980.
- [146] T. T. McMahon, L. Szczotka-Flynn, J. T. Barr, R. J. Anderson, M. E. Slaughter *et al.*, "A new method for grading the severity of keratoconus: the Keratoconus Severity Score (KSS)," *Cornea*, vol. 25, no. 7, pp. 794-800, 2006.
- [147] T. T. McMahon, J. B. Robin, K. M. Scarpulla, and J. L. Putz, "The spectrum of topography found in keratoconus," (in eng), *The CLAO journal : official publication of the Contact Lens Association of Ophthalmologists, Inc*, vol. 17, no. 3, pp. 198-204,

1991/07// 1991.

- [148] A. J. Kanellopoulos and G. Asimellis, "Revisiting keratoconus diagnosis and progression classification based on evaluation of corneal asymmetry indices, derived from Scheimpflug imaging in keratoconic and suspect cases," (in eng), *Clinical ophthalmology (Auckland, N.Z.)*, vol. 7, pp. 1539-1548, 2013.
- [149] J. B. Randleman, B. Russell, M. A. Ward, K. P. Thompson, and R. D. Stulting, "Risk factors and prognosis for corneal ectasia after LASIK," *Ophthalmology*, vol. 110, no. 2, pp. 267-275, 2003/02/01/ 2003.
- [150] P. S. Binder, R. L. Lindstrom, R. D. Stulting, E. Donnenfeld, H. Wu *et al.*, "Keratoconus and corneal ectasia after LASIK," *Journal of refractive surgery*, vol. 21, no. 6, pp. 749-752, 2005.
- [151] R. K. Chiang, A. J. Park, C. J. Rapuano, E. J. Cohen, and c. lens, "Bilateral keratoconus after LASIK in a keratoconus patient," *Eye*, vol. 29, no. 2, pp. 90-92, 2003.
- [152] A. M. Mahmoud, C. J. Roberts, R. G. Lembach, M. D. Twa, E. E. Herderick *et al.*, "CLMI: the cone location and magnitude index," (in eng), *Cornea*, vol. 27, no. 4, pp. 480-487, 2008.
- [153] Y. S. Rabinowitz and K. Rasheed, "KISA% index: a quantitative videokeratography algorithm embodying minimal topographic criteria for diagnosing keratoconus," *Journal of Cataract & Refractive Surgery*, vol. 25, no. 10, pp. 1327-1335, 1999/10/01/ 1999.
- [154] J. T. Schwiegerling, J. E. Greivenkamp, and J. M. Miller, "Keratoconus detection from videokeratoscopic height data," *Investigative Ophthalmology Visual Science*, vol. 37, no. 3, 1996.
- [155] N. Maeda, S. D. Klyce, and M. K. Smolek, "Neural network classification of corneal topography. Preliminary demonstration," *Investigative Ophthalmology & Visual Science*, vol. 36, no. 7, pp. 1327-1335, 1995.

- [156] M. K. Smolek and S. D. Klyce, "Current keratoconus detection methods compared with a neural network approach," *Investigative Ophthalmology & Visual Science*, vol. 38, no. 11, pp. 2290-2299, 1997.
- [157] N. Maeda, S. D. Klyce, M. K. Smolek, and H. W. Thompson, "Automated keratoconus screening with corneal topography analysis," *Investigative Ophthalmology & Visual Science*, vol. 35, no. 6, pp. 2749-2757, 1994.
- [158] Y. S. Rabinowitz and P. J. McDonnell, "Computer-assisted corneal topography in keratoconus," *Journal of Refractive Surgery*, vol. 5, no. 6, pp. 400-408, 1989.
- [159] Y. Li, D. M. Meisler, M. Tang, A. T. H. Lu, V. Thakrar *et al.*, "Keratoconus diagnosis with optical coherence tomography pachymetry mapping," *Ophthalmology*, vol. 115, no. 12, pp. 2159-2166, 2008/12/01/ 2008.
- [160] M. Gobbe and M. Guillon, "Corneal wavefront aberration measurements to detect keratoconus patients," *Contact Lens and Anterior Eye*, vol. 28, no. 2, pp. 57-66, 2005/06/01/ 2005.
- [161] S. Emre, S. Doganay, and S. Yologlu, "Evaluation of anterior segment parameters in keratoconic eyes measured with the Pentacam system," *Journal of Cataract & Refractive Surgery*, vol. 33, no. 10, pp. 1708-1712, 2007/10/01/ 2007.
- [162] U. de Sanctis, C. Loiacono, L. Richiardi, D. Turco, B. Mutani, and F. M. Grignolo, "Sensitivity and specificity of posterior corneal elevation measured by pentacam in discriminating keratoconus/subclinical keratoconus," *Ophthalmology*, vol. 115, no. 9, pp. 1534-1539, 2008/09/01/ 2008.
- [163] M. M. Sinjab, "Classifications and patterns of keratoconus and keratectasia," in *Quick Guide to the Management of Keratoconus*: Springer, 2012, pp. 13-58.
- [164] D. P. Piñero, J. L. Alió, A. Alesón, M. Escaf, and M. Miranda, "Pentacam posterior and anterior corneal aberrations in normal and keratoconic eyes," vol. 92, no. 3, pp. 297-303, 2009.

- [165] S. Sawaguchi, T. Fukuchi, H. Abe, T. Kaiya, J. Sugar, and B. Y. J. T. Yue, "Three-dimensional scanning electron microscopic study of keratoconus corneas," *Archives of Ophthalmology*, vol. 116, no. 1, pp. 62-68, 1998.
- [166] K. H. Weed, C. J. MacEwen, A. Cox, and C. N. J. McGhee, "Quantitative analysis of corneal microstructure in keratoconus utilising in vivo confocal microscopy," *Eye, Clinical Study* vol. 21, p. 614, 02/24/online 2006.
- [167] T. Sherwin and N. H. Brookes, "Morphological changes in keratoconus: pathology or pathogenesis," *Clinical & experimental ophthalmology*, vol. 32, no. 2, pp. 211-217, 2004.
- [168] J. Y. F. Ku, R. L. Niederer, D. V. Patel, T. Sherwin, and C. N. J. McGhee, "Laser scanning in vivo confocal analysis of keratocyte density in keratoconus," *Ophthalmology*, vol. 115, no. 5, pp. 845-850, 2008/05/01/ 2008.
- [169] E. S. Bennett and B. A. Weissman, *Clinical contact lens practice*. Lippincott Williams & Wilkins, 2005.
- [170] D. V. Patel, J. Y. F. Ku, R. Johnson, and C. N. J. McGhee, "Laser scanning in vivo confocal microscopy and quantitative aesthesiometry reveal decreased corneal innervation and sensation in keratoconus," *Eye, Clinical Study* vol. 23, p. 586, 03/14/online 2008.
- [171] A. J. Bron and Y. S. Rabinowitz, "Corneal dystrophies and keratoconus," (in eng), *Current opinion in ophthalmology*, vol. 7, no. 4, pp. 71-82, 1996/08// 1996.
- [172] M. L. FeRACO, J. Douglas, A. J. P. M. Phil, and M. L. FRACO, "Keratoconus: diagnosis and management," *Australian and New Zealand journal of ophthalmology*, vol. 17, no. 1, pp. 33-60, 1989.
- [173] H. R. Vellara and D. V. Patel, "Biomechanical properties of the keratoconic cornea: a review," *Clinical and Experimental Optometry*, vol. 98, no. 1, pp. 31-38, 2015.
- [174] J. S. Friedenwald, "Contribution to the theory and practice of tonometry*," *American*

Journal of Ophthalmology, vol. 20, no. 10, pp. 985-1024, 1937/10/01/ 1937.

- [175] J. Hartstein and B. Becker, "Research into the pathogenesis of keratoconus: a new syndrome: low ocular rigidity, contact lenses, and keratoconus," *Archives of Ophthalmology*, vol. 84, no. 6, pp. 728-729, 1970.
- [176] C. Edmund, "Corneal elasticity and ocular rigidity in normal and keratoconic eyes," *Acta Ophthalmologica*, vol. 66, no. 2, pp. 134-140, 1988.
- [177] R. N. Weinreb, T. Aung, and F. A. Medeiros, "The pathophysiology and treatment of glaucoma: a review," *Journal of the American Medical Association*, vol. 311, no. 18, pp. 1901-1911, 2014.
- [178] H. A. Quigley and A. T. Broman, "The number of people with glaucoma worldwide in 2010 and 2020," *British journal of ophthalmology*, vol. 90, no. 3, pp. 262-267, 2006.
- [179] A. P. Rotchford, J. F. Kirwan, M. A. Muller, G. J. Johnson, and P. Roux, "Temba glaucoma study: a population-based cross-sectional survey in urban South Africa," *Ophthalmology*, vol. 110, no. 2, pp. 376-382, 2003/02/01/ 2003.
- [180] M. T. Leite, L. M. Sakata, and F. A. Medeiros, "Managing glaucoma in developing countries " *Arquivos Brasileiros de Oftalmologia*, vol. 74, pp. 83-84, 2011.
- [181] M. F. Armaly, "Ocular pressure and visual fields: a ten-year follow-up study," *Archives of ophthalmology*, vol. 81, no. 1, pp. 25-40, 1969.
- [182] E. S. Perkins, "The Bedford glaucoma survey. I. Long-term follow-up of borderline cases," (in eng), *The British journal of ophthalmology*, vol. 57, no. 3, pp. 179-185, 1973.
- [183] R. A. Hitchings, "Low tension glaucoma--its place in modern glaucoma practice," (in eng), *The British journal of ophthalmology*, vol. 76, no. 8, pp. 494-496, 1992.
- [184] Y. Kitazawa, S. Shirato, and T. Yamamoto, "Optic disc hemorrhage in low-tension glaucoma," *Ophthalmology*, vol. 93, no. 6, pp. 853-857, 1986/06/01/ 1986.

- [185] J. Gloster, "Incidence of optic disc haemorrhages in chronic simple glaucoma and ocular hypertension," *British Journal of Ophthalmology*, vol. 65, no. 7, pp. 452-456, 1981.
- [186] H. A. Quigley, E. M. Addicks, W. R. Green, and A. E. Maumenee, "Optic nerve damage in human glaucoma: II. The site of injury and susceptibility to damage," *Archives of ophthalmology*, vol. 99, no. 4, pp. 635-649, 1981.
- [187] A. Sommer, "Intraocular pressure and glaucoma," *American Journal of Ophthalmology*, vol. 107, no. 2, pp. 186-188, 1989.
- [188] H. H. Markiewitz, "The so-called imbert-fick law," *JAMA Ophthalmology*, vol. 64, no. 1, pp. 159-159, 1960.
- [189] H. H. Mark, "Armand Imbert, Adolf Fick, and their tonometry law," *Eye*, Review vol. 26, p. 13, 10/21/online 2011.
- [190] J. Gloster and E. S. Perkins, "The validity of the Imbert-Fick law as applied to applanation tonometry," *Experimental Eye Research*, vol. 2, no. 3, pp. 274-283, 1963/07/01/ 1963.
- [191] A. A. Patwardhan, M. Khan, S. P. Mollan, and P. J. B. O. Haigh, "The importance of central corneal thickness measurements and decision making in general ophthalmology clinics: a masked observational study," journal article vol. 8, no. 1, p. 1, January 20 2008.
- [192] M. M. Whitacre, R. A. Stein, and K. Hassanein, "The effect of corneal thickness on applanation tonometry," *American Journal of Ophthalmology*, vol. 115, no. 5, pp. 592-596, 1993/05/01/ 1993.
- [193] M. A. Shah, K. B. Saleem, and T. Mehmood, "Intraocular pressure measurement: Goldmann applanation tonometer vs non contact airpuff tonometer," *Journal of Ayub Medical College Abbottabad*, vol. 24, no. 3-4, pp. 21-24, 2012.
- [194] R. L. Stamper, "A history of intraocular pressure and its measurement," *Optometry*

Vision Science, vol. 88, no. 1, pp. E16-E28, 2011.

- [195] C. J. Roberts and J. Liu, *Corneal biomechanics: from theory to practice*. Kugler Publications, 2017.
- [196] D. A. Luce, "Non-contact tonometry method," Washington, DC, 2002.
- [197] D. A. Luce, "Determining in vivo biomechanical properties of the cornea with an ocular response analyzer," *Journal of Cataract & Refractive Surgery*, vol. 31, no. 1, pp. 156-162, 2005/01/01/ 2005.
- [198] D. Luce, "Air-jet temporal and spatial pressure properties of the reichert ocular response analyzer (ORA)," *Investigative ophthalmology & visual science*, vol. 46, no. 13, pp. 5009-5009, 2005.
- [199] H. Kasprzak, E. Mazur, and M. Widlicka, "Measurement and analysis of the air pressure curve on the rigid lenses by use of ocular response analyzer," *Acta of bioengineering biomechanics* vol. 16, no. 4, 2014.
- [200] G. Grabner, R. Eilmsteiner, C. Steindl, J. Ruckhofer, R. Mattioli, and W. Husinsky, "Dynamic corneal imaging," *Journal of Cataract & Refractive Surgery*, vol. 31, no. 1, pp. 163-174, 2005/01/01/ 2005.
- [201] C. J. Roberts, A. M. Mahmoud, J. P. Bons, A. Hossain, A. Elsheikh *et al.*, "Introduction of two novel stiffness parameters and interpretation of air Puff-Induced biomechanical deformation parameters with a dynamic scheimpflug analyzer," *Journal of Refractive Surgery*, vol. 33, no. 4, pp. 266-273, 2017.
- [202] S. Kling, N. Bekesi, C. Dorronsoro, D. Pascual, and S. Marcos, "Corneal viscoelastic properties from finite-element analysis of in vivo air-puff deformation," *PloS one*, vol. 9, no. 8, p. e104904, 2014.
- [203] S. Kling and S. Marcos, "Contributing factors to corneal deformation in air puff measurements," *Investigative*

Ophthalmology & Visual Science, vol. 54, no. 7, pp. 5078-5085, 2013.

- [204] M. C. Leske, A. Heijl, M. Hussein, B. Bengtsson, L. Hyman *et al.*, "Factors for Glaucoma Progression and the Effect of Treatment: The Early Manifest Glaucoma Trial," *JAMA Ophthalmology*, vol. 121, no. 1, pp. 48-56, 2003.
- [205] A. Pelit, R. Altan-Yaycioglu, A. Pelit, and Y. A. Akova, "Effect of corneal thickness on intraocular pressure measurements with the Pascal dynamic contour, Canon TX-10 non-contact and Goldmann applanation tonometers in healthy subjects," *Clinical and Experimental Optometry*, vol. 92, no. 1, pp. 14-18, 2009.
- [206] Y. C. Ko, C. J. I. Liu, and W. M. Hsu, "Varying effects of corneal thickness on intraocular pressure measurements with different tonometers," *Eye*, vol. 19, no. 3, pp. 327-332, 2005/03/01 2005.
- [207] H. H. Mark, "Corneal curvature in applanation tonometry," *American Journal of Ophthalmology*, vol. 76, pp. 223-224, 1973.
- [208] K. E. Hamilton, D. C. Pye, S. Aggarwala, S. Evian, J. Khosla, and R. Perera, "Diurnal variation of central corneal thickness and Goldmann applanation tonometry estimates of intraocular pressure," *Journal of glaucoma*, vol. 16, no. 1, pp. 29-35, 2007.
- [209] P. A. Tonnu, T. Ho, T. Newson, A. El Sheikh, K. Sharma *et al.*, "The influence of central corneal thickness and age on intraocular pressure measured by pneumotonometry, non-contact tonometry, the Tono-Pen XL, and Goldmann applanation tonometry," *British Journal of Ophthalmology*, vol. 89, no. 7, pp. 851-854, 2005.
- [210] A. Kotecha, E. T. White, J. M. Shewry, and D. F. Garway-Heath, "The relative effects of corneal thickness and age on Goldmann applanation tonometry and dynamic contour tonometry," *British Journal of Ophthalmology*, vol. 89, no. 12, pp. 1572-1575, 2005.
- [211] N. EHLERS, T. BRAMSEN, and S. SPERLING, "Applanation tonometry and central corneal thickness," *Acta ophthalmologica*, vol. 53, no. 1, pp. 34-43, 1975.

- [212] B. Ceska, K. Ferrova, A. Filous, K. Oskorypová, P. Lezatková, and P. Sedlácková, "Comparative study of intraocular pressure measurements by Goldmann applanation tonometer, noncontact tonometer and TonoPen," *Ceska a slovenska oftalmologie: casopis Ceske oftalmologicke spolecnosti a Slovenske oftalmologicke spolecnosti*, vol. 68, no. 1, pp. 43-46, 2012.
- [213] C. Y. Shih, J. S. G. Zivin, S. L. Trokel, and J. C. Tsai, "Clinical Significance of Central Corneal Thickness in the Management of Glaucoma," *Archives of ophthalmology*, vol. 122, no. 9, pp. 1270-1275, 2004.
- [214] E. M. Kirstein and A. Hüsler, "Evaluation of the Orssengo-Pye IOP corrective algorithm in LASIK patients with thick corneas," *Optometry-Journal of the American Optometric Association*, vol. 76, no. 9, pp. 536-543, 2005.
- [215] A. Elsheikh, D. Wang, P. Rama, M. Campanelli, and D. Garway-Heath, "Experimental assessment of human corneal hysteresis," *Current eye research*, vol. 33, no. 3, pp. 205-213, 2008.
- [216] A. Elsheikh, D. Alhasso, P. Gunvant, and D. Garway-Heath, "Multiparameter correction equation for Goldmann applanation tonometry," *Optometry and Vision Science*, vol. 88, no. 1, pp. E102-E112, 2011.
- [217] S. Z. Amin, L. Smith, P. J. Luthert, M. E. Cheetham, and R. J. Buckley, "Minimising the risk of prion transmission by contact tonometry," *British journal of ophthalmology*, vol. 87, no. 11, pp. 1360-1362, 2003.
- [218] L. M. Abraham, N. C. R. Epasinghe, D. Selva, and R. Casson, "Comparison of the ICare® rebound tonometer with the Goldmann applanation tonometer by experienced and inexperienced tonometrists," *Eye*, vol. 22, no. 4, p. 503, 2008.
- [219] S. Shah, A. Chatterjee, M. Mathai, S. P. Kelly, J. Kwartz *et al.*, "Relationship between corneal thickness and measured intraocular pressure in a general ophthalmology clinic," *Ophthalmology*, vol. 106, no. 11, pp. 2154-2160, 1999.
- [220] R. Stodtmeister, "Applanation tonometry and correction according to corneal

thickness," *Acta Ophthalmologica Scandinavica*, vol. 76, no. 3, pp. 319-324, 1998/06/01 1998.

- [221] A. K. C. Lam, R. Wu, Z. Wang, V. Woo, E. Chan *et al.*, "Effect of laser in situ keratomileusis on rebound tonometry and Goldmann applanation tonometry," *Journal of Cataract & Refractive Surgery*, vol. 36, no. 4, pp. 631-636, 2010.
- [222] D. Zadok, D. B. Tran, M. Twa, M. Carpenter, and D. J. Schanzlin, "Pneumotonometry versus Goldmann tonometry after laser in situ keratomileusis for myopia1," *Journal of Cataract & Refractive Surgery*, vol. 25, no. 10, pp. 1344-1348, 1999.
- [223] D. S. Siganos, G. I. Papastergiou, and C. Moedas, "Assessment of the Pascal dynamic contour tonometer in monitoring intraocular pressure in unoperated eyes and eyes after LASIK," *Journal of Cataract & Refractive Surgery*, vol. 30, no. 4, pp. 746-751, 2004.
- [224] J. S. Pepose, S. K. Feigenbaum, M. A. Qazi, J. P. Sanderson, and C. J. Roberts, "Changes in corneal biomechanics and intraocular pressure following LASIK using static, dynamic, and noncontact tonometry," *American journal of ophthalmology*, vol. 143, no. 1, pp. 39-47. e1, 2007.
- [225] R. Sinha, H. Shekhar, S. Tinwala, A. Gangar, and J. S. Titiyal, "Late post-traumatic flap dislocation and macrostriae after laser in situ keratomileusis," *Oman journal of ophthalmology*, vol. 7, no. 1, p. 25, 2014.
- [226] W. E. Philipp, L. Speicher, and W. Göttinger, "Histological and immunohistochemical findings after laser in situ keratomileusis in human corneas1," *Journal of Cataract & Refractive Surgery*, vol. 29, no. 4, pp. 808-820, 2003.
- [227] S. Sudesh, M. J. Moseley, and J. R. Thompson, "Accuracy of Goldmann tonometry in clinical practice," *Acta ophthalmologica*, vol. 71, no. 2, pp. 185-188, 1993.
- [228] M. Nakamura, U. Darhad, Y. Tatsumi, M. Fujioka, A. Kusuhara *et al.*, "Agreement of rebound tonometer in measuring intraocular pressure with three types of applanation tonometers," *American journal of ophthalmology*, vol. 142, no. 2, pp.

332-334, 2006.

- [229] P. Tonnu, T. Ho, K. Sharma, E. White, C. Bunce, and D. Garway-Heath, "A comparison of four methods of tonometry: method agreement and interobserver variability," *British journal of ophthalmology*, vol. 89, no. 7, pp. 847-850, 2005.
- [230] M. A. El Danasoury, A. El Maghraby, and S. J. Coopender, "Change in intraocular pressure in myopic eyes measured with contact and non-contact tonometers after laser in situ keratomileusis," *Journal of Refractive Surgery*, vol. 17, no. 2, pp. 97-99, 2001.
- [231] T. Eysteinnsson, F. Jonasson, H. Sasaki, A. Arnarsson, T. Sverrisson *et al.*, "Central corneal thickness, radius of the corneal curvature and intraocular pressure in normal subjects using non-contact techniques: Reykjavik Eye Study," *Acta Ophthalmologica Scandinavica*, vol. 80, no. 1, pp. 11-15, 2002.
- [232] F. J. Bao, B. Geraghty, Q. M. Wang, and A. Elsheikh, "Consideration of corneal biomechanics in the diagnosis and management of keratoconus: is it important?," *Eye and Vision*, vol. 3, no. 1, p. 18, 2016.
- [233] A. Elsheikh, C. Whitford, R. Hamarashid, W. Kassem, A. Joda, and P. Büchler, "Stress free configuration of the human eye," *Medical engineering & physics*, vol. 35, no. 2, pp. 211-216, 2013.
- [234] M. Guillon, D. P. Lydon, and C. Wilson, "Corneal topography: a clinical model," *Ophthalmic and Physiological Optics*, vol. 6, no. 1, pp. 47-56, 1986.
- [235] L. R. Baker, "Aberrations of Optical Systems," *Journal of Modern Optics*, vol. 34, no. 1, pp. 4-4, 1987.
- [236] M. S. De La Maza, J. Tauber, and C. S. Foster, *The sclera*. Springer Science & Business Media, 2012.
- [237] F. Rüfer, A. Schröder, and C. Erb, "White-to-white corneal diameter: normal values in healthy humans obtained with the Orbscan II topography system," *Cornea*, vol. 24,

no. 3, pp. 259-261, 2005.

- [238] C. Khng and R. H. Osher, "Evaluation of the relationship between corneal diameter and lens diameter," *Journal of Cataract & Refractive Surgery*, vol. 34, no. 3, pp. 475-479, 2008.
- [239] S. Al-Ageel and A. M. Al-Muammar, "Comparison of central corneal thickness measurements by Pentacam, noncontact specular microscope, and ultrasound pachymetry in normal and post-LASIK eyes," *Saudi journal of ophthalmology : official journal of the Saudi Ophthalmological Society*, vol. 23, no. 3-4, pp. 181-187, 2009.
- [240] D. Gatinel, T. Hoang-Xuan, and D. T. Azar, "Determination of corneal asphericity after myopia surgery with the excimer laser: a mathematical model," *Investigative ophthalmology & visual science*, vol. 42, no. 8, pp. 1736-1742, 2001.
- [241] A. Villamarin, S. Roy, R. Hasballa, O. Vardoulis, P. Reymond, and N. Stergiopoulos, "3D simulation of the aqueous flow in the human eye," *Medical engineering & physics*, vol. 34, no. 10, pp. 1462-1470, 2012.
- [242] A. Elsheikh, D. Alhasso, A. Kotecha, and D. Garway-Heath, "Assessment of the ocular response analyzer as a tool for intraocular pressure measurement," *Journal of biomechanical engineering*, vol. 131, no. 8, p. 081010, 2009.
- [243] O. Maklad, V. Theofilis, and A. Elsheikh, "Fluid structure interaction (FSI) simulation of the human eye under the air puff tonometry using Computational Fluid Dynamics (CFD)," 2018.
- [244] K.-J. Chen, A. Joda, R. Vinciguerra, A. Eliasy, S. M. M. Sefat *et al.*, "Clinical evaluation of a new correction algorithm for dynamic Scheimpflug analyzer tonometry before and after laser in situ keratomileusis and small-incision lenticule extraction," *Journal of Cataract & Refractive Surgery*, 2018.
- [245] M. Shimmyo, A. J. Ross, A. Moy, and R. Mostafavi, "Intraocular pressure, Goldmann applanation tension, corneal thickness, and corneal curvature in Caucasians, Asians, Hispanics, and African Americans," *American journal of ophthalmology*, vol. 136, no.

4, pp. 603-613, 2003.

- [246] R. Shah, S. Shah, and S. Sengupta, "Results of small incision lenticule extraction: all-in-one femtosecond laser refractive surgery," *Journal of Cataract & Refractive Surgery*, vol. 37, no. 1, pp. 127-137, 2011.
- [247] S. M. M. Sefat, R. Wiltfang, M. Bechmann, W. J. Mayer, A. Kampik, and D. Kook, "Evaluation of changes in human corneas after femtosecond laser-assisted LASIK and small-incision lenticule extraction (SMILE) using non-contact tonometry and ultra-high-speed camera (Corvis ST)," *Current eye research*, vol. 41, no. 7, pp. 917-922, 2016.
- [248] H. Altinkaynak, C. Kocasarac, H. Dundar, N. Sayin, N. Kara *et al.*, "Which tonometry in eyes with keratoconus?," *Eye*, vol. 30, no. 3, p. 431, 2016.
- [249] Y. Goldich, Y. Barkana, I. Avni, and D. Zadok, "Goldmann applanation tonometry versus ocular response analyzer for intraocular pressure measurements in keratoconic eyes," *Cornea*, vol. 29, no. 9, pp. 1011-1015, 2010.
- [250] A. Bayer, A. Sahin, V. Hürmeriç, and G. Özge, "Intraocular pressure values obtained by ocular response analyzer, dynamic contour tonometry, and Goldmann tonometry in keratocornic corneas," *Journal of glaucoma*, vol. 19, no. 8, pp. 540-545, 2010.
- [251] J. D. Unterlauff, N. Schädle, K. Kasper, T. Klink, and G. Geerling, "Comparison of dynamic contour tonometry and Goldmann applanation tonometry in keratoconus," *Cornea*, vol. 30, no. 10, pp. 1078-1082, 2011.
- [252] O. F. Villavicencio, F. Gilani, M. A. Henriquez, L. Izquierdo Jr Jr, R. R. Ambrosio Jr, and M. W. Belin, "Independent population validation of the Belin/Ambrosio enhanced ectasia display: implications for keratoconus studies and screening," *International Journal of Keratoconus and Ectatic Corneal Diseases*, vol. 3, no. 1, p. 1, 2014.
- [253] E. Rohtchina, P. Mitchell, and J. J. Wang, "Relationship between age and intraocular pressure: the Blue Mountains Eye Study," *Clinical & experimental ophthalmology*, vol. 30, no. 3, pp. 173-175, 2002.

- [254] H. Nomura, F. Ando, N. Niino, H. Shimokata, and Y. Miyake, "The relationship between age and intraocular pressure in a Japanese population: the influence of central corneal thickness," *Current eye research*, vol. 24, no. 2, pp. 81-85, 2002.
- [255] S. Goebels, T. Eppig, S. Wagenpfeil, A. Cayless, B. Seitz, and A. Langenbacher, "Staging of keratoconus indices regarding tomography, topography, and biomechanical measurements," *American journal of ophthalmology*, vol. 159, no. 4, pp. 733-738. e3, 2015.
- [256] J. Kennedy and R. Eberhart, "Particle swarm optimization," in *Neural Networks, 1995. Proceedings., IEEE International Conference on*, 1995, vol. 4, pp. 1942-1948: IEEE.
- [257] G. Nemeth, Z. Hassan, A. Csutak, E. Szalai, A. Berta, and L. Modis Jr, "Repeatability of ocular biomechanical data measurements with a Scheimpflug-based noncontact device on normal corneas," *Journal of Refractive Surgery*, vol. 29, no. 8, pp. 558-563, 2013.
- [258] K. D. Solomon, L. E. F. de Castro, H. P. Sandoval, J. M. Biber, B. Groat *et al.*, "LASIK world literature review: quality of life and patient satisfaction," *Ophthalmology*, vol. 116, no. 4, pp. 691-701, 2009.
- [259] K. E. Brown and N. G. Congdon, "Corneal structure and biomechanics: impact on the diagnosis and management of glaucoma," *Current opinion in ophthalmology*, vol. 17, no. 4, pp. 338-343, 2006.
- [260] A. Eliasy, K.-J. Chen, R. Vinciguerra, O. Maklad, P. Vinciguerra *et al.*, "Ex-vivo experimental validation of biomechanically-corrected intraocular pressure measurements on human eyes using the CorVis ST," *Experimental eye research*, 2018.
- [261] F. J. Bao, M. L. Deng, Q. M. Wang, J. H. Huang, J. Yang *et al.*, "Evaluation of the relationship of corneal biomechanical metrics with physical intraocular pressure and central corneal thickness in ex vivo rabbit eye globes," *Experimental eye research*, vol. 137, pp. 11-17, 2015.
- [262] T. H. Kwon, J. Ghaboussi, D. A. Pecknold, and Y. M. A. Hashash, "Effect of cornea

material stiffness on measured intraocular pressure," *Journal of biomechanics*, vol. 41, no. 8, pp. 1707-1713, 2008.

- [263] P. G. Davey, A. Elsheikh, and D. F. Garway-Heath, "Clinical evaluation of multiparameter correction equations for Goldmann applanation tonometry," *Eye*, vol. 27, no. 5, p. 621, 2013.
- [264] S. McCafferty, J. Levine, J. Schwiegerling, and E. T. Enikov, "Goldmann applanation tonometry error relative to true intracameral intraocular pressure in vitro and in vivo," *BMC ophthalmology*, vol. 17, no. 1, p. 215, 2017.
- [265] N. Ehlers, F. K. Hansen, and H. Aasved, "Biometric correlations of corneal thickness," *Acta ophthalmologica*, vol. 53, no. 4, pp. 652-659, 1975.
- [266] L. W. Herndon, S. A. Choudhri, T. Cox, K. F. Damji, M. B. Shields, and R. R. Allingham, "Central corneal thickness in normal, glaucomatous, and ocular hypertensive eyes," *Archives of Ophthalmology*, vol. 115, no. 9, pp. 1137-1141, 1997.
- [267] H. E. Kanngiesser, C. Kniestedt, and Y. C. Robert, "Dynamic contour tonometry: presentation of a new tonometer," *Journal of glaucoma*, vol. 14, no. 5, pp. 344-350, 2005.
- [268] R. Montard, R. Kopito, O. Touzeau, C. Allouch, I. Letaief *et al.*, "Ocular Response Analyzer: Étude de fiabilité et de corrélation sur des yeux normaux," *Journal Français d'Ophthalmologie*, vol. 30, no. 10, pp. 978-984, 2007.
- [269] J. Hong, J. Xu, A. Wei, S. X. Deng, X. Cui *et al.*, "A new tonometer—the Corvis ST tonometer: clinical comparison with noncontact and Goldmann applanation tonometers," *Investigative ophthalmology & visual science*, vol. 54, no. 1, pp. 659-665, 2013.
- [270] R. Vinciguerra, A. Elsheikh, C. J. Roberts, D. S. Y. Kang, B. T. Lopes *et al.*, "Influence of pachymetry and intraocular pressure on dynamic corneal response parameters in healthy patients," *Journal of Refractive Surgery*, vol. 32, no. 8, pp. 550-561, 2016.

- [271] I. Sánchez, R. R. Martin, and F. Ussa, "Measurement of Intraocular Pressure in a Porcine Ex Vivo Model Eye," *Ophthalmology Research: An International Journal*, vol. 2, pp. 55-64, 2014.
- [272] L. K. K. Leung, M. W. L. Ko, and D. C. C. Lam, "Individual-specific tonometry on porcine eyes," *Medical Engineering & Physics*, vol. 36, no. 1, pp. 96-101, 2014.
- [273] C. L. Passaglia, X. Guo, J. Chen, and J. B. Troy, "Tono-Pen XL® calibration curves for cats, cows and sheep," *Veterinary Ophthalmology*, vol. 7, no. 4, pp. 261-264, 2004/07/01 2004.
- [274] C. L. Passaglia, X. Guo, J. Chen, and J. B. Troy, "Tono-Pen XL® calibration curves for cats, cows and sheep," *Veterinary Ophthalmology*, vol. 7, no. 4, pp. 261-264, 2004.
- [275] J. Stoiber, V. Fernandez, P. D. Lamar, W. Hitzl, F. Fantès, and J. M. Parel, "Ex vivo Evaluation of Tono-Pen and Pneumotonometry in Cat Eyes," *Ophthalmic Research*, vol. 38, no. 1, pp. 13-18, 2006.
- [276] O. R. Ioseliani, *New Developments in Eye Research: Nova Biomedical Books*. Nova Publishers, 2006.
- [277] I. Riva, L. Quaranta, A. Russo, A. Katsanos, E. Rulli, and I. Floriani, "Dynamic contour tonometry and Goldmann applanation tonometry: correlation with intracameral assessment of intraocular pressure," *European journal of ophthalmology*, vol. 22, no. 1, pp. 55-62, 2012.
- [278] C. Kniestedt, M. Nee, and R. L. Stamper, "Accuracy of dynamic contour tonometry compared with applanation tonometry in human cadaver eyes of different hydration states," *Graefe's Archive for Clinical and Experimental Ophthalmology*, vol. 243, no. 4, pp. 359-366, 2005.
- [279] G. Simon, R. H. Small, Q. Ren, and J. M. Parel, "Effect of corneal hydration on Goldmann applanation tonometry and corneal topography," *Journal of Refractive Surgery*, vol. 9, no. 2, pp. 110-117, 1993.

- [280] R. A. Moses, "The Goldmann applanation tonometer," *American Journal of Ophthalmology*, vol. 46, no. 6, pp. 865-869, 1958.
- [281] J. D. Brandt, "Central corneal thickness - tonometry artifact, or something more?," *Ophthalmology*, vol. 114, no. 11, pp. 1963-1964, 2007.
- [282] P. Gunvant, M. Baskaran, L. Vijaya, I. Joseph, R. Watkins *et al.*, "Effect of corneal parameters on measurements using the pulsatile ocular blood flow tonograph and Goldmann applanation tonometer," *British journal of ophthalmology*, vol. 88, no. 4, pp. 518-522, 2004.
- [283] D. H. Chang and R. D. Stulting, "Change in intraocular pressure measurements after LASIK: the effect of the refractive correction and the lamellar flap," *Ophthalmology*, vol. 112, no. 6, pp. 1009-1016, 2005.
- [284] A. Elsheikh, A. Joda, R. Vinciguerra, P. Vinciguerra, D. Kook *et al.*, "Clinical evaluation of correction algorithm for Corvis ST tonometry," *Investigative Ophthalmology & Visual Science*, vol. 56, no. 7, pp. 101-101, 2015.
- [285] E. Chihara, "Assessment of true intraocular pressure: the gap between theory and practical data," *Survey of ophthalmology*, vol. 53, no. 3, pp. 203-218, 2008.
- [286] A. Elsheikh, P. Gunvant, S. W. Jones, D. Pye, and D. Garway-Heath, "Correction factors for Goldmann tonometry," *Journal of glaucoma*, vol. 22, no. 2, pp. 156-163, 2013.
- [287] P. Ceruti, R. Morbio, M. Marraffa, and G. Marchini, "Comparison of Goldmann applanation tonometry and dynamic contour tonometry in healthy and glaucomatous eyes," *Eye*, vol. 23, no. 2, p. 262, 2009.
- [288] M. L. Salvetat, M. Zeppieri, C. Tosoni, and P. Brusini, "Comparisons between Pascal dynamic contour tonometry, the TonoPen, and Goldmann applanation tonometry in patients with glaucoma," *Acta Ophthalmologica Scandinavica*, vol. 85, no. 3, pp. 272-279, 2007.
- [289] J. L. Alió, O. Muftuoglu, D. Ortiz, J. J. Pérez-Santonja, A. Artola *et al.*, "Ten-year follow-

- up of laser in situ keratomileusis for myopia of up to– 10 diopters," *American journal of ophthalmology*, vol. 145, no. 1, pp. 46-54. e1, 2008.
- [290] S. G. Slade, "The use of the femtosecond laser in the customization of corneal flaps in laser in situ keratomileusis," *Current opinion in ophthalmology*, vol. 18, no. 4, pp. 314-317, 2007.
- [291] M. A. Qazi, J. P. Sanderson, A. M. Mahmoud, E. Y. Yoon, C. J. Roberts, and J. S. Pepose, "Postoperative changes in intraocular pressure and corneal biomechanical metrics: laser in situ keratomileusis versus laser-assisted subepithelial keratectomy," *Journal of Cataract & Refractive Surgery*, vol. 35, no. 10, pp. 1774-1788, 2009.
- [292] J. Shin, T. W. Kim, S. J. Park, M. Yoon, and J. W. Lee, "Changes in biomechanical properties of the cornea and intraocular pressure after myopic laser in situ keratomileusis using a femtosecond laser for flap creation determined using ocular response analyzer and Goldmann applanation tonometry," *Journal of glaucoma*, vol. 24, no. 3, pp. 195-201, 2015.
- [293] L. Reznicek, D. Muth, A. Kampik, A. S. Neubauer, and C. Hirneiss, "Evaluation of a novel Scheimpflug-based non-contact tonometer in healthy subjects and patients with ocular hypertension and glaucoma," *British Journal of Ophthalmology*, pp. bjophthalmol-2013-303400, 2013.
- [294] F. J. Bao, Z. X. Huang, J. H. Huang, J. J. Wang, M. L. Deng *et al.*, "Clinical Evaluation of Methods to Correct Intraocular Pressure Measurements by the Goldmann Applanation Tonometer, Ocular Response Analyzer, and Corvis ST Tonometer for the Effects of Corneal Stiffness Parameters," *Journal of Glaucoma*, vol. 25, no. 6, pp. 510-519, 2016.
- [295] W. J. Dupps and C. Roberts, "Effect of acute biomechanical changes on corneal curvature after photokeratectomy," *Journal of Refractive Surgery*, vol. 17, no. 6, pp. 658-669, 2001.
- [296] J. B. Randleman, D. G. Dawson, H. E. Grossniklaus, B. E. McCarey, and H. F.

Edelhauser, "Depth-dependent cohesive tensile strength in human donor corneas: implications for refractive surgery," *Journal of refractive surgery*, vol. 24, no. 1, pp. S85-S89, 2008.

- [297] M. K. Smolek, "Interlamellar cohesive strength in the vertical meridian of human eye bank corneas," *Investigative ophthalmology & visual science*, vol. 34, no. 10, pp. 2962-2969, 1993.
- [298] D. Z. Reinstein, T. J. Archer, and J. B. Randleman, "Mathematical model to compare the relative tensile strength of the cornea after PRK, LASIK, and small incision lenticule extraction," *Journal of Refractive Surgery*, vol. 29, no. 7, pp. 454-460, 2013.
- [299] Z. X. Dong, X. T. Zhou, J. H. Wu, Z. H. Zhang, T. Li *et al.*, "Small incision lenticule extraction (SMILE) and femtosecond laser LASIK: comparison of corneal wound healing and inflammation," *British Journal of Ophthalmology*, vol. 98, no. 2, pp. 263-269, 2014.
- [300] V. M.-B. Tham and R. K. Maloney, "Microkeratome complications of laser in situ keratomileusis," *Ophthalmology*, vol. 107, no. 5, pp. 920-924, 2000.
- [301] T. M. AlMubrad and K. C. Ogbuehi, "The effect of repeated applanation on subsequent IOP measurements," *Clinical and Experimental Optometry*, vol. 91, no. 6, pp. 524-529, 2008.
- [302] S. Senthil, N. S. Choudhari, P. K. Vaddavalli, S. Murthy, J. Reddy, and C. S. Garudadri, "Etiology and management of raised intraocular pressure following posterior chamber phakic intraocular lens implantation in myopic eyes," *PloS one*, vol. 11, no. 11, p. e0165469, 2016.
- [303] R. Vinciguerra, M. R. Romano, F. I. Camesasca, C. Azzolini, S. Trazza *et al.*, "Corneal cross-linking as a treatment for keratoconus: four-year morphologic and clinical outcomes with respect to patient age," *Ophthalmology*, vol. 120, no. 5, pp. 908-916, 2013.
- [304] Z. Ozbek, E. J. Cohen, K. M. Hammersmith, and C. J. Rapuano, "Dynamic contour

- tonometry: a new way to assess intraocular pressure in ectatic corneas," *Cornea*, vol. 25, no. 8, pp. 890-894, 2006.
- [305] F. Özcura, N. Yıldırım, E. Tambova, and A. Şahin, "Evaluation of Goldmann applanation tonometry, rebound tonometry and dynamic contour tonometry in keratoconus," *Journal of optometry*, vol. 10, no. 2, pp. 117-122, 2017.
- [306] M. G. Gkika, G. Labiris, and V. P. Kozobolis, "Tonometry in keratoconic eyes before and after riboflavin/UVA corneal collagen crosslinking using three different tonometers," *European journal of ophthalmology*, vol. 22, no. 2, pp. 142-152, 2012.
- [307] P. G. Firat, G. Orman, S. Doganay, and S. Demirel, "Influence of corneal parameters in keratoconus on IOP readings obtained with different tonometers," *Clinical and Experimental Optometry*, vol. 96, no. 2, pp. 233-237, 2013.
- [308] J. O. Hjortdal, "Extensibility of the normo-hydrated human cornea," *Acta Ophthalmologica Scandinavica*, vol. 73, no. 1, pp. 12-17, 1995.
- [309] M. Ahearne, Y. Yang, K. Y. Then, and K.-K. Liu, "An indentation technique to characterize the mechanical and viscoelastic properties of human and porcine corneas," *Annals of biomedical engineering*, vol. 35, no. 9, pp. 1608-1616, 2007.
- [310] E. Lanchares, B. Calvo, J. A. Cristóbal, and M. Doblaré, "Finite element simulation of arcuates for astigmatism correction," *Journal of biomechanics*, vol. 41, no. 4, pp. 797-805, 2008.
- [311] A. Gefen, R. Shalom, D. Elad, and Y. Mandel, "Biomechanical analysis of the keratoconic cornea," *Journal of the mechanical behavior of biomedical materials*, vol. 2, no. 3, pp. 224-236, 2009.
- [312] A. Pandolfi, G. Fotia, and F. Manganiello, "Finite element simulations of laser refractive corneal surgery," *Engineering with computers*, vol. 25, no. 1, p. 15, 2009.
- [313] A. S. Roy, K. M. Rocha, J. B. Randleman, R. D. Stulting, and W. J. Dupps Jr, "Inverse computational analysis of in vivo corneal elastic modulus change after collagen

crosslinking for keratoconus," *Experimental eye research*, vol. 113, pp. 92-104, 2013.

- [314] A. S. Roy, M. Kurian, H. Matalia, and R. Shetty, "Air-puff associated quantification of non-linear biomechanical properties of the human cornea in vivo," *Journal of the mechanical behavior of biomedical materials*, vol. 48, pp. 173-182, 2015.
- [315] C. Whitford, A. Joda, S. Jones, F. Bao, P. Rama, and A. Elsheikh, "Ex vivo testing of intact eye globes under inflation conditions to determine regional variation of mechanical stiffness," *Eye and Vision*, vol. 3, no. 1, p. 21, 2016.
- [316] C. Edmund, "Assessment of an elastic model in the pathogenesis of keratoconus," *Acta ophthalmologica*, vol. 65, no. 5, pp. 545-550, 1987.
- [317] Y. M. Michelacci, "Collagens and proteoglycans of the corneal extracellular matrix," *Brazilian Journal of Medical and Biological Research*, vol. 36, no. 8, pp. 1037-1046, 2003.
- [318] K. M. Meek and C. Knupp, "Corneal structure and transparency," *Progress in retinal and eye research*, vol. 49, pp. 1-16, 2015.
- [319] S. Akhtar, T. Almubrad, I. Paladini, and R. Mencucci, "Keratoconus corneal architecture after riboflavin/ultraviolet A cross-linking: ultrastructural studies," *Molecular vision*, vol. 19, p. 1526, 2013.
- [320] C. S. Foster and G. K. Yamamoto, "Ocular rigidity in keratoconus," *American journal of ophthalmology*, vol. 86, no. 6, pp. 802-806, 1978.
- [321] R. Vinciguerra, R. Ambrósio, A. Elsheikh, C. J. Roberts, B. Lopes *et al.*, "Detection of keratoconus with a new biomechanical index," *Journal of Refractive Surgery*, vol. 32, no. 12, pp. 803-810, 2016.
- [322] R. Ambrósio, B. T. Lopes, F. Faria-Correia, M. Q. Salomão, J. Bühren *et al.*, "Integration of Scheimpflug-based corneal tomography and biomechanical assessments for enhancing ectasia detection," *Journal of Refractive Surgery*, vol. 33, no. 7, pp. 434-443, 2017.

- [323] R. Ambrósio, Jr., F. F. Correia, B. Lopes, M. Q. Salomão, A. Luz *et al.*, "Corneal Biomechanics in Ectatic Diseases: Refractive Surgery Implications," *The open ophthalmology journal*, vol. 11, pp. 176-193, 2017.
- [324] B. C. Dominiak, P. S. Gillespie, and G. Tom, "Changes in data management and the impediments to change-a case study for fruit fly surveillance," *Plant Protection Quarterly*, vol. 22, no. 3, p. 95, 2007.
- [325] G. Scarcelli, S. Kling, E. Quijano, R. Pineda, S. Marcos, and S. H. Yun, "Brillouin microscopy of collagen crosslinking: noncontact depth-dependent analysis of corneal elastic modulus," *Investigative ophthalmology & visual science*, vol. 54, no. 2, pp. 1418-1425, 2013.
- [326] S. H. Chang, A. Mohammadvali, K. J. Chen, Y. R. Ji, T. H. Young *et al.*, "The Relationship Between Mechanical Properties, Ultrastructural Changes, and Intrafibrillar Bond Formation in Corneal UVA/Riboflavin Cross-linking Treatment for Keratoconus," *Journal of Refractive Surgery*, vol. 34, no. 4, pp. 264-272, 2018.
- [327] A. Eliasy, K.-J. Chen, and A. Elsheikh, "Intraocular Pressure Measurement Pre-and Post Refractive Surgery Using GAT and CorVis ST bIOP Algorithm," presented at the 6th European Conference on Computational Mechanics (ECCM 6); 7th European Conference on Computational Fluid Dynamics (ECFD 7), Glasgow, UK, 2018.
- [328] G. Scarcelli, S. Besner, R. Pineda, and S. H. Yun, "Biomechanical Characterization of Keratoconus Corneas Ex Vivo With Brillouin Microscopy Evaluation of Brillouin Microscopy for Keratoconus," *Investigative Ophthalmology & Visual Science*, vol. 55, no. 7, pp. 4490-4495, 2014.
- [329] A. K. Jain, R. P. W. Duin, and M. Jianchang, "Statistical pattern recognition: a review," *IEEE Transactions on Pattern Analysis and Machine Intelligence*, vol. 22, no. 1, pp. 4-37, 2000.
- [330] C. J. Roberts and J. W. J. Dupps, "Biomechanics of corneal ectasia and biomechanical treatments," *Journal of Cataract & Refractive Surgery*, Review Article vol. 40, no. 6,

pp. 991-998, 06/01/June 2014 2014.

- [331] Y. Lu, V. Vitart, K. P. Burdon, C. C. Khor, Y. Bykhovskaya *et al.*, "Genome-wide association analyses identify multiple loci associated with central corneal thickness and keratoconus," *Nature Genetics*, vol. 45, no. 2, pp. 155-163, 2013.
- [332] N. Morishige, A. J. Wahlert, M. C. Kenney, D. J. Brown, K. Kawamoto *et al.* (2007) Second-Harmonic Imaging Microscopy of Normal Human and Keratoconus Cornea. [Periodical]. 1087.
- [333] L. J. Maguire and W. M. Bourne, "Corneal topography of early keratoconus," *American Journal of Ophthalmology*, vol. 108, no. 2, pp. 107-112, 1989.
- [334] X. Li, H. Yang, and Y. S. Rabinowitz, "Keratoconus: classification scheme based on videokeratography and clinical signs," *Journal of Cataract & Refractive Surgery*, Article vol. 35, no. 9, pp. 1597-1603, 01/01/January 2009 2009.
- [335] N. Q. Ali, D. V. Patel, and C. N. J. McGhee, "Biomechanical Responses of Healthy and Keratoconic Corneas Measured Using a Noncontact Scheimpflug-Based Tonometer," vol. 55, ed, 2014, pp. 3651-3659.
- [336] P. R. R. Vazquez, M. Delrivo, F. F. Bonthoux, T. Pfortner, and J. G. Galletti. (2013) Combining Ocular Response Analyzer Metrics for Corneal Biomechanical Diagnosis. [Periodical]. 596.
- [337] A. Luz, B. Lopes, K. M. Hallahan, B. Valbon, B. Fontes *et al.*, "Discriminant Value of Custom Ocular Response Analyzer Waveform Derivatives in Forme Fruste Keratoconus," (in eng), *American journal of ophthalmology*, vol. 164, pp. 14-21, 2016.
- [338] J. D. Galletti, P. R. Ruiseñor Vázquez, F. Fuentes Bonthoux, T. Pfortner, and J. G. Galletti, "Multivariate Analysis of the Ocular Response Analyzer's Corneal Deformation Response Curve for Early Keratoconus Detection," (in eng), *Journal of ophthalmology*, vol. 2015, pp. 496382-496382, 2015.